

**Gaseous and Liquid Fuel Generation and Material
Recovery from Waste Electrical and Electronic
Equipment (WEEE) through Green Processes**

Thesis Submitted By
BISWAJIT DEBNATH

DOCTOR OF PHILOSOPHY (ENGINEERING)

DEPARTMENT OF CHEMICAL ENGINEERING

JADAVPUR UNIVERSITY

KOLKATA – 700 032

2023

Dedicated to my lovely wife Ankita

And

My alter-ego

Jon Bisu Debnath

NAME, DESIGNATION AND INSTITUTIONS OF THE SUPERVISORS

NAME: *RANJANA CHOWDHURY*

DESIGNATION: *PROFESSOR*

DEPARTMENT: *CHEMICAL ENGINEERING*

INSTITUTE: *JADAVPUR UNIVERSITY, KOLKATA-700032*

NAME: *SADHAN KUMAR GHOSH*

DESIGNATION: *PROFESSOR (Retired)*

DEPARTMENT: *MECHANICAL ENGINEERING*

INSTITUTE: *JADAVPUR UNIVERSITY, KOLKATA-700032*

LIST OF PUBLICATIONS

Journals

1. Debnath, B., Chowdhury, R., & Ghosh, S. K. (2018). Sustainability of metal recovery from E-waste. *Frontiers of environmental science & engineering*, 12, 1-12.

Book Chapters

1. Debnath, B., Chowdhury, R., & Ghosh, S. K. (2019). An analysis of e-waste recycling technologies from the chemical engineering perspective. In *Waste Management and Resource Efficiency: Proceedings of 6th IconSWM 2016* (pp. 879-888). Springer Singapore.

2. Debnath, B., Chowdhury, R., & Ghosh, S. K. (2019). Urban mining and the metal recovery from E-waste (MREW) supply chain. In *Waste Valorisation and Recycling: 7th IconSWM—ISWMAW 2017, Volume 2* (pp. 341-347). Springer Singapore.

LIST OF PRESENTATIONS IN NATIONAL/INTERNATIONAL CONFERENCES

1. Debnath., B., Kayal., S., Layek., P. and Chowdhury., R. (2023). Pyrolytic Urban Mining of FR-4 type Printed Circuit Boards: An Enviro-economic Analysis. In: International Conference on Chemical Engineering Innovation & Sustainability (ICEIS 2023), Jadavpur University, Kolkata, India, 26-27 February, 2023.
2. Debnath., B., Das., A., Chowdhury., R. & Ghosh, S.K. (2019). Kinetic Studies on FR-2 type Waste Printed Circuit Board (PCB) Pyrolysis. In Proceedings of 9th International Conference on Sustainable Waste Management towards Circular Economy (9thIconSWM-CE), pp. 1162 – 1167, Kalinga Institute of Industrial Technology (KIIT), Bhubaneswar, Odisha, India, 27-29 November, 2019. (Accepted for publication and Oral Presentation).
3. Debnath, B., Chowdhury, R., Ghosh, S.K. (2018). Towards Circular Economy in E-waste recycling via Metal Recovery from E-waste (MREW) facilities. In: Proceedings of ISWA 2018 World Congress, Kuala Lumpur, Malaysia, 22-24 October 2018.
4. Debnath., B., Banerji., A., Chowdhury., R. & Ghosh, S.K. (2018). Kinetic Studies on FR-4 type Waste Printed Circuit Board (PCB) Pyrolysis. In Proceedings of Recycle 2018, 2nd International Conference on Waste Management. IIT Guwahati, India, 22-24 February, 2018. (Abstract Published in book only)
5. Debnath., B., Chowdhury., R. & Ghosh, S.K. (2017). Studies on sustainable material recovery via Pyrolysis of WEEE. In Proceedings of Indian Chemical Engineering Congress (Chemcon 2017) pp. 31-33, Haldia, India, 27-30 December, 2017. (Extended Abstract Only) [Best Paper Award]
6. Debnath., B., Chowdhury., R., & Ghosh, S.K. (2017). Studies on Resource Recovery from E-waste via Thermochemical Route. In Proceedings of 4th 3R International Scientific Conference on Material Cycles and Waste Management, India Habitat Centre, New Delhi, India, 8-10 March, 2017. (Extended Abstract only).

“Statement of Originality”

I, Biswajit Debnath, registered on 5th May, 2016 do hereby declare that this thesis entitled **“Gaseous and Liquid Fuel Generation and Material Recovery from Waste Electrical and Electronic Equipment (WEEE) through Green Processes”** contains literature survey and original research work done by the undersigned candidate as part of Doctoral studies.

All information in this thesis have been obtained and presented in accordance with existing academic rules and ethical conduct. I declare that, as required by these rules and conduct, I have fully cited and referred all materials and results that are not original to this work.

I also declare that I have checked this thesis as per the “Policy on Anti Plagiarism, Jadavpur University, 2019”, and the level of similarity as checked by iThenticate software is 8 %.

Signature of Candidate: *Biswajit Debnath*

Date : *02/05/2023*

Certified by Supervisor(s):

1. *Ranjana Chowdhury 2-5-2023*
Dr. Ranjana Chowdhury
Professor
Chemical Engineering Department
JADAVPUR UNIVERSITY
Kolkata-700 032

2. *Sadg* *23/5/2023*

CERTIFICATE FROM THE SUPERVISOR/S

This is to certify that the thesis entitled “*Gaseous and Liquid Fuel Generation and Material Recovery from Waste Electrical and Electronic Equipment (WEEE) through Green Processes*” submitted by Shri Biswajit Debnath, who got his/her name registered on *5th May, 2016* for the award of Ph. D. (Engg.) degree of Jadavpur University is absolutely based upon his/her own work under the supervision of (1) **Prof. (Dr.) Ranjana Chowdhury** and (2) **Prof. (Dr.) Sadhan Kumar Ghosh** and that neither his/her thesis nor any part of the thesis has been submitted for any degree/diploma or any other academic award anywhere before.

Ranjana Chowdhury 2-5-2023

1. **Prof. (Dr.) Ranjana Chowdhury**

Sadhan Kumar Ghosh 3/5/23

2. **Prof. (Dr.) Sadhan Kumar Ghosh**

Dr. Ranjana Chowdhury
Professor
Chemical Engineering Department
JADAVPUR UNIVERSITY
Kolkata-700 032

ACKNOWLEDGEMENT

I take this opportunity to express my sincere gratitude and respect to my research supervisors, Prof. Ranjana Chowdhury, Chemical Engineering Department, Jadavpur University and Prof. Sadhan Kumar Ghosh, Mechanical Engineering Department, Jadavpur University for their guidance, constant help and encouragement without which it would not have been possible for me to finalize the thesis in the present form.

My heartfelt thanks to State Fellowship Scheme of Government of West Bengal, for providing necessary funding to carry out my Ph.D research work.

My sincere thanks to Commonwealth Scholarships Commission (CSC) for funding my research work on Supply Chain Kinetics of MREW plant at Aston University, Birmingham, UK. I would like to sincerely thank Prof. Sadhan Kumar Ghosh for helping me to achieve the prestigious Commonwealth Split-site scholarship. My sincere gratitude to Dr. Amit Kumar Chattopadhyay for his guidance and help during my visits at Aston University, Birmingham, UK.

My heartfelt gratitude goes to Prof. Laxminarayan Samavedam and National University of Singapore for providing the GeMS software. My sincere thanks go to members of workshop, staff members, library members and faculty members of Chemical Engineering Department, Jadavpur University for their help and support. I am also thankful to the HOD of Chemical Engineering Department, Jadavpur University, who have helped me in a number of occasions to make things right.

My genuine thanks to Prof. Papita Das for allowing me to use the FTIR machine, Dr. Sudhir Ghosh, Metallurgy Department, Jadavpur University for helping with the XRD analysis, Dr. Saswati Gharami, Chemistry Department, Jadavpur University for helping with ¹H NMR analysis, Mr. Soumitra Pati, Research Scholar, Mechanical Engineering Department, Jadavpur University for his inputs and help during Life Cycle Assessment. In addition to that, my thanks go to Physics Department, Jadavpur University for helping out with FESEM and EDX analysis. My sincere thanks are also due to all fellow scholars for their kind co-operation and support. I am really thankful to my wife who had been super supportive through my kith and kin. I would also like to mention Prof. Amar C. Das and Mrs. Ratna Das for their continuous support during this journey. I would like to acknowledge Late Guru Ramkrishna Goswami for his blessings. I am sincerely thankful to my parents for their unwavering support both humanly and financially and bearing up with me. Above all, I am really thankful to almighty god without the grace and blessings of whom the journey of Ph.D would have been meaningless.

LIST OF TABLES

CHAPTER - 1	
Table 1.1 Composition of PCB	
Table 1.2: Gasification Reactions	
CHAPTER - 4	
Table 4.1: FR-2 PCB Pyrolysis Reaction Pathway	
Table 4.2: FR-4 PCB Pyrolysis Reaction Pathway	
CHAPTER - 5	
Table 5.1: Proximate Analysis Results of Feedstock	
Table 5.2: Ultimate Analysis Results of Feedstock	
Table 5.3 Data of weight loss profile of FR-2 WPCB pyrolysis at different temperature	
Table 5.4 Data of Kinetic Constants of FR-2 WPCB pyrolysis	
Table 5.5 Data of weight loss profile of FR-4 WPCB pyrolysis at different temperature	
Table 5.6 Data of Kinetic Constants of FR-4 WPCB pyrolysis	
Table 5.7: The Kinetic Parameters determined using Friedman, KAS, FWO, Tang, Starink and Bosewell method for FR-2 VPCB Pyrolysis	
Table 5.8: The Kinetic Parameters determined using Friedman, KAS, FWO, Tang, Starink and Bosewell method for FR-2 WPCB Pyrolysis	
Table 5.9: The Kinetic Parameters determined using Friedman, KAS, FWO, Tang, Starink and Bosewell method for FR-4 VPCB Pyrolysis	
Table 5.10: The Kinetic Parameters determined using Friedman, KAS, FWO, Tang, Starink and Bosewell method for FR-4 WPCB Pyrolysis	
Table 5.11: The values of compensation effect for FR-2 WPCB Pyrolysis	
Table 5.12: The values of compensation effect for FR-4 WPCB Pyrolysis	
Table 5.13: Fitting Results of the Šesták-Berggren model for FR-2 PCBs	
Table 5.14: Fitting Results of the Šesták-Berggren model for FR-4 PCBs	
Table 5.15: Thermodynamic Triplets and Pre-exponential Factors for FR2 VPCB and WPCB at $\beta=10\text{K/min}$	
Table 5.16: Thermodynamic Triplets and Pre-exponential Factors for FR2 VPCB and WPCB at $\beta=20\text{K/min}$	
Table 5.17: Thermodynamic Triplets and Pre-exponential Factors for FR2 VPCB and WPCB at $\beta=30\text{K/min}$	

Table 5.18: Thermodynamic Triplets and Pre-exponential Factors for FR4 VPCB and WPCB at $\beta=10\text{K/min}$	
Table 5.19: Thermodynamic Triplets and Pre-exponential Factors for FR4 VPCB and WPCB at $\beta=20\text{K/min}$	
Table 5.20: Thermodynamic Triplets and Pre-exponential Factors for FR4 VPCB and WPCB at $\beta=30\text{K/min}$	
Table 5.21: Metal content mapping of FR-2 VPCB and WPCB before and after pyrolysis	
Table 5.22: Metal content mapping of FR-4 VPCB and WPCB before and after pyrolysis	
Table 5.23: Metal content mapping of mixed WPCB before and after pyrolysis	
Table 5.24: FTIR spectra analysis of FR2 VPCB Raw, Char and Oil	
Table 5.25: FTIR spectra analysis of FR2 WPCB Raw, Char and Oil	
Table 5.26: FTIR spectra analysis of FR4 VPCB Raw, Char and Oil	
Table 5.27: FTIR spectra analysis of FR4 WPCB Raw, Char and Oil	
Table 5.28: FTIR spectra analysis of Mixed WPCB Raw, Char and Oil	
Table 5.29: Composition of FR-2 WPCB Oil determined via Pyrolysis	
Table 5.30: Composition of FR-4 WPCB Oil determined via Pyrolysis	
Table 5.31: Composition of mixed WPCB Oil determined via Pyrolysis	
CHAPTER - 6	
Table 6.1: Experimental Set following DOE of BBD Method	
Table 6.2: Parameter for GP analysis	
Table 6.3: BBD matrix of three input process variables and their corresponding experimental outputs of metal+glass fibre recovery and pyro-oil yield.	
Table 6.4: ANOVA and the summary statistics of quadratic model for yield of metal mixture	
Table 6.5: ANOVA and the summary statistics of quadratic model for yield of pyro-oil	
Table 6.6 Maximum Yield of Metal+Glass Fibre and Pyro-oil at optimal conditions	
CHAPTER - 7	

Table 7.1: Data for the yield of solid residue of FR-2 and FR-4 and Mixed WPCB steam gasification aided pyrolysis	
Table 7.2: Syn-gas Composition obtained from Steam gasification aided pyrolysis of FR-2 and FR-4 WPCB	
Table 7.3: Metal content mapping of FR-2 and FR-4 WPCB before and after gasification	
Table 7.4: FTIR spectra analysis of FR-2 and FR-4 WPCB Steam Gasification aided Pyrolysis Char	
CHAPTER-8	
Table 8.1 Proximate and Ultimate analysis of FR-2 and FR-4 WPCB	
Table 8.2: Rate constants for gasification reactions	
Table 8.3: Simulation results of mixed WPCB Pyrolysis	
Table 8.4: Simulation results of mixed WPCB pyrolysis at different temperature	
Table 8.5: Simulation results of mixed WPCB gasification aided pyrolysis at different temperature	
Table 8.6: ASPEN predicted composition of metal stream from gasification aided pyrolysis	
CHAPTER-10	
Table 10.1: Midpoint Results of LCA of FR-2 WPCB Pyrolysis	
Table 10.2: Midpoint Results of LCA of FR-4 WPCB Pyrolysis	
Table 10.3: Midpoint Results of LCA of Mixed WPCB steam gasification aided pyrolysis	
Table 10.4: Economic Analysis of FR-2 and FR-4 WPCB Pyrolysis plant	
Table 10.5: Economic Analysis of mixed WPCB steam gasification aided pyrolysis plant	
Table 10.6: Stakeholder category and sub-categories for social aspects of MREW	

LIST OF FIGURES

CHAPTER-1	
Figure 1.1: Composition of E-waste	
Figure 1.2 (a): Structure of FR-2 PCB	
Figure 1.2 (b): Composition of FR-2 PCB	
Figure 1.3 (a): Structure of FR-4 PCB	
Figure 1.3 (b): Composition of FR-4 PCB	
Figure 1.4: Pyrolysis Scheme	
CHAPTER-4	
Figure 4.1 (a): FR-2 Waste PCB recovered from old TV set	
Figure 4.1 (b): FR-4 Waste PCB recovered from Personal Computer	
Figure 4.1 (c): FR-2 Virgin PCB store bought	
Figure 4.1 (d): FR-4 Virgin PCB procured online	
Figure 4.2 (a): FR-2 Waste PCB samples	
Figure 4.2 (b): FR-2 Virgin PCB samples	
Figure 4.2 (c): FR-4 Waste PCB samples	
Figure 4.2 (d): FR-4 Virgin PCB samples	
Figure 4.3: Experimental Setup	
Figure 4.4: Experimental Setup for Lumped Kinetics	
CHAPTER-5	
Figure 5.1: FR-2 WPCBs before and after pyrolysis	
Figure 5.2 (a): Weight loss profile of FR-2 WPCB pyrolysis	
Figure 5.2 (b): Kinetic Constants of FR-2 WPCB pyrolysis	
Figure 5.3: FR-4 WPCBs before and after pyrolysis	
Figure 5.4 (a): Weight loss profile of FR-4 WPCB pyrolysis	
Figure 5.4 (b): Kinetic Constants of FR-4 WPCB pyrolysis	
Figure 5.5 (a): TG curve of FR-2 WPCB at 10, 20 and 30K per min	
Figure 5.5 (b): TG curve of FR-2 VPCB at 10, 20 and 30K per min	
Figure 5.6 (a): DTG curve of FR-2 WPCB at 10, 20 and 30K per min	
Figure 5.6 (b): DTG curve of FR-2 VPCB at 10, 20 and 30K per min	
Figure 5.7 (a): TG curve of FR-4 WPCB at 10, 20 and 30K per min	
Figure 5.7 (b): TG curve of FR-4 VPCB at 10, 20 and 30K per min	
Figure 5.8 (a): DTG curve of FR-4 WPCB at 10, 20 and 30K per min	

Figure 5.8 (b): DTG curve of FR-4 VPCB at 10, 20 and 30K per min	
Figure 5.9 (a): Kinetic Plot for determination of kinetic parameters using Friedman method for FR-2 VPCB pyrolysis	
Figure 5.9 (b): Kinetic Plot for determination of kinetic parameters using KAS method for FR-2 VPCB pyrolysis	
Figure 5.9 (c): Kinetic Plot for determination of kinetic parameters using FWO method for FR-2 VPCB pyrolysis	
Figure 5.9 (d): Kinetic Plot for determination of kinetic parameters using Starink method for FR-2 VPCB pyrolysis	
Figure 5.9 (e): Kinetic Plot for determination of kinetic parameters using Tang method for FR-2 VPCB pyrolysis	
Figure 5.9 (f): Kinetic Plot for determination of kinetic parameters using Bosewell method for FR-2 VPCB pyrolysis	
Figure 5.10: Plot of R^2 vs Conversion (α) using Friedman, KAS, FWO, Starink, Tang and Bosewell method for FR-2 VPCB pyrolysis	
Figure 5.11 (a): Comparison of Activation Energies obtained using Friedman, KAS, FWO, Starink, Tang and Bosewell method for FR-2 VPCB pyrolysis	
Figure 5.11 (b): Evolution trend of Activation Energies obtained using Friedman, KAS, FWO, Starink, Tang and Bosewell method for FR-2 VPCB pyrolysis	
Figure 5.12 (a): Kinetic Plot for determination of kinetic parameters using Friedman method for FR-2 WPCB pyrolysis	
Figure 5.12 (b): Kinetic Plot for determination of kinetic parameters using KAS method for FR-2 WPCB pyrolysis	
Figure 5.12 (c): Kinetic Plot for determination of kinetic parameters using FWO method for FR-2 WPCB pyrolysis	
Figure 5.12 (d): Kinetic Plot for determination of kinetic parameters using Starink method for FR-2 WPCB pyrolysis	
Figure 5.12 (e): Kinetic Plot for determination of kinetic parameters using Tang method for FR-2 WPCB pyrolysis	
Figure 5.12 (f): Kinetic Plot for determination of kinetic parameters using Bosewell method for FR-2 WPCB pyrolysis	

Figure 5.13: Plot of R^2 vs Conversion (α) using Friedman, KAS, FWO, Starink, Tang and Bosewell method for FR-2 WPCB pyrolysis	
Figure 5.14 (a): Comparison of Activation Energies obtained using Friedman, KAS, FWO, Starink, Tang and Bosewell method for FR-2 WPCB pyrolysis	
Figure 5.14 (b): Evolution trend of Activation Energies obtained using Friedman, KAS, FWO, Starink, Tang and Bosewell method for FR-2 WPCB pyrolysis	
Figure 5.15 (a): Kinetic Plot for determination of kinetic parameters using Friedman method for FR-4 VPCB pyrolysis	
Figure 5.15 (b): Kinetic Plot for determination of kinetic parameters using KAS method for FR-4 VPCB pyrolysis	
Figure 5.15 (c): Kinetic Plot for determination of kinetic parameters using FWO method for FR-4 VPCB pyrolysis	
Figure 5.15 (d): Kinetic Plot for determination of kinetic parameters using Starink method for FR-4 VPCB pyrolysis	
Figure 5.15 (e): Kinetic Plot for determination of kinetic parameters using Tang method for FR-4 VPCB pyrolysis	
Figure 5.15 (f): Kinetic Plot for determination of kinetic parameters using Bosewell method for FR-4 VPCB pyrolysis	
Figure 5.16: Plot of R^2 vs Conversion (α) using Friedman, KAS, FWO, Starink, Tang and Bosewell method for FR-4 VPCB pyrolysis	
Figure 5.17 (a): Comparison of Activation Energies obtained using Friedman, KAS, FWO, Starink, Tang and Bosewell method for FR-4 VPCB pyrolysis	
Figure 5.17 (b): Evolution trend of Activation Energies obtained using Friedman, KAS, FWO, Starink, Tang and Bosewell method for FR-4 VPCB pyrolysis	
Figure 5.18 (a): Kinetic Plot for determination of kinetic parameters using Friedman method for FR-4 WPCB pyrolysis	
Figure 5.18 (b): Kinetic Plot for determination of kinetic parameters using KAS method for FR-4 WPCB pyrolysis	
Figure 5.18 (c): Kinetic Plot for determination of kinetic parameters using FWO method for FR-4 WPCB pyrolysis	

Figure 5.18 (d): Kinetic Plot for determination of kinetic parameters using Starink method for FR-4 WPCB pyrolysis	
Figure 5.18 (e): Kinetic Plot for determination of kinetic parameters using Tang method for FR-4 WPCB pyrolysis	
Figure 5.18 (f): Kinetic Plot for determination of kinetic parameters using Bosewell method for FR-4 WPCB pyrolysis	
Figure 5.19: Plot of R^2 vs Conversion (α) using Friedman, KAS, FWO, Starink, Tang and Bosewell method for FR-4 WPCB pyrolysis	
Figure 5.20 (a): Comparison of Activation Energies obtained using Friedman, KAS, FWO, Starink, Tang and Bosewell method for FR-4 WPCB pyrolysis	
Figure 5.20 (b): Evolution trend of Activation Energies obtained using Friedman, KAS, FWO, Starink, Tang and Bosewell method for FR-4 WPCB pyrolysis	
Figure 5.21: Distribution of Activation Energy of FR-2 VPCB and WPCB Pyrolysis	
Figure 5.22: Distribution of Activation Energy of FR-4 VPCB and WPCB Pyrolysis	
Figure 5.23 (a): Compensation Effect of FR-2 PCBs using Arrhenius Parameters obtained from Friedman method	
Figure 5.23 (b): Compensation Effect of FR-2 PCBs using Arrhenius Parameters obtained from KAS method	
Figure 5.23 (c): Compensation Effect of FR-2 PCBs using Arrhenius Parameters obtained from FWO method	
Figure 5.24 (a): Compensation Effect of FR-4 PCBs using Arrhenius Parameters obtained from Friedman method	
Figure 5.24 (b): Compensation Effect of FR-4 PCBs using Arrhenius Parameters obtained from KAS method	
Figure 5.24 (c): Compensation Effect of FR-4 PCBs using Arrhenius Parameters obtained from FWO method	
Figure 5.25 (a): Contribution analysis of interface reaction ($n \ln(1-\alpha)$), diffusion ($m \ln \alpha$), and nucleation reaction ($p \ln(-\ln(1-\alpha))$) to pyrolysis of FR-2 VPCB	

Figure 5.25 (b): Contribution analysis of interface reaction ($n \ln(1-\alpha)$), diffusion ($m \ln \alpha$), and nucleation reaction ($p \ln(-\ln(1-\alpha))$) to pyrolysis of FR-2 WPCB	
Figure 5.26 (a): Contribution analysis of interface reaction ($n \ln(1-\alpha)$), diffusion ($m \ln \alpha$), and nucleation reaction ($p \ln(-\ln(1-\alpha))$) to pyrolysis of FR-4 VPCB	
Figure 5.26 (b): Contribution analysis of interface reaction ($n \ln(1-\alpha)$), diffusion ($m \ln \alpha$), and nucleation reaction ($p \ln(-\ln(1-\alpha))$) to pyrolysis of FR-4 WPCB	
Figure 5.27 (a): Product Distribution of FR-2 VPCB pyrolysis	
Figure 5.27 (b): Product Distribution of FR-2 WPCB pyrolysis	
Figure 5.28 (a): Product Distribution of FR-4 VPCB pyrolysis	
Figure 5.28 (b): Product Distribution of FR-4 WPCB pyrolysis	
Figure 5.29 (a): Pyro-oil recovered from 90% FR2 and 10% FR4 WPCB combination feedstock	
Figure 5.29 (b): Pyro-oil recovered from 90% FR4 and 10% FR2 WPCB combination feedstock	
Figure 5.30: Variation of pyro-oil yield with different percentage of FR-2 WPCB in a mixture of FR2 and FR4	
Figure 5.31(a): Copper recovered via Pyrolysis of mixed WPCB	
Figure 5.31 (b): Variation of yield of metals with different percentage of FR-2 WPCB in a mixture of FR2 and FR4	
Figure 5.32 (a): Recovered Glass Fibre from mixed WPCB	
Figure 5.32 (b): Variation of yield of glass fibre and char of FR-2 WPCB in a mixture of FR2 and FR4	
Figure 5.33 (a): FESEM images of FR2 VPCB before pyrolysis	
Figure 5.33 (b): FESEM images of FR2 VPCB after pyrolysis	
Figure 5.34 (a): FESEM images of FR2 WPCB before pyrolysis	
Figure 5.34 (b): FESEM images of FR2 WPCB before pyrolysis	
Figure 5.35 (a): FESEM images of FR4 VPCB before pyrolysis	
Figure 5.35 (b): FESEM images of FR4 VPCB before pyrolysis	
Figure 5.36 (c): FESEM images of FR4 WPCB before pyrolysis	
Figure 5.36 (d): FESEM images of FR4 WPCB before pyrolysis	

Figure 5.37: FESEM images of mixed WPCB sample before pyrolysis	
Figure 5.38: FESEM images of mixed WPCB sample after pyrolysis	
Figure 5.39 (a): XRD Spectra of FR2 VPCB Raw	
Figure 5.39 (b): XRD Spectra of FR2 VPCB Pyro Char	
Figure 5.39 (c): XRD Spectra of FR2 WPCB Raw	
Figure 5.39 (d): XRD Spectra of FR2 WPCB pyro-char	
Figure 5.40 (a): XRD Spectra of FR4 VPCB Raw	
Figure 5.40 (b): XRD Spectra of FR4 VPCB Pyro Char	
Figure 5.40 (c): XRD Spectra of FR4 WPCB Raw	
Figure 5.40 (d): XRD Spectra of FR4 WPCB pyro-char	
Figure 5.41 (a): XRD Spectra of mixed WPCB Raw	
Figure 5.41 (b): XRD Spectra of mixed WPCB Pyro Char	
Figure 5.42 (a): IR spectra of FR2 VPCB before pyrolysis	
Figure 5.42 (b): IR spectra of FR2 VPCB char (after pyrolysis)	
Figure 5.42 (c): IR spectra of FR2 WPCB before pyrolysis	
Figure 5.42 (d): IR spectra of FR2 WPCB char (after pyrolysis).	
Figure 5.43 (a): IR spectra of Pyro-oil recovered from FR2 VPCB pyrolysis	
Figure 5.43 (b): IR spectra of Pyro-oil recovered from FR2 WPCB pyrolysis	
Figure 5.44 (a): IR spectra of FR4 VPCB before pyrolysis	
Figure 5.44 (b): IR spectra of FR4 VPCB char (after pyrolysis)	
Figure 5.44 (c): IR spectra of FR4 WPCB before pyrolysis	
Figure 5.44 (d): IR spectra of FR4 WPCB char (after pyrolysis).	
Figure 5.45 (a): IR spectra of Pyro-oil recovered from FR4 VPCB pyrolysis	
Figure 5.45 (b): IR spectra of Pyro-oil recovered from FR4 WPCB pyrolysis	
Figure 5.46 (a): IR spectra of mixed WPCB before pyrolysis	
Figure 5.46 (b): IR spectra of mixed WPCB char (after pyrolysis).	
Figure 5.47: IR spectra of Pyro-oil recovered from mixed WPCB pyrolysis	
Figure 5.48 (a): ^1H NMR spectra of FR-2 VPCB Pyro-oil	
Figure 5.48 (b): ^1H NMR spectra of FR-2 WPCB Pyro-oil	
Figure 5.49 (a): ^1H NMR spectra of FR-4 VPCB Pyro-oil	
Figure 5.49 (b): ^1H NMR spectra of FR-4 WPCB Pyro-oil	
Figure 5.50: ^1H NMR spectra of mixed WPCB Pyro-oil	

CHAPTER-6	
Figure 6.1: TGA-DTG plot of mixed WPCB at 20K per min heating rate	
Figure 6.2 (a): Plot of predicted vs. actual response for metal+glass fibre recovery	
Figure 6.2 (b): Plot of normal % probability vs. externally studentized residuals for metal+glass fibre recovery	
Figure 6.3: Perturbation plot showing the effect of three process variables on the response metal+glass fibre recovery	
Figure 6.4 (a): 3D surface plot of metal + glass fibre recovery showing effect of time and %FR-4 WPCB in a mixture of FR-2 and FR-4 WPCB,	
Figure 6.4 (b): 3D surface plot of metal + glass fibre recovery showing effect of time and N ₂ Flowrate	
Figure 6.4 (c): 3D surface plot of metal + glass fibre recovery showing effect of N ₂ Flowrate and %FR-4 WPCB in a mixture of FR-2 and FR-4 WPCB	
Figure 6.5 (a): Plot of predicted vs. actual response for pyro-oil recovery	
Figure 6.5 (b): Plot of normal % probability vs. externally studentized residuals for pyro-oil recovery	
Figure 6.6: Perturbation plot showing the effect of three process variables on the response Pyro-oil yield	
Figure 6.7 (a): 3D surface plot of pyro-oil recovery showing effect of time and %FR-4 WPCB in a mixture of FR-2 and FR-4 WPCB,	
Figure 6.7 (b): 3D surface plot of pyro-oil recovery showing effect of time and N ₂ Flowrate	
Figure 6.7 (c): 3D surface plot of pyro-oil recovery showing effect of N ₂ Flowrate and %FR-4 WPCB in a mixture of FR-2 and FR-4 WPCB	
Figure 6.8: Model Fitting using GP for Metal + glass fibre recovery	
Figure 6.9: Model Fitting using GP for Pyro-oil recovery	
CHAPTER-7	
Figure 7.1 (a): Solid Residue of FR-2 WPCB steam gasification	
Figure 7.1 (b): Solid Residue of FR-4WPCB steam gasification	
Figure 7.2 (a): Yield of Solid Residue of FR-2 steam gasification aided pyrolysis	

Figure 7.2 (b): Yield of Solid Residue of FR-4WPCB steam gasification aided pyrolysis	
Figure 7.3 (a): FESEM images of FR-2WPCB Raw	
Figure 7.3 (b): FESEM images of FR-2WPCB Steam gasification aided pyrolysis char	
Figure 7.3 (c): FESEM images of FR-4 WPCB Raw	
Figure 7.3 (d): FESEM images of FR-4 WPCB Steam gasification aided pyrolysis char	
Figure 7.4 (a): XRD Spectra of FR-2WPCB Raw	
Figure 7.4 (b): XRD Spectra of FR-2WPCB Steam gasification aided pyrolysis Char	
Figure 7.4 (c): XRD Spectra of FR-4 WPCB Raw	
Figure 7.4 (d): XRD Spectra of FR-4 WPCB Steam gasification aided pyrolysis char	
Figure 7.5 (a): IR spectra of FR-2WPCB	
Figure 7.5 (b): IR spectra of FR-4 WPCB steam gasification aided pyrolysis char	
CHAPTER-8	
Figure 8.1: Process of E-waste Recycling in Indian Unit	
Figure 8.2: Process for CRT recycling in Indian Unit	
Figure 8.3: Process for e-waste recycling in Chinese Unit	
Figure 8.4: Schematic Diagram of MREW Facility	
Figure 8.5: Conceptual Framework with conventional mechanical pre-treatment followed by metallurgical processing for MREW (Option-1)	
Figure 8.6: Conceptual Framework with light mechanical recycling and pyrolysis as pre-treatment followed by metallurgical processing for MREW (Option-2)	
Figure 8.7: Conceptual Framework with light mechanical recycling and steam gasification aided pyrolysis as pre-treatment followed by metallurgical processing for MREW (Option-3)	
Figure 8.8: Aspen Plus Simulation of mixed WPCB pyrolysis and product separation	

Figure 8.9: Aspen Plus Simulation of mixed WPCB steam gasification aided pyrolysis and product separation	
CHAPTER-9	
Figure 9.1: Boundaries of Supply Chain based on LCA	
Figure 9.2: Supply chain network for MREW facility	
Figure 9.3: Working Flowchart of the problem to solution approach	
Figure 9.4: AHP model 1 to determine the general alterative rankings.	
Figure 9.5: Layered AHP model for determination of interrelationship values	
Figure 9.6: Time dependency of V_{CO_2} in constrained environment, using AHP for ranking (dash-dotted line) and hybrid AHP-PCA for ranking (solid line) obtained from simultaneous solution of Eqs. (9.9) and (9.12): (a) 1-year time span; (b) 5-year time span.	
Figure 9.7: Time dependency of V_{CO_2} in constrained environment, using AHP for ranking (dash-dotted line) and hybrid AHP-PCA for ranking (solid line) obtained from simultaneous solution of Eqs. (9.9) and (9.12) in 3-year time span	
Figure 9.8: Time dependency of E_c in a constrained environment, using AHP for ranking (dash-dotted line) and hybrid AHP-PCA for ranking (solid line) obtained from simultaneous solution of Eqs. (9.9) and (9.12): (a) 1-year time span; (b) 5-year time span.	
Figure 9.9: Time dependency of E_c : (a) in constrained environment, using AHP for ranking (dash-dotted line) and hybrid AHP-PCA for ranking (solid line) and (b) in unconstrained environment using hybrid AHP-PCA for ranking obtained from simultaneous solution of Eqs. (9.9) and (9.12) in a 3-year timespan	
Figure 9.10: Time dependency of N_3 in constrained environment, using AHP for ranking (dash-dotted line) and hybrid AHP-PCA for ranking (solid line) obtained from simultaneous solution of Eqs. (9.9) and (9.12): (a) 1-year time span; (b) 5-year time span	
Figure 9.11: Time dependency of N_3 : (a) in constrained environment, using AHP for ranking (dash-dotted line) and hybrid AHP-PCA for ranking (solid line) and (b) in unconstrained environment using hybrid AHP-PCA for ranking	

and AHP for ranking (provided in the insets) obtained from simultaneous solution of Eqs. (9.9) and (9.12)	
Figure 9.12: Time dependency of N_4 in constrained environment, using AHP for ranking (dash-dotted line) and hybrid AHP-PCA for ranking (solid line) obtained from simultaneous solution of Eqs. (9.9) and (9.12): (a) 1-year time span; (b) 5-year time span	
Figure 9.13: Time dependency of N_4 : (a) in constrained environment, using AHP for ranking (dash-dotted line) and hybrid AHP-PCA for ranking (solid line) and (b) in unconstrained environment using hybrid AHP-PCA for ranking and AHP for ranking (provided in the insets) obtained from simultaneous solution of Eqs. (9.9) and (9.12)	
CHAPTER-10	
Figure 10.1: LCA Framework according to ISO 14040 series	
Figure 10.2 (a): System Boundary of LCA of FR-2 WPCB Pyrolysis	
Figure 10.2 (b): System Boundary of LCA of FR-4 WPCB Pyrolysis	
Figure 10.2 (c): System Boundary of LCA of Mixed WPCB Gasification based pyrolysis	
Figure 10.3: LCA midpoint results of FR-2 WPCB pyrolysis	
Figure 10.4: LCA midpoint results of FR-4 WPCB pyrolysis	
Figure 10.5: LCA midpoint results of mixed WPCB steam gasification aided pyrolysis	

CONTENTS

	Page no.
List of Figures	
List of Tables	
CHAPTER-1: INTRODUCTION	1 - 13
Preamble	1
1.1 Global Scenario of E-waste Management	2
1.2 Composition of E-waste	2
1.3 Printed Circuit Boards	3
1.3.1 FR-2 type PCB	3
1.3.2 FR-4 type PCB	3
1.4 Existing Technologies for PCB treatment	4
1.4.1 Physical Recycling Methods	4
1.4.2 Pyro-metallurgical Methods	5
1.4.3 Hydro-metallurgical Methods	5
1.4.4 Bio-metallurgical Processes	6
1.5 Non-conventional Thermochemical Processes for PCB Treatment	6
1.5.1 Pyrolysis	6
1.5.2 Gasification	7
1.6 Rationale Behind Research	8
References	10
CHAPTER-2: LITERATURE REVIEW	14-46
2.1 Printed Circuit Board (PCB) Pyrolysis	14
2.2 Printed Circuit Board Gasification	22
2.3 Process Modelling of Thermochemical Treatment of PCBs	25
2.4 Supply Chain Performance of E-waste Processing Plant	27
2.5 Life Cycle Assessment of E-waste	31
2.6 Research Gap	40
References	41
CHAPTER-3: AIMS AND OBJECTIVES	47-55
CHAPTER-4: MATERIALS AND METHODS	56-75

4.1 Materials and methods	56
4.1.1 Printed Circuit Board (PCB) collection	56
4.1.2 Sample Preparation	56
4.1.3 Chemicals	57
4.1.4 Description of Experimental Setup	57
4.1.5 Experimental Setup for Lumped Kinetics	58
4.1.6 Equipment and Apparatus	59
4.1.7 Software Packages	59
4.2 Analytical Methods	59
4.2.1 Proximate and Ultimate Analysis	60
4.2.2 Thermo-gravimetric Analysis (TGA)	60
4.2.3. Field Emission Scanning Electron Microscope (FESEM)	60
4.2.4 Energy-dispersive X-ray spectroscopy (EDX) analysis	60
4.2.5 FTIR Analysis	60
4.2.6 X-Ray Diffraction (XRD) Analysis	61
4.2.7 ¹ H NMR Analysis	61
4.2.8 GC-MS Analysis	61
4.2.9 GC Analysis of pyro-gas and syngas	61
4.3 Theoretical Analysis	61
4.3.1 Fundamentals Chemistry of Kinetic Studies	61
4.3.1.1 FR-2 PCB Reaction Chemistry	61
4.3.1.2 FR-4 PCB Reaction Chemistry	63
4.3.2 Lumped Kinetic Modelling	65
4.3.3 Isoconversional Kinetic Modelling and DAEM	66
4.3.3.1 Friedman Method	67
4.3.3.2 KAS Method	68
4.3.3.3 FWO Method	68
4.3.3.4 Starink Method	69
4.3.3.5 Tang Method	69
4.3.3.6 Bosewell Method	69
4.3.4 DAEM Method	69
4.3.5 Thermodynamic Analysis	70

4.3.6 Reaction Mechanism	71
4.3.7 Solution Algorithm	71
4.3.7.1 Determination of Kinetic Parameters	71
4.3.7.2 Determination of Reaction Mechanisms	71
4.3.7.3 Determination of Thermodynamic Parameters	71
4.3.7.4 Calculation of E and f(E)	72
4.3.8 Calculation of Theoretical Yield	72
4.3.9 Calculation of Higher Heating Value of Pyro-oil	72
4.3.10 AHP Analysis	72
References	74
CHAPTE-5: PYROLYSIS OF PRINTED CIRCUIT BOARDS	76-143
5.1 Background	76
5.2 Experimental	77
5.2.1 Lumped Kinetics	77
5.2.2 PCB Pyrolysis	77
5.3 Results and Discussion	78
5.3.1 Proximate and Ultimate Analysis	78
5.3.2 Lumped Kinetics	78
5.3.2.1 Lumped Kinetics of FR-2 WPCB	78
5.3.2.2 Lumped Kinetics of FR-4 WPCB	80
5.3.3. Thermogravimetric Analysis	82
5.3.3.1 FR-2 Virgin PCB	82
5.3.3.2 FR-2 Waste PCB	83
5.3.3.3 FR-4 Virgin PCB	84
5.3.3.4 FR-4 Waste PCB	85
5.3.4. Iso-conversional Kinetics	85
5.3.4.1 Kinetic Analysis of FR-2 type VPCB	85
5.3.4.2 Analysis of Activation Energies of FR-2 VPCB	87
5.3.4.3 Kinetic Analysis of FR-2 type WPCB	87
5.3.4.4 Analysis of Activation Energies for FR-2 WPCB.	91
5.3.4.5. Kinetic Analysis of FR-4 type VPCB	93
5.3.4.6 Analysis of Activation Energies of FR-4 VPCB	95

5.3.4.7 Kinetic Analysis of FR-4 type WPCB	96
5.3.4.8 Analysis of Activation Energies of FR-4 WPCB	99
5.3.5 Distribution of Activation Energies (DAEM)	100
5.3.5.1 DAEM of FR-2 PCBs	100
5.3.5.2 DAEM of FR-4 PCBs	101
5.3.6. Compensation Effect	101
5.3.6.1 FR-2 PCBs	101
5.3.6.2 FR-4 PCBs	103
5.3.7. Determination of Reaction Mechanism Function	105
5.3.7.1 FR-2 PCBs	105
5.3.7.2 FR-4 PCBs	107
5.3.8. Determination of Pre-exponential Factor & Thermodynamic Triplets	109
5.3.8.1 FR-2 PCBs	109
5.3.8.2 FR-4 PCBs	112
5.3.9. Product Distribution	116
5.3.9.1 FR-2 PCBs	116
5.3.9.2 FR-4 PCBs	116
5.3.10 Product Recovery from mixed WPCB pyrolysis	117
5.3.10.1 Recovery of Pyro-oil	117
5.3.10.2 Recovery of Metals	119
5.3.10.3 Recovery of Char and Glass Fibre	119
5.3.11. Characterizations of Pyro-products	120
5.3.11.1 FESEM and EDX analysis of FR-2 PCBs	120
5.3.11.2 FESEM and EDX analysis of FR-4 PCBs	122
5.3.11.3 FESEM and EDX analysis of mixed WPCBs	124
5.3.11.4 XRD analysis of FR-2 PCBs	125
5.3.11.5 XRD analysis of FR-4 PCBs	127
5.3.11.6 XRD analysis of mixed WPCBs	128
5.3.11.7 FTIR Analysis of FR-2 PCBs	129
5.3.11.8 FTIR Analysis of FR-4 PCBs	133
5.3.11.9 FTIR Analysis of mixed PCBs	137
5.3.11.10 ¹ H NMR Results of FR-2 PCBs	139

5.3.11.11 ¹ H NMR Results of FR-4 PCBs	140
5.3.11.12 ¹ H NMR Results of mixed WPCBs pyro-oil	140
5.3.11.13 GC-MS analysis of FR-2 WPCBs	141
5.3.11.14 GC-MS analysis of FR-4 WPCBs	143
5.3.11.15 GC-MS analysis of mixed WPCB pyro-oil	144
References	147
CHAPTER – 6: Optimization of mixed Waste Printed Circuit Board (WPCB) pyrolysis	150-171
6.1 Background	150
6.2 Experimental	150
6.3 TGA analysis of Mixed WPCB	151
6.4 Optimization of mixed WPCB pyrolysis	152
6.5.1 Methodology	153
6.5.1.1 Response surface methodology (RSM)	153
6.5.1.2 Genetic Programming (GP)	154
6.6 Results and Discussion	155
6.6.1 Response surface model and ANOVA	155
6.6.1.1 Metal + glass fibre recovery	156
6.6.1.2 Effect of individual variables on metal mixture recovery: perturbation analysis	158
6.6.1.3. Effect of process variables on metal mixture recovery: response surface plots	159
6.6.1.4 Pyro Oil Yield	161
6.6.1.5 Effect of individual variables on pyro-oil yield: perturbation analysis	163
6.6.1.6. Effect of process variables on pyro-oil recovery: response surface plots	164
6.6.2 Genetic Programming (GP)	166
6.6.2.1 Metal + glass fibre recovery	166
6.6.2.2 Pyro-oil Yield	167
6.6.3 Model Critique	169
References	170
CHAPTER – 7: Steam Gasification aided Pyrolysis of Waste Printed Circuit Boards	172-181

7.1 Background	172
7.2 Experimental	173
7.3 Results and Discussion	173
7.4 Characterizations of Steam Gasification aided Pyrolysis Char	175
7.4.1 FESEM and EDX analysis	175
7.4.2 XRD analysis	178
7.4.3 FTIR Analysis	179
References	181
CHAPTER – 8: MREW FRAMEWORK AND PROCESS MODELING USING ASPEN	182 – 197
8.1 Background	182
8.2 Methodology	182
8.3 Case Studies	183
8.3.1 Case Study Organization A:	183
8.3.2 Case Study Organization B:	185
8.4 The Concept of MREW	186
8.4.1 Description of MREW Facility	186
8.4.2 Three Scopes of MREW	187
8.5 Process Modelling	190
8.6 Process Modelling Methods	191
8.7 Simulation model of Mixed PCB Pyrolysis	191
8.8 Simulation model of Mixed PCB Gasification	193
8.9 Results and Discussions	194
8.9.1 Results of simulation of mixed WPCB pyrolysis	194
8.9.2 Results of simulation of mixed WPCB gasification aided pyrolysis	195
References	197
CHAPTER-9: Supply Chain Kinetics of MREW Plant	198-221
9.1 BACKGROUND	198
9.2 Description of the MREW Supply Chain Network	199
9.3 Methodology	200
9.4 Mathematical Modelling	202
9.4.1 Model Assumptions	202

9.4.2. Model Descriptions	202
9.4.3 Determination of weight factors and Interaction Terms	204
9.4.3.1 Analytical Hierarchical Process (AHP)	204
9.4.3.2 Multivariate Study - Principal Component Analysis (PCA)	205
9.4.3.3. Hybrid AHP-PCA method	206
9.4.4 Optimization Algorithm	207
9.5 Unconstrained Problem	208
9.6 Constrained Problem	210
9.7 Results & Discussion	211
9.7.1 Volume of Carbon Dioxide Emission	212
9.7.2 Energy Consumption	214
9.7.3 Number of Awareness Activities	216
9.7.4 Recycled Product Sales	218
References	220
CHAPTER-10: SUSTAINABILITY ANALYSIS OF MREW	222-232
10.1 BACKGROUND	222
10.2.1 LCA Methodology	222
10.2.1.1 Goal & Scope Definition	223
10.2.1.2 Life Cycle Inventory Analysis (LCI)	224
10.2.1.3 Life Cycle Impact Assessment (LCIA)	224
10.2.2 Economic Analysis	225
10.3 Sustainability Analysis	225
10.3.1 Environmental Sustainability	225
10.3.1.1 LCA of FR-2 &FR-4 WPCB pyrolysis process	225
10.3.1.2 LCA of mixed WPCB steam gasification aided pyrolysis process	228
10.3.2 Economic Sustainability	229
10.3.3 Social Sustainability	231
References	232
CHAPTER-11: CONCLUSION	233 - 236
Conclusion	233
Future Scope	236

CHAPTER-1

INTRODUCTION

CHAPTER – 1

Preamble

Valorisation of waste materials and utilisation of the recovered products is a key process to achieve a sustainable system. There is a wide array of waste materials – Biomass, Plastic waste, Industrial wastes etc., suitable for utilisation for sustainability. Electronic Waste (E-waste) is a mini catastrophe and a threat to the modern developed society (Rathinakumar et al. 2023). The definition of e-waste varies depending on the regulatory body. According to Basel Action Network, “*E-waste includes a wide and developing range of electronic appliances ranging from large household appliances, such as refrigerators, air-conditioners, cell phones, stereo systems, and consumable electronic items to computers discarded by their users*” (Basel Convention 2014). If utilized judiciously, e-waste is a highly potent candidate for urban mining and developing a sustainable system (Murthy & Ramakrishna 2022).

E-waste is a complex and heterogeneous material. Printed circuit boards (PCBs) are vital part of electronic systems and are commonly found in different electronic appliances. PCBs are the core element in all electronic units. Used PCBs contribute to 3% -6% of the total mass of the total e-waste generated. It is a self-contained board with interconnected electrical and electronic component found in various devices ranging from beepers to pagers, radios, radars and computer systems. Nearly, 2 million tons of waste printed circuit boards (PCBs) are estimated to generate worldwide annually, which contain approximately 70% of non-metallic fractions (NMF) which are primarily resin-based compounds (Ma et al. 2021). Waste PCB generation from e-waste alone is 0.5 million tons in China every year excluding the 0.1 tons of scraps generated during manufacturing process (Zhang et al. 2012). PCB contains a lot of materials including metals, polymers and glass fibres. Since, PCB manufactured by different manufactures has different compositions it is considered a heterogeneous material and the properties may vary widely. E-waste is a big mine of several resources and it can be a source of secondary raw materials (Tipre et al. 2021). In the pre-processing step of recovery of metals and glass fibres from the PCBs, the polymer part can be handled through thermo-chemical processes to generate fuels and chemicals (Charitopoulou et al. 2021). Given the rich composition, PCBs are potential candidates for resource valorisation. PCB valorisation can help in achieving circular economy ensuring the economic and environmental sustainability.

1.1 Global Scenario of E-waste Management

Growth of electronics industry has been tremendous in the last two decades which ensured a lot of cash flow, but it also contributed to the material flow stream of electronic waste. According to the business research company, the global electrical and electronics market grew from \$3454.94 billion in 2022 to \$3739.37 billion in 2023 at a CAGR of 8.2% (The business research company 2023). Globally, e-waste is the fastest expanding waste stream, increasing at an annual rate of 3-5% (Yao et al. 2020). The demand of Electronic and Electrical Equipment (EEE) is ever increasing and the driving force behind this demand is often the technological advancement coupled with short innovation cycles and business strategies which shortens the lifespan of EEEs (Forti et al. 2020). The high rate of desuetude of EEE is not only due to the abovementioned reasons, but also due to intelligent marketing gimmicks of electronics industry. The electronic industry is one of the gigantic industries worldwide. As reported by International Solid Waste Association (ISWA), in the year 2019, approximately 53.6 million metric tons of e-waste was generated worldwide (Forti et al. 2020). India generated nearly 3.2 million metric tons of e-waste in 2019 and ranks third in the world (Forti et al. 2020). While Asia was the highest generator of e-waste (24.9 million metric tons), highest amount of e-waste was documented to be collected and properly recycled in Europe (5.1 million metric tons, ~42.5%) (Forti et al. 2020). The BRICS nations generated 25% of the total global e-waste generated in 2014 which increased to nearly 33% in 2019 (Ghosh et al. 2016; Forti et al. 2020).

1.2 Composition of E-waste

E-waste contains a wide range of materials including metals, polymers, cables and wires, PCBs, glass, hazardous materials, ceramics, concrete, woods, rubbers, etc. as represented in Figure 1.1 (Jia et al. 2022; Widmer et al., 2005).

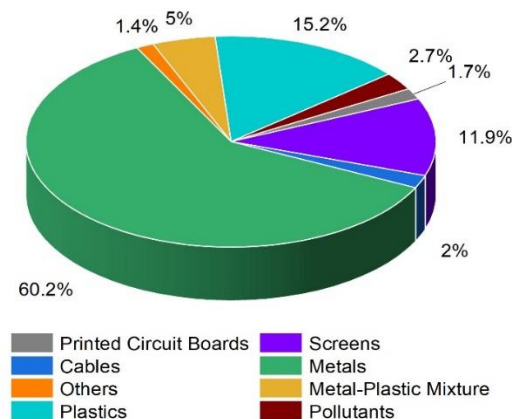


Figure 1.1: Composition of E-waste

1.3 Printed Circuit Boards

Printed circuit boards (PCBs) are key parts of e-wastes. Two most common PCBs, i.e., Fire Retardant Type-2 (FR-2) PCBs are widely used in small electronics, toys, old CRT television etc whereas Fire Retardant Type-4 (FR-4) PCBs are used in electronics where mechanical rigidity is required such as laptop, computers, LCD televisions etc (Argumedo-Delira et al. 2020). The main constituents of PCBs are represented in Table 1.1.

Table 1.1 Composition of PCB

Material	Percentage
Non-Metal	>70%
Copper	~ 16%
Solder	~ 4%
Iron and other metals	~ 10%

1.3.1 FR-2 type PCB

FR-2 PCBs are phenolic paper laminated single-sided printed circuit boards. FR-2 PCBs are often used in low grade electronics where mechanical rigidity is not required, such as small electronics, toys, old CRT television etc. As represented in Figure 1.2 (b), FR-2 PCBs contain nearly 38% carbon; 51.5% metal and metal oxides; 2.2% SiO₂ and rest are others.

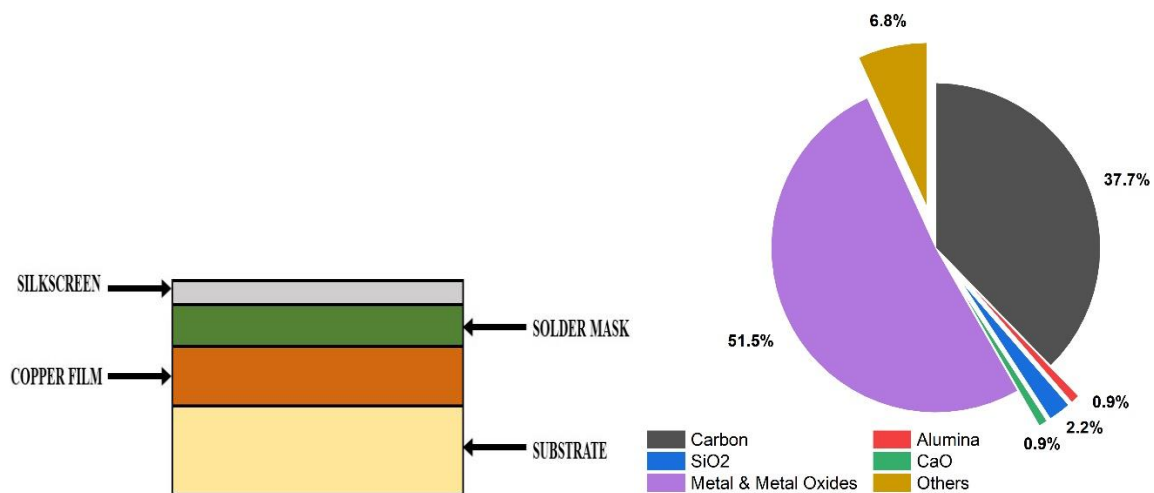


Figure 1.2 (a): Structure of FR-2 PCB and (b) Composition of FR-2 PCB

1.3.2 FR-4 type PCB

FR-4 laminates are the most common printed circuit boards. Fire Retardant Type-4 (FR-4) PCBs are used in electronics where mechanical rigidity is required such as laptop, computers,

LCD televisions etc (Argumedo-Delira et al. 2020). FR-4 PCBs contain nearly 12% carbon; 54% metal and metal oxides; 20.1% SiO₂ and rest are alumina, calcium and others.

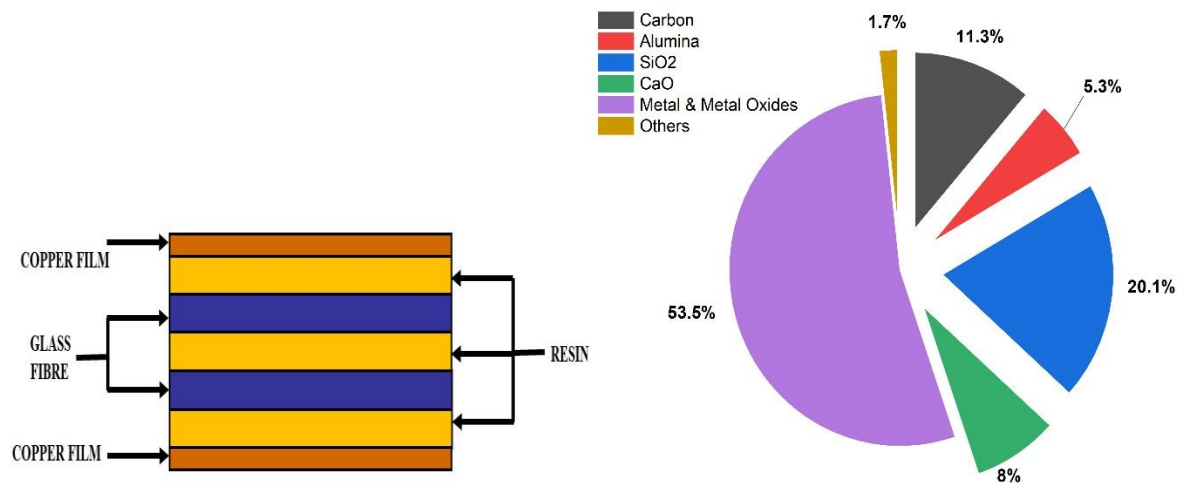


Figure 1.3 (a): Structure of FR-4 PCB and (b) Composition of FR-4 PCB

1.4 Existing Technologies for PCB treatment

Metal recovery from e-waste is a lucrative business opportunity for the small and medium enterprises (SMEs). Many conventional thermo-chemical and bio-chemical processes have been tested both in pilot and laboratory scale for metal recovery from e-waste. Various researchers have used hydro-metallurgical (Kim et al. 2011), pyro-metallurgical (Hall & Williams 2007) and bio-metallurgical (Ilyas & Lee 2014) methods for this purpose. However, physical processes for metal recovery are quite in practice for easier operation and lower carbon footprint.

1.4.1 Physical Recycling Methods

Physical recycling includes disassembling, dismantling, chopping, shredding, crushing etc. These steps are achieved by using machineries like shredder, pre-granulator, granulator etc shredding. After this, the separations of metal from the non-metals are achieved. Different methods such as magnetic separation, eddy current separation and density separation are used (Kang & Schoenung 2005). It is possible to recover metal fraction containing more than 50% of copper, 24% of tin, and 8% of lead by implementing a combination of electrostatic and magnetic separation which separates the metal part from the non-metal ones (Veit et al. 2005). There are other methods reported in literature such as corona discharge method (Li et al. 2007; Zhang & Forssberg 1998) (suitable for separation of metallic and non-metallic fractions),

density-based separation (Peng et al. 2004), milling (Koyanaka et al. 1997), froth floatation (Vidyadhar and Das 2012; Ogunniyi and Vermaak 2009) etc.

1.4.2 Pyro-metallurgical Methods

The state-of-art facilities available in the smelting and refining facilities are capable of extracting valuable metals from the complex matrix and are quite efficient (Khaliq et al. 2014; Antrekowitsch et al. 2006). A typical pyro-metallurgical treatment process is smelting followed by electro-chemical refining. First e-waste or metals recovered by physical recycling are fed into the furnace. The metals are collected in a molten bath and the oxides are obtained from the slag phase. Umicore, Outotec TSL, Aurubis recycling are to name a few that employs pyro-metallurgical processes for metal recovery from e-waste (Khaliq et al. 2014).

1.4.3 Hydro-metallurgical Methods

Hydro-metallurgical methods implemented for metal recovery from e-waste are the modified version of the traditional hydro-metallurgical methods used for metal extraction from primary ores. Leaching is carried out by means of acid, alkali or other solvents to leach out metals in form of soluble salts. Impurities are removed with the gangue materials and the isolation of metals from the solution is achieved by processes such as adsorption, solvent extraction etc. Final forms of metals are achieved through electro-refining or chemical reduction processes (Khaliq et al. 2014; Shamsuddin 1986). Four types of common leaching processes, namely – cyanide leaching (Kołodziej & Adamski 1984), halide leaching (Quinet et al. 2005), thiourea leaching (Sheng & Etsell 2007) and thiosulfate leaching (Chmielewski et al. 1997) are usually used. Copper and other precious metals such as gold, silver etc can be recovered via hydrometallurgical route and a detailed discussion can be found in the study by Wu and group (Wu et al. 2017). Rare Earth Elements (REE) can also be recovered via this route and consolidated studies have been reported (Sun et al. 2016). Aqua regia was used as leaching agent for recovery of gold from printed circuit board (Sheng & Etsell 2007). Metals such as nickel (Kim et al. 2007), tin (Gibson et al. 2003), copper (Veit et al. 2006), silver (Shibata & Matsumoto 1999), palladium (Quinet et al. 2005) has been reported to be recovered from e-waste. It was found that nitric acid; sulphuric acid and muriatic acid-based solutions are majorly implemented for primary leaching of precious metals from e-waste. Recent focus on tin recycling from e-waste has been found among the researchers (Yang et al. 2017; Mecucci & Scott 2002). A green hydrometallurgical process has been developed for recovery of tin from PCBs via co-processing of waste PCBs and spent tin stripping solution which is generated

during production of PCBs (Yang et al. 2017). Umicore uses hydro-metallurgical processes for metal recovery. Industrial applications of such green processes are essential for sustainability.

1.4.4 Bio-metallurgical Processes

Bio-metallurgical processing of e-waste is an emerging and a very promising area. Bio-metallurgical processes can be classified into two sections – a) Biosorption and b) Bioleaching. Biosorption means adsorption of metals by means of adsorbents prepared from waste biomass or abundant biomass. Metal recovery from e-waste by biosorption has been achieved by using algae (*Chlorella vulgaris*), fungi (*Aspergillus niger*), bacteria (*Penicillium chrysogenum*), hen eggshell membrane, ovalbumin, alfalfa etc (Niu & Volesky 1999; Darnall et al. 1986; Kuyucak & Volesky 1988). The mechanism associated with biosorption is complex and no clear picture is available. There are certain factors that affect the process – a) Type of biological ligands accessible for metal binding, b) Type of the biosorbent (living, non-living), c) Chemical, stereo-chemical and co-ordination characteristics of the targeted metals and d) Characteristics of the metal solution such as pH and the competing ions (Tsezos et al. 2006).

According to Ilyas and Lee (2014), the mobilization of metal cations from often almost insoluble materials by biological oxidation and complexation processes is referred to as bioleaching. There are three major group of bacteria associated with in bioleaching of e-waste are – a) Autotrophic bacteria (e.g. Thiobacilli sp.), b) Heterotrophic bacteria (e.g. Pseudomonas sp., Bacillus sp.) and c) Heterotrophic fungi (e.g. Aspergillus sp., Penicillium sp.) (Schinner & Burgstaller 1989). Typically bioleaching occurs in four steps – a) Acidolysis, b) Complexolysis, c) Redoxolysis and d) Bioaccumulation (Bosshard et al. 1996). Bioleaching has been explored by researchers for recovery of Gold, Aluminium, Copper, Nickel, Zinc and Lead from e-waste (Faramarzi et al. 2004; Brandl et al. 2001; Yang et al. 2009; Wang et al. 2009; Bas et al. 2013). There is no example of any industrialized process in the bio-metallurgical route.

1.5 Non-conventional Thermochemical Processes for PCB Treatment

1.5.1 Pyrolysis

Pyrolysis is a thermo-chemical process which ensures thermal degradation of a targeted material in absence of air. Pyrolysis (573 – 973K) leads to formation of char and volatiles. The condensable part of the volatiles lead to tar or pyro-oil, while the non-condensable part remains gaseous and known as pyro-gas containing CO, CO₂, H₂ and light hydrocarbons. The schematic of pyrolysis is presented in the figure below –

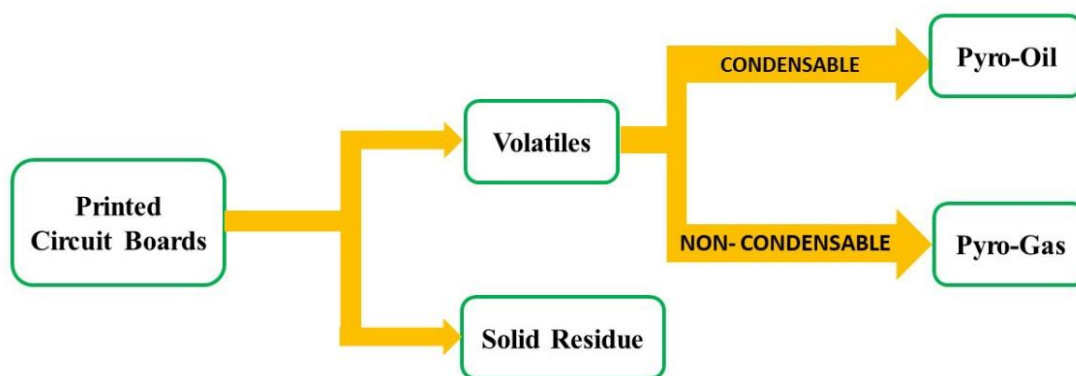


Figure 1.4: Pyrolysis Scheme

A few studies have been carried out on pyrolysis of e-waste (Boro and Tiwari 2023; Joo et al. 2021; Guo et al. 2010). Vacuum pyrolysis (Chen et al. 2017), microwave induced pyrolysis (Sun et al. 2012; Risco et al. 2021), catalytic pyrolysis (Hall et al. 2008) and co-pyrolysis (with biomass) (Liu et al. 2013) are different types of pyrolysis that have been reported. Though pyrolysis of e-waste is mostly limited within the laboratory, Jectec (a company from Japan) has already implemented pyrolysis in their facility. Another process which has gained attention these days is the plasma process that is being implemented for e-waste treatment and metal recovery. Plasma Technology is a high temperature and environment friendly technology. High enthalpy plasma jet (Mitrasinovic et al. 2013), plasma reactor (Rath et al. 2012) and plasma torch (Tippayawong & Khongkrapan 2009) has been explored for processing of e-waste. Pyrolysis not only serves as a pre-treatment process of metal recovery from e-wastes, it can also generate liquid and gaseous fuels and char as byproducts.

1.5.2 Gasification

E-waste gasification is a comparatively unexplored area and only a few research articles are available in this direction. High-impact polystyrene (HIPS) resin containing poly-brominated diphenyl ethers (PBDE; mainly decabromo-diphenyl oxide), which is a brominated flame retardant, has been used as feedstock for a zero-emission recycling process which implements gasification followed by shock cooling. A gaseous by-product, rich in hydrogen can be produced through this process. The list of standard gasification reactions has been provided in Table 1.1 (Pati et al. 2023).

Table 1.1: Gasification Reactions

Reaction	Reaction Name	Heat of reaction (ΔH) (kJ/mol)	Reaction Number
<i>Pyrolysis</i>			
$E - waste_{dry} \rightarrow Gas + Tar + Char$	-	-	(R2)
<i>Heterogeneous reaction</i>			
$C + O_2 \rightarrow CO_2$	Complete combustion	-394	(R3)
$C + 0.5 O_2 \rightarrow CO$	Char partial combustion	-111	(R4)
$C + CO_2 \leftrightarrow 2CO$	Boudouard reaction	+172	(R5)
$C + H_2O \leftrightarrow CO + H_2$	Water-gas	+131	(R6)
$C + 2H_2 \rightarrow CH_4$	Methane formation	-74.8	(R7)
<i>Homogeneous reactions</i>			
$CO + 0.5O_2 \rightarrow CO_2$	CO partial combustion	-284	(R8)
$H_2 + 0.5 O_2 \rightarrow H_2O$	Hydrogen combustion	-242	(R9)
$CO + H_2O \leftrightarrow CO_2 + H_2$	Water-gas shift (WGS)	-41.2	(R10)
$CH_4 + H_2O \leftrightarrow CO + 3H_2$	Methane reforming	+206	(R11)
$CH_4 + 1.5 O_2 \rightarrow CO + 2H_2O$	Methane partial combustion	-520	(R12)

1.6 Rationale Behind Research

Among the pyro-, hydro- and bio-metallurgical processes, although the first two are followed in industrial scale, the last one is still under research stage. None of these processes are capable of either recovering the non-metallic part or generating any useful by-products from that part. Therefore, none of them is a sustainable option for the treatment of PCBs, a heterogeneous matrix of metal, glass fibre and polymer. In case of pyro-metallurgical treatment based on conventional thermal process, namely combustion, all components, other than metals are fully combusted. In case of hydrometallurgy, metal part of PCBs is leached out and the other parts are treated as waste. Moreover, a waste liquid stream is generated simultaneously with the recovery of the metallic part. Following bio-metallurgy, although the recovery of metals is possible either through bio-sorption or bioleaching, the other parts are wasted.

In contrary, through the non-conventional thermochemical processes, namely, pyrolysis and gasification, the achievements over the pyro-, hydro- and bio-metallurgical processes are as follows:

- i) They allow simultaneous recovery of metal mixture and production of liquid oil and char in case pyrolysis and syngas in case of gasification
- ii) The non-metallic fraction i.e., glass fibre can be recovered.
- iii) Ensures the zero-waste concept of sustainability

To explore the possibility of implementation of non-conventional thermo-chemical processes, namely pyrolysis and gasification, for material recovery from printed circuit boards, in details, the current investigation will delve deeper in the following aspects – (i) Evaluation of product distribution and dynamics of non-conventional thermo-chemical conversion of PCB in laboratory scale; (ii) Assessment of suitability of thermo-chemical processes to be used as pre-treatment process for material recovery from e-waste and supply chain performance of e-waste processing plant (iii) Assessment of large scale implementation of suitable thermo-chemical processes using the predictions of Process modelling using standard software (ASPEN PLUS), incorporating kinetic data generated on laboratory scale; (iv) evaluation of sustainability of the thermochemical processes for material recovery from e-waste through life cycle analysis, economic analysis and qualitative social analysis considering the three pillars of sustainability — environment, economics and social.

References

- Antrekowitsch, H., Potesser, M., Spruzina, W., & Prior, F. (2006, March). Metallurgical recycling of electronic scrap. In *EPD Congress* (pp. 899-908).
- Bas, A. D., Deveci, H., & Yazici, E. Y. (2013). Bioleaching of copper from low grade scrap TV circuit boards using mesophilic bacteria. *Hydrometallurgy*, *138*, 65-70.
- Basel Convention (2014). Basel Convention on The Control of Transboundary Movements of Hazardous Wastes and Their Disposal Protocol on Liability and Compensation for Damage Resulting from Transboundary Movements of Hazardous Wastes and Their Disposal Texts and Annexes. UNEP.
- Bosshard, P. P., Bachofen, R., & Brandl, H. (1996). Metal leaching of fly ash from municipal waste incineration by *Aspergillus niger*. *Environmental science & technology*, *30*(10), 3066-3070.
- Brandl, H., Bosshard, R., & Wegmann, M. (2001). Computer-munching microbes: metal leaching from electronic scrap by bacteria and fungi. *Hydrometallurgy*, *59*(2), 319-326.
- Charitopoulou, M. A., Kalogiannis, K. G., Lappas, A. A., & Achilias, D. S. (2021). Novel trends in the thermo-chemical recycling of plastics from WEEE containing brominated flame retardants. *Environmental Science and Pollution Research*, *28*, 59190-59213.
- Chen, Y., Zhang, L., & Xu, Z. (2017). Vacuum pyrolysis characteristics and kinetic analysis of liquid crystal from scrap liquid crystal display panels. *Journal of hazardous materials*, *327*, 55-63.
- Chmielewski, A. G., Urbański, T. S., & Migdał, W. (1997). Separation technologies for metals recovery from industrial wastes. *Hydrometallurgy*, *45*(3), 333-344.
- Darnall, D. W., Greene, B., Henzl, M. T., Hosea, J. M., McPherson, R. A., Sneddon, J., & Alexander, M. D. (1986). Selective recovery of gold and other metal ions from an algal biomass. *Environmental science & technology*, *20*(2), 206-208.
- Faramarzi, M. A., Stagars, M., Pensini, E., Krebs, W., & Brandl, H. (2004). Metal solubilization from metal-containing solid materials by cyanogenic *Chromobacterium violaceum*. *Journal of Biotechnology*, *113*(1), 321-326.
- Gibson, R. W., Goodman, P. D., Holt, L., Dalrymple, I. M., & Fray, D. J. (2003). *U.S. Patent No. 6,641,712*. Washington, DC: U.S. Patent and Trademark Office.
- Guo, Q., Yue, X., Wang, M., & Liu, Y. (2010). Pyrolysis of scrap printed circuit board plastic particles in a fluidized bed. *Powder Technology*, *198*(3), 422-428.
- Hall, W. J., & Williams, P. T. (2007). Analysis of products from the pyrolysis of plastics recovered from the commercial scale recycling of waste electrical and electronic equipment. *Journal of Analytical and Applied Pyrolysis*, *79*(1), 375-386.
- Hall, W. J., Miskolczi, N., Onwudili, J., & Williams, P. T. (2008). Thermal processing of toxic flame-retarded polymers using a waste fluidized catalytic cracker (FCC) catalyst. *Energy & Fuels*, *22*(3), 1691-1697.

- Ilyas, S., & Lee, J. C. (2014). Biometallurgical recovery of metals from waste electrical and electronic equipment: a review. *ChemBioEng Reviews*, 1(4), 148-169.
- Jia, C., Das, P., Kim, I., Yoon, Y. J., Tay, C. Y., & Lee, J. M. (2022). Applications, treatments, and reuse of plastics from electrical and electronic equipment. *Journal of Industrial and Engineering Chemistry*. Volume 110, Pages 84-99, DOI: 10.1016/j.jiec.2022.03.026
- Joo, J., Kwon, E. E., & Lee, J. (2021). Achievements in pyrolysis process in E-waste management sector. *Environmental Pollution*, 287, 117621.
- Kang, H. Y., & Schoenung, J. M. (2005). Electronic waste recycling: A review of US infrastructure and technology options. *Resources, Conservation and Recycling*, 45(4), 368-400.
- Khaliq, A., Rhamdhani, M. A., Brooks, G., & Masood, S. (2014). Metal extraction processes for electronic waste and existing industrial routes: a review and Australian perspective. *Resources*, 3(1), 152-179.
- Kim, E. Y., Lee, J. C., Kim, B. S., Kim, M. S., & Jeong, J. (2007). Leaching behavior of nickel from waste multi-layer ceramic capacitors. *Hydrometallurgy*, 86(1), 89-95.
- Kim, E., Kim, M., Lee, J., Jeong, J., Pandey, B.D., 2011. Selective recovery of gold from waste mobile phone PCBs by hydrometallurgical process. *J. Hazard. Mater.* 198, 206–215.
- Kołodziej, B., & Adamski, Z. (1984). A ferric chloride hydrometallurgical process for recovery of silver from electronic scrap materials. *Hydrometallurgy*, 12(1), 117-127.
- Koyanaka, S., Endoh, S., Ohya, H., & Iwata, H. (1997). Particle shape of copper milled by swing-hammer-type impact mill. *Powder technology*, 90(2), 135-140.
- Kuyucak, N., & Volesky, B. (1988). Biosorbents for recovery of metals from industrial solutions. *Biotechnology letters*, 10(2), 137-142.
- Li, J., Xu, Z., & Zhou, Y. (2007). Application of corona discharge and electrostatic force to separate metals and nonmetals from crushed particles of waste printed circuit boards. *Journal of Electrostatics*, 65(4), 233-238.
- Liu, W. W., Hu, C. W., Yang, Y., Tong, D. M., Zhu, L. F., Zhang, R. N., & Zhao, B. H. (2013). Study on the effect of metal types in (Me)-Al-MCM-41 on the mesoporous structure and catalytic behavior during the vapor-catalyzed co-pyrolysis of pubescens and LDPE. *Applied Catalysis B: Environmental*, 129, 202-213.
- Ma, C., Sánchez-Rodríguez, D., & Kamo, T. (2021). A comprehensive study on the oxidative pyrolysis of epoxy resin from fiber/epoxy composites: product characteristics and kinetics. *Journal of Hazardous Materials*, 125329.
- Mecucci, A., & Scott, K. (2002). Leaching and electrochemical recovery of copper, lead and tin from scrap printed circuit boards. *Journal of Chemical Technology and Biotechnology*, 77(4), 449-457.
- Mitrasinovic, A., Pershin, L., & Mostaghimi, J. (2013). Electronic waste treatment by high enthalpy plasma jet. *International plasma chemistry society (IPCS20) Philadelphia USA*.

- Murthy, V., & Ramakrishna, S. (2022). A review on global e-waste management: urban mining towards a sustainable future and circular economy. *Sustainability*, 14(2), 647.
- Niu, H., & Volesky, B. (1999). Characteristics of gold biosorption from cyanide solution. *Journal of Chemical technology and Biotechnology*, 74(8), 778-784.
- Ogunniyi, I. O., & Vermaak, M. K. G. (2009). Investigation of froth flotation for beneficiation of printed circuit board comminution fines. *Minerals Engineering*, 22(4), 378-385.
- Pati, S., Manna, D., De, S., & Chowdhury, R. (2023). Thermodynamic and phase equilibrium models of syngas generation through gasification. In *Advances in Synthesis Gas: Methods, Technologies and Applications* (pp. 3-42). Elsevier
- Peng, M., Layiding, W., Dong, X., Jiangang, G., & Guanghong, D. (2004, May). A physical process for recycling and reusing waste printed circuit boards. In *Electronics and the Environment, 2004. Conference Record. 2004 IEEE International Symposium on* (pp. 237-242). IEEE.
- Quinet, P., Proost, J., & Van Lierde, A. (2005). Recovery of precious metals from electronic scrap by hydrometallurgical processing routes. *Minerals and Metallurgical Processing*, 22(1), 17-22.
- Rath, S. S., Nayak, P., Mukherjee, P. S., Chaudhury, G. R., & Mishra, B. K. (2012). Treatment of electronic waste to recover metal values using thermal plasma coupled with acid leaching—A response surface modeling approach. *Waste management*, 32(3), 575-583.
- Rathinakumar, V., Sriram, G. A., & Gunarani, G. I. (2022). Integrated Electronic Waste Management: Issues and Strategies. In *Handbook of Solid Waste Management: Sustainability through Circular Economy* (pp. 1479-1497). Singapore: Springer Nature Singapore.
- Risco, A., Sucunza, D., & Gonzalez-Egido, S. (2021). Chemical recovery of waste electrical and electronic equipment by microwave-assisted pyrolysis: A review. *Journal of Analytical and Applied Pyrolysis*, 159, 105323.
- Schinner, F., & Burgstaller, W. (1989). Extraction of zinc from industrial waste by a *Penicillium* sp. *Applied and Environmental Microbiology*, 55(5), 1153-1156.
- Shamsuddin, M. (1986). Metal recovery from scrap and waste. *JOM*, 38(2), 24-31.
- Sheng, P. P., & Etsell, T. H. (2007). Recovery of gold from computer circuit board scraps using aqua regia. *Waste management & research*, 25(4), 380-383.
- Shibata, J., & Matsumoto, S. (1999). Development of environmentally friendly leaching and recovery process of gold and silver from wasted electronic parts. Available from: <http://www.environmentalcenter.com/articles/article320/article320.htm> N.
- Sun, J., Wang, W., Liu, Z., Ma, Q., Zhao, C., & Ma, C. (2012). Kinetic study of the pyrolysis of waste printed circuit boards subject to conventional and microwave heating. *Energies*, 5(9), 3295-3306.

- Sun, Z., Cao, H., Xiao, Y., Sietsma, J., Jin, W., Agterhuis, H., & Yang, Y. (2016). Toward sustainability for recovery of critical metals from electronic waste: the hydrochemistry processes. *ACS Sustainable Chemistry & Engineering*, 5(1), 21-40.
- Tippayawong, N., P. Khongkrapan, P., (2009). Development of a laboratory scale air plasma torch and its application to electronic waste treatment. *Int. J. Environ. Sci. Tech.*, 6 (3), 407-414.
- Tipre, D. R., Khatri, B. R., Thacker, S. C., & Dave, S. R. (2021). The brighter side of e-waste—a rich secondary source of metal. *Environmental Science and Pollution Research*, 1-16.
- Tsezos, M., Remoundaki, E., & Hatzikioseyan, A. (2006, October). Biosorption-principles and applications for metal immobilization from waste-water streams. In *Proceedings of EU-Asia Workshop on Clean Production and Nanotechnologies* (pp. 23-33). Seoul.
- Veit, H. M., Bernardes, A. M., Ferreira, J. Z., Tenório, J. A. S., & de Fraga Malfatti, C. (2006). Recovery of copper from printed circuit boards scraps by mechanical processing and electrometallurgy. *Journal of Hazardous Materials*, 137(3), 1704-1709.
- Veit, H. M., Diehl, T. R., Salami, A. P., Rodrigues, J. D. S., Bernardes, A. M., & Tenório, J. A. S. (2005). Utilization of magnetic and electrostatic separation in the recycling of printed circuit boards scrap. *Waste management*, 25(1), 67-74.
- Vidyadhar, A., & Das, A. (2012). Kinetics and Efficacy of Froth Flotation for the Recovery of Metal Values from Pulverized Printed Circuit Boards.
- Wang, J., Bai, J., Xu, J., & Liang, B. (2009). Bioleaching of metals from printed wire boards by *Acidithiobacillus ferrooxidans* and *Acidithiobacillus thiooxidans* and their mixture. *Journal of Hazardous Materials*, 172(2), 1100-1105.
- Wu, Z., Yuan, W., Li, J., Wang, X., Liu, L., & Wang, J. (2017). A critical review on the recycling of copper and precious metals from waste printed circuit boards using hydrometallurgy. *Frontiers of Environmental Science & Engineering*, 11(5), 8.
- Yang, C., Li, J., Tan, Q., Liu, L., & Dong, Q. (2017). Green Process of Metal Recycling: Co-processing Waste Printed Circuit Boards and Spent Tin Stripping Solution. *ACS Sustainable Chemistry & Engineering*, 5(4), 3524-3534.
- Yang, C., Tan, Q., Liu, L., Dong, Q., & Li, J. (2017). Recycling Tin from Electronic Waste: A Problem That Needs More Attention. *ACS Sustainable Chemistry & Engineering*.
- Yang, T., Xu, Z., Wen, J., & Yang, L. (2009). Factors influencing bioleaching copper from waste printed circuit boards by *Acidithiobacillus ferrooxidans*. *Hydrometallurgy*, 97(1), 29-32.
- Yao, Z., Xiong, J., Yu, S., Su, W., Wu, W., Tang, J., & Wu, D. (2020). Kinetic study on the slow pyrolysis of nonmetal fraction of waste printed circuit boards (NMF-WPCBs). *Waste Management & Research*, 38(8), 903-910.
- Zhang, S., & Forssberg, E. (1998). Optimization of electrodynamic separation for metals recovery from electronic scrap. *Resources, conservation and recycling*, 22(3), 143-162.
- Zhang, S., Yoshikawa, K., Nakagome, H., & Kamo, T. (2012). Steam gasification of epoxy circuit board in the presence of carbonates. *Journal of Material Cycles and Waste Management*, 14(4), 294-300.

CHAPTER-2
LITERATURE REVIEW

CHAPTER – 2

An intense literature survey over last fifteen years have been performed to focus on the research rationale of the study, described in chapter 1. This includes the literature review of product distribution and dynamics of non-conventional thermo-chemical conversion, namely, pyrolysis and gasification of PCBs in laboratory scale; supply chain performance of e-waste plants; Process modelling of large scale non-conventional thermo-chemical process plants of e-wastes using standard software (ASPEN PLUS), sustainability analysis of the non-conventional thermochemical processes for material recovery considering the three pillars of sustainability — environment, economics and social. The topic-wise, research status has been discussed and the research gaps have also been identified.

2.1 Printed Circuit Board (PCB) Pyrolysis

Year	Parameters	Salient Outcomes	References
2023	<ul style="list-style-type: none"> • PCB Type: FR4. • Pyrolysis in a tubular reactor in N₂ atmosphere. • Response Surface Methodology based on Central composite design (CCD). • Inputs - Temp: 673 – 873K, Heating Rate: 10 – 30K/min and N₂ flowrate: 0.1, 0.3, 0.5 lpm. Output – Weight Loss. 	<ul style="list-style-type: none"> • Order of significance: Temperature > Heating rate > N₂ flow rate. Significant quadratic term: Temperature (T²). Interaction terms have little or no influence. • Maximum weight loss of ~ 27% at Temperature ≥ 823K while heating rate >15 K/min and N₂ flow >0.2 lpm. • Optimal point: Temp = 786K, Heating Rate = 22 K/min and N₂ flow = 0.3 lpm • XRD analysis shows increase in crystallinity in pyrolyzed WPCBs. 	Kurniawan et al. 2023

		<ul style="list-style-type: none"> • FTIR spectra demonstrated the vanishing of various organic peaks. 	
2023	<ul style="list-style-type: none"> • PCB Type: FR4. • Pyrolysis in semi-batch lab scale vertical reactor with tubular furnace in N₂ atmosphere at varying temperatures – 723K, 773K, 873K. • Pyrolysis followed by acid leaching for metal recovery in H₂SO₄ and H₂O₂ mixture. 	<ul style="list-style-type: none"> • 873K was found suitable for maximum removal of epoxy resin. • Pyro-oil contains phenolics, aromatics and brominated compounds. • Acid leaching effectively leached out copper lining. 	Boro and Tiwari 2023
2021	<ul style="list-style-type: none"> • PCB Type: FR4 (Cu-coated and Cu free versions). • Tubular furnace pyrolyzer with Ar atmosphere, 873K and 20 min residence time. • TG-FTIR-MS and GC-MS of PCBs and volatiles respectively. • Thermogravimetric experiments at 10, 15, 20, 25, 30 K per min. • Kinetic modelling – Arrhenius method with different models. • Reaction mechanism using Šesták-Berggren method. 	<ul style="list-style-type: none"> • Conversion range with high R² value: 0.1 – 0.6 • Average Activation energy: 175.62 kJ/mol (Cu-free) and 164.45 kJ/mol (With Cu). • Reaction mechanism was found to be random nucleation followed by random growth. • Presence of copper facilitates phase boundary reaction slightly. • Pyro-oil contains phenols, cresols, and brominated compounds. <p>Cu helps in reducing the activation energy by catalytic effect on the cleavage of C-Br bond.</p>	Gao et al. 2021

2020	<ul style="list-style-type: none"> • PCB Type: FR4 (Non-metallic part) • Thermogravimetric experiments at 5, 15, 25K per min. • Kinetic modelling – Friedman, FWO, Starink, Tang, Bosewell method and DAEM using Miura-Maki method. • Reaction model determined using Criado method. 	<ul style="list-style-type: none"> • Conversion range with high R² value: 0.05 – 0.35 • Average Activation energy: 336.71 kJ/mol (Friedman), 329.66 kJ/mol (FWO), 337.16 kJ/mol (Starink), 337.07 kJ/mol (Tang), 341.93 kJ/mol (Bosewell), 337.05 kJ/mol (Miura and Maki). • For DAEM, the major peak of f(E) curve was at 402.98 kJ/mol. • Reaction order: 2. 	Yao et al. 2020
2020	<ul style="list-style-type: none"> • PCB Type: FR4. • Thermogravimetric experiments at 10, 120, 30 K per min. • Kinetic modelling – FWO and Kissinger method • Reaction mechanism using Škvára-Šesták method. 	<ul style="list-style-type: none"> • Conversion range with high R² value: 0.1 – 0.6 • Average Activation energy: 173.6 kJ/mol (FWO) and 172.62 kJ/mol (Kissinger). • Reaction mechanism was found to be random nucleation followed by random growth. • Pyro-oil contains phenols and aromatic compounds as well as brominated compounds. 	Gao et al. 2020
2020	<ul style="list-style-type: none"> • PCB Type: FR4. • Recovery of metallic fraction from e-waste using combined method of pyrolysis and ultrasonication. 	<ul style="list-style-type: none"> • 35 wt% combustible gases and 60 wt% solid products were obtained. • 90 wt% metal recovery in 30 min ultrasonication. 	Jadhao et al. 2020

	<ul style="list-style-type: none"> Vertical fixed bed reactor in N₂ atmosphere at Temp: 673K 		
2019	<ul style="list-style-type: none"> PCB Type: Mixed PCB. Pyrolysis in fixed bed reactor to determine kinetics and enhance pyro-oil yield. Temp: 648K Kinetic modelling – Broido, Coats-Redfern and Horowitz- Metzger method. Thermodynamics triplets calculated. Response Surface Methodology based on Central composite design (CCD). Inputs – Temp (A): 398 – 898K, Particle Size (B): 1 – 3 mm, Retention time (C): 15 – 60 min and Feed Quantity (D): 25 – 125 gm. Output – Pyro-oil Yield. 	<ul style="list-style-type: none"> Average Activation energy: 112.36 kJ/mol (Broido), 61.79 kJ/mol (Coats-Redfern) and 162.61 kJ/mol (Horowitz- Metzger). Entropy: -106.956 kJ/mol (Broido), -111.561 kJ/mol (Coats-Redfern) and -102.87 kJ/mol (Horowitz- Metzger). Enthalpy: -52.75 kJ/mol x 10² (Broido), -53.25 kJ/mol x 10² (Coats-Redfern) and -52.24 kJ/mol x 10² (Horowitz- Metzger). Gibbs Free Energy: 25.241 kJ/mol x 10³ (Broido), 27.902 kJ/mol x 10³ (Coats-Redfern) and 24.08 kJ/mol x 10³ (Horowitz- Metzger). Quadratic terms and cross term AC suppress oil yield whereas linear cross terms favour the oil yield. Optimal point: Temp = 648K, Particle Size = 3 mm, retention time = 45min and Feed Quantity = 75gm 	Jayapradha et al. 2019

2018	<ul style="list-style-type: none"> • PCB Type: FR4. • Comparative analysis about degradation mechanisms of PCBs in slow & fast pyrolysis. • Separate setup for slow and fast pyrolysis. • Temp: 573 -973K • The analysis was made based on continuous off-gas analysis by FTIR, kinetic analysis on slow pyrolysis and measurement of total carbon (TC), TOC & elemental carbon (EC). • DTA & TGA curves are obtained. 	<ul style="list-style-type: none"> • Degradation of organics occurs in three different stages. • During Pyrolysis the long-chain-hydrocarbons are cracked to form tar and other gaseous compounds 	Diaz et al. 2018
2018	<ul style="list-style-type: none"> • Pyrolysis of flexible PCB wastes. • Carbonization of polyimide by dual pyrolysis process. 	<ul style="list-style-type: none"> • The organic matter was recovered as pyro-oil at low temp. and valuable metals, polyimide-derived carbon was recovered through secondary high temp. pyrolysis. • The major component of organics extracted from FPCB waste comprised of epoxy resins were identified as pyro-oil containing bisphenol-A. • The valuable metals (Cu, Ni, Ag, Sn, Au, Pd) in waste 	Won Kim et al. 2018

		FPCB were recovered and quantitatively analyzed via ICP-OES.	
2017	<ul style="list-style-type: none"> • PCB Type: FR4. • Thermochemical treatment of Non-Metallic Fraction (NMF) from waste printed circuit boards. • Both pyrolysis and combustion of NMF-WPCB was done, pretreated by alkalis, acids, and alkali-salts. 	<ul style="list-style-type: none"> • Si (28.3%) and Br (26.4%) were the predominant non-metallic constituents. • Cu (2.5%), Ca (28.7%) and Al (6.9%) were the main metal constituents. • Metals such as Cu was significantly reduced by 92.4% with the acid (e.g., HCl) pre-treatment. 	Shen et al. 2017
2017	<ul style="list-style-type: none"> • PCB Type: FR4. • Experimental investigation of the influence of reaction of reaction atmosphere on the pyrolysis of printed circuit boards. • The decomposition of two diff. PCB fractions in inert and steam atmospheres has been investigated by means of TGA and lab-scale fixed bed reactor experiments. 	<ul style="list-style-type: none"> • The decomposition of the tested materials in steam atmosphere starts at lower temp. and proceeds slower compared to N₂ atmosphere. • Presence of steam influence the pyrolysis gas composition and promotes additional vaporization of antimony as verified by powder XRD and SEM. • Liquid fraction has been analysed using GC-MS. 	Evangelopoulos et al. 2017
2017	<ul style="list-style-type: none"> • PCB Type: FR4. • Thermal degradation of waste PCBs is investigated using TGA 	<ul style="list-style-type: none"> • PCB considered as two pseudo-polymers. • Pseudo-polymer 1 degrades below 600 K and follows first order kinetics. 	Alenezi & Al-Fadhli 2017

	<p>in the temp. range of 350-1200K.</p> <ul style="list-style-type: none"> Pyrolysis was carried out on PCB samples at six diff. heating rates of 5,10,20,30,40 and 50 K/min. Kinetic modelling – Friedman, Kissinger, FWO and Coats-Redfern method 	<ul style="list-style-type: none"> Pseudo-polymer 2 degrades above 600 K and follows 5th. order kinetics. The apparent activation energy for the upper range is $E_{a1}= 130-97\text{kJ/mol}$ is always higher than the lower range i.e., $E_{a2}=97-75\text{kJ/mol}$. 	
2015	<ul style="list-style-type: none"> PCB Type: FR-2 Thermogravimetric experiments at 10, 15, 30 K per min. Kinetic modelling using FWO method. Py-GC/MS and EGA-GC/MS were done. 	<ul style="list-style-type: none"> Four zones of thermal degradation identified. Average Activation energies in four steps of thermal degradation are 108.3, 213.7, 397.45 and 501 kJ/mol respectively. Pyro-oil contains Triphenyl Phosphate, Tribromobisphenol A, cresols, toluene as well as brominated compounds. 	Kim et al. 2015
2014	<ul style="list-style-type: none"> PCB Type: FR-4 Horizontal cylinder fixed-bed pyrolyzer at 773K temp, N₂ atmosphere and 1 hour retention time. Thermogravimetric experiments at 10, 15, 30 K per min. 	<ul style="list-style-type: none"> Pyrolysis Yield: 71.60 wt% residue, 18.23 wt% Oil and 10.71 wt% pyro-gas. Pyro-gas contains CO, CO₂, Propylene and Bromomethane. Pyro-oil contains phenols, cresols, acetone and brominated compounds. 	Guo et al. 2014

	<ul style="list-style-type: none"> • GC-MS and FTIR were done. 	<ul style="list-style-type: none"> • The endothermic heat of FR4 WPCB pyrolysis is 19.69 MJ/kg. 	
2012	<ul style="list-style-type: none"> • PCB Type: FR-4 • Pyrolysis of PCB using TGA followed by leaching. • Kinetic study – Criado Method. • Temp: 473K-873K • Atm: Air & nitrogen separately. 	<ul style="list-style-type: none"> • Activation Energy in nitrogen atmosphere is $E_A=110.7$ kJ/mol whereas activation energy in air is $E_A=90.2$ kJ/mol. • Copper recoveries from untreated, pyrolyzed and air burned PCB were 30.4%, 92.5% and 96.2% respectively 	Mankhand et al. 2012
2008	<ul style="list-style-type: none"> • PCB Type: FR-2 • Thermogravimetric experiments at 0.5, 1, 2, 4 K per min. • TGA-MS used for kinetics and degradation behaviour. • Large samples pyrolyzed in quartz glass reactor. • GC-MS and GC-ECD were done for qualitative and quantitative analysis of pyro-oil. IC was done for Br and Cl determination. 	<ul style="list-style-type: none"> • Maximum weight loss in TGA around 65% around 573K. • Activation energies in three steps of thermal degradation are 151, 176 and 205 kJ/mol respectively. • Pyro-oil contains phenols and aromatic compounds as well as brominated compounds. 	Grause et al. 2008
2007	<ul style="list-style-type: none"> • PCB Type:FR-2 +FR-4. 	<ul style="list-style-type: none"> • FR-4 PCB: 68.9 wt% residue, 22.7 wt% oil, and 4.7 wt% gas. 	Hall and Willams 2007

<ul style="list-style-type: none"> • Fixed bed vertical reactor with N₂ atmosphere. • Residence time: 135 min. • GC-MS, GC-ECD, and GC-FID were used for product analysis. 	<ul style="list-style-type: none"> • FR-4 PCB: 60.0% residue, 28.5% oil, and 6.5% gas. • Pyro gas consist of CO, CO₂, C₁ – C₄ gases and inorganic bromine. • Pyro-oil contained phenols, phenol derivatives and TBBPA. • Ash contained copper, calcium, iron, nickel, zinc, aluminium and silver. 	
------------------------------------------------------------------------------------------------------------------------------------------------------------------------------------------------------------------------	------------------------------------------------------------------------------------------------------------------------------------------------------------------------------------------------------------------------------------------------------------------------------------------------------------------------------------------------------------------------------	--

2.2 Printed Circuit Board Gasification

Year	Parameters	Salient Outcomes	References
2022	<ul style="list-style-type: none"> • PCB Type: FR-4 • Steam gasification assisted pyrolysis was carried out. • Tubular reactor used with 3 hours of residence time. • Temperature range: 673 – 1273K • Steam flow rate: 1-4 ml/min. • Heating rate: 10 – 30K per min with 5K interval. 	<ul style="list-style-type: none"> • Utilization of steam helped in achieving higher concentration of metals in the residue. • Syn-gas is rich in hydrogen (55%). • Steam also reduced the amount of bromine in the solid products. 	Li et al. 2022
2018	<ul style="list-style-type: none"> • PCB Type: FR-4. • Gasification, pyrolysis and incineration 	<ul style="list-style-type: none"> • Gasification was found to be most effective as nearly 19% weight loss was observed. 	Gurgul et al. 2018

	<p>comparison of Laptop Screen Inverter PCB.</p> <ul style="list-style-type: none"> • Quartz tube reactor with multiple zones for steam gasification, air aided incineration and argon aided pyrolysis. • Syn-gas is enriched in hydrogen and may be used for chemical synthesis or energy recovery. 	<ul style="list-style-type: none"> • Gasification eliminates organic fractions without high oxygen potential of the gaseous phase. • Volatile contaminants (including halides) are collected in the aqueous condensate. 	
2015	<ul style="list-style-type: none"> • PCB Type: FR-2 • Steam gasification of phenolic printed circuit boards (PCB) in presence of molten ternary (Lithium Carbonate, Sodium Carbonate and Potassium Carbonate) eutectic carbonates for hydrogen generation has been studied. • Nickel powders were added with existing nickel in PCB. • Temp: 823-948 K. 	<ul style="list-style-type: none"> • The existing nickel in the PCB and the nickel powder plays a catalytic role that can improve hydrogen generation from the plastics. • Metals are oxidized at high temp. decreasing the catalytic power. • E-waste should be mixed with metal powder recovered from e-waste and gasified with steam at low temperature. 	Salbidegoitia et al. 2015
2013	<ul style="list-style-type: none"> • A novel two steps process - pyrolysis followed by steam gasification using Ni/Al₂O₃ catalyst for 	<ul style="list-style-type: none"> • Filamentous and layered carbon formation was observed. • The introduction of steam and catalyst produced best result. 	Acomb et al. 2013

	<p>thermal processing of plastics from WEEE for hydrogen production has been reported.</p> <ul style="list-style-type: none"> Plastics recovered from WEEE, fresh high-impact polystyrene (HIPS) and acrylonitrile-butadiene-styrene (ABS) were used as feedstock. No steam, catalyst replaced by sand condition and variation of nickel loading in catalyst. 	<ul style="list-style-type: none"> Higher nickel loading resulted in higher yield of hydrogen. 	
2013	<ul style="list-style-type: none"> PCB Type: FR-2 Steam gasification of phenolic PCB was carried out in presence of molten LNK carbonates (Lithium Carbonate, Sodium Carbonate and Potassium Carbonate) for metal recovery and hydrogen generation. Temp: 773K and Quartz Reactor used. 	<ul style="list-style-type: none"> Homogeneous model and the shrinking core model were used to describe the kinetics ($p \leq 0.15\text{mm}$). Initial rapid pyrolysis, homogenous model gasification and the shrinking core model gasification was observed ($p > 1\text{mm}$). 	Zhang et al. 2013
2012	<ul style="list-style-type: none"> PCB Type: FR-4 Recovery of metals and hydrogen generation from WEEE by steam 	<ul style="list-style-type: none"> Kinetic study revealed that the reaction follows pseudo first order kinetics. The order was 	Zhang et al. 2012

	gasification of epoxy PCBs in presence of molten eutectic carbonate (Lithium Carbonate, Sodium Carbonate and Potassium Carbonate) mixture.	0.91th power of the partial pressure. • The activation energy was 122 kJ/mol.	
2009	<ul style="list-style-type: none"> Gasification of waste keyboards, mouse, waste printers and telephones conducted. Temp. range: 973 – 1123K. 	<ul style="list-style-type: none"> Gasification was found to be helpful for convenient recovery of metals such as Fe, Cu, Pb, Zn, Cu, Cr, Cd and Ni etc. 	Wang et al. 2009

2.3 Process Modelling of Thermochemical Treatment of PCBs

Year	Parameters	Salient Findings	References
2023	<ul style="list-style-type: none"> Steady state ASPEN Plus simulation model for pyrolysis and steam gasification of Organic Fraction of FR-4 type Printed Circuit Boards. Global Flow: MIXCINC; specific property methods for enthalpy: HCOALGEN and Density method: DCOALIGT. Property method: Peng–Robinson equation of state with 	<ul style="list-style-type: none"> Bisphenol A (C₁₅H₁₆O₂) was considered the main decomposition product of the organic fraction of PCBs. Pyrolysis and Gasification simulated using RYIELD followed by RGIBBS block. Temp: 873K. Model validated using experimental data reported by Evangelopoulos et al. (2017). Simulation data overpredicts the char and gas where as underpredicts pyro-oil compared to experimental data. 	Romano et al. 2023

	<p>Boston–Mathias (PR-BM) modifications</p> <ul style="list-style-type: none"> • PCB simulated as Nonconventional Component using Ultimate and Proximate analysis data. 	<ul style="list-style-type: none"> • Sensitivity analysis reveals that a mass ratio of 0.4 between steam and feed at 873 K gives best results for conversion. 	
2022	<ul style="list-style-type: none"> • Chemical looping reforming (CLR) plant has been simulated utilizing pyrolysis of PCB to generate high quality syn-gas and metallic components for the CLR process. Metal oxides act as oxygen carrier. • Global Flow: MIXCINC; specific property methods for enthalpy: HCOALGEN and Density method: DCOALIGT. • Property method: Peng–Robinson equation of state with Boston–Mathias (PR-BM) modifications • PCB simulated as Nonconventional Component using Ultimate and Proximate analysis data. 	<ul style="list-style-type: none"> • Pyrolysis and Gasification simulated using RYIELD followed by RGIBBS block. Temp: 1173K. • Energy and economic analysis carried out. • Calorific value of the PCB syngas 12 - 14 MJ/m³. • Thermal efficiency: 32.72% for PCB based syngas, further raised by 13.02% and more 17.17% with PCB-coal blend and PCB-coal-PP blend respectively. • Syngas production cost from PCB gasifier: 0.0026\$/kWh to 0.0034 \$/kWh. • Cost of metals extracted from PCB treatment: 15.94 \$/ton to 24.38 \$/ton. 	Rai et al. 2022

	<ul style="list-style-type: none"> • Three reactor configurations explored – fuel reactor (FR), air reactor (AR), and steam reactor (SR) • Comparison made with PCB, Coal and PolyProlylene Plastics ad source of energy. 		
2021	<ul style="list-style-type: none"> • Mixed oxygen carrier particles derived from PCB are proposed for simulation of Chemical looping combustion (CLC) process. • Aspen Plus used for simulations of integrated CLC system with a combined cycle power plant (Net capacity: 150 MW). • High ash coal (HAC) (33%) and low ash coal (LAC) (2.1%) along with rice straw (RS) are used in a co-combustion mode for the CLC operation. 	<ul style="list-style-type: none"> • Pyrolysis and Gasification simulated using RYIELD followed by RGIBBS block. Temp: 1173K. • Net thermal efficiency of 42.4% for HAC, 40.6% for LAC and 37.9% for RS based fuels. • Economic analysis reveals the Levelized cost of electricity (LCOE) of PCB based combined cycle power system are 88.3 \$/MWh, 85.9 \$/MWh and 94.3 \$/MWh for HAC, LAC and RS respectively. 	Bhui and Babu 2021

2.4 Supply Chain Performance of E-waste Processing Plant

Year	Parameters	Salient Outcomes	References
2023	<ul style="list-style-type: none"> • Mathematical model of e-waste reverse 	<ul style="list-style-type: none"> • Electronic items might be developed to benefit from this 	Singh et al. 2023

	<p>supply chain considering multi-electronic products, considering multi-manufacturers and multi-retailers.</p> <ul style="list-style-type: none"> • Cost based model solved using fixed point iteration with numerical example. • Sensitivity analysis was carried out. 	<p>reverse supply chain, in which the accumulation of e-waste is reduced to address current environmental concerns.</p> <ul style="list-style-type: none"> • The plant can optimise the quantity and ordering time, hence reducing waste output. • Model can be extended to three pillars of sustainability i.e., environment, economic and social aspects. 	
2022	<ul style="list-style-type: none"> • E-waste supply chain performance using the SCOR method. • BWM method used for weightage of criteria • Sustainability parameter: Environment and Social. 	<ul style="list-style-type: none"> • Costs, quality and GreenScor attributes and measures have the highest scores. • GreenScor includes attributes such as Energy, Emissions, Water, • Recycling utilization rate, • Environmentally friendly process, • Landfill reduction, Life cycle assessment etc. 	Jain et al. 2022
2021	<ul style="list-style-type: none"> • Evaluates the sustainable e-waste collection • chain in urban and rural regions of India for hazard mitigation. • Sustainability aspects: Environment, Economic, Social, 	<ul style="list-style-type: none"> • Take-back and retail store collection system are suitable for urban area. • Retail store and curbside collection are better for rural area. • For urban area most important attribute is Economical sustainability and potential risk of business 	Singh et al. 2021

	<p>Business Risk</p> <ul style="list-style-type: none"> Fuzzy-Analytical Hierarchy Process (FAHP) and Fuzzy-VlseKriterijumska Optimizacija I Kompromisno Resenje (FVIKOR) has been used. 	<p>is the least important attribute.</p> <ul style="list-style-type: none"> For rural area most important attribute is social awareness and potential risk of business is the least important attribute. 	
2020	<ul style="list-style-type: none"> Game theory has been used to model an e-waste supply chain. Three players: the government, a recycling center, and a collection center. Sustainability aspect: Economic Different scenarios are analyzed for material recovery, sustainability and supply chain profits 	<ul style="list-style-type: none"> E-waste supply chain profit maximum when recycling center and collection center work in a centralized manner. Dealing with customers with higher sensitivity towards material recovery sustainability are more profitable for business. When fixed released emissions increases, improving the material recovery process is not beneficial, rather sorting of material is more helpful. 	Ghalehkhondabi and Ardjmand 2020
2017	<ul style="list-style-type: none"> Explores the barriers restricting the proper implementation of e-waste reverse supply chain in India. Based on literature review and interviews. 	<ul style="list-style-type: none"> Consumer awareness, developing infrastructure, collection efficiency, legal issues and informal sector were found to be the major barriers. Provisions for capacity enhancement and incentive 	Chaudhary et al. 2017

	<ul style="list-style-type: none"> • Uses interpretive structural modelling methodology. • Three pillars of sustainability have been considered. 	<ul style="list-style-type: none"> • Mechanisms were proposed. • Inefficiency of the Producer Responsibility Organizations (PROs) are also highlighted. 	
2016	<ul style="list-style-type: none"> • E-waste supply chain network (SCN) in BRICS nations has been mapped. • Issues and challenges in the e-waste SCN in BRICS nations are highlighted. 	<ul style="list-style-type: none"> • Social awareness, informal sector, policy loopholes, trans-boundary movement were found to be common issues and challenges for the BRICS nations. • Generic high-level e-waste SCN for BRICS nations proposed for sustainable e-waste recycling. 	Ghosh et al. 2016
2015	<ul style="list-style-type: none"> • Discusses the pre-requisites for design of sustainable e-waste supply chain. • Based on interviews and literature. • Triple-bottom-line of sustainability considered. 	<ul style="list-style-type: none"> • Setting design goals with respect to Sustainability; • Setting design goals to comply the regulations; • Setting relevant Key Performance Indicators (KPIs) to be monitored and assessed; • Using of research methods and research tools for plant design etc were established as theoretical pre-requisites. 	Barletta et al. 2015
2014	<ul style="list-style-type: none"> • Quality Function Deployment (QFD) tool used to analyze issues and challenges 	<ul style="list-style-type: none"> • The study identified formal e-waste collection, technology availability and storage of e-waste as most challenging 	Ghosh et al. 2014

	<p>in e-waste supply chain in India.</p> <ul style="list-style-type: none"> • Three pillars of sustainability is considered. 	<p>issues for e-waste supply chain stakeholders.</p>	
--	---------------------------------------------------------------------------------------------------------------------------------------------	------------------------------------------------------	--

2.5 Life Cycle Assessment of E-waste

Year	Parameters	Salient Outcomes	References
2022	<ul style="list-style-type: none"> • E-waste Type/Component: Generic e-waste • Method: Impact 2002+ & ReCiPe 2016 v1.1 • Software: SimaPro • Database: Ecoinvent v3.5 • 	<ul style="list-style-type: none"> • The LCA determined the avoided emissions and damages (human health, ecosystem quality, climate change, and resource use) per kg material recovered, per product, and for an entire recycling community, with a benefit of 2.7 to 25.4 kg CO2 eq avoided per product piece. • This study has shown that informal e-waste recycling can provide net human health, ecosystem quality, climate change, and resources benefits in the form of avoided emissions for some products. 	Arain et al., 2022
2022	<ul style="list-style-type: none"> • E-waste Type/Component: Laptops and Desktop Computers • Method: ReCiPe 2016 midpoint 	<ul style="list-style-type: none"> • Five impact categories are Climate change potential, Stratospheric ozone depletion, Terrestrial ecotoxicity, Human non-carcinogenic toxicity, Mineral resource depletion. 	Rasheed et al., 2022

	<ul style="list-style-type: none"> • Software: SimaPro V 8.5 • Analyzes the environmental sustainability and economic benefits of e-waste management in the developing economies like Pakistan. 		
2021	<ul style="list-style-type: none"> • E-waste Type/Component: Generic e-waste • Method: Eco-Indicator 99 • Software: SimaPro & GaBi • Database: Ecoinvent v3 • Environmental performance of Landfill disposal, incineration with energy recovery, materials recovery without energy recovery and materials recovery with energy recovery for e-waste management in Malaysia. 	<ul style="list-style-type: none"> • Waste reduction rate (WRR) and environmental cost-benefit ratio (eCBR) used as indicator. • direct incineration with energy recovery is best alternative for Malaysian e-waste management. • Landfill (0) has the worst eCBR while Incineration had the highest (4.6). 	Ismail and Hanafiah, 2021

	<ul style="list-style-type: none"> Life cycle assessment (LCA) and material flow analysis (MFA) used. 		
2021	<ul style="list-style-type: none"> E-waste Type/Component: WEEE Method: EF (adapted) v1.00 Software: SimaPro 9 Database: Ecoinvent Considers transportation, dismantling and recycling operations. Material consumption and energy resources causing environmental impacts were considered. 	<ul style="list-style-type: none"> The results indicate that the benefits of reverse logistics outweigh its impacts, remarkably due to the saving of metals and mineral resources resulting mainly from recycling printed circuit boards, and to the reduction of the potential environmental impact in human toxicity categories. 	Rocha, pentead. 2021
2021	<ul style="list-style-type: none"> E-waste Type/Component: LCD Display of Cell phone Method: LCA Software: SimaPro Database: Ecoinvent 	<ul style="list-style-type: none"> The results highlight the materials that cause the most damage to the soil in the long term and point out Cadmium (63%) and Zinc (24%) as the toxic elements with the highest representation in the incineration of the LCD screen of cell phones. The results of this work confirm the toxicity and negative impacts related to 	Nunes et al., 2021

		the handling and processing of WEEE at the end of its useful life cycle.	
2017	<ul style="list-style-type: none"> • E-waste Type/Component: Waste Electrical and Electronic Equipment • Method: CML-IA • Software: SimaPro • Database: Ecoinvent v.3.1 • Treatment of small WEEE via Hydrometallurgical process through LCA methodology. • Cradle-to-gate approach taken. • Impacts comparison between copper and gold recovery for a) mass allocation and b) economic allocation. 	<ul style="list-style-type: none"> • All impact category biotic depletion, Abiotic depletion (fossil fuels), Global warming, Ozone layer depletion, Human toxicity, Fresh water aquatic ecotoxicity, Marine aquatic ecotoxicity, Terrestrial ecotoxicity, Photochemical oxidation, Acidification, Eutrophication. • The obtained outcomes allow to point out the critical steps of the process and consequently improve the eco-design phase of the plant. 	Iannicelli - Zubiani et al., 2017
2017	<ul style="list-style-type: none"> • E-waste Type/Component: Waste Printed Circuit Board. • Method: Eco-Indicator 99 • Software: GaBi environmental • Database: ecoinvent 	<ul style="list-style-type: none"> • Impact of the Scenario 1 for climate change, freshwater eutrophication and fossil depletion are significantly higher scenario 2. • Sensitivity analysis reveals, in scenario 1, a reduction of 10% in electricity has more environmental benefit in 	Ghodrat et al. 2017

	<ul style="list-style-type: none"> Two scenarios compared – a) Precious metal recovery from PCB through Secondary Copper smelting (pyrometallurgy) and b) Secondary Copper Recycling via pyrometallurgy. Cradle-to-gate approach taken. 	<p>majorly affected categories, except human toxicity, terrestrial eco-toxicity and photochemical oxidant formation.</p>	
2017	<ul style="list-style-type: none"> E-waste Type/Component: Obsolete Refrigerator and Desktop PC Power Supply Unit (PSU) Method: Eco-Indicator 99 Software: SimaPro Two scenarios explored – i) Unit Reuse Scenario (URS) and ii) Materials Recovery Scenario (MRS). 	<ul style="list-style-type: none"> Two lifespans considered – 2 years and 3 years. In both cases, respirable inorganics, climate change, ozone layer depletion and fossil fuels are the top damage impact categories. In case of 2-year lifespan Materials Recovery Scenario have higher end-point impact than Unit Reuse Scenario. For 3-year lifespan, the case is reversed. 	Lu et al. 2017
2016	<ul style="list-style-type: none"> E-waste Type/Component: Refrigerator Method: CML 2001 Software: GaBi 	<ul style="list-style-type: none"> Environmental benefits of 7 impact categories (AP, EP, ADP elements, FAETP, HTP, POCP and TETP) 	Xiao et al. 2016

	<ul style="list-style-type: none"> • Database: Ecoinvent V2.2 	<ul style="list-style-type: none"> • Upstream production, such as in the HIPS recycling (P3) (22.17%), the steel recycling (P2) (23.94%), and the copper recycling of (P5) (8.10%) phases, which together account for over 50% of the total GWP benefits. • As recycling of materials such as iron, copper etc. can bring environmental benefits, the values of some environmental categories are negative. 	
2015	<ul style="list-style-type: none"> • E-waste • Type/Component: Waste Management of Printed Wiring Boards • Method: Eco-Indicator 99 • Software: SimaPro 7 • Database: GaBi & Ecoinvent 	<ul style="list-style-type: none"> • Global warming potential was the most significant environmental impact category after normalization and weighting, followed by fossil abiotic depletion potential, and marine aquatic eco-toxicity potential. 	Xue et al., 2015
2015	<ul style="list-style-type: none"> • E-waste • Type/Component: Electronic E-Waste • Method: ReCiPe • Software: SimaPro • Database: Ecoinvent • ET-ND scenario 	<ul style="list-style-type: none"> • E-waste recycling with an end-life disposal scenario is environmentally beneficial because of the low environmental burden generated from human toxicity, terrestrial 	Hong et al., 2015

		<p>ecotoxicity, freshwater ecotoxicity, and marine ecotoxicity categories.</p> <ul style="list-style-type: none"> The key factors in reducing the overall environmental impact of e-waste recycling are optimizing energy consumption efficiency, reducing wastewater and solid waste effluent, increasing proper e-waste treatment amount, avoiding e-waste disposal to landfill and incineration sites, and clearly defining the duties of all stakeholders (e.g., manufacturers, retailers, recycling companies, and consumers). 	
2014	<ul style="list-style-type: none"> E-waste Type/Component: washing machines, refrigerator, air conditioners & televisions Method: IPCC (2006) Software: Excel Calculation 	<ul style="list-style-type: none"> This study aims to provide an in-depth investigation of the efficiency of e-waste recycling on GHG mitigation. Recycling of unit weight of washing machines, refrigerators, air conditioners and televisions could contribute to 17.70, 27.34, 45.62 and 3.61 kg CO₂-eq of GHG emissions reduction respectively. 	Menikpura et al. 2014

2014	<ul style="list-style-type: none"> • E-waste • Type/Component: Mobile Phone PCB • Method: IMPACT 2002+ • Comparison of formal mobile phone PCB recycling through the recycling in Malaysia and Australia. 	<ul style="list-style-type: none"> • Aquatic ecotoxicity, non-carcinogens and aquatic acidification are the highly affected categories. • Malaysian facilities have higher environmental impact over Australian facilities. • The extraction of materials for reuse is strongly based on their financial gains in the industry that has high market demand. 	Soo & Doolan 2014
2014	<ul style="list-style-type: none"> • E-waste • Type/Component: Printed Circuit Board • Method: EDIP • Software: LCA 	<ul style="list-style-type: none"> • Material recovery from printed circuit board (PCB) scrap may contribute to reduce the environmental impacts caused by the extraction of high-valued and/or highly toxic materials from nature. • Recovery of copper from PCB scraps. 	Rubin et al., 2014
2014	<ul style="list-style-type: none"> • E-waste • Type/Component: CRT MONITOR • Method: Eco-Indicator 99 • Software: CML 	<ul style="list-style-type: none"> • Glass-to-glass recycling of parts of the end-of-life CRTs, for the manufacturing of new CRT screen. • This analysis confirms the environmental advantage of all the considered scenarios for CRT recycling 	Rocchetti and Beolchini 2014
2014	<ul style="list-style-type: none"> • E-waste • Type/Component: Generic E-Waste 	<ul style="list-style-type: none"> • The key factors that contribute to overall environmental burden are the 	Chen et al., 2014

	<ul style="list-style-type: none"> • Method: Eco-Indicator 99 • Software: SimaPro 7 • Database: Ecoinvent 	<p>direct emissions of nitrogen oxides, particulates, and carbon dioxide (CO₂) into the atmosphere, as well as the use of coal during cement production. The amounts of CO₂, sulfur dioxide (SO₂).</p>	
2012	<ul style="list-style-type: none"> • E-waste Type/Component: CRT Display • Method: Eco-Indicator 99 • Software: SimaPro 7 	<ul style="list-style-type: none"> • The incineration is the main contribution factor in the life cycle assessment of treatment on CRT. So in order to decrease the environmental impact in the process of incineration, reducing the amount of CRT for incineration is necessary. • The result suggests that the CRT display should be separately treated and not be mixed with municipal solid waste which is treated by incineration. 	Niu et al., 2012
2007	<ul style="list-style-type: none"> • E-waste Type/Component: Generic E-Waste • Method: Eco-Indicator 99 • Software: SimaPro 7 • Database: Ecoinvent • Different appliances were analyzed (washing machines, refrigerators, TV sets) 	<ul style="list-style-type: none"> • LCA was applied, highlighting the final phase of product life and calculating the threshold beyond which collection is harmful for each type of equipment. • The categories most affected were Respiratory Inorganics (winter smog), Fossil Fuels, 	Gutierrez et al., 2007

	and personal computers).	Acidification, Eutrophication and Radiation.	
--	--------------------------	----------------------------------------------	--

2.6 Research Gap

The literature review on thermochemical pre-treatment processes for material recovery from e-wastes, namely, pyrolysis and gasification indicate that the existing plethora of studies are focused on kinetic analysis and product distribution of FR-4 type printed circuit boards pyrolysis. Some studies have focused on FR-2 type printed circuit boards pyrolysis, but they have not explicitly mentioned the same as well as focused only on product analysis. Some of the articles have delved deeper in reaction mechanism and removal of bromine. However, no attempt has so far been made to study the detailed kinetics, i.e., both lumped and iso-conversional kinetics, along with product recovery schemes, of FR-2 and FR-4 type PCBs. Additionally, no comparison of kinetic parameters obtained for virgin and waste PCBs are available in the literature. Although it is understandable that the heterogeneity of PCBs has to be faced to reuse the e-wastes in real life, there is scarcity of literature data on pyrolysis of mixed (FR-2 and FR-4) PCBs. Although it is claimed in the literature that gasification of PCBs is an important technology for resource recovery from PCBs, it appears to be overlooked with respect to research focus. From the literature review it is also clear that the important aspects regarding efficient utilization of e-waste, namely, process modelling, environmental impact analysis and the time evolution dynamics of e-waste processing plant encompassing three pillars of sustainability - environment, economic and social, need more research attention.

References

- Acomb, J. C., Nahil, M. A., & Williams, P. T. (2013). Thermal processing of plastics from waste electrical and electronic equipment for hydrogen production. *Journal of Analytical and Applied Pyrolysis*, *103*, 320-327.
- Alenezi, R. A., & Al-Fadhli, F. M. (2018). Thermal degradation kinetics of waste printed circuit boards. *Chemical Engineering Research and Design*, *130*, 87-94
- Arain, A. L., Neitzel, R. L., Nambunmee, K., Hischier, R., Jindaphong, S., Austin-Breneman, J., & Jolliet, O. (2022). Material flow, economic and environmental life cycle performances of informal electronic waste recycling in a Thai community. *Resources, Conservation and Recycling*, *180*, 106129.
- Barba-Gutiérrez, Y., Adenso-Diaz, B., & Hopp, M. (2008). An analysis of some environmental consequences of European electrical and electronic waste regulation. *Resources, Conservation and Recycling*, *52*(3), 481-495.
- Barletta, I., Johansson, B., Reimers, J., Stahre, J., & Berlin, C. (2015). Prerequisites for a high-level framework to design sustainable plants in the e-waste supply chain. *Procedia CIRP*, *29*, 633-638.
- Bhui, B., & Prabu, V. (2021). Techno-economic evaluation of electronic waste based oxygen carriers for co-chemical looping combustion of coal and biomass integrated combined cycle power generating systems. *Energy Conversion and Management*, *236*, 114075.
- Boro, B., & Tiwari, P. (2023). Material Recovery from Waste Printed Circuit Board Using Pyrolysis and Metal Extraction. In *Sustainable Environment: Proceedings of NERC 2022* (pp. 199-210). Singapore: Springer Nature Singapore.
- Chaudhary, K., Mathiyazhagan, K., & Vrat, P. (2017). Analysis of barriers hindering the implementation of reverse supply chain of electronic waste in India. *International Journal of Advanced Operations Management*, *9*(3), 143-168.
- Chen, W., Hong, J., & Xu, C. (2015). Pollutants generated by cement production in China, their impacts, and the potential for environmental improvement. *Journal of Cleaner Production*, *103*, 61-69.
- Diaz, F., Flerus, B., Nagraj, S., Bokelmann, K., Stauber, R., & Friedrich, B. (2018). Comparative analysis about degradation mechanisms of printed circuit boards (PCBs) in slow

and fast pyrolysis: The influence of heating speed. *Journal of Sustainable Metallurgy*, 4, 205-221.

Evangelopoulos, P., Kantarelis, E., & Yang, W. (2017). Experimental investigation of the influence of reaction atmosphere on the pyrolysis of printed circuit boards. *Applied Energy*, 204, 1065-1073.

Gao, R., Liu, B., Zhan, L., Guo, J., Zhang, J., & Xu, Z. (2021). Catalytic effect and mechanism of coexisting copper on conversion of organics during pyrolysis of waste printed circuit boards. *Journal of Hazardous Materials*, 403, 123465.

Gao, R., Zhan, L., Guo, J., & Xu, Z. (2020). Research of the thermal decomposition mechanism and pyrolysis pathways from macromonomer to small molecule of waste printed circuit board. *Journal of hazardous materials*, 383, 121234

Ghalekhondabi, I., & Ardjmand, E. (2020). Sustainable E-waste supply chain management with price/sustainability-sensitive demand and government intervention. *Journal of Material Cycles and Waste Management*, 22, 556-577.

Ghodrat, M., Rhamdhani, M. A., Brooks, G., Rashidi, M., & Samali, B. (2017). A thermodynamic-based life cycle assessment of precious metal recycling out of waste printed circuit board through secondary copper smelting. *Environmental Development*, 24, 36-49.

Ghosh, S. K., Baidya, R., Debnath, B., Biswas, N. T., & De D, L. M. (2014, November). E-waste supply chain issues and challenges in India using QFD as analytical tool. In *Proceedings of international conference on computing, communication and manufacturing, ICCCM* (pp. 22-23).

Ghosh, S. K., Debnath, B., Baidya, R., De, D., Li, J., Ghosh, S. K., ... & Tavares, A. N. (2016). Waste electrical and electronic equipment management and Basel Convention compliance in Brazil, Russia, India, China and South Africa (BRICS) nations. *Waste Management & Research*, 34(8), 693-707.

Grause, G., Furusawa, M., Okuwaki, A., & Yoshioka, T. (2008). Pyrolysis of tetrabromobisphenol-A containing paper laminated printed circuit boards. *Chemosphere*, 71(5), 872-878.

Guo, Q., Yue, X., Wang, M., & Liu, Y. (2010). Pyrolysis of scrap printed circuit board plastic particles in a fluidized bed. *Powder Technology*, 198(3), 422-428

- Guo, Qingjie, Xuehai Yue, Minghua Wang, & Liu, Yongzhuo. (2010). Pyrolysis of scrap printed circuit board plastic particles in a fluidized bed. *Powder Technology*, 198(3), 422–428.
- Guo, X., Qin, F. G., Yang, X., & Jiang, R. (2014). Study on low-temperature pyrolysis of large-size printed circuit boards. *Journal of Analytical and Applied Pyrolysis*, 105, 151-156.
- Gurgul, A., Szczepaniak, W., & Zabłocka-Malicka, M. (2018). Incineration and pyrolysis vs. steam gasification of electronic waste. *Science of the total environment*, 624, 1119-1124.
- Hall, W. J., & Williams, P. T. (2007). Separation and recovery of materials from scrap printed circuit boards. *Resources, Conservation and Recycling*, 51(3), 691-709.
- Hong, J., Shi, W., Wang, Y., Chen, W., & Li, X. (2015). Life cycle assessment of electronic waste treatment. *Waste management*, 38, 357-365.
- Iannicelli-Zubiani, E. M., Giani, M. I., Recanati, F., Dotelli, G., Puricelli, S., & Cristiani, C. (2017). Environmental impacts of a hydrometallurgical process for electronic waste treatment: A life cycle assessment case study. *Journal of Cleaner Production*, 140, 1204-1216.
- Islam, M. T., & Huda, N. (2018). Reverse logistics and closed-loop supply chain of Waste Electrical and Electronic Equipment (WEEE)/E-waste: A comprehensive literature review. *Resources, Conservation and Recycling*, 137, 48-75.
- Ismail, H., & Hanafiah, M. M. (2021). Evaluation of e-waste management systems in Malaysia using life cycle assessment and material flow analysis. *Journal of Cleaner Production*, 308, 127358.
- Jadhao, P. R., Ahmad, E., Pant, K. K., & Nigam, K. D. P. (2020). Environmentally friendly approach for the recovery of metallic fraction from waste printed circuit boards using pyrolysis and ultrasonication. *Waste Management*, 118, 150-160.
- Jain, V., Kumar, S., Mostofi, A., & Momeni, M. A. (2022). Sustainability performance evaluation of the E-waste closed-loop supply chain with the SCOR model. *Waste Management*, 147, 36-47.
- Jayapradha, A., AbbasMohaideen, J., Senthil Kumar, P., Kavitha, V., & Narendrakumar, G. (2019). Management of printed circuit boards by newly designed thermal pyrolytic process: Process optimization by RSM approach. *Environmental Progress & Sustainable Energy*, 38(2), 489-499.

- Kim, J. W., Lee, A. S., Yu, S., & Han, J. W. (2018). En masse pyrolysis of flexible printed circuit board wastes quantitatively yielding environmental resources. *Journal of hazardous materials*, 342, 51-57.
- Kim, Y. M., Han, T. U., Watanabe, C., Teramae, N., Park, Y. K., Kim, S., & Hwang, B. (2015). Analytical pyrolysis of waste paper laminated phenolic-printed circuit board (PLP-PCB). *Journal of Analytical and Applied Pyrolysis*, 115, 87-95.
- Krishna, J. V. J., Prashanth, P. F., & Vinu, R. (2022). Distributed Activation Energy Modeling and Py-GC/MS Studies on Pyrolysis of Different Printed Circuit Boards for Resource Recovery. *ACS omega*, 7(36), 31713-31725.
- Kurniawan, K., Kim, S., & Lee, J. C. (2023). Pyrolysis of Waste Printed Circuit Boards: Optimization Using Response Surface Methodology and Characterization of Solid Product. In *Rare Metal Technology 2023* (pp. 227-238). Cham: Springer Nature Switzerland.
- Li, C., Xia, H., Liu, C., & Zeng, K. (2022). Steam gasification assisted pyrolysis directional debromination of waste printed circuit boards and comprehensive utilization of products. *Journal of Cleaner Production*, 366, 132979.
- Liu, J., Jiang, Q., Wang, H., Li, J., & Zhang, W. (2021). Catalytic effect and mechanism of in-situ metals on pyrolysis of FR4 printed circuit boards: insights from kinetics and products. *Chemosphere*, 280, 130804.
- Lu, B., Song, X., Yang, J., & Yang, D. (2017). Comparison on End-of-Life strategies of WEEE in China based on LCA. *Frontiers of Environmental Science & Engineering*, 11, 1-12.
- Ma, C., Yu, J., Wang, B., Song, Z., Xiang, J., Hu, S., Su, S. & Sun, L. (2016). Chemical recycling of brominated flame retarded plastics from e-waste for clean fuels production: a review. *Renewable and Sustainable Energy Reviews*, 61, 433-450.
- Mankhand, T. R., Singh, K. K., Gupta, S. K., & Das, S. (2012). Pyrolysis of printed circuit boards. *International Journal of Metallurgical Engineering*, 1(6), 102-107.
- Menikpura, S. N., Santo, A., & Hotta, Y. (2014). Assessing the climate co-benefits from Waste Electrical and Electronic Equipment (WEEE) recycling in Japan. *Journal of cleaner production*, 74, 183-190.
- Nunes, I. C., Kohlbeck, E., Beuren, F. H., Fagundes, A. B., & Pereira, D. (2021). Life cycle analysis of electronic products for a product-service system. *Journal of Cleaner Production*, 314, 127926.

- Park, Y. K., Han, T. U., Jeong, J., & Kim, Y. M. (2019). Debrominated high quality oil production by the two-step catalytic pyrolysis of phenolic printed circuit boards (PPCB) using natural clays and HY. *Journal of hazardous materials*, 367, 50-58.
- Rai, C., Bhui, B., & Prabu, V. (2022). Techno-economic analysis of e-waste based chemical looping reformer as hydrogen generator with co-generation of metals, electricity and syngas. *International Journal of Hydrogen Energy*, 47(21), 11177-11189.
- Rasheed, R., Rizwan, A., Javed, H., Sharif, F., Yasar, A., Tabinda, A. B., ... & Su, Y. (2022). Analysis of environmental sustainability of e-waste in developing countries—a case study from Pakistan. *Environmental Science and Pollution Research*, 29(24), 36721-36739.
- Rocha, T. B., & Penteadó, C. S. G. (2021). Life cycle assessment of a small WEEE reverse logistics system: Case study in the Campinas Area, Brazil. *Journal of Cleaner Production*, 314, 128092.
- Romano, P., Melchiorre, E., & Vegliò, F. (2023, January). ASPEN PLUS Predictive Simulation of Printed Circuit Boards Pyrolysis and Steam Gasification for Organic Fraction Valorization. In *Waste* (Vol. 1, No. 1, pp. 281-292). MDPI.
- Salbidegoitia, J. A., Fuentes-Ordóñez, E. G., González-Marcos, M. P., González-Velasco, J. R., Bhaskar, T., & Kamo, T. (2015). Steam gasification of printed circuit board from e-waste: Effect of coexisting nickel to hydrogen production. *Fuel Processing Technology*, 133, 69-74.
- Shen, Y., Chen, X., Ge, X., & Chen, M. (2018). Thermochemical treatment of non-metallic residues from waste printed circuit board: Pyrolysis vs. combustion. *Journal of Cleaner Production*, 176, 1045-1053.
- Singh, S. K., Chauhan, A., & Sarkar, B. (2023). Supply Chain Management of E-Waste for End-of-Life Electronic Products with Reverse Logistics. *Mathematics*, 11(1), 124.
- Soo, V. K., & Doolan, M. (2014). Recycling mobile phone impact on life cycle assessment. *Procedia cirp*, 15, 263-271.
- Wang, W., Sun, J., Ma, C., Dong, Y., Wang, Z., Xu, X., & Song, Z. (2009, October). Study on the gasification and melting characteristics of electronic waste. In *2009 International Conference on Energy and Environment Technology* (Vol. 3, pp. 574-577). IEEE.
- Xiao, R., Zhang, Y., & Yuan, Z. (2016). Environmental impacts of reclamation and recycling processes of refrigerators using life cycle assessment (LCA) methods. *Journal of Cleaner Production*, 131, 52-59.

Yao, Z., Xiong, J., Yu, S., Su, W., Wu, W., Tang, J., & Wu, D. (2020). Kinetic study on the slow pyrolysis of nonmetal fraction of waste printed circuit boards (NMF-WPCBs). *Waste Management & Research*, 38(8), 903-910.

Zhang, S., Yoshikawa, K., Nakagome, H., & Kamo, T. (2012). Steam gasification of epoxy circuit board in the presence of carbonates. *Journal of Material Cycles and Waste Management*, 14(4), 294-300.




Zhang, S., Yoshikawa, K., Nakagome, H., & Kamo, T. (2013). Kinetics of the steam gasification of a phenolic circuit board in the presence of carbonates. *Applied Energy*, 101, 815-821.




CHAPTER-3
AIMS AND OBJECTIVES



CHAPTER – 3

Aims and Objectives





As illustrated in chapter 2, the research gap clearly points out that detailed kinetics i.e., both lumped and iso-conversional kinetics of pyrolysis of FR-2 and FR-4 type WPCBs are rare. While pyrolysis is a well-researched area, gasification has been a less intervened area for e-waste treatment. Given the fact that PCBs are heterogeneous material recovery from mixed WPCBs is another area of concern. Sustainability of thermochemical pre-treatment processes, i.e., pyrolysis and gasification of PCBs also need further intervention. Understanding the fact that the resource recovery from PCBs is a very important and timely area of intervention, the current research study intends to address the research gaps, identified through extensive literature review, with the aims and objectives detailed below:




AIM 1: Selection and Characterization of PCBs from local electronic waste		
Objectives		Work Plan
Collection of FR-2 & FR-4 type Printed Circuit Boards (PCBs)		<ul style="list-style-type: none"> • Collection of FR-2 & FR-4 type Waste PCB from waste dealers in Kolkata, West Bengal. • Procurement of FR-2 & FR-4 type Virgin PCBs from local shops.
Sample preparation for experimental studies		<ul style="list-style-type: none"> • Removal of electronic components from WPCBs using basic tools. • Cutting VPCB and WPCB in small sizes (1 mm x 1 mm approx.) using a cutter. • Grinding of PCBs followed by sieving for characterization purpose.
Primary characterisation of FR-2 virgin and waste PCBs		<ul style="list-style-type: none"> • Proximate analysis of FR-2 & FR-4 virgin and waste PCBs using ground samples following standard protocol. • Ultimate analysis (CHNS) of FR-2 & FR-4 virgin and waste PCBs using ground samples in an elemental analyser. • Morphological characterization of FR-2 & FR-4 virgin and waste ground PCBs through FESEM.


		<ul style="list-style-type: none"> • Metal content analysis of FR-2 & FR-4 virgin and waste ground PCBs through EDX. • Identification of bonds present in FR-2 & FR-4 virgin and waste ground PCBs through FTIR analysis.
AIM 2: Studies on pyrolytic valorisation of FR-2 and FR-4 type Printed Circuit Board with kinetic analysis, product characterization and distribution		
Objectives		Work Plan
Thermogravimetric analysis (TGA) of FR-2 & FR-4 virgin and waste PCBs		<ul style="list-style-type: none"> • Performance of TGA analysis of ground FR-2 & FR-4 virgin and waste PCBs at three heating rates. • Performance of DTG analysis by processing recorded TGA data.
Lumped Kinetics of FR-2 & FR-4 waste PCBs		<ul style="list-style-type: none"> • Performance of batch experiments on FR-2 & FR-4 waste PCBs at different temperatures in a muffle furnace. • Evaluation of the lumped kinetic triplets using the batch experiments data.
Experimental investigation on FR-2 & FR-4 virgin and waste PCBs pyrolysis in custom made pyrolyzer for product recovery		<ul style="list-style-type: none"> • Performance of pyrolysis experiments of FR-2 & FR-4 virgin PCBs in a semi-batch reactor at varying temperatures. • Recovery of pyro-oil via solvent rising and recovery of copper, glass fibre and pyro-char from pyro-residues via mild crushing and sieving. • Performance of pyrolysis experiments of FR-2 & FR-4 waste PCBs in a semi-batch reactor at varying temperatures. • Recovery of pyro-oil via solvent rising and recovery of metal mixture, glass fibre and pyro-char from pyro-residues via mild crushing and sieving.

<p>Characterization of pyrolysis products of FR-2 & FR-4 virgin and waste PCBs</p>		<ul style="list-style-type: none"> • Morphological characterization pyro-char of FR-2 & FR-4 virgin and waste PCBs through FESEM. • Metal content analysis of pyro-char of FR-2 virgin and waste PCBs through EDX. • Identification of bonds present in pyro-char of FR-2 & FR-4 virgin and waste PCBs through FTIR analysis. • CHNS analysis of pyro-oil of FR-2 & FR-4 virgin and waste PCB. • Identification of bonds and types of compound mixture present in pyro-oil of FR-2 & FR-4 virgin and waste PCB through FTIR and ¹H NMR analysis. • Identification of compounds present in pyro-oil of FR-2 & FR-4 virgin and waste PCB through GC-MS analysis. • Identification of phases and crystallinity of pyro-char of FR-2 & FR-4 virgin and waste PCB using XRD analysis.
<p>Kinetic analysis using isoconversional methods and DAEM of FR-2 & FR-4 virgin and waste PCB pyrolysis.</p>		<ul style="list-style-type: none"> • Calculation of kinetic triplets of FR-2 & FR-4 virgin and waste PCB pyrolysis using Friedman, KAS, FWO, Tang, Starink and Bosewell isoconversional methods using the TGA data. • Calculation of thermodynamic triplets of FR-2 & FR-4 virgin and waste PCB pyrolysis using the activation energy obtained from the kinetic method with best results. • Calculation of Distribution of Activation Energy using the Miura and Maki DAEM method for FR-2 & FR-4 virgin and waste PCB pyrolysis using the TGA data.


AIM 3: Studies on pyrolytic valorisation of mixed Waste Printed Circuit Board with product characterization and optimization.





Objectives		Work Plan
Development of experiment matrix using Design of Experiments (DoE) methodology.		<ul style="list-style-type: none"> • Development of experiment matrix using Design of Experiments (DoE) considering mixture of FR-2 and FR-4 WPCB, Nitrogen gas flow rate and reaction time as input parameters, while pyro-oil, glass fibre and metal recovery was considered as output parameters.
Experimental investigation on mixed waste PCBs pyrolysis in custom made pyrolyzer for product recovery		<ul style="list-style-type: none"> • Performance of experiments on pyrolysis of mixed waste PCBs according to design matrix in a semi-batch reactor • Recovery of pyro-oil via solvent rising and recovery of metal mixture, glass fibre and pyro-char from pyro-residues via mild crushing and sieving.
Characterization of mixed waste PCB pyrolysis products		<ul style="list-style-type: none"> • Morphological characterization pyro-char of mixed waste PCBs through FESEM. • Metal content analysis of pyro-char of mixed waste PCBs through EDX. • Identification of bonds present in pyro-char of mixed waste PCBs through FTIR analysis. • CHNS analysis of pyro-oil of mixed waste PCB. • Identification of bonds and types of compound mixture present in pyro-oil of mixed waste PCB through FTIR and ¹H NMR analysis. • Identification of compounds present in pyro-oil of mixed waste PCB through GC-MS analysis. • Identification of phases and crystallinity of pyro-char of mixed PCB using XRD analysis.
Thermogravimetric analysis (TGA) of mixed waste PCBs		<ul style="list-style-type: none"> • TGA analysis of mixed waste PCBs at three heating rates.







		<ul style="list-style-type: none"> • DTG analysis from recorded TGA data.
Optimization of mixed WPCB pyrolysis using Response Surface Methodology (RSM) and Genetic Programming (GP)		<ul style="list-style-type: none"> • Performance of optimization of mixed WPCB pyrolysis using Response Surface Methodology (RSM) focusing on metal, glass fibre and pyro-oil recovery as output parameters using the semi-batch reactor data obtained from pyrolysis of mixed WPCB Design Expert software. • Optimization of mixed WPCB pyrolysis using Genetic Programming (GP) focusing on metal, glass fibre and pyro-oil recovery as output parameters using the semi-batch reactor data obtained from pyrolysis of mixed WPCB GeMS software.
AIM 4: Studies on steam gasification aided pyrolysis of individual Printed Circuit Board (FR2 and FR4)		
Objectives		Work Plan
Experimental investigation on gasification aided pyrolysis using FR-2 WPCB		<ul style="list-style-type: none"> • Performance of experiments on steam gasification aided pyrolysis of FR-2 WPCBs in a semi-batch reactor at varying temperatures. • Recovery of metal mixture and char from solid residues via mild crushing and sieving. • Analysis of composition of product gas from the reactor fed on FR-2 WPCBs using gas chromatograph.
Experimental investigation on gasification aided pyrolysis using FR-4 WPCB.		<ul style="list-style-type: none"> • Performance of experiments on steam gasification aided pyrolysis of FR-2 WPCBs in a semi-batch reactor at varying temperatures. • Recovery of metal mixture and char from solid residues via mild crushing and sieving. • Analysis of composition of product gas from the reactor fed on FR-4 WPCBs using gas chromatograph.





<p>Characterization of Char</p>		<ul style="list-style-type: none"> • Morphological characterization gasification aided pyrolysis-char of FR-2 waste PCBs through FESEM. • Metal content analysis of gasification aided pyrolysis-char of FR-2 waste PCBs through EDX. • Identification of bonds present in gasification aided pyrolysis-char of FR-2 waste PCBs through FTIR analysis. • Morphological characterization gasification aided pyrolysis-char of FR-4 waste PCBs through FESEM. • Metal content analysis of gasification aided pyrolysis-char of FR-4 waste PCBs through EDX. • Identification of bonds present in gasification aided pyrolysis-char of FR-4 waste PCBs through FTIR analysis. • Identification of phases and crystallinity of gasification aided pyrolysis-char of FR-2 & FR-4 waste PCB using XRD analysis.
---------------------------------	-----------------------------------------------------------------------------------	------------------------------------------------------------------------------------------------------------------------------------------------------------------------------------------------------------------------------------------------------------------------------------------------------------------------------------------------------------------------------------------------------------------------------------------------------------------------------------------------------------------------------------------------------------------------------------------------------------------------------------------------------------------------------------------------------------------------------------------------------------------------------------------------------------------------------------------------------------------------------------

AIM 5: Development of sustainable framework for simultaneous fuel generation and material recovery using pyrolysis and steam gasification aided pyrolysis as pre-treatment process

Objectives		Work Plan
<p>Conceptualization of Metal Recovery from E-waste (MREW) will be done using pyrolysis and steam gasification aided pyrolysis as a pre-treatment process.</p>		<ul style="list-style-type: none"> • E-waste plant visits for data collection and information collation. • Coining of the term Material Recovery from E-waste (MREW) • Conceptualization of MREW considering pyrolysis and Steam gasification aided pyrolysis as a pre-treatment process for printed circuit boards.

<p>Development of MREW plant layout with detailed input and output.</p>		<ul style="list-style-type: none"> • Development of three scenario of MREW plant layout i.e., without pyrolysis or steam gasification aided pyrolysis, with pyrolysis and with steam gasification aided pyrolysis as pre-treatment process. • Identification of system boundary of MREW plant layouts with detailed input, output and emissions from the principles of Life Cycle Assessment (LCA).
<p>AIM 6: Process Modelling of MREW focusing on Pyrolysis and Steam gasification aided pyrolysis as pre-treatment processes.</p>		
<p>Objectives</p>		<p>Work Plan</p>
<p>Process modelling of mixed WPCB Pyrolysis using Aspen PLUS</p>		<ul style="list-style-type: none"> • Process modelling of mixed WPCB pyrolysis plant having 200kg/hour capacity with material recovery are done using Aspen PLUS process modelling software and experimental outputs,
<p>Process modelling of mixed WPCB steam gasification aided pyrolysis using Aspen PLUS</p>		<ul style="list-style-type: none"> • Process modelling of mixed WPCB steam gasification aided pyrolysis plant having 200kg/hour capacity with material recovery and energy recovery from syn-gas are done using Aspen PLUS process modelling software and experimental outputs.
<p>AIM 7: Time Evolution Dynamics of Metal Recovery from E-waste (MREW) plant focusing on plant operation and its sustainability</p>		
<p>Objectives</p>		<p>Work Plan</p>
<p>Data collection for model development and validation</p>		<ul style="list-style-type: none"> • Data collection from published literature to identify the constructs of e-waste supply chain performance are done. • Data collection from Indian E-waste Recycler for model validation are done.
<p>Development of cost function for e-waste supply chain network</p>		<ul style="list-style-type: none"> • Variables and parameters of e-waste supply chain network are identified.

		<ul style="list-style-type: none"> • Identified variables and parameters are categorised into three cost components based on the three pillars of sustainability. • Cost function model for e-waste supply chain network is developed
Evaluation of weight factor and interrelation co-efficient		<ul style="list-style-type: none"> • Ranking of the cost components and the individual parameters are done using Analytical Hierarchic Process (AHP). • Further refining of the values is done obtained from the generic AHP followed by Principal Component Analysis (PCA).
Optimization of cost function and conversion into dynamic system		<ul style="list-style-type: none"> • The cost function is optimized (minimized) by evaluating the second order derivative. • The system is converted into a dynamic problem by introducing Euler-Lagrange equation.
Development of constrained problem		<ul style="list-style-type: none"> • Lagrange multipliers are introduced to develop a constrained version of the problem.
Model validation for both unconstrained and constrained scenarios.		<ul style="list-style-type: none"> • Boundary values are identified from e-waste recycler. • Simultaneous solution of unconstrained and constrained system equations is done using data gathered from e-waste recycler via MATLAB.
AIM 8: Sustainability analysis of MREW plant featuring pyrolysis and steam gasification aided pyrolysis as alternative green treatment technologies.		
Objectives		Work Plan
Life Cycle Analysis (LCA) of FR-2 WPCB and FR-4 WPCB pyrolysis process		<ul style="list-style-type: none"> • Goal and scope definition for WPCB pyrolysis for LCA. • Data collation from literature and experimental outcomes. • Standalone LCA of FR-2 WPCB pyrolysis process is done using SimaPro software.

		<ul style="list-style-type: none"> • Standalone LCA of FR-4 WPCB pyrolysis process is done using SimaPro software.
Life Cycle Analysis (LCA) of mixed WPCB steam gasification aided pyrolysis process		<ul style="list-style-type: none"> • Goal and scope definition for mixed WPCB steam gasification aided pyrolysis process for LCA. • Data collation from literature and process modelling outputs. • Standalone LCA of mixed WPCB steam gasification aided pyrolysis process is done using SimaPro software.
Economic analysis of FR-2 WPCB and FR-4 WPCB pyrolysis plant		<ul style="list-style-type: none"> • Economic analysis of FR-2 WPCB pyrolysis plant using is done Aspen Economic Analyzer. • Economic analysis of FR-4 WPCB pyrolysis plant using is done Aspen Economic Analyzer.
Economic analysis of mixed WPCB steam gasification aided pyrolysis plant		<ul style="list-style-type: none"> • Economic analysis of mixed WPCB steam gasification aided pyrolysis plant is done using Aspen Economic Analyzer.
Qualitative Analysis of social aspects of MREW plant		<ul style="list-style-type: none"> • Social aspects of MREW are explored qualitatively.

CHAPTER-4
MATERIALS AND METHODS

CHAPTER – 4

4.1 Materials and methods

4.1.1 Printed Circuit Board (PCB) collection

The FR2 WPCBs (Fig. 4.1a) was collected from a local scrap shop located in Kolkata, India. The FR2 VPCBs were procured from local shop in Kolkata, India. FR-4 type Waste PCBs (Fig. 4.1 b) were recovered from End-of-Life (EoL) computers (MSI-7349 VER 2) from the department of chemical engineering, Jadavpur University, India. FR-4 type Virgin PCBs (Fig. 4.1d) were procured from Amazon India website.

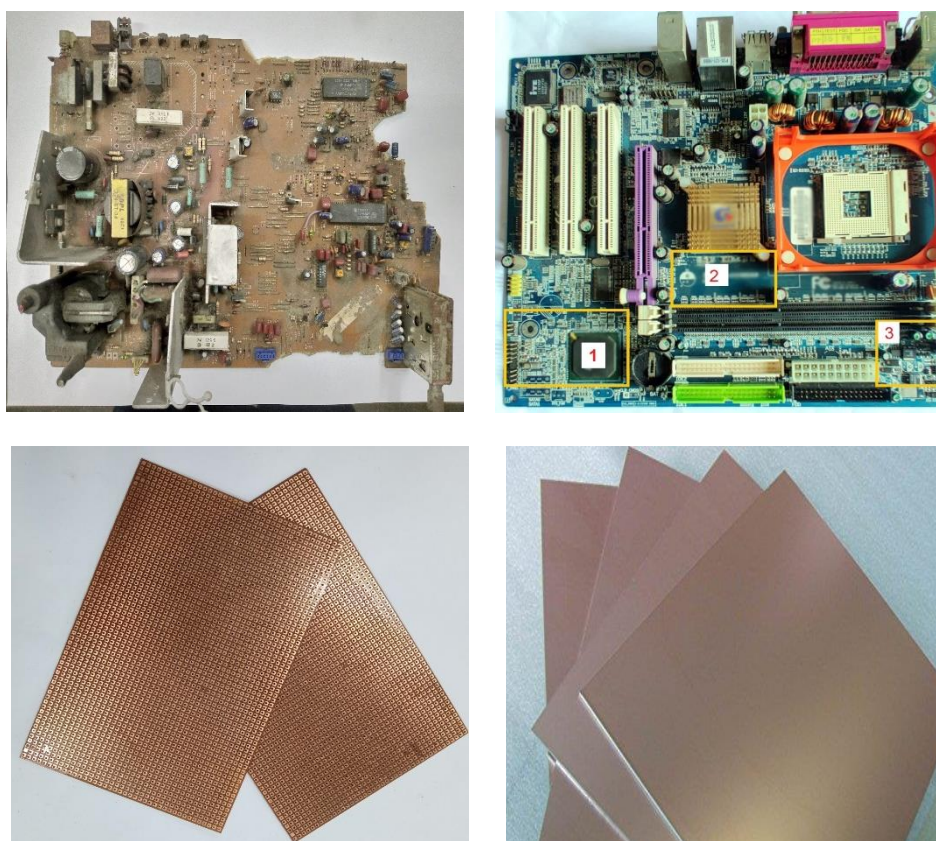


Figure 4.1 (a) FR-2 Waste PCB recovered from old TV set; (b) FR-4 Waste PCB recovered from Personal Computer; (c) FR-2 Virgin PCB store bought and (d) FR-4 Virgin PCB procured online

4.1.2 Sample Preparation

Electronic Components (ECs) including FETs, diodes, transistors etc, mounted on the WPCBs were removed using hot-air gun and de-soldering rods. For VPCBs this step was not required as they do not contain any EC (Figure 4.2 b, d). The PCBs were broken into pieces of average 1 cm x 1 cm. Since the FR-2 type PCBs (Fig. 4.2 a, b) are brittle in nature they were broken

into pieces, whereas FR-4 type PCBs (Fig. 4.2 c, d) are reinforced with glass fibre fabric, they were cut into the aforementioned dimension using a mechanical hand cutter. For characterization purpose, FR-2 and FR-4 type PCBs were ground using heavy duty mixer grinder (Bajaj Pvt. Ltd). The resulting mass was sieved to obtain the finely ground PCBs. Grinding was carried out separately for both FR-2 and FR-4 type VPCB and WPCBs. FR-2 and FR-4 feed mixture was prepared by varying the percentage of FR-2 in the range of 10 – 90%.

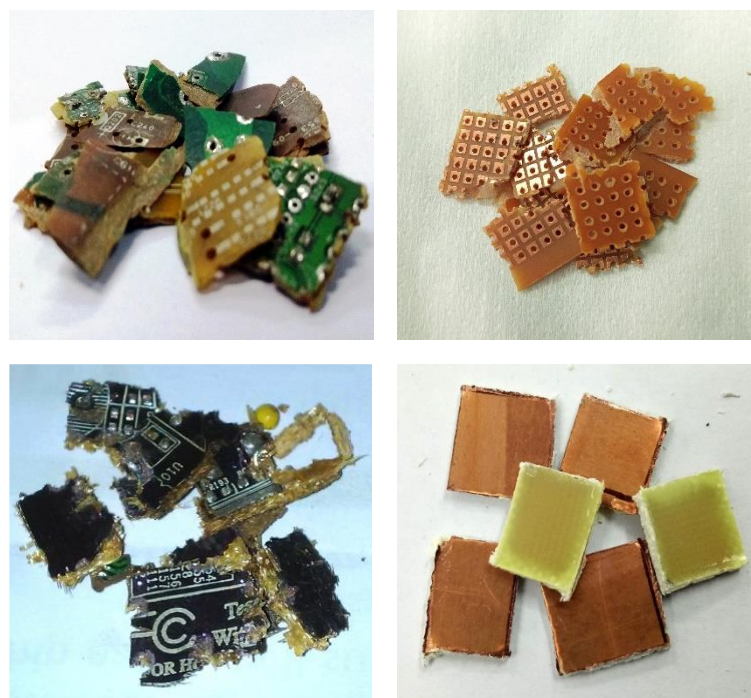


Figure 4.2 (a) FR-2 Waste PCB samples; (b) FR-2 Virgin PCB samples; (c) FR-4 Waste PCB samples and (d) FR-4 Virgin PCB samples.

4.1.3 Chemicals

Acetone (99.5%) procured from Central Drug House (CDH) limited (New Delhi, India) was used in the experiment. CDCl_3 and DMSO-d_6 used in NMR analysis was purchased from Sigma Aldrich.

4.1.4 Description of Experimental Setup

The experimental setup (Figure 4.3) is a custom-made stainless-steel fixed bed reactor (L:D = 4:1) with a furnace just to accommodate the reactor in it. The furnace can be heated up to a temperature of 1273K and can be programmed with a PID controller (Honeywell Make) attached with it. The same reactor was used for pyrolysis and gasification.

During pyrolysis nitrogen was flown through the reactor to maintain inert and oxygen-free atmosphere. The volatile products were passed through series of condensers, one continuous bulb type condenser and two batch mode condensers, using constant temperature water of 283K as the cooling fluid in each case. The condensable volatiles were collected as liquid product and the non-condensable volatiles were collected as gaseous product of pyrolysis. The solid residues, mainly the char, metal mixture and glass fibre were collected from the reactor after atmospheric cooling to ambient temperature.



Figure 4.3: Experimental Setup

During gasification, mixture of steam and air was as the gasifying agent. Air was supplied in a fashion so that the molar flow rate of oxygen lied much below that required for complete combustion of the polymeric portion of PCBs. The gaseous product was collected and the solid residues, mainly the char, metal mixture and glass fibre were collected from the reactor after atmospheric cooling to ambient temperature.

4.1.5 Experimental Setup for Lumped Kinetics

The experimental setup (Figure 4.3) is a custom-made stainless-steel fixed bed horizontal reactor (L:D = 13:1) equipped with a furnace, a precise temperature controller utilizing a PID controller, and a digital weight box. The furnace can be heated upto a temperature of 973K and

can be programmed with a PID controller attached with it. As depicted in figure 4.4, the pyrolyzer was suspended using a stainless-steel chain and connected to a weighing machine to enable continuous monitoring of the remaining solid mass inside the pyrolyzer. The furnace temperature was varied within the range of 573 K to 973 K. Upon reaching the predetermined temperature, the pyrolyzer was introduced into the furnace. Isothermal conditions were strictly maintained throughout the entire duration of the pyrolysis process.

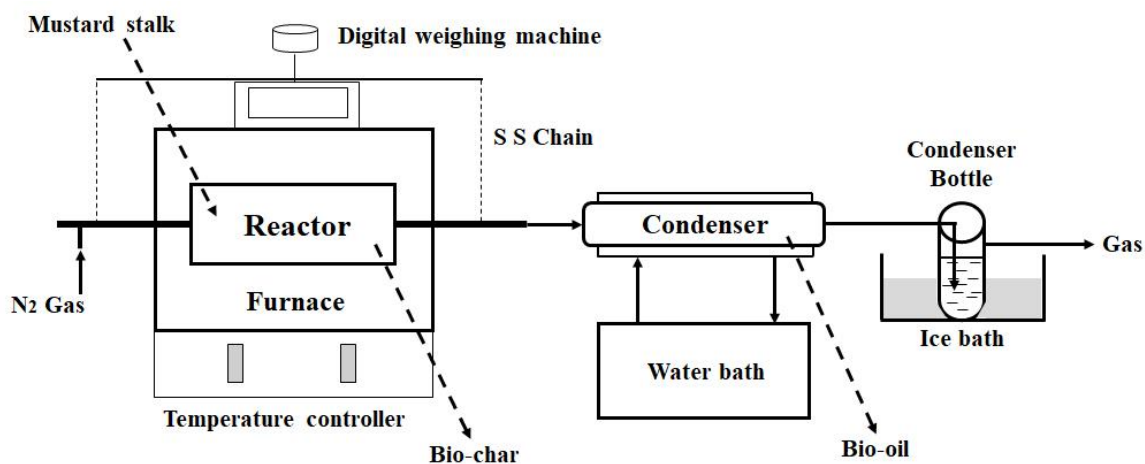


Figure 4.4: Experimental Setup for Lumped Kinetics

4.1.6 Equipment and Apparatus

- Digital weighing balance (Sartorius, Germany)
- Hot air oven (G.B. Enterprises, Kolkata, India)
- Muffle Furnace (G.B. Enterprises, Kolkata, India)
- Heater
- Chiller
- Semi-batch Horizontal Pyrolyzer (G.B. Enterprises, Kolkata, India)
- Semi-batch Vertical Pyrolyzer-cum-Gasifier (G.B. Enterprises, Kolkata, India)
- Custom furnace for Pyrolyzer and Gasifier (G.B. Enterprises, Kolkata, India)

4.1.7 Software Packages

- MATLAB 2019b
- Super Decisions Pro
- GeMS
- Design Expert 13
- Simapro 8
- Aspen Plus 10
- ChemDraw Ultra 12.0

4.2 Analytical Methods

4.2.1 Proximate and Ultimate Analysis

Proximate analysis of FR-2 and FR-4 type PCB were carried out following ASTM method D-3172-89. The CHNS elemental analyzer (vario MACRO cube, Elementar, Germany) was used for ultimate analysis of FR-2 and FR-4 type VPCB and WPCB.

4.2.2 Thermo-gravimetric Analysis (TGA)

The Thermogravimetric Analysis (TGA) experiments were carried out in the 325 – 1250 K temperature range in a Pyris Diamond TG/DTA, STA 6000 (PerkinElmer). The TG experiment was carried out using approximately 4 mg of the sample in an alumina bed placed in a crucible. The nitrogen flow was 20 ml/min.

4.2.3. Field Emission Scanning Electron Microscope (FESEM)

The analysis of surface morphology of raw and pyrolyzed samples of FR-2 and FR-4 type VPCB and WPCBs were carried out by using FESEM. All samples were crushed and sieved to obtain the finest fraction. The samples were then thinly coated with gold. The analysis was done using INSPECT F50 (FEI) at 600-5000x magnification. FESEM was carried out with two aims – i) to observe the surface morphology and ii) to identify pores on the surface along with their dimension.

4.2.4 Energy-dispersive X-ray spectroscopy (EDX) analysis

EDX analysis was carried out to find out the presence of prevalent metals in PCBs using Bruker EDX. EDX was carried out before and after thermochemical pre-treatment i.e., pyrolysis and gasification of the feedstocks.

4.2.5 FTIR Analysis

Samples of PCBs, pyro-char and gasification char were pelletized using KBr and the IR spectra was captured on a RX-1 PerkinElmer spectrometer in the range of 4500–450 cm^{-1} . While pyro-oil samples were diluted with acetone in the ratio of 1:10, filtered using nitro-cellulose filter before IR analysis. IR spectra of the oil samples were recorded on a Perkin Elmer spectrophotometer (Magma -IR 560 E.S.P) utilizing KBr disk.

4.2.6 X-Ray Diffraction (XRD) Analysis

Powder x-ray diffraction (XRD) patterns were performed in 10° – 90° 2θ range using Ultima III, (Rigaku, Japan) which employs “Cu K α radiation” as target applying 40 kV voltage, 30 mA current, 1.2 kW power.

4.2.7 ^1H NMR Analysis

CDCl_3 and DMSO-d_6 were used as solvents using TMS as an internal standard for NMR spectra. ^1H NMR spectra were recorded on a Bruker (AC) 300 MHz FT-NMR spectrometer.

4.2.8 GC-MS Analysis

Pyro-oil samples were diluted with acetone in the ratio of 1:100, filtered using nitro-cellulose filter before GC-MS analysis. The analysis was carried out using a GC/MS (Thermo-Scientific) in TR-WAX column (30 m x 0.25 mm x 0.25 μm) with helium as carrier gas. The oven temperature was programmed to 423K with $10^{\circ}\text{C}/\text{min}$ heating rate before raising the temperature to 503K. The injector and MS detector temperature was 503 K and 483K respectively. The mass line range was set in the range 50 – 600 amu.

4.2.9 GC Analysis of pyro-gas and syngas

Pyro gas and syngas were analyzed using gas chromatograph (GC, TRACE 1100, Thermo Fisher Scientific, India) equipped with TCD detector and stainless-steel column (3m x 3.2 mm) packed with 5 \AA molecular sieve (TG-5MS). Samples were collected using a tedlar bag and injected in GC with a gas tight glass syringe. Operational temperatures of the detector, oven and injector were kept at 393K, 333K and 373K respectively.

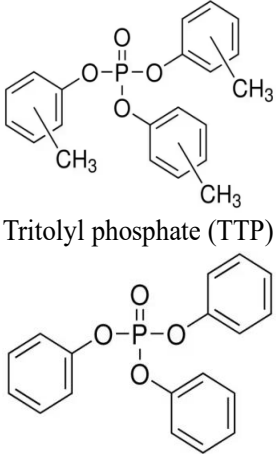
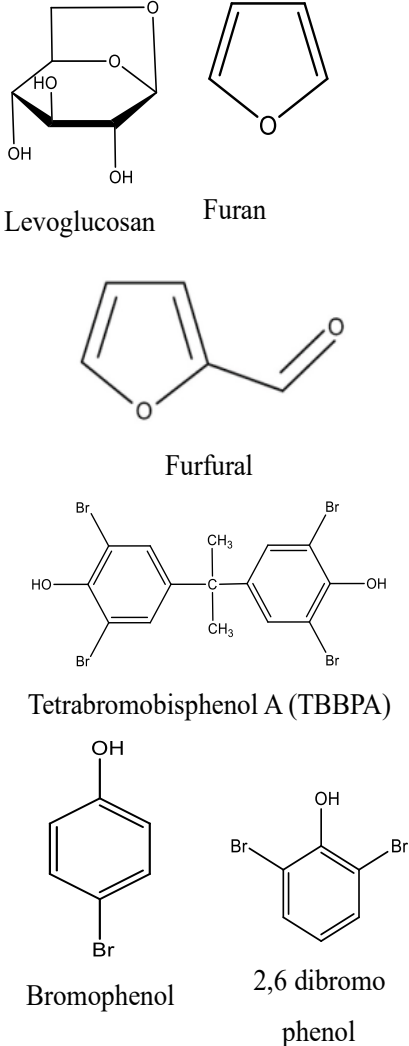
4.3 Theoretical Analysis

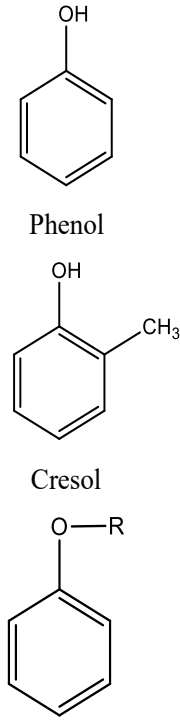
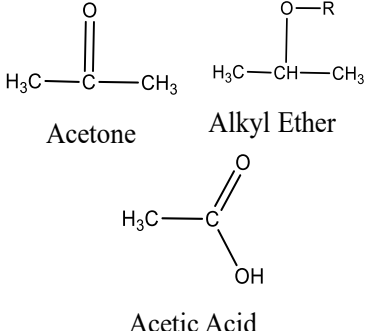
4.3.1 Fundamentals Chemistry of Kinetic Studies

4.3.1.1 FR-2 PCB Reaction Chemistry

Based on the literature data, pyrolysis of FR-2 PCB follows of four stages occurring at different temperature regimes (Kim et al. 2015; Kumagai et al. 2017). Table 4.1 represents the stages according to temperature zone of their occurrence, probable reactions and products.

Table 4.1: FR-2 PCB Pyrolysis Reaction Pathway

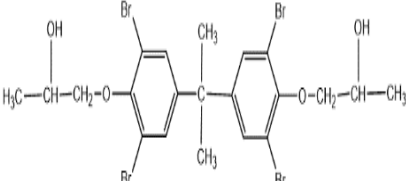
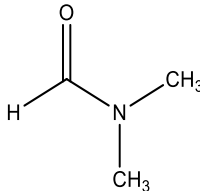
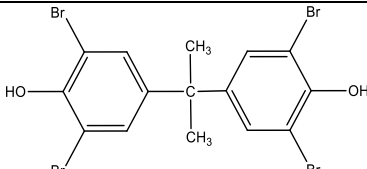
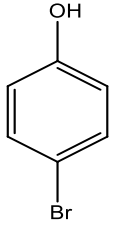
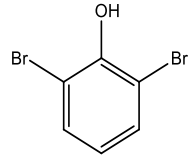
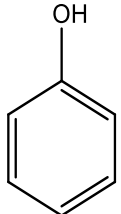
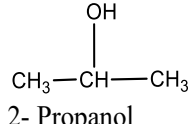
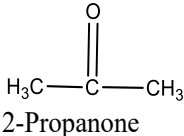
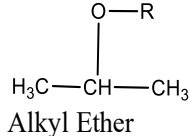
Stage	Temperature Range (°C)	Probable Reactions	Possible Products
1	<280	<p>FR-2 PCBs are paper laminated phenolic resins that contain both phosphate and brominated flame retardants. In stage 1, vaporization of Phosphate Flame Retardants (PFRs) takes place generating PFRs such as Triphenyl phosphate (TPP), Tritolyl phosphate (TTP) etc and a Reaction Intermediate (RI1) is formed.</p> <p>$FR2\ PCB \rightarrow TTP + TPP + RI1$</p>	 <p>Tritolyl phosphate (TTP)</p> <p>Triphenyl phosphate (TPP)</p>
2	280-370	<p>Reaction Intermediate generated in stage 1 contains paper, TBBPA and Phenolic resin. In this stage the reaction occurs in two steps.</p> <p>i) Pyrolysis of paper occurs where cellulose decomposes generating volatile compounds such as levoglucosan, furan, furfural etc.</p> <p>$Cellulose \rightarrow Levoglucosan + Furan + Furfural$</p> <p>ii) Decomposition of RI1 to Tetrabromobisphenol A (TBBPA) and intermediate, RI2 and further decomposition of TBBPA to Bisphenol A, brominated phenols and an intermediate RI3.</p> <p>$RI1 \rightarrow TBBPA + RI2$</p> <p>$TBBPA \rightarrow Bisphenol\ A + Brominated\ compounds + RI3$</p> <p>Thus, in step 2, two reaction intermediates (RI2 and RI3) are formed.</p>	 <p>Levoglucosan</p> <p>Furan</p> <p>Furfural</p> <p>Tetrabromobisphenol A (TBBPA)</p> <p>Bromophenol</p> <p>2,6 dibromo phenol</p>

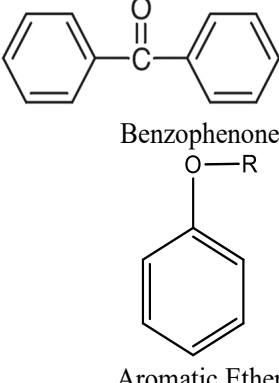
3	370-500	<p>The reaction intermediates, RI2 and RI3, generated in the previous stage primarily contains the phenolic resin which undergoes thermal decomposition in this stage. This process produces phenol and phenolic derivatives (cresol etc.). Phenols go through further intramolecular reactions and rearrangement reactions which produces carbonyl compounds and aromatic ethers. In this step, another reaction intermediate (RI4) is generated.</p> <p>$RI2 + RI3 \rightarrow Phenol + Cresol + RI4$</p>	 <p>Phenol</p> <p>Cresol</p> <p>Aromatic Ether</p>
4	>500	<p>The reaction intermediate, RI4 generated in stage 3 undergoes stabilization reaction forming char and volatile products.</p> <p>$Phenol\ and\ derivatives \rightarrow Carbonyl\ compounds + Ether$</p> <p>$RI4 \rightarrow Char + Volatile\ Products$</p>	 <p>Acetone</p> <p>Alkyl Ether</p> <p>Acetic Acid</p>

4.3.1.2 FR-4 PCB Reaction Chemistry

According to the literature, the pyrolysis of FR-4 PCB is characterized by four distinct stages, each occurring within specific temperature ranges (Kim et al. 2013; Liu et al. 2018). Table 4.2 outlines these stages, detailing the temperature zones, along with the probable reactions and resulting products.

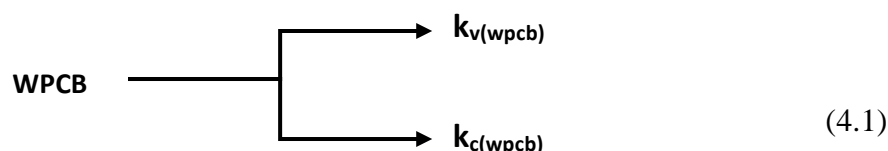
Table 4.2: FR-4 PCB Pyrolysis Reaction Pathway

Stage	Temperature Range (°C)	Reactions	Possible Products
1	<298	<p>FR-4 PCBs are epoxy resins, cross-linked with brominated flame retardants such as TBBPA. In stage 1, the breakage of N-containing cross-linkage occurs to form dimethyl formamide and brominated epoxy resin (BER) monomers.</p> <p>$BER_{polymer} \rightarrow Dimethyl Formamide + BER_{monomer}$</p>	 <p>Brominated Epoxy Resin (BER) monomers</p>  <p>Dimethyl Formamide</p>
2	298-351	<p>$BER_{monomer}$ undergoes thermal decomposition producing TBBPA and aliphatic alcohols.</p> <p>$BER_{monomer} \rightarrow TBBPA + Alcohol$</p> <p>TBBPA further decomposes to Bisphenol A, brominated phenols, phenols and alkanes.</p> <p>$TBBPA \rightarrow Bisphenol A + Phenol + Brominated Phenol + Alkane$</p> <p>Alcohols further undergoes intramolecular reactions and rearrangement reactions which produces carbonyl compounds and aliphatic ethers.</p> <p>$Aliphatic Alcohols \rightarrow Carbonyl Compounds + Aliphatic Ether$</p> <p>Carbonyl compounds decomposes to gaseous products like carbon dioxide, monoxide and methane.</p> <p>$Ketones \rightarrow CO + CO_2 + CH_4$</p>	 <p>TBBPA</p>  <p>Bromophenol</p>  <p>2,6-dibromophenol</p>  <p>Phenol</p>  <p>2-Propanol</p>  <p>2-Propanone</p>  <p>Alkyl Ether</p> <p>Carbon monoxide</p> <p>Carbon dioxide</p> <p>Methane</p>

3	351-494	Phenols experience intramolecular reactions and rearrangement reactions which produces aromatic carbonyl compounds (Benzophenone etc.) and aromatic ethers. <i>Phenols → Aromatic Carbonyls + Aromatic Ethers</i>	 <p>Benzophenone</p> <p>Aromatic Ether</p>
4	>494	The residues undergo stabilization reaction forming char and volatile small molecules such as carbon dioxide, carbon monoxide and HBr are evolved. <i>Residues → Char + Volatiles</i>	<p>Hydrogen Bromide</p> <p>Carbon monoxide</p> <p>Carbon dioxide</p>

4.3.2 Lumped Kinetic Modelling

The lump kinetic parameters were estimated using the method proposed by Bandopadhyay et al. (1999). The reaction pathway may be represented as –



The weight loss profile of solid sample M_{wpcb} with time may be given by:

$$-\frac{dM_{\text{wpcb}}}{dt} = (k_v(\text{wpcb}) + k_c(\text{wpcb}))M_{\text{wpcb}} \quad (4.2)$$

Let,

$$k_v(\text{wpcb}) + k_c(\text{wpcb}) = k_{\text{wpcb}} \quad (4.3)$$

Hence,

$$-\frac{dM_{\text{wpcb}}}{dt} = k_{\text{wpcb}}M_{\text{wpcb}} \quad (4.4)$$

$$\frac{dM_{v(\text{wpcb})}}{dt} = k_v(\text{wpcb})M_{\text{wpcb}} = k_v(\text{wpcb})M_{\text{wpcb}(o)} \exp(-k_{\text{wpcb}}t) \quad (4.5)$$

$$\frac{dM_{c(\text{wpcb})}}{dt} = k_c(\text{wpcb})M_{\text{wpcb}} = k_c(\text{wpcb})M_{\text{wpcb}(o)} \exp(-k_{\text{wpcb}}t) \quad (4.6)$$

Initial Condition,

$$M_{\text{wpcb}}(t=0) = M_{\text{wpcb}(o)}, M_{v(\text{wpcb})}(t=0) = M_{v(o)(\text{wpcb})} \text{ and } M_{c(\text{wpcb})}(t=0) = M_{c(o)(\text{wpcb})} \quad (4.7)$$

Hence,

$$\frac{dM_{wpcb}}{dM_{V(wpcb)}} = \frac{k_c(wpcb)}{k_v(wpcb)} = \frac{M_{C(wpcb)} - M_{Co(wpcb)}}{M_{V(wpcb)} - M_{Vo(wpcb)}} = \frac{M_{C(wpcb)}(t_\infty) - M_{Co(wpcb)}}{M_{V(wpcb)}(t_\infty) - M_{Vo(wpcb)}} \quad (4.8)$$

Now, according to Thurner and Mann (1981),

$$M_{C(wpcb)}(t_\infty) = M_{R(wpcb)}(t_\infty) \quad (4.9)$$

$$M_{V(wpcb)}(t_\infty) = M_{wpcb(o)} - M_{R(wpcb)}(t_\infty) \quad (4.10)$$

Hence,

$$\frac{M_{C(wpcb)} - M_{Co(wpcb)}}{M_{V(wpcb)} - M_{Vo(wpcb)}} = \frac{M_{R(wpcb)}(t_\infty) - M_{Co(wpcb)}}{M_{wpcb(o)} - M_{R(wpcb)}(t_\infty)} \quad (4.11)$$

So, the weight of the unreacted sample after any time t is given by,

$$M_{wpcb}(t) = M_{wpcb(o)} - (M_{V(wpcb)} - M_{Vo(wpcb)}) * \left[1 + \frac{M_{R(wpcb)}(t_\infty) - M_{Co(wpcb)}}{M_{wpcb(o)} - M_{R(wpcb)}(t_\infty)} \right] \quad (4.12)$$

Using this above equation to find $M_{wpcb}(t)$ we find $M_{wpcb(avg)}$ and plot $\frac{\Delta M_{V(wpcb)}}{\Delta t}$ and

$\frac{\Delta M_{C(wpcb)}}{\Delta t}$ vs $M_{wpcb(avg)}$ to get k_v and k_c respectively at different temperatures.

According to Arrhenius Equation –

$$\ln k = \ln A - \frac{E_a}{RT} \quad (4.13)$$

where, E_a is the activation energy for the reaction and A is the pre-exponential factor.

Similar equations can be written for $k_{v(wpcb)}$, $k_{c(wpcb)}$ corresponding to the activation energies E_c and E_v respectively. A plot $\ln k$, $\ln k_c$ and $\ln k_v$ vs $1/T$ gives the corresponding activation energies.

4.3.3 Isoconversional Kinetic Modelling and DAEM

Thermal decomposition of complex waste materials such as PCB is a heterogeneous process, where the solid particles undergo thermal cracking producing char and volatile products. A lot of models have been established based on the Arrhenius Equation as this equation is extensively utilized to illustrate the homogeneous kinetic of solid-state pyrolysis in linear non-isothermal TGA (Cai et al. 2014). The distributed activation energy model (DAEM) has been used to study pyrolysis under non-isothermal conditions (Poddar et al. 2015). As suggested by researchers, during the pyrolysis process a huge number of distinct series and parallel reactions occur illustrated with different Activation Energies (E_a), resulting into distributions of activation energy (Yao et al. 2020; Poddar et al. 2015; Chowdhury and Sarkar 2012). The main cause behind the irregularity of E_a 's can be attributed to the deviation of bond strengths of multiple components (Wu et al. 2013). In general, isoconversional methods are employed along with TGA data to find the activation energy (Mortezaeikia et al., 2021). Isoconversional

methods are extensively used because they do not require information about the reaction model and can predict the activation energy quite accurately (Yao et al. 2020).

The TG findings can be demonstrated as a function of conversion (α)

$$\alpha = \frac{w_i - w_t}{w_i - w_f} \quad (4.14)$$

where w_i and w_f are the initial and final weight of sample respectively, whereas w_t represents the instantaneous weight of solid.

The conversion rate ($d\alpha/dt$) of solids can be illustrated as

$$\frac{d\alpha}{dt} = \frac{d\alpha}{dT} \cdot \frac{dT}{dt} = \beta \frac{d\alpha}{dT} = k(T) \times f(\alpha) \quad (4.15)$$

where β is the heating rate (dT/dt , $K \text{ min}^{-1}$); $k(T)$ refers to the reaction rate constant; $f(\alpha)$ is the kinetic model function.

$k(T)$ can be expressed as per the Arrhenius equation

$$k(T) = A e^{-\frac{E_a}{RT}} \quad (4.16)$$

where A is the frequency factor or the pre-exponential factor (min^{-1}) and E_a refers to the apparent activation energy (kJ mol^{-1}). R is the universal gas constant ($8.314 \text{ J (mol} \cdot \text{K)}^{-1}$) and T is the absolute temperature (K).

Under constant temperature ramp conditions, combining Equations (15) and (16) yields

$$\frac{d\alpha}{dT} = \frac{A}{\beta} e^{-\frac{E_a}{RT}} f(\alpha) \quad (4.17)$$

Integrating equation (17) yields the integral form as follows:

$$g(\alpha) = \int_0^\alpha \frac{d\alpha}{f(\alpha)} = \frac{A}{\beta} \int_0^T e^{-\frac{E_a}{RT}} dT = \frac{AE_a}{\beta R} \int_x^\alpha \frac{e^{-x}}{x^2} dx = \frac{AE_a}{\beta R} p(x) \quad (4.18)$$

Where,

$$p(x) = \int_x^\alpha \frac{e^{-x}}{x^2} dx \quad (4.19)$$

As per the recommendation of the ICTAC committee (Vyazovkin et al. 2011), Friedman iso-conversion method is not reliable alone due to the inherent issue of being a differential method. Hence, KAS method, based on integral method, has also been used for our analysis. All calculations have been carried out using Microsoft Excel.

4.3.3.1 Friedman Method

According to the ICTAC committee recommendation, Friedman Method is an efficient iso-conversion method (Vyazovkin et al. 2011). The Friedman method is grounded on a key assumption i.e., “solids decomposition depends only on the rate of mass loss and is independent

of the temperature” (Friedman 1964). Hence, $f(\alpha)$ can be assumed to be constant. Taking the natural logarithms on both sides for equation (4) yields –

$$\ln\left(\beta \frac{d\alpha}{dT}\right) = \ln[Af(\alpha)] - \frac{E_\alpha}{RT} \quad (4.20)$$

Since $\ln[Af(\alpha)]$ is a constant, hence for a particular value of α and β , the E_α values can be computed from the slope the $\ln\left(\beta \frac{d\alpha}{dT}\right)$ versus $\frac{1}{T}$ straight lines. It was assumed that all the reactions occurring during the experiments are of first-order irreversible type.

4.3.3.2 KAS Method

Kissinger–Akahira–Sunose (KAS) method is one of the best model free iso-conversional methods for estimation of activation energy. According to the ICTAC Committee recommendation, KAS method offers a significant improvement in the accuracy of the E_α values. KAS method provided better solutions than the well-known Flynn–Wall–Ozawa or the FWO method (Vyazovkin et al. 2011). For the constant heating rate program, the general form of an iso-conversional integral method (Starink 2003) can be expressed as follows:

$$\ln\left(\frac{\beta}{T^B}\right) = \text{Constant} - C\left(\frac{E_\alpha}{RT_\alpha}\right) \quad (4.21)$$

Using the Murray and White approximation, we obtain $B=2$ and $C=1$ (Vyazovkin et al. 2011). This leads to the popular equation of Kissinger–Akahira–Sunose (KAS) equation (Akahira and Sunose 1971):

$$\ln\left(\frac{\beta}{T_\alpha^2}\right) = \ln\left(\frac{AR}{E_\alpha g(\alpha)}\right) - \left(\frac{E_\alpha}{RT}\right) \quad (4.22)$$

The E_α values has been calculated from the slope of straight line by plotting $\ln\left(\frac{\beta}{T_\alpha^2}\right)$ versus $\frac{1}{T}$.

4.3.3.3 FWO Method

The FWO method named after Flynn, Wall and Ozawa (Flynn and Wall, 1966; Ozawa, 1965) utilises the Doyle’s temperature integral approximation, i.e., $\ln p(x) = -5.331 - 1.052x$. Using this approximation, equation 5 can be written as,

$$\ln\beta = \ln\frac{AE_\alpha}{Rg(\alpha)} - 5.331 - 1.052\frac{E_\alpha}{RT} \quad (4.23)$$

For a particular α value, each plot of $\ln\beta$ vs $1/T$ produces a straight line. The E_α values has been determined through the slope of $-1.052E_\alpha/R$ over a series of α .

4.3.3.4 Starink Method

For the Starink method (Starink 2003), the following approximation is used –

$$p(x) = \frac{e^{-1.0008x-0.312}}{x^{1.92}} \quad (4.24)$$

the relation between heating rate and inverse temperature takes the following form –

$$\ln\left(\frac{\beta}{T^{1.92}}\right) = -1.0008\left(\frac{E_\alpha}{RT}\right) + C \quad (4.25)$$

The E_α values has been calculated from the slope of straight line by plotting $\ln\left(\frac{\beta}{T^{1.92}}\right)$ versus $\frac{1}{T}$ over a series of α .

4.3.3.5 Tang Method

An estimation of the Arrhenius temperature integral was reported by Tang et al. (2003) as follows –

$$p(x) = \frac{e^{-x}}{x} \left(\frac{1}{1.001989x + 1.873912} \right) \quad (4.26)$$

the relation between heating rate and inverse temperature takes the following form –

$$\ln\left(\frac{\beta}{T^{1.894661}}\right) = -1.00145033\left(\frac{E_\alpha}{RT}\right) + C \quad (4.27)$$

The E_α values has been determined through the slope of $-1.000145033E_\alpha/R$ over straight lines of $\ln\left(\frac{\beta}{T^{1.894661}}\right)$ versus $\frac{1}{T}$ over a series of α .

4.3.3.6 Bosewell Method

The Bosewell method (Bosewell 1980) is a well-known isoconversional method which can be represented as –

$$\ln\left(\frac{\beta}{T}\right) = -\left(\frac{E_\alpha}{RT}\right) + C \quad (4.28)$$

The E_α values has been calculated from the slope of straight line by plotting $\ln\left(\frac{\beta}{T^{1.92}}\right)$ versus $\frac{1}{T}$ over a series of α .

4.3.4 DAEM Method

The common equation of this model can be illustrated as:

$$1 - \frac{d\alpha}{dt} = \int_0^\infty \exp\left[-A \int_0^t \exp\left(-\frac{E}{RT}\right) dt\right] f(E) dE \quad (4.29)$$

where A , E and R are the pre-frequency factor, activation energy and the universal gas constant ($8.314 \text{ J (mol}\cdot\text{K)}^{-1}$) respectively. $f(E)$ is distribution function that sums up the range and variation in the activation energies of the concurrent first-order irreversible reactions and is normalized as –

$$\int_0^{\infty} f(E)dE = 1 \quad (4.30)$$

Considering the correlation among T , t and β , Equation (10) can be depicted as

$$1 - \frac{d\alpha}{dT} = \int_0^{\infty} \exp\left[-\frac{A}{\beta} \int_{T_0}^T \exp\left(-\frac{E}{RT}\right) dT\right] f(E)dE \quad (4.31)$$

To simplify, Equation (31) can be rewritten as

$$\frac{d\alpha}{dT} = 1 - \int_{E_s}^{\infty} f(E)dE = \int_0^{E_s} f(E)dE \quad (4.32)$$

Miura and Maki (1998) achieved a straightforward technique to estimate the E and A values as follows

$$\ln \frac{\beta}{T^2} = \ln \frac{AR}{E_{\alpha}} + 0.6075 - \frac{E_{\alpha}}{RT} \quad (4.33)$$

4.3.5 Thermodynamic Analysis

The thermodynamic analysis was carried out using the data obtained from TGA-DTG and kinetic parameters evaluated using Microsoft Excel. The analysis has been carried out based on equations provided in Liu et al. (2021) and Ali et al. (2021). The enthalpy change (ΔH), Gibbs free energy change (ΔG), and entropy change (ΔS) have been calculated by using the equations below:

$$\Delta H = E_{\alpha} - RT_{\alpha} \quad (4.34)$$

$$\Delta G = E_{\alpha} + RT_m \ln\left(\frac{k_B T_m}{hA}\right) \quad (4.35)$$

$$\Delta S = \frac{\Delta H - \Delta G}{T_m} \quad (4.36)$$

where E_{α} is the activation energy; T_{α} is the temperature at a particular α ; T_m is the highest temperature at which extreme mass loss occurs; k_B is the Boltzmann constant ($1.381 \times 10^{-23} \text{ J/K}$); and h is the Planck constant ($6.626 \times 10^{-34} \text{ J s}$).

4.3.6 Reaction Mechanism

The mechanism function was determined using the Šesták-Berggren model [29], as expressed in Equation 9 –

$$f(\alpha) = (1 - \alpha)^n \alpha^m [-\ln(1 - \alpha)]^p \quad (4.37)$$

Equation (9) can be logarithmically expressed as –

$$\ln\left(\frac{d\alpha}{dt}\right) + \frac{E_a}{RT} = \ln A + n \ln(1 - \alpha) + m \ln \alpha + p \ln[-\ln(1 - \alpha)] \quad (4.38)$$

Where, the terms $(1-\alpha)^n$, α^m , $[-\ln(1-\alpha)]^p$ are associated with phase boundary reaction, diffusion reaction and nucleation reaction mechanisms. Estimation of the parameters n, m and p has been obtained with the help of multiple linear regression using MATLAB R2021 software.

4.3.7 Solution Algorithm

4.3.7.1 Determination of Kinetic Parameters

Step 1: Perform TGA of the sample at least three different heating rates.

Step 2: Calculate conversion (α) from TG data and convert Temperature in Kelvin scale.

Step 3: Calculate the values of $\ln \beta$ and $\frac{1}{T}$.

Step 4: Plot $\ln \beta$ versus $\frac{1}{T}$ for all heating rates at each α .

Step 5: For each α in the plot, the data of different heating rates must be linearised. Activation energy is determined from the slope of the plot in step 4 and frequency factor is determined from the intercept.

4.3.7.2 Determination of Reaction Mechanisms

Step 1: Calculate $\ln \alpha$, $\ln(1-\alpha)$, $\ln[-\ln(1-\alpha)]$, $\ln\left(\frac{d\alpha}{dt}\right)$ and $\frac{E_a}{RT}$ for different α .

Step 2: Use equation 10 segregate X and Ys.

Step 3: Use multiple regression to determine the $\ln A$, n, m and p.

4.3.7.3 Determination of Thermodynamic Parameters

Step 1: Perform TGA of the sample at three different heating rates.

Step 2: Compute kinetic parameters as stated above.

Step 3: Calculate the enthalpy change (ΔH), Gibbs free energy change (ΔG), and entropy change (ΔS) as per equation 4.34 – 4.36.

4.3.7.4 Calculation of E and $f(E)$

Step 1: Calculate conversion (α) from TG data and convert Temperature in Kelvin scale.

Step 2: Calculate the values of $\ln(\beta/T^2)$ and $1/T$.

Step 3: For each value of α , plot $\ln(\beta/T^2)$ against $1/T$ at different values of β i.e., heating rate.

Step 4: For each α in the plot, the data of different β must be linearized and calculate $E\alpha$ and A values from slope and intercept respectively.

Step 5: Plot α against E and differentiate the relationship by E to achieve $f(E)$.

4.3.8 Calculation of Theoretical Yield

Theoretical yields of pyro-oil (Y_{PO}), glass fibre (Y_{GF}), metal (Y_M) and char (Y_{Char}) have been calculated using the following correlations –

$$Y_{PO}(\%) = \frac{\text{Mass of Pyro-oil produced}}{\text{Mass of Total Feed}} \times 100 \quad (4.39)$$

$$Y_{GF}(\%) = \frac{\text{Mass of Glass Fibre produced}}{\text{Mass of Total Feed}} \times 100 \quad (4.40)$$

$$Y_M(\%) = \frac{\text{Mass of Metals produced}}{\text{Mass of Total Feed}} \times 100 \quad (4.41)$$

$$Y_{Char}(\%) = \frac{\text{Mass of Char produced}}{\text{Mass of Total Feed}} \times 100 \quad (4.42)$$

4.3.9 Calculation of Higher Heating Value of Pyro-oil

The higher heating values (HHV) of the pyro-oil recovered from pyrolysis of VPCBs and WPCBs have been calculated using the Dulong's equation (Sarkar 2009) –

$$HHV (kJ/Kg) = \left[(337.7 \times C) + \left\{ 1437.9 \times \left(H - \left(\frac{O}{8} \right) \right) \right\} \right] \quad (4.43)$$

4.3.10 AHP Analysis

The Analytic Hierarchy Process (AHP), developed by T.L. Saaty (Saaty 1980), was employed to derive the weight factors of the uncertainty variables in the 'free-energy' model. The general steps of performing AHP is described below (Debnath et al. 2022):

Step 1: Defining the problem and determining its goal and structuring the hierarchy from the top through the intermediate levels to the lowest level containing the list of alternatives.

Step 2: Construction of a set of pair-wise comparison matrices (size $n \times n$) for each of the lower levels with one matrix for each element in the level immediately above by using the relative scale measurement. The pair-wise comparisons are done in terms of which element dominates the other.

Step 3: Picked in groups of two over a set of n terms, this produces $n(n-1)/2$ judgments to develop the set of matrices in step 2. Reciprocals are automatically assigned in each pair-wise comparison.

Step 4: Hierarchical synthesis is now used to weight the eigenvectors (normalized representation in the generalized vector space) by the weights of the criteria and the sum is taken over all weighted eigenvector entries corresponding to those in the next lower level of the hierarchy. The AHP eigenvalues represent the normalized weights of the respective quantities, more in the mold of PCA.

Step 5: The consistency ratio (CR) confirms the reliability of the pairwise comparisons and it is determined as follows

$$CR = \frac{\lambda_{max} - n}{n - 1} \frac{CI}{RandomConsistency} \quad CI/RI \quad (4.43)$$

Here consistency index $CI = (\lambda_{max} - n) / (n - 1)$, where λ_{max} is the maximum average value and n is the matrix size. The random consistency index (RI) depends on the value of n. CR is acceptable, if it is ≤ 0.10 to have a consistency level. Beyond this value, the judgment matrix gets inconsistent. To obtain a consistent matrix, judgments should be reviewed and improved.

Step 6: Steps 2-5 are performed for all levels in the hierarchy.

References

Akahira, T. and Sunose, T., 1971. Method of determining activation deterioration constant of electrical insulating materials. *Res Rep Chiba Inst Technol (Sci Technol)*, 16(1971), pp.22-31.

Bandyopadhyay, S., Chowdhury, R., & Biswas, G. K. (1999). Thermal deactivation studies of coconut shell pyrolysis. *The Canadian Journal of Chemical Engineering*, 77(5), 1028-1036.

Cai, J., Wu, W., & Liu, R. (2014). An overview of distributed activation energy model and its application in the pyrolysis of lignocellulosic biomass. *Renewable and Sustainable Energy Reviews*, 36, 236-246.

Chowdhury, R., & Sarkar, A. (2012). Reaction kinetics and product distribution of slow pyrolysis of Indian textile wastes. *International Journal of Chemical Reactor Engineering*, 10(1).

Debnath, B., El-Hassani, R., Chattopadhyay, A. K., Kumar, T. K., Ghosh, S. K., & Baidya, R. (2022). Time evolution of a supply chain network: Kinetic Modeling. *Physica A: Statistical Mechanics and its Applications*, 607, 128085.

Flynn, J.H. and Wall, L.A., 1966. A quick, direct method for the determination of activation energy from thermogravimetric data. *J. Polym. Sci. Part B: Polymer Letters*, 4(5), pp.323-328.

Friedman, H. L. (1964). Kinetics of thermal degradation of char-forming plastics from thermogravimetry. Application to a phenolic plastic. In *Journal of polymer science part C: polymer symposia* (Vol. 6, No. 1, pp. 183-195). New York: Wiley Subscription Services, Inc., A Wiley Company.

Miura, K. (1995). A new and simple method to estimate $f(E)$ and $k_0(E)$ in the distributed activation energy model from three sets of experimental data. *Energy & Fuels*, 9(2), 302-307.

Mortezaeikia, V., Tavakoli, O., & Khodaparasti, M. S. (2021). A review on kinetic study approach for pyrolysis of plastic wastes using thermogravimetric analysis. *Journal of Analytical and Applied Pyrolysis*, 160, 105340.

Murray, P., & White, J. (1955). Kinetics of the thermal dehydration of clays. Part IV. Interpretation of the differential thermal analysis of the clay minerals. *Trans Br Ceram Soc*, 54, 204-238.

- Kim, Y. M., Kim, S., Lee, J. Y., & Park, Y. K. (2013). Pyrolysis reaction pathways of waste epoxy-printed circuit board. *Environmental Engineering Science*, 30(11), 706-712.
- Kim, Y. M., Han, T. U., Watanabe, C., Teramae, N., Park, Y. K., Kim, S., & Hwang, B. (2015). Analytical pyrolysis of waste paper laminated phenolic-printed circuit board (PLP-PCB). *Journal of analytical and applied pyrolysis*, 115, 87-95.
- Kumagai, S., Grause, G., Kameda, T., & Yoshioka, T. (2017). Thermal decomposition of tetrabromobisphenol-A containing printed circuit boards in the presence of calcium hydroxide. *Journal of Material Cycles and Waste Management*, 19, 282-293.
- Liu, W., Xu, J., Han, J., Jiao, F., Qin, W., & Li, Z. (2018). Kinetic and mechanism studies on pyrolysis of printed circuit boards in the absence and presence of copper. *ACS sustainable chemistry & engineering*, 7(2), 1879-1889.
- Ozawa, T., 1965. A new method of analyzing thermogravimetric data. *Bull. Chem. Soc. Jpn.*, 38(11), pp.1881-1886.
- Poddar, S., De, S., & Chowdhury, R. (2015). Catalytic pyrolysis of lignocellulosic bio-packaging (jute) waste—kinetics using lumped and DAE (distributed activation energy) models and pyro-oil characterization. *RSC advances*, 5(120), 98934-98945.
- Saaty, T.L., 1980. *The analytic hierarchy process*. New York: McGraw- Hill.
- Sarkar, S. (2009). *Fuels and combustion*. Universities Press.
- Vyazovkin, S. (2015). Isoconversional methodology. In *Isoconversional Kinetics of Thermally Stimulated Processes* (pp. 27-62). Springer, Cham.
- Vyazovkin, S., Burnham, A. K., Criado, J. M., Pérez-Maqueda, L. A., Popescu, C., & Sbirrazzuoli, N. (2011). ICTAC Kinetics Committee recommendations for performing kinetic computations on thermal analysis data. *Thermochimica acta*, 520(1-2), 1-19.
- Wu, W., Cai, J., & Liu, R. (2013). Isoconversional kinetic analysis of distributed activation energy model processes for pyrolysis of solid fuels. *Industrial & Engineering Chemistry Research*, 52(40), 14376-14383.
- Yao, Z., Xiong, J., Yu, S., Su, W., Wu, W., Tang, J., & Wu, D. (2020). Kinetic study on the slow pyrolysis of nonmetal fraction of waste printed circuit boards (NMF-WPCBs). *Waste Management & Research*, 38(8), 903-910.

CHAPTER-5
PYROLYSIS OF PRINTED
CIRCUIT BOARDS

CHAPTER – 5

5.1 Background

Printed circuit boards (PCBs) are a crucial constituent of electronic objects which ends up as waste PCB (WPCB) (Yao et al. 2020). Fire Retardant Type-2 (FR-2) PCBs are widely used in small electronics, toys, old CRT television etc (Argumedo-Delira et al. 2020). On the other hand, FR-2 type Virgin Printed Circuit Boards (VPCBs) are widely used for manufacturing of low-grade electronics (Kaya 2016). Fire Retardant Type-4 (FR-4) PCBs are used in electronics where mechanical rigidity is required such as laptop, computers, LCD televisions etc (Argumedo-Delira et al. 2020). Whereas FR-4 type Virgin Printed Circuit Boards (VPCBs) are widely used various projects (Kaya 2016). VPCBs are usually manufactured in sheets and generates a trimming of VPCBs during cutting (Hossain et al. 2022). These are usually manufactured in sheets. During the production stage, the VPCBs are punched and cut into custom shapes which generates a trimming of VPCBs (Hossain et al. 2022). Due to the absence of the circuit lines in VPCBs, they contain more copper than the WPCBs. Both the components of WPCB and VPCBs are fit for resource recovery (Kaya 2016). It is expected that the more the fraction of VPCBs, the more will be the fraction of copper in the recovered metal part. This chapter is focused on (a) *Studies on pyrolytic valorisation of FR-2 and FR-4 type Printed Circuit Boards with kinetic analysis, product characterization and distribution* and (b) *studies on pyrolytic valorisation of mixed Waste Printed Circuit Board with product characterization*. ICTAC-IUPAC nomenclatures have been used throughout the chapter (Lever et al. 2014). The chapter encompasses the following objectives described in **Chapter 3** under aim 2 and aim 3 –

- Thermogravimetric analysis (TGA) of FR-2 & FR-4 virgin and waste PCBs
- Lumped Kinetics of FR-2 & FR-4 waste PCBs
- Thermogravimetric analysis (TGA) of FR-2 & FR-4 virgin and waste PCBs.
- Experimental investigation on FR-2 & FR-4 virgin and waste PCBs pyrolysis in semi-batch pyrolyzer for product recovery
- Experimental investigation on mixed waste PCBs pyrolysis in custom made pyrolyzer for product recovery
- Kinetic analysis using isoconversional methods and DAEM of FR-2 & FR-4 virgin and waste PCB pyrolysis.
- Characterization of pyrolysis products of FR-2 & FR-4 virgin and waste PCBs pyrolysis.
- Characterization of mixed waste PCB pyrolysis products.

5.2 Experimental

5.2.1 Lumped Kinetics

The FR-2 and FR-4 PCBs were subjected to pyrolysis within the temperature range of 573 K to 973 K in a pre-heated tubular furnace using a horizontal fixed bed reactor suspended using a stainless-steel chain and connected to a weighing machine. Initially, the furnace was heated to the desired temperature at a constant rate of 20K/min. Once the temperature was attained, the pre-weighed pyrolyzer containing the feedstock was inserted into the furnace and was exposed to that temperature. After positioning the reactor, the temperature was held constant for different time period. After the reaction period is over, weight of the reactor set-up was again noted. Experiments were conducted by within the temperature range of 573 K to 973 K. The weighing arrangement was integrated with the furnaces and the dynamic weight variation of the reactor was noted without dismantling.

5.2.2 PCB Pyrolysis

The FR-2 and FR-4 PCBs were subjected to pyrolysis in a pre-heated furnace using the fixed bed reactor. On the other hand, in case of mixed WPCBs, samples of FR-2 and FR-4 WPCB were mixed in the ratio of 1:1. Nitrogen flow at 1-3 lpm was introduced to maintain an inert atmosphere and to provide necessary residence time for the volatiles to condense in the condensing units. The volatiles were passed through a bulb type condenser followed by two auxiliary condensing units. The average time of pyrolysis was 45 minutes. Pyro-oil was recovered from the condenser and the auxiliary units after the experiment by rinsing with acetone. The non-condensable portion was scrubbed with water and NaOH solution before it was vented out. The solid residues were collected after cooling down the reactor to the room temperature and weighed in a precision weighing balance. The residues were crushed and sieved to recover the carbonaceous part. The glass fibres were found to be laden with carbon particles and they were inseparable. To recover the glass fibre, the pyrolyzed glass fibres were subjected to combustion at a temperature of 773 K which removed the carbon particles. The total mass of char was determined by summing up 1) the mass of free char and 2) that associated with glass fibre. The mass of the second part of char was determined by the difference of mass of (Glass fibre+ Char) and carbon-free glass fibre after combustion. The yield of pyro-oil, % recovery of glass fibre and metal mixture and yield of pyro-char were determined by Equation 4.39-4.42 using the values of collected mass of the corresponding product (pyro-oil, glass fibre, metal mixture and pyro-char) and initial mass of feed PCBs. The characterization of pyro-char and pyro-oil were performed through FESEM, EDX, XRD, FTIR and NMR, GC-MS, FTIR analyses respectively.

5.3 Results and Discussion

5.3.1 Proximate and Ultimate Analysis

Proximate analysis was carried out to determine the moisture, volatile matter, ash and fixed carbon of FR-2 & FR-4 VPCB and WPCBs. The result obtained from our study are presented in Table 5.1.

Table 5.1: Proximate Analysis Results of Feedstock

Sample	Moisture	Volatiles	Ash	Fixed Carbon
FR-2 VPCB	1.27	24.8	25.3	48.2
FR-2 WPCB	2	21.30	33	43.70
FR-4 VPCB	1.5	25.32	69.5	3.68
FR-4 WPCB	0.50	24.25	73.2	2.05

The elemental analysis of FR-2 & FR-4 VPCB and WPCBs has been carried out in order to obtain the percentage of carbon, hydrogen and nitrogen present in it. The analysis results are presented in Table 5.2.

Table 5.2: Ultimate Analysis Results of Feedstock

Sample	Carbon	Hydrogen	Nitrogen	Sulphur	Bromine
FR-2 VPCB	49.73	4.289	3.39	0.366	12.12
FR-2 WPCB	42	6.3	1.7	0.266	4.32
FR-4 VPCB	42.54	3.823	0.15	0.216	1.42
FR-4 WPCB	24.83	0.412	0.58	0.325	5.98

5.3.2 Lumped Kinetics

5.3.2.1 Lumped Kinetics of FR-2 WPCB

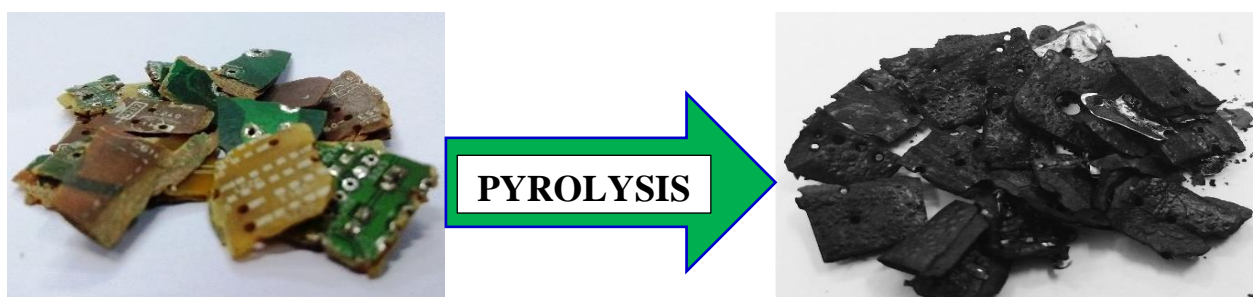


Figure 5.1: FR-2 WPCBs before and after pyrolysis

The lumped kinetics of the FR-2 type WPCBs were determined experimentally in a pyrolyzer in batch mode. Figure 5.1 shows the before and after pyrolysis samples of FR-2 WPCB. Experiments of

pyrolysis were carried out in an inert atmosphere at varying temperatures ranging within 573 – 973 K. The changes in weight were recorded in 2 minutes interval. The recorded data from the experiments were used for the kinetic studies. The kinetic rate constants and the activation energy were estimated using the method proposed by Bandopadhyay et al. (1999).

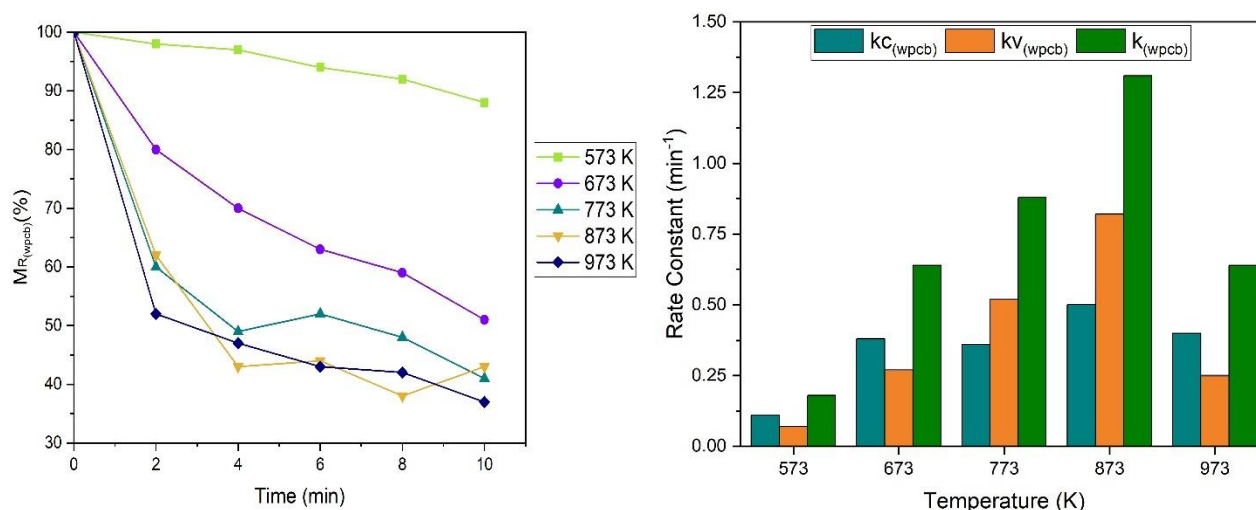


Figure 5.2 (a): Weight loss profile and (b) Kinetic Constants of FR-2 WPCB pyrolysis

Table 5.3 Data of weight loss profile of FR-2 WPCB pyrolysis at different temperature

Time (min)	Weight of Residue ($M_{R(wpcb)}$) (%)				
	573 K	673 K	773 K	873 K	973 K
0	100	100	100	100	100
2	98	80	60	62	52
4	97	70	49	43	47
6	94	63	52	44	43
8	92	59	48	38	42
10	88	51	41	43	37

Table 5.4 Data of Kinetic Constants of FR-2 WPCB pyrolysis

Temperature (K)	kc	kv	k
	(min ⁻¹)		
573	0.11	0.07	0.18
673	0.38	0.27	0.64
773	0.36	0.52	0.88
873	0.5	0.82	1.31
973	0.4	0.25	0.64

Figure 5.2 (a) shows a decreasing profile with time which is evident as mass loss increases with residence time. The data is presented in table 5.3. The study reveals that the decomposition reaction

follows the first order kinetics with respect to the reactant and the temperature dependence of the rate constant is administered by Arrhenius equation. The activation energy and the frequency factor have been determined to be 27.39 kJ/mole and 57.32 min⁻¹ respectively. These values are much lower compared to reported literature.

As can be seen from figure 5.2 (b), the $k_{v(wpcb)}$, $k_{c(wpcb)}$ and k_{wpcb} values have increased with temperature till 873K. The data of figure 5.2 (b) is presented in table 5.4. At 973K, these values have decreased. However, the value of $k_{c(wpcb)}$ obtained at 773K is less than the value of $k_{c(wpcb)}$ obtained at 673K. Within the temperature range of 573 – 673K the $k_{c(wpcb)}$ values are higher than the $k_{v(wpcb)}$ value. Beyond 873K, similar phenomenon is observed. This implies that the rate of char formation is higher than the rate of volatilisation in these regions. A reverse phenomenon is observed within the temperature range of 773 – 873K. In this case, the value of $k_{v(wpcb)}$ values are higher than the value of $k_{c(wpcb)}$. These non-linearity of kinetic rate constant values indicate that the activation energies are possibly distributed over the conversion range. It also indicates that beyond 873K, the pyrolysis process may not be guided by solely kinetics, other driving forces, such as mass transfer could be controlling the rate. These are further unveiled later in section 5.3.5 and 5.7.

5.3.2.2 Lumped Kinetics of FR-4 WPCB

The lumped kinetics of the FR-4 type WPCBs were determined experimentally in a pyrolyzer in batch mode similar to FR-2 WPCB. Figure 5.3 shows the before and after pyrolysis samples of FR-4 WPCB

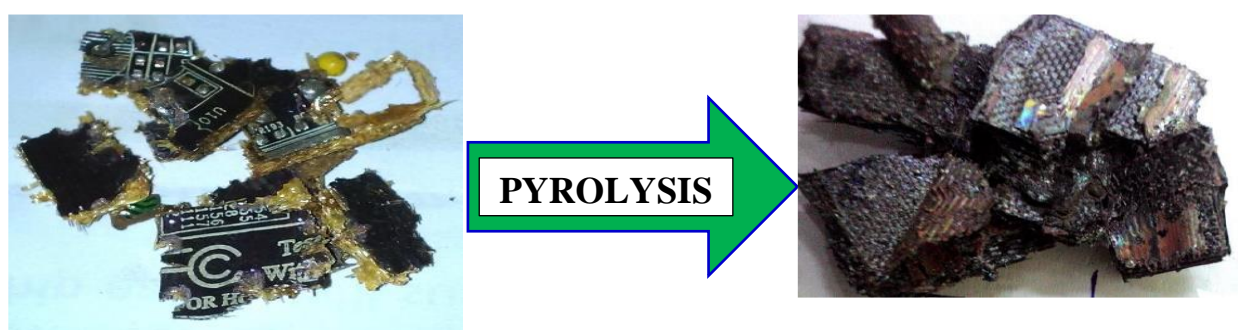


Figure 5.3: FR-4 WPCBs before and after pyrolysis

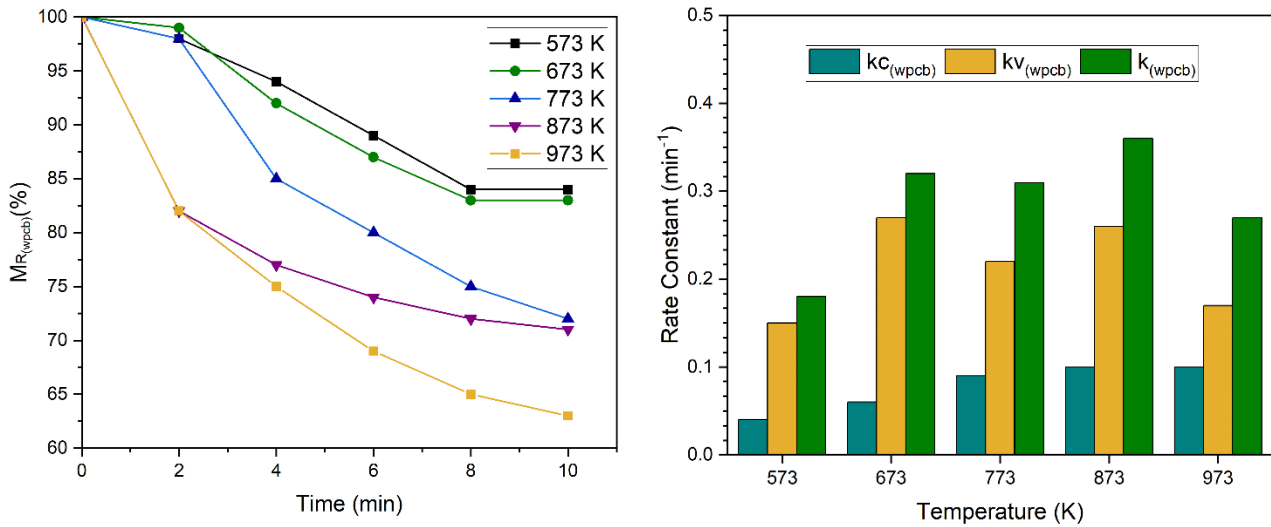


Figure 5.4 (a): Weight loss profile and (b) Kinetic Constants of FR-4 WPCB pyrolysis

Table 5.3 Data of weight loss profile of FR-4 WPCB pyrolysis at different temperature

Time (min)	Weight of Residue ($M_{R(wpcb)}$) (%)				
	573 K	673 K	773 K	873 K	973 K
0	100	100	100	100	100
2	98	99	98	82	82
4	94	92	85	77	75
6	89	87	80	74	69
8	84	83	75	72	65
10	84	83	72	71	63

Table 5.4 Data of Kinetic Constants of FR-2 WPCB pyrolysis

Temperature (K)	k_c	k_v	k
	(min^{-1})		
573	0.04	0.15	0.18
673	0.06	0.27	0.32
773	0.09	0.22	0.31
873	0.1	0.26	0.36
973	0.1	0.17	0.27

Figure 5.4 (a) shows a decreasing profile with time which is evident as mass loss increases with residence time. The data is presented in table 5.3. The study reveals that the decomposition reaction follows the first order kinetics with respect to the reactant and the temperature dependence of the rate constant is administered by Arrhenius equation. The activation energy and the frequency factor have been determined to be 11.5 kJ/mole and 0.44 min^{-1} respectively.

As can be seen from figure 5.4 (b), the $k_{v(wpcb)}$, $k_{c(wpcb)}$ and k_{wpcb} values have increased with temperature till 873K. The data of figure 5.4 (b) is presented in table 5.4. At 973K, the value of $k_{c(wpcb)}$ becomes constant, but the values of $k_{v(wpcb)}$ and k_{wpcb} decreases. Over the whole range of temperature, no particular pattern of k values has been observed. In addition to that, $k_{v(wpcb)}$ values are higher than the $k_{c(wpcb)}$ values implying higher rate of volatilization. These non-linearity of kinetic rate constant values indicate that the activation energies are possibly distributed over the conversion range. These anomalies found can be attributed to the catalytic effect of the in-situ metals in the PCBs as well.

5.3.3. Thermogravimetric Analysis

5.3.3.1 FR-2 Virgin PCB

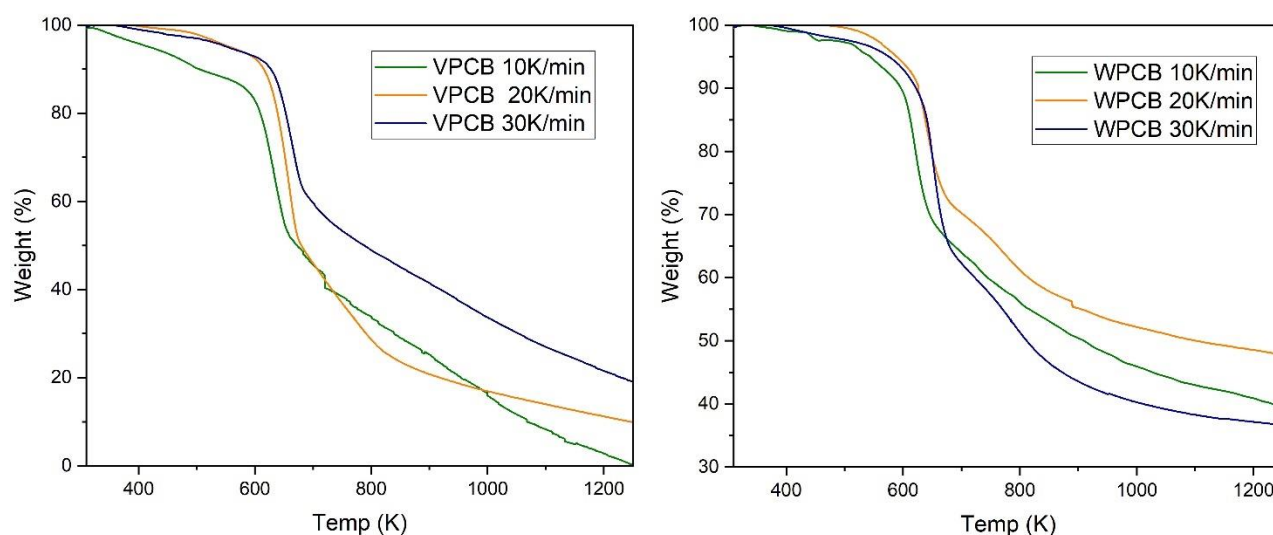


Figure 5.5: TG curve of FR-2 WPCB and VPCB at 10, 20 and 30K per min

The profiles of thermogravimetry (TG) and derivative thermogravimetry (DTG) of VPCB and WPCB at three heating rates are exhibited in Figures 5.5 and 5.6 respectively. In the case of VPCBs, the thermal pyrolysis process occurs in three stages 308 – 610 K, 610 – 720 K, and 720 – 1250 K. The mass loss at three heating rates has been determined as 7.65–14.95%, 31.18–44.74%, and 39.4–41.65% for these stages, respectively. Since FR-2 PCB is a phenolic resin-based material three-stage degradation mechanism proposed by Trick and Saliba is the best representative (Trick and Salida 1995; Wang et al. 2021). Stage 1 is the primary decomposition stage where the material is heated up, moisture is removed and it starts to degrade as condensation reaction between phenolic hydroxyl groups or methylene ($-\text{CH}_2-$) groups occurs (Wang et al. 2021). In stage 2, major weight loss is observed where ether bonds and methylene bonds are ruptured which produces methane, carbon monoxide, and hydrogen (Wang et al. 2021). Degradation of TBBPA also occurs in this stage which produces

Bisphenol A and other phenolic derivatives (Evangelopoulos et al. 2015). In the third stage, the phenolic resin undergoes degradation. In addition to that, hydrogen atoms get separated from the carbon skeleton which generates a carbonaceous residue and hydrogen (Wang et al. 2021).

From Figure 5.5 (b), the peak temperatures are observed at 665K, 669K, and 685K for three heating rates respectively. It can be observed that the peak temperature is shifting to a higher value with increase in heating rate. Similar phenomenon has been observed for waste biomass (Cortés et al. 2015) and coal samples (Song et al. 2016). This phenomenon can be mainly accredited to the heat and mass transport constraints, which gives rise to temperature gradients within the sample itself and inside each particle.

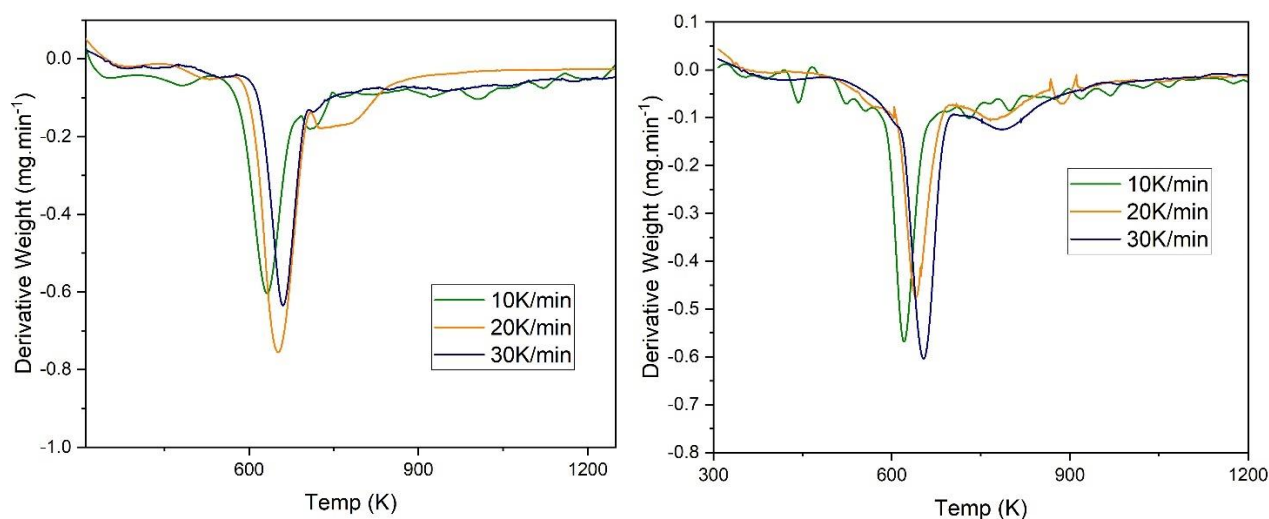


Figure 5.6 (a): DTG curve of FR-2 WPCB and (b) VPCB at 10, 20 and 30K per min

5.3.3.2 FR-2 Waste PCB

In the case of WPCBs, it is observed that thermal pyrolysis process is split into three stages 308 – 580 K, 580 – 690K, and 690 – 1250 K. The mass loss at three heating rates have been determined as 3.39 – 4.05%, 24.33–32.71% and 23.61–27.85% for these stages, respectively. The thermal degradation mechanism has been elucidated in the above subsection. From Figure 5.6 (a), the peak temperatures for WPCB have been observed at 621K, 641K, and 655K for three heating rates respectively. Hao et al. (2014) have reported observed peak temperature at 631 K. The peak temperature shift is similar to the case of VPCB and the reason remains unaltered.

5.3.3.3 FR-4 Virgin PCB

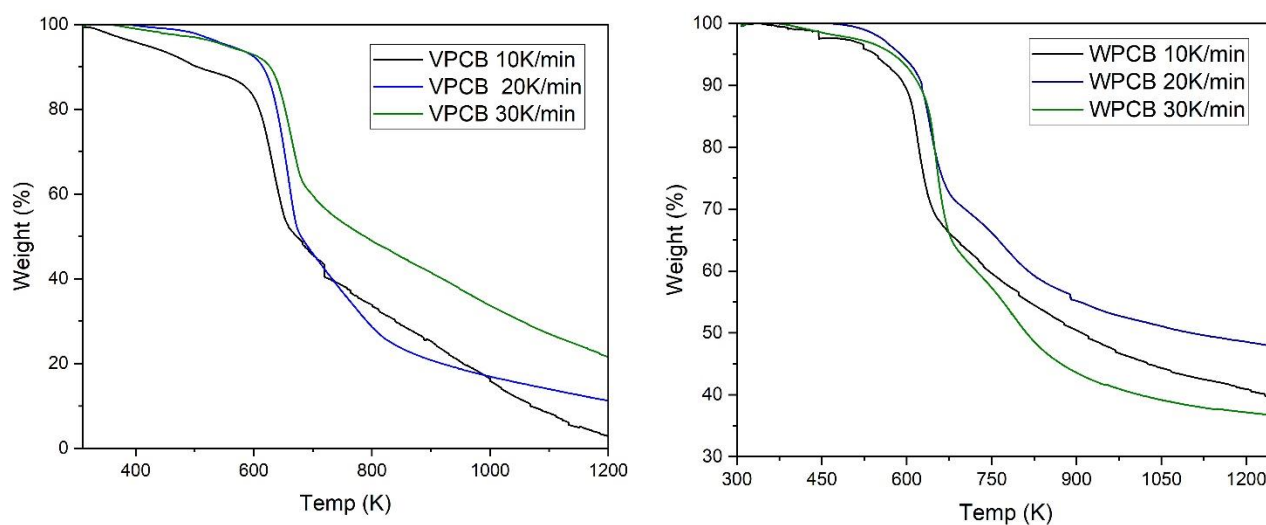


Figure 5.7: TG curve of FR-4 VPCB and WPCB at 10, 20 and 30K per min

The thermogravimetry (TG) and derivative thermogravimetry (DTG) profiles of FR-4 VPCB and WPCBs at different heating rates are displayed in Figures 5.7 and 5.8 respectively. The pyrolysis of VPCBs takes place in three stages 308 – 640 K, 640 – 823 K, and 823 – 1250 K. The mass loss has been determined as 2.98–4.64%, 46.74–62.34%, and 8.89–14.63% respectively for these stages at three heating rates. FR4 PCB is an epoxy resin-based material which undergoes degradation in three-stages (Wang et al. 2021). The primary decomposition occurs in stage 1 where the material is heated to remove any moisture and the material just starts to degrade. The highest mass loss occurs in stage 2 where the ether bonds disintegrate to form bisphenol A, propyl alcohol and tetrabromobisphenol A. Additionally, the epoxy group breaks down to smaller molecules. At higher temperature, tetrabromobisphenol A undergoes further decomposition which produces methane, carbon monoxide, and hydrogen. (Evangelopoulos et al., 2015; Yao et al. 2020). In stage 3, hydrogen atoms get separated from the carbon skeleton which generates a carbonaceous residue and hydrogen. In this stage, there is some amount of mass loss but the decomposition rate saturates towards higher temperature with a very small conversion rate.

The DTG curve (Figure 5.8a) indicates the two significant weight losses occurring during the pyrolysis process with maximum decomposition temperature zone at 610 – 630K and 650 – 730K. This is more prominent for $\beta=10\text{K/min}$. These results are in line with reported literature (Barontini et al., 2015; Ciecierska et al., 2016; Yao et al. 2020). The peak temperatures are observed at 633K, 659K and 667K for three heating rates respectively. This indicates that the peak temperature is shifting towards higher value with increase in heating rate. This phenomenon occurs as at higher temperature diffusion of volatiles are inhibited which translates to heat and mass transport constraints.

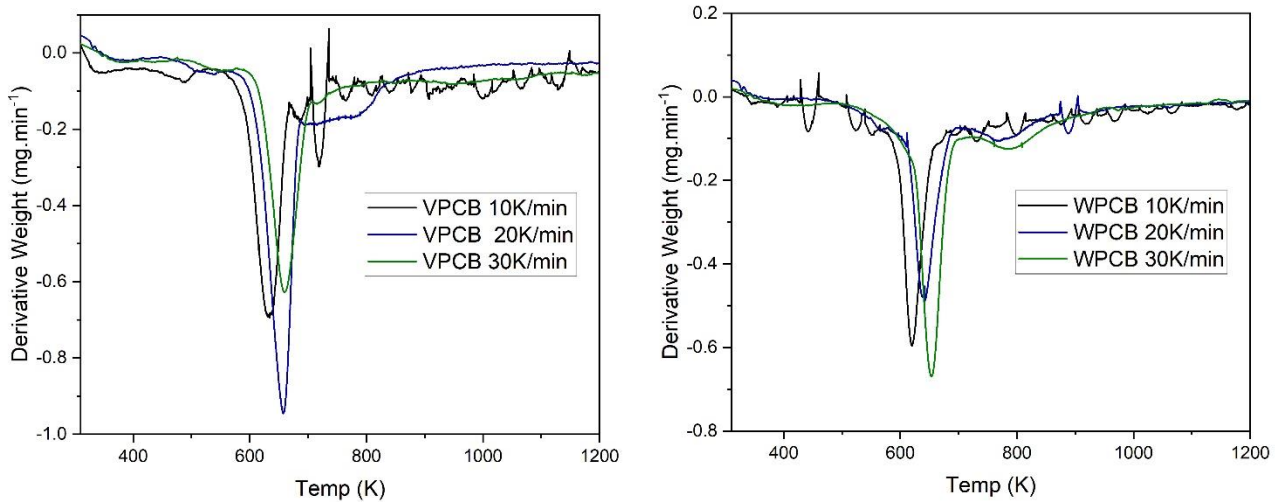


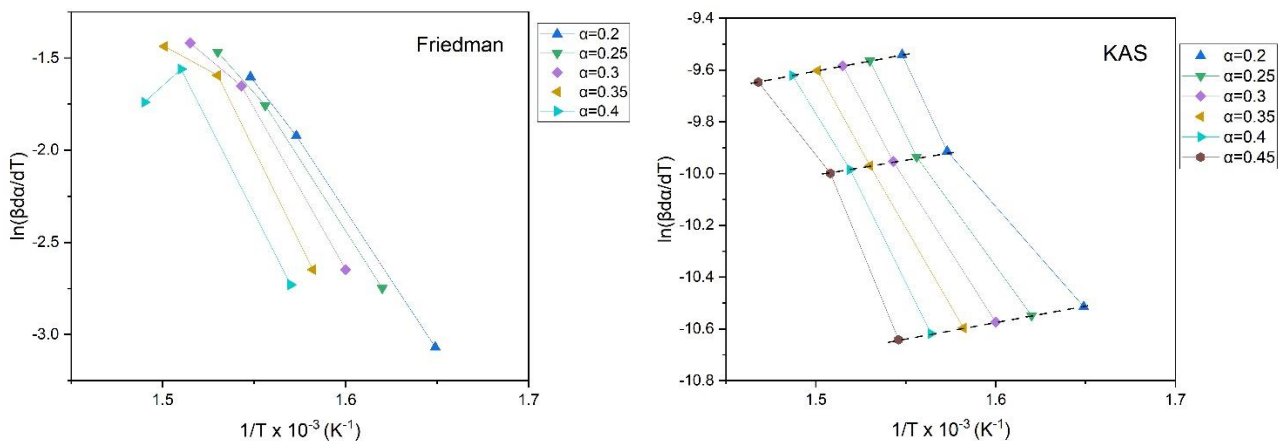
Figure 5.8 (a): DTG curve of FR-4 VPCB and (b) WPCB at 10, 20 and 30K per min

5.3.3.4 FR-4 Waste PCB

The three stages FR-4 WPCB pyrolysis process is split into three stages 308 – 654 K, 654 – 718K, and 718 – 1250 K. The mass loss has been determined as 2.18–8.16%, 12.12–18.45%, and 11.41–13.93% respectively for these stages at three heating rates. In case of WPCB, the overall mass loss is restricted to 40% compared to 80% in case of VPCBs. This is attributed to the heterogeneity of WPCBs as the assortment of metals present in WPCBs are more than VPCBs. The thermal degradation mechanism has been elucidated in the above subsection. From Figure 5.8(b), the peak temperatures for WPCB have been observed at 628K, 658K and 691K for three heating rates respectively. Reported literature have observed peak temperature at 631 K (Hao et al. 2014). The peak temperature shift is similar to the case of VPCB and the reason remains the same.

5.3.4. Iso-conversional Kinetics

5.3.4.1 Kinetic Analysis of FR-2 type VPCB



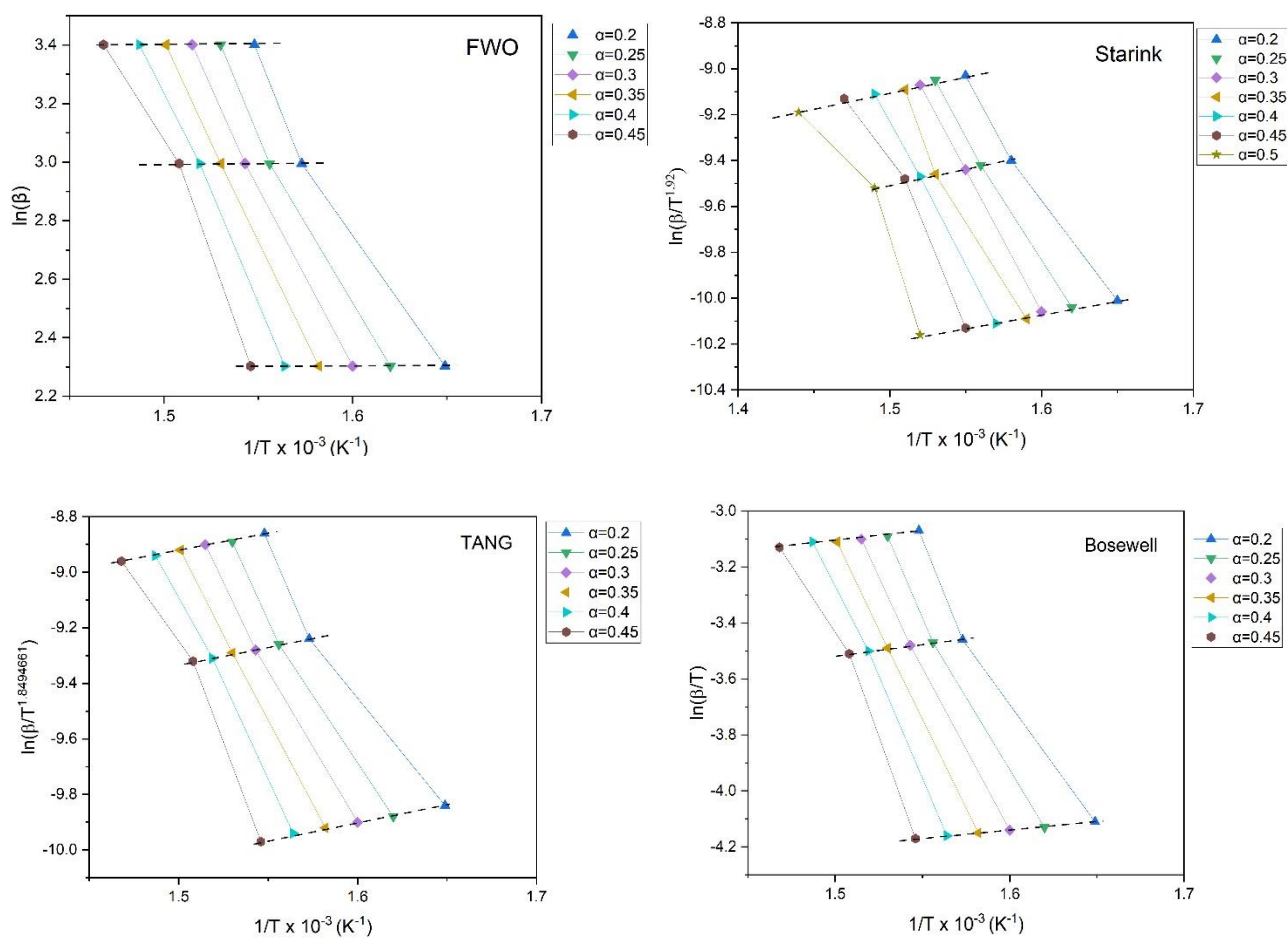


Figure 5.9: Kinetic Plot for determination of kinetic parameters using (a) Friedman, (b) KAS, (c) FWO, (d) Starink, (e) Tang and (f) Bosewell method for FR-2 VPCB pyrolysis

Figure 5.9 (a-f) shows the linear fitting obtained through the Friedman, KAS, FWO, Starink, Tang and Bosewell methods. Parallel straight lines have been obtained with satisfactory regression coefficients i.e., 0.94–0.99 for Friedman, 0.93 – 0.99 for KAS, 0.95 – 0.99 for FWO, 0.93 – 1 for Starink, 0.95 – 1 for Tang and 0.95 – 1 for Bosewell. The low R^2 value for $\alpha > 0.45$ for all methods, except Friedman method ($\alpha > 0.35$), can be accredited to the variation of thermal disintegration process with increase in the heating rate. Additionally, the mass interval of sample is often defined arbitrarily. In other words, the values of initial (w_i) and final mass (w_f) of the substrate is not clearly explained, which induces further uncertainty in the system (Anca-Couche et al. 2014; Alves et al. 2014). The E_a values in the range of $\alpha=0.1$ to 0.15 are not reliable due to lower R^2 values which might result from slow conversion rate of FR-2 VPCB. In other words, at a lower temperature, the energy is not enough to initiate the rupture of bonds. Thereafter, the temperature increases to break the molecules resulting in the straight line beyond the conversion of 0.15. At $\alpha > 0.5$ (for Friedman $\alpha > 0.4$) the undesirable R^2 values indicates complex decomposition of the substrate.

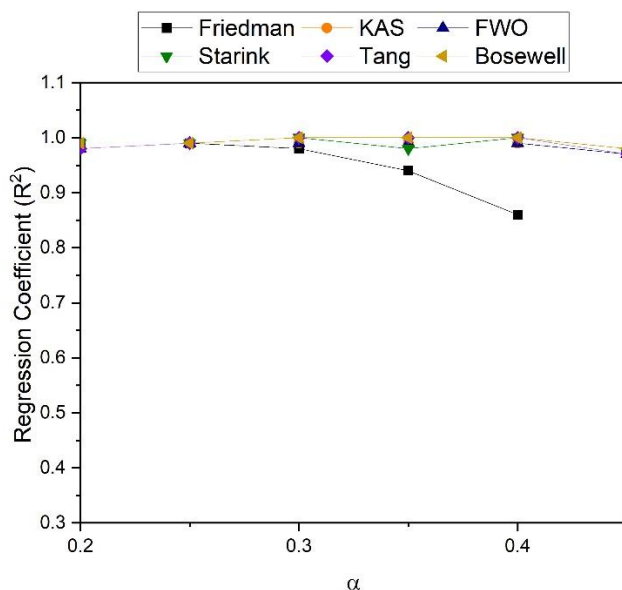


Figure 5.10: Plot of R^2 vs Conversion (α) using Friedman, KAS, FWO, Starink, Tang and Bosewell method for FR-2 VPCB pyrolysis

Parallel straight lines are attained in the 0.15 to 0.45 conversion range (for Friedman $0.15 < \alpha < 0.35$ range) (Figure 5.9). The parallel profile of the acquired straight lines signifies that the activation energies are distributed in close vicinity. Conversely, at lower ($\alpha = 0.1-0.15$) and higher ($\alpha > 0.5$) conversion ranges signify the possibility distinctly different pyrolysis reactions occurring compared to those happening at the intermediate range i.e., $\alpha = 0.2-0.45$. It is usual that the conversion up to 0.15 symbolizes mainly the exclusion of moisture and the starting point of the primary pyrolysis of phenolic resin. Again, at middle to higher conversion levels ($\alpha > 0.5$), the pyrolysis of major components leads towards rupture of ether and methylene bonds following a certain pattern, perhaps significantly dominated primary pyrolysis of phenolic resins.

5.3.4.2 Analysis of Activation Energies of FR-2 VPCB

The values of E_a , obtained are displayed in Table 6.3 and figure 6.7 for all six methods. Figures 5.10 and 5.11 (a) display the development of E_a with fitting correlation coefficients (R^2) and conversion with the conversion for the Friedman, KAS, FWO, Starink, Tang and Bosewell methods respectively. In case of Friedman method, it is observed that the values of E_a increase from 114.33 kJ/mol ($\alpha = 0.15$) to 129.53 kJ/mol ($\alpha = 0.35$) then decreases. The values of E_a beyond $\alpha = 0.4$ are not reliable. In case of KAS method, the values of E_a follow an increasing trend from 47.47 kJ/mol ($\alpha = 0.15$) to 105.82 kJ/mol ($\alpha = 0.45$). The values of E_a in the remaining range are not reliable. In case of, FWO method the values of E_a increase from 54.69 kJ/mol ($\alpha = 0.15$) to 113.83 kJ/mol ($\alpha = 0.4$) then decrease to 110.96 kJ/mol ($\alpha = 0.45$). Starink, Tang and Bosewell methods produce similar trend to KAS and

FWO (Figure 6.7 b). For Starink method, Ea values increase from 49.22 kJ/mol ($\alpha = 0.15$) to 104.1 kJ/mol exponentially ($\alpha = 0.4$) then decrease to 103.85 kJ/mol ($\alpha = 0.45$). In case of Tang method, Ea values increase from 48.47 kJ/mol ($\alpha = 0.15$) to 108.37 kJ/mol exponentially ($\alpha = 0.4$) then decrease to 107.22 kJ/mol ($\alpha = 0.45$). Bosewell method follows the same trend as well with Ea values in the range of 52.63 kJ/mol ($\alpha = 0.15$) to 113.99 kJ/mol ($\alpha = 0.4$) then decreasing to 110.58 kJ/mol ($\alpha = 0.45$). Beyond $\alpha = 0.55$, the Ea values are not reliable.

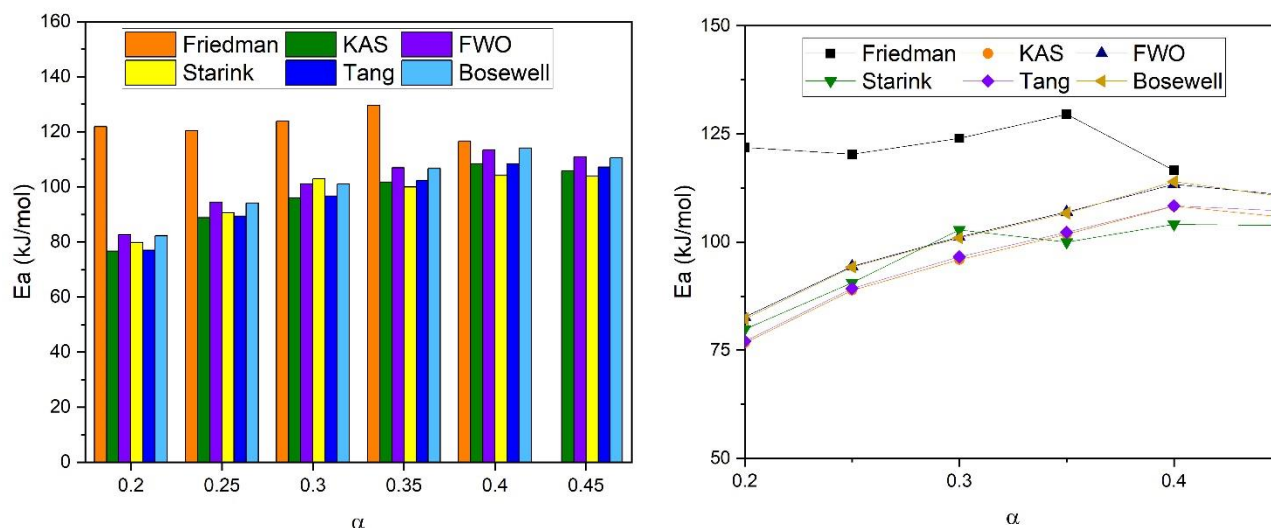


Figure 5.11 (a): Comparison of Activation Energies and (b) Evolution trend of Activation Energies obtained using Friedman, KAS, FWO, Starink, Tang and Bosewell method for FR-2 WPCB pyrolysis

Table 5.5: The Kinetic Parameters determined using Friedman, KAS, FWO, Tang, Starink and Bosewell method for FR-2 VPCB Pyrolysis

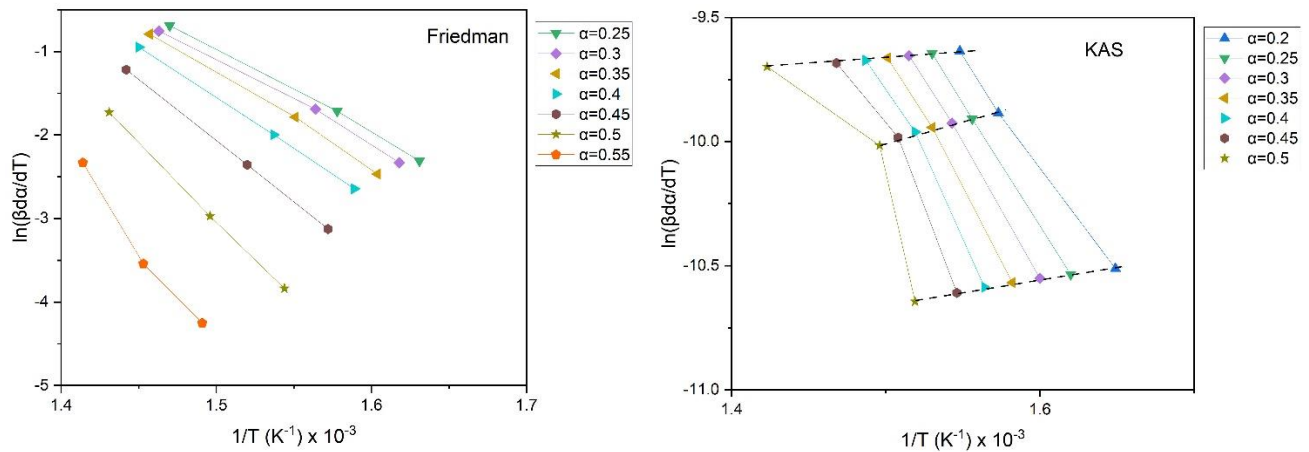
α	Friedman		KAS		FWO		STARINK		TANG		BOSEWELL	
	Ea (kJ/mol)	R ²	Ea (kJ/mol)	R ²	Ea (kJ/mol)	R ²	Ea (kJ/mol)	R ²	Ea (kJ/mol)	R ²	Ea (kJ/mol)	R ²
0.15	114.33	0.99	47.47	0.93	54.69	0.95	49.22	0.92	48.47	0.94	52.63	0.95
0.2	121.86	0.99	76.68	0.98	82.67	0.98	79.82	0.99	77.05	0.98	82.23	0.99
0.25	120.30	0.99	88.84	0.99	94.37	0.99	90.6	0.99	89.27	0.99	94.2	0.99
0.3	124	0.98	95.92	0.99	101.16	0.99	102.83	1	96.59	1	100.94	1
0.35	129.53	0.95	101.81	0.99	106.93	0.99	100.01	0.98	102.27	1	106.67	1
0.4	116.56	0.86	108.3	0.99	113.33	0.99	104.1	1	108.37	1	113.99	1
0.45	-	-	105.82	0.97	110.96	0.97	103.85	0.97	107.22	0.97	110.58	0.98

The progressive increase of the activation energy ($\alpha = 0.15 - 0.45$) indicates the huge array of bonds and the multiphasic nature of its conversion. It may also signify the occurrence of competitive or consecutive reactions (Carrier et al. 2016). These variations in the values might be a consequence of the variation in raw materials and equipment. The fitting correlation coefficients (R²) are over 0.95 in

the conversion range of 0.15 – 0.45 for all methods except Friedman method. It has been observed that at $\alpha = 0.4$ for Friedman method, the fitting co-efficient is not good. The anomaly might have been the result of experimental errors in monitoring the mass which is because of the minute alterations at these phases and material heterogeneity. The average Ea values have been determined as 121.1, 89.26, 94.87, 90.06, 89.89 and 94.46 kJ/mol for Friedman, KAS, FWO, Starink, Tang and Bosewell methods respectively.

5.3.4.3 Kinetic Analysis of FR-2 type WPCB

Figure 5.12 (a-f) shows the linear fitting obtained through the Friedman, KAS, FWO, Starink, Tang and Bosewell methods. The parallel straight lines obtained offer satisfactory regression coefficients i.e., 0.98–1 for Friedman, 0.94 – 0.99 for KAS, 0.88 – 0.98 for FWO, 0.93 – 1 for Starink, 0.9 – 1 for Tang and 0.9 – 1 for Bosewell. The low R^2 value for $\alpha > 0.55$ for all (except KAS) methods can be accredited to the alteration of thermal breakdown mechanism with the increasing heating rate. Similar to VPCB, the tricky definition of the mass interval, also plays a part here (Anca-Couche et al. 2014). The undesirable R^2 values in the range $\alpha=0.1 – 0.15$ indicates a slow conversion rate of FR2 WPCB. A larger gap between the lines at $\alpha > 0.4$ is also noticed and this indicates the change of the thermal decomposition mechanism.



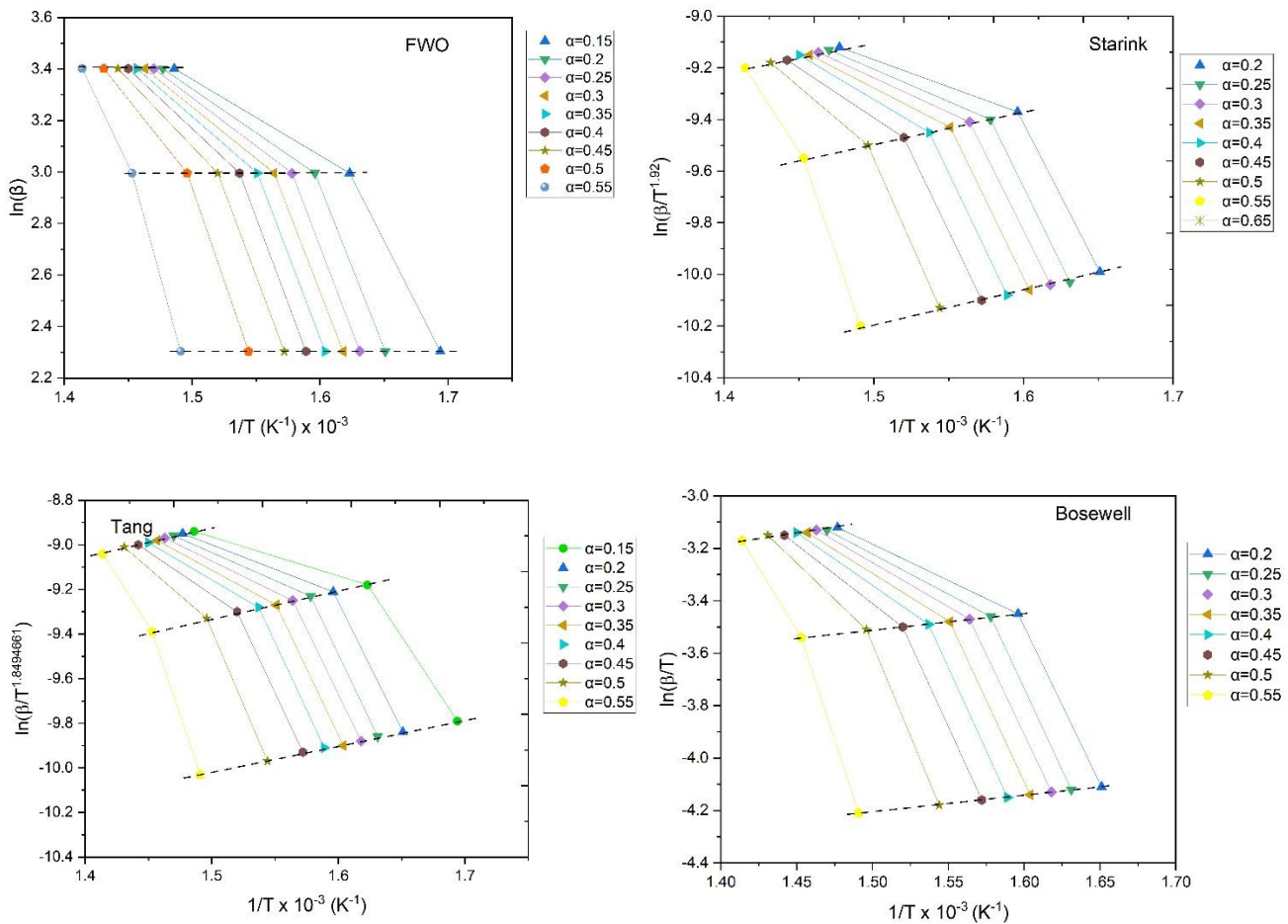


Figure 5.12: Kinetic Plot for determination of kinetic parameters using (a) Friedman, (b) KAS, (c) FWO, (d) Starink, (e) Tang and (f) Bosewell method for FR-2 WPCB pyrolysis

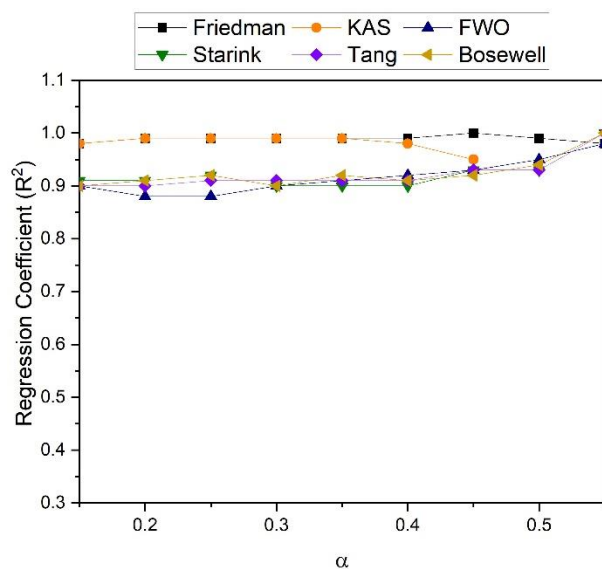


Figure 5.13: Plot of R^2 vs Conversion (α) using Friedman, KAS, FWO, Starink, Tang and Bosewell method for WPCB pyrolysis

In the 0.2 to 0.5 conversion range (Figure 5.12), parallel lines have been obtained for all six methods which suggests close distribution of activation energies. Conversely, at lower (0.1–0.15) and higher (> 0.5) ranges lower R^2 values indicate the possibility of distinctly different pyrolysis reactions occurring compared to those happening at the intermediate range i.e., $\alpha = 0.2$ –0.5. Conversion up to 0.2 symbolizes typically the elimination of moisture and the beginning of primary condensation of phenolic and methylene groups. Alternatively, at higher conversion levels ($\alpha > 0.45$) the pyrolysis of intermediates occurs.

5.3.4.4 Analysis of Activation Energies for FR-2 WPCB.

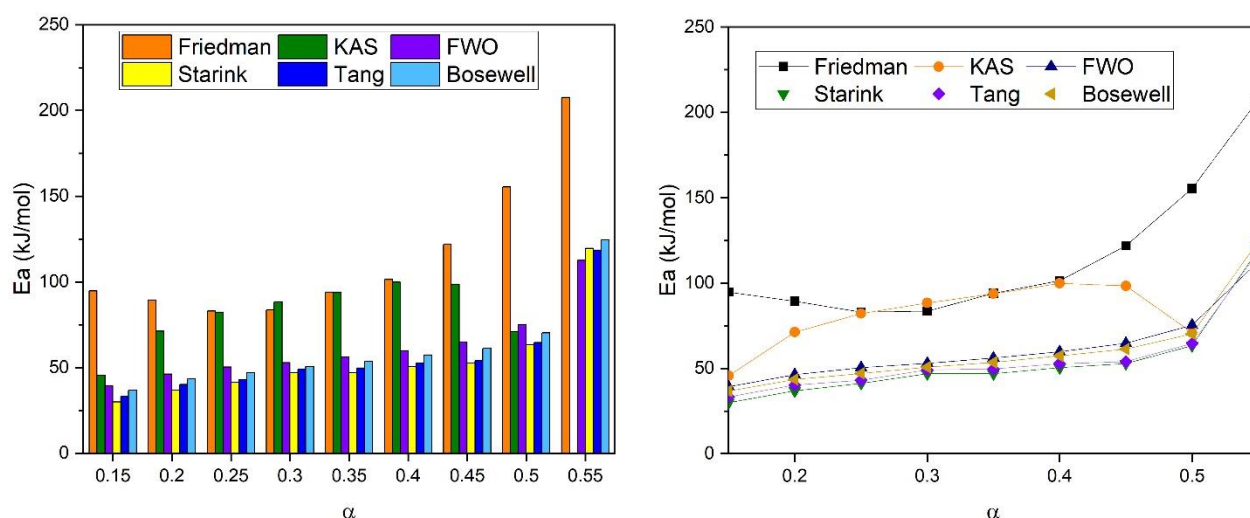


Figure 5.14 (a): Comparison of Activation Energies and (b) Evolution trend of Activation Energies obtained using Friedman, KAS, FWO, Starink, Tang and Bosewell method for FR-2 WPCB pyrolysis

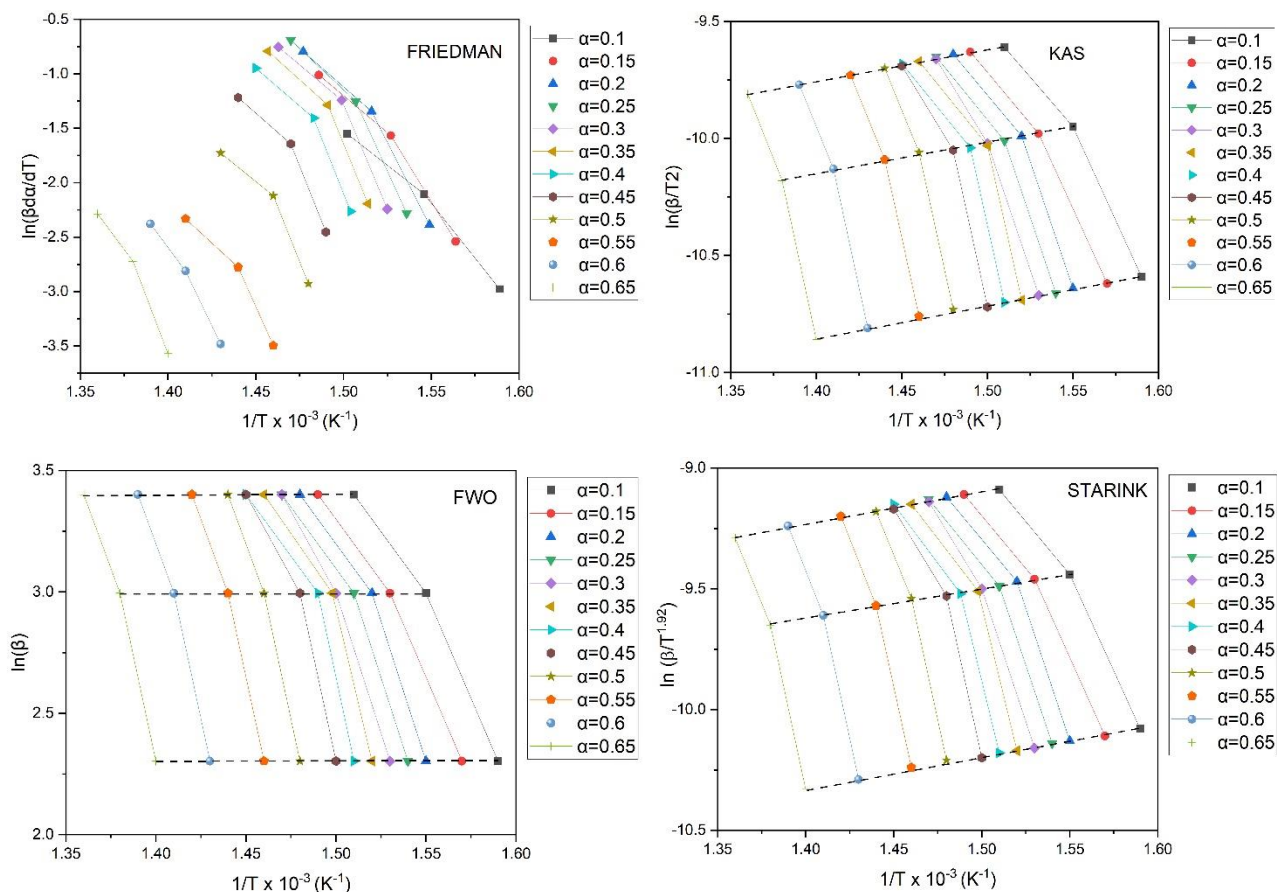
The values of E_a are displayed in Figure 5.14 (a). Figures 5.14 (b) display the development of E_a collectively for Friedman, KAS, FWO, Starink, Tang and Bosewell methods respectively. As can be seen, in Friedman method, the E_a values increases exponentially from 82.99 kJ/mol ($\alpha = 0.25$) to 207.43 kJ/mol linearly ($\alpha = 0.55$). Similar exponential profile is obtained in FWO method as well where E_a values increase from 46.24 kJ/mol ($\alpha = 0.2$) to 112.54 kJ/mol linearly ($\alpha = 0.55$). In case of KAS method, the plot profile is similar to the VPCB case. E_a values increase from 71.27 kJ/mol ($\alpha = 0.2$) to 99.84 kJ/mol ($\alpha = 0.4$) then decreases to 98.33 kJ/mol ($\alpha = 0.45$). In case of Starink, Tang and Bosewell methods, the trends resemble that of FWO methods but the values are closely distributed (Figure 5.14b). For Starink method, E_a values increase from 36.78 kJ/mol ($\alpha = 0.2$) to 119.56 kJ/mol exponentially ($\alpha = 0.55$). In case of Tang method, 40.19 kJ/mol ($\alpha = 0.2$) to 118.25 kJ/mol exponentially ($\alpha = 0.55$). Bosewell method follows the same trend as well with E_a values in the range of 43.49 kJ/mol ($\alpha = 0.2$) to 124.38 kJ/mol ($\alpha = 0.55$). The exponential increase of activation energy is illustrative of the large assortment of bonds and the multiphasic nature of its conversion

corresponding to consecutive reactions (Carrier et al. 2016). The differences in the values might be caused by the heterogeneity of the WPCBs and equipment noise. The average Ea values have been determined as 116.99, 88.94, 64.73, 57.24, 58.93 and 63.52 kJ/mol for Friedman, KAS, FWO, Starink, Tang and Bosewell methods respectively.

Table 5.6: The Kinetic Parameters determined using Friedman, KAS, FWO, Tang, Starink and Bosewell method for FR-2 WPCB Pyrolysis

α	Friedman		KAS		FWO		STARINK		TANG		BOSEWELL	
	Ea (kJ/mol)	R ²	Ea (kJ/mol)	R ²	Ea (kJ/mol)	R ²	Ea (kJ/mol)	R ²	Ea (kJ/mol)	R ²	Ea (kJ/mol)	R ²
0.2	89.30	0.99	71.27	0.99	46.24	0.88	36.78	0.91	40.19	0.9	43.49	0.91
0.25	82.99	0.99	82.10	0.99	50.35	0.88	41.2	0.92	43.05	0.91	47.06	0.92
0.3	83.58	0.99	88.34	0.99	52.88	0.9	46.93	0.9	49.09	0.91	50.72	0.90
0.35	93.95	0.99	93.76	0.99	56.12	0.91	46.93	0.9	49.67	0.91	53.55	0.92
0.4	101.33	0.99	99.84	0.98	59.75	0.92	50.43	0.9	52.72	0.91	57.37	0.91
0.45	121.91	1	98.33	0.95	64.73	0.93	52.77	0.93	53.91	0.93	61.36	0.92
0.5	155.39	0.99	70.86	0.79	75.24	0.95	63.34	0.93	64.59	0.93	70.26	0.94
0.55	207.43	0.98	48.59	0.45	112.54	0.98	119.56	1	118.25	1	124.38	1

5.3.4.5. Kinetic Analysis of FR-4 type VPCB



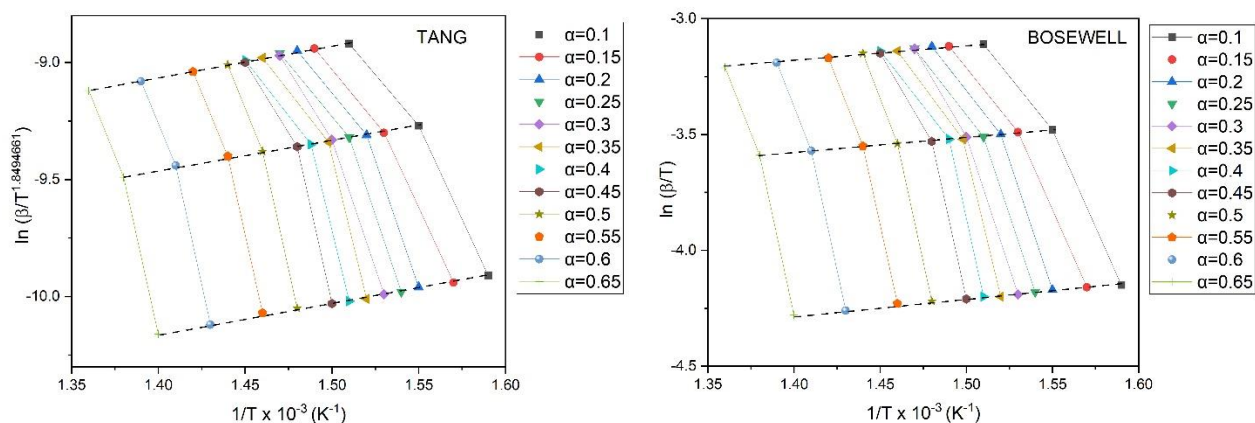


Figure 5.15: Kinetic Plot for determination of kinetic parameters using (a) Friedman, (b) KAS, (c) FWO, (d) Starink, (e) Tang and (f) Bosewell method for FR-4 VPCB pyrolysis

Figure 5.15 (a-f) shows the linear fitting obtained through the Friedman, KAS, FWO, Starink, Tang and Bosewell methods. Parallel straight lines have been obtained with satisfactory regression coefficients i.e., 0.91–0.99 for Friedman, 0.9 – 0.97 for KAS, 0.9 – 0.98 for FWO, 0.9 – 0.97 for Starink, 0.9 – 0.98 for Tang and 0.91 – 0.98 for Bosewell. The low R^2 value for $\alpha > 0.65$ in all six methods, can be accredited to the variation of thermal disintegration process with increase in the heating rate. Additionally, the mass interval of sample is often defined arbitrarily. In other words, the values of initial (w_i) and final mass (w_f) of the substrate is not clearly explained, which induces further uncertainty in the system (Anca-Couche et al. 2014; Alves et al. 2014). The gap between the straight lines around $\alpha=0.1$ to 0.2 indicates a slow conversion rate of FR4 VPCB. In other words, at a lower temperature, the energy is not enough to initiate the rupture of bonds. Thereafter, the temperature increases to break the molecules resulting in the straight line beyond the conversion of 0.2. A greater gap between the lines at $\alpha > 0.45$ is also noticed indicating the modification of thermal decomposition mechanism.

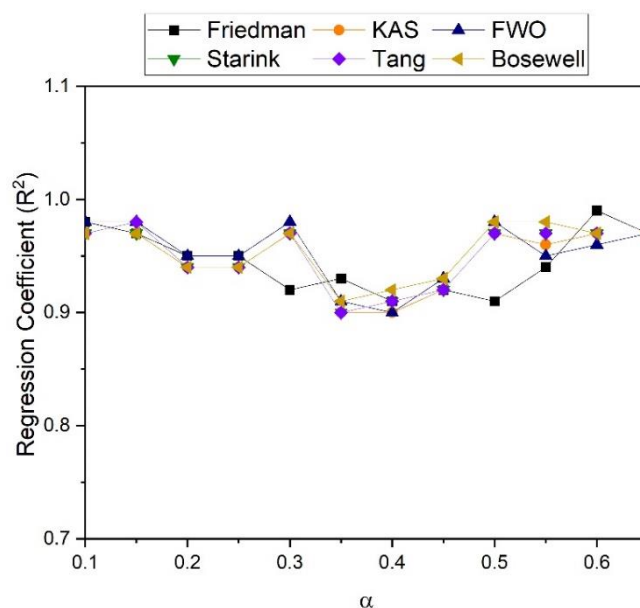


Figure 5.16: Plot of R^2 vs Conversion (α) using Friedman, KAS, FWO, Starink, Tang and Bosewell method for FR-4 VPCB pyrolysis

Parallel straight lines are attained in the 0.1 to 0.65 conversion range (Figure 5.15). The parallel profile of the acquired straight lines signifies that the activation energies are distributed in close vicinity. Conversely, the non-parallel association at lower (0.1–0.2) and higher (0.45–0.65) conversion ranges signify the possibility of the pyrolysis reactions. This trend is noticeably different from those happening at the previous intermediate-range i.e., $\alpha = 0.2$ –0.45. It is usual that the conversion up to 0.15 symbolizes mainly the exclusion of moisture and the starting point of the primary pyrolysis of epoxy resin. Again, at middle to higher conversion levels ($\alpha > 0.45$), signify dominated primary pyrolysis of epoxy resins.

5.3.4.6 Analysis of Activation Energies of FR-4 VPCB

The values of E_a , obtained are displayed in Table 5.7 for all six methods. Figures 5.15 (a – f) display the development of E_a simultaneously with the fitting correlation coefficients (R^2) for the Friedman, KAS, FWO, Starink, Tang and Bosewell methods respectively. In case of Friedman method, it is observed that the values of E_a increase from 136.35 kJ/mol ($\alpha = 0.05$) to 197.09 kJ/mol ($\alpha = 0.25$) followed by minuscule alteration until α reaches 0.5 (192.37 kJ/mol). The values of E_a beyond $\alpha = 0.55$ increases and reaches the highest value at $\alpha = 0.65$ i.e., 266.68 kJ/mol. In case of KAS method, the values of E_a increase from 101.85 kJ/mol ($\alpha = 0.1$) to 165.63 kJ/mol ($\alpha = 0.45$) then again increases to 218.25 kJ/mol ($\alpha = 0.65$). The values of E_a in the remaining range are not reliable. FWO method produces similar trend to KAS method. The values of E_a increase from 108.47 kJ/mol ($\alpha = 0.1$) to 165.5 kJ/mol ($\alpha = 0.4$) then increases to 277.11 kJ/mol ($\alpha = 0.65$). Starink, Tang and Bosewell methods

produce similar trend to KAS and FWO. The Ea values lies within the range of 102.74 kJ/mol ($\alpha = 0.1$) to 222.4 kJ/mol ($\alpha = 0.65$). Overall highest activation energy values have been obtained in case of Friedman method. Activation energy values for $\alpha > 0.65$ are not reliable.

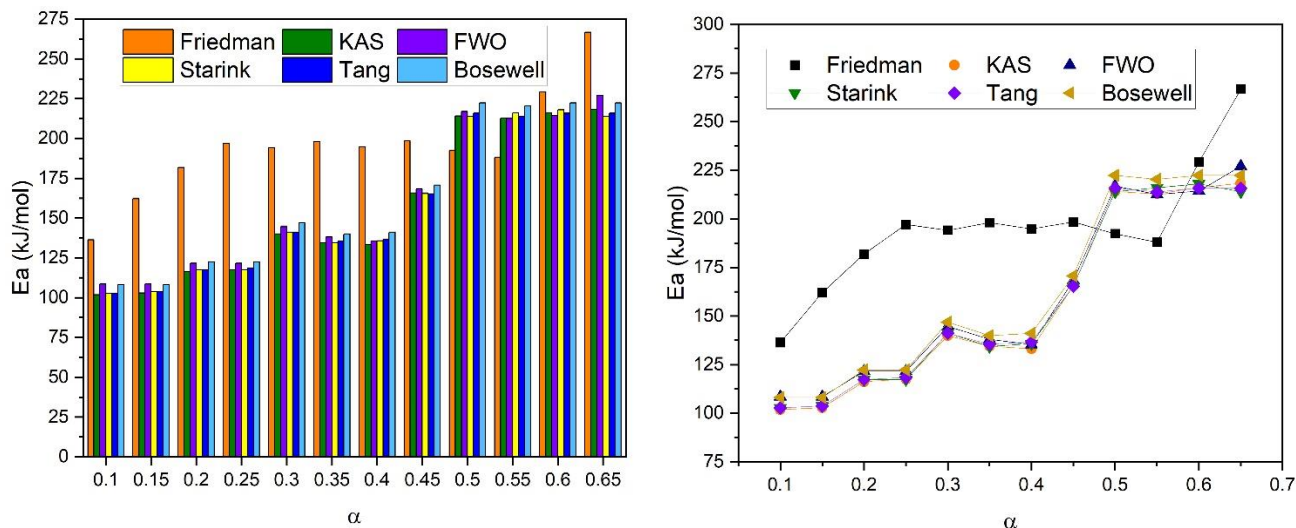


Figure 5.17 (a): Comparison of Activation Energies and (b) Evolution trend of Activation Energies obtained using Friedman, KAS, FWO, Starink, Tang and Bosewell method for VPCB pyrolysis

The progressive increase of the activation energy ($\alpha = 0.1 - 0.65$) indicates the huge array of bonds and the multiphasic nature of its conversion. It may also signify the occurrence of competitive or consecutive reactions (Carrier et al. 2016). These variations in the values might be a consequence of the variation in raw materials and equipment. The fitting correlation coefficients (R^2) are more than 0.9 throughout the range of $\alpha = 0.1 - 0.65$. The average activation energy has been determined as 194.94, 156.09, 159.79, 156.69, 156.87 and 162.44 kJ/mol for Friedman, KAS, FWO, Starink, Tang and Bosewell methods respectively.

Table 5.7: The Kinetic Parameters determined using Friedman, KAS, FWO, Tang, Starink and Bosewell method for FR-4 VPCB Pyrolysis

α	Friedman		KAS		FWO		STARINK		TANG		BOSEWELL	
	Ea (kJ/mol)	R^2	Ea (kJ/mol)	R^2	Ea (kJ/mol)	R^2	Ea (kJ/mol)	R^2	Ea (kJ/mol)	R^2	Ea (kJ/mol)	R^2
0.1	136.35	0.98	101.85	0.97	108.47	0.98	102.81	0.97	102.74	0.97	108.09	0.97
0.15	162.19	0.97	102.89	0.97	108.47	0.98	103.85	0.97	103.78	0.98	108.09	0.97
0.2	181.84	0.95	116.28	0.94	121.6	0.95	117.32	0.94	117.35	0.94	122.3	0.94
0.25	197.09	0.95	117.52	0.94	121.6	0.95	117.43	0.94	118.47	0.94	122.3	0.94
0.3	194.15	0.92	139.95	0.97	144.63	0.98	141.23	0.97	141.14	0.97	146.91	0.97

0.35	198.04	0.93	134.46	0.9	138.01	0.91	134.35	0.9	135.5	0.9	139.93	0.91
0.4	194.88	0.91	133.19	0.9	135.43	0.9	135.82	0.91	136.71	0.91	141.09	0.92
0.45	198.44	0.92	165.63	0.92	168.3	0.93	165.5	0.92	165.38	0.92	170.69	0.93
0.5	192.37	0.91	214.09	0.97	216.94	0.98	213.92	0.97	215.86	0.97	222.4	0.98
0.55	187.99	0.94	212.84	0.96	212.53	0.95	216	0.97	213.78	0.97	220.33	0.98
0.6	229.26	0.99	216.17	0.97	214.34	0.96	218.07	0.97	215.86	0.97	222.4	0.97
0.65	266.68	0.97	218.25	0.97	227.11	0.97	213.92	0.97	215.86	0.97	222.4	0.97

5.3.4.7 Kinetic Analysis of FR-4 type WPCB

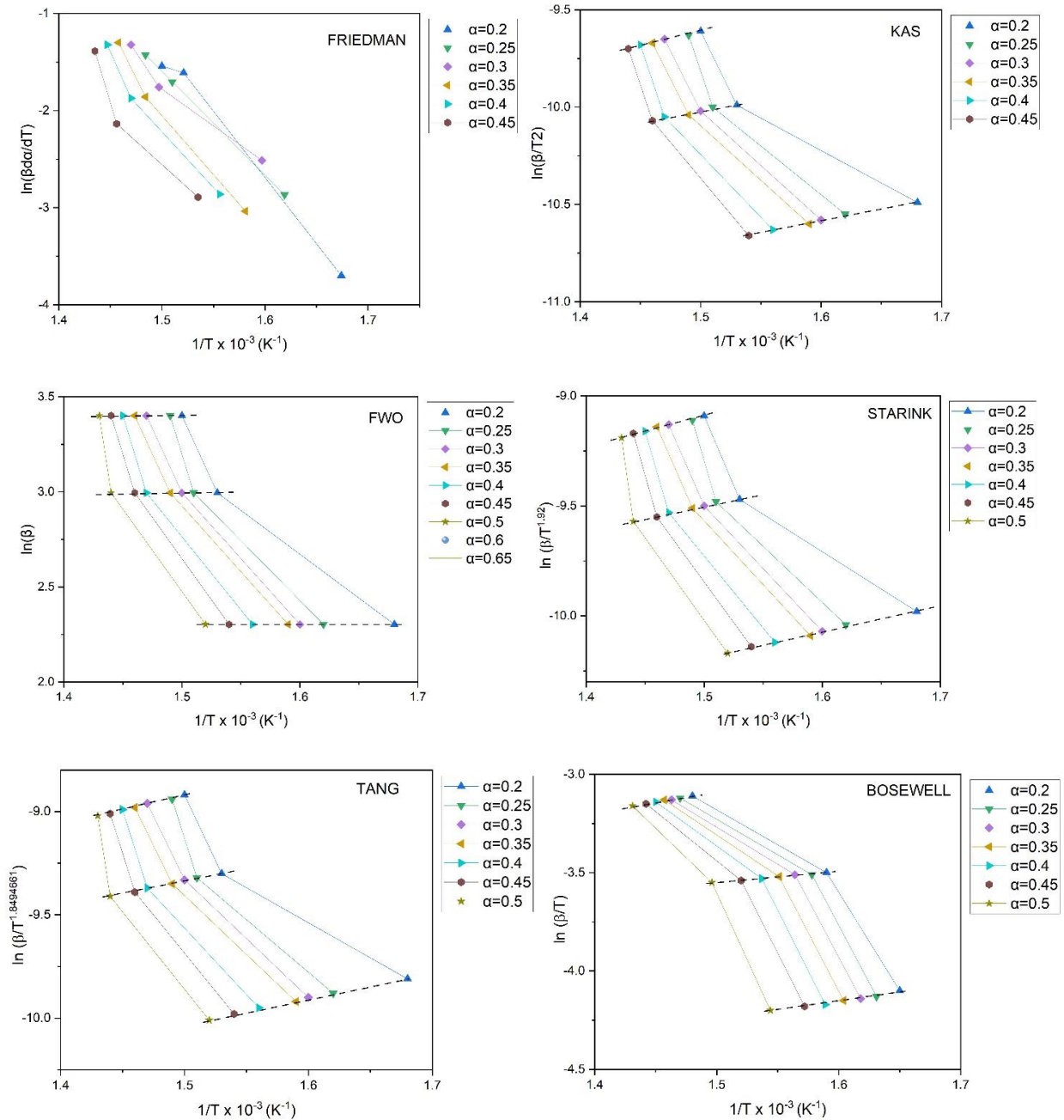


Figure 5.18: Kinetic Plot for determination of kinetic parameters using (a) Friedman, (b) KAS, (c) FWO, (d) Starink, (e) Tang and (f) Bosewell method for FR-4 WPCB pyrolysis

Figure 5.18 (a-f) shows the linear fitting obtained through the Friedman, KAS, FWO, Starink, Tang and Bosewell methods. The parallel straight lines obtained offer satisfactory regression coefficients i.e., 0.9–1 for Friedman, 0.91 – 0.97 for KAS, 0.95 – 0.98 for FWO, 0.92 – 0.97 for Starink, 0.91 – 0.97 for Tang and 0.9 – 95 for Bosewell. The low R^2 value for $\alpha > 0.55$ for all (except Friedman) methods can be accredited to the alteration of thermal breakdown mechanism with the increasing heating rate. Similar to VPCB, the tricky definition of the mass interval, also plays a part here (Anca-Couche et al. 2014). At $\alpha = 0.15 - 0.2$, lower R^2 values indicates a slow conversion rate of FR4 WPCB. A larger gap between the lines at $\alpha > 0.45$ (for Friedman $\alpha > 0.4$) is also noticed and this indicates the change of the thermal decomposition mechanism.

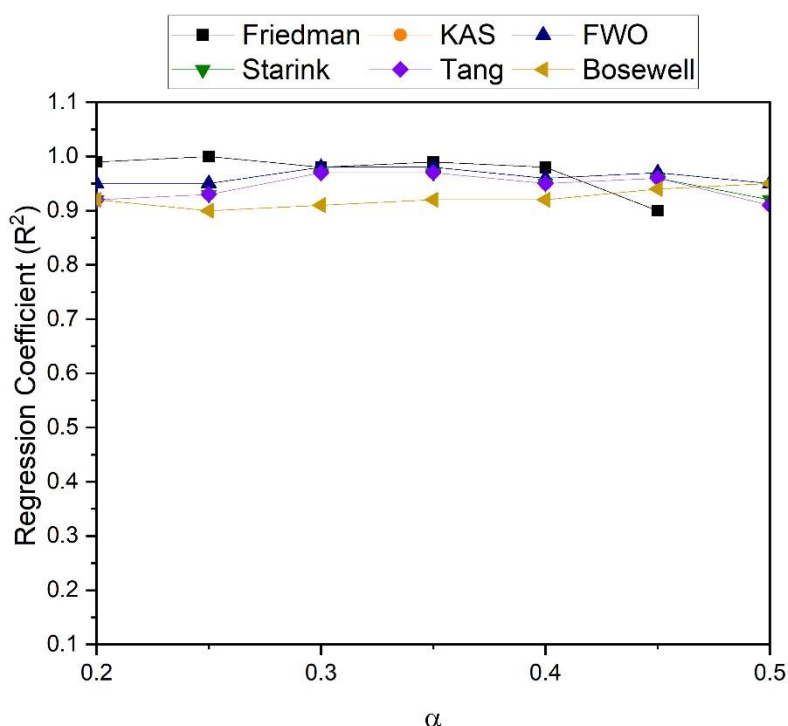


Figure 5.19: Plot of R^2 vs Conversion (α) using Friedman, KAS, FWO, Starink, Tang and Bosewell method for FR-4 WPCB pyrolysis

In the 0.2 to 0.5 conversion range (Figure 5.18), parallel lines have been obtained for all six methods which suggests close distribution of activation energies. Conversely, at lower (0.15–0.12) and higher (> 0.5) ranges of conversion unreliable R^2 values indicates the possibility of distinctly different and complex pyrolysis reactions. Conversion up to 0.2 symbolizes typically the elimination of moisture and the beginning of primary condensation of phenolic and methylene groups. Alternatively, at higher conversion levels ($\alpha > 0.5$) the pyrolysis of intermediates occurs.

5.3.4.8 Analysis of Activation Energies of FR-4 WPCB

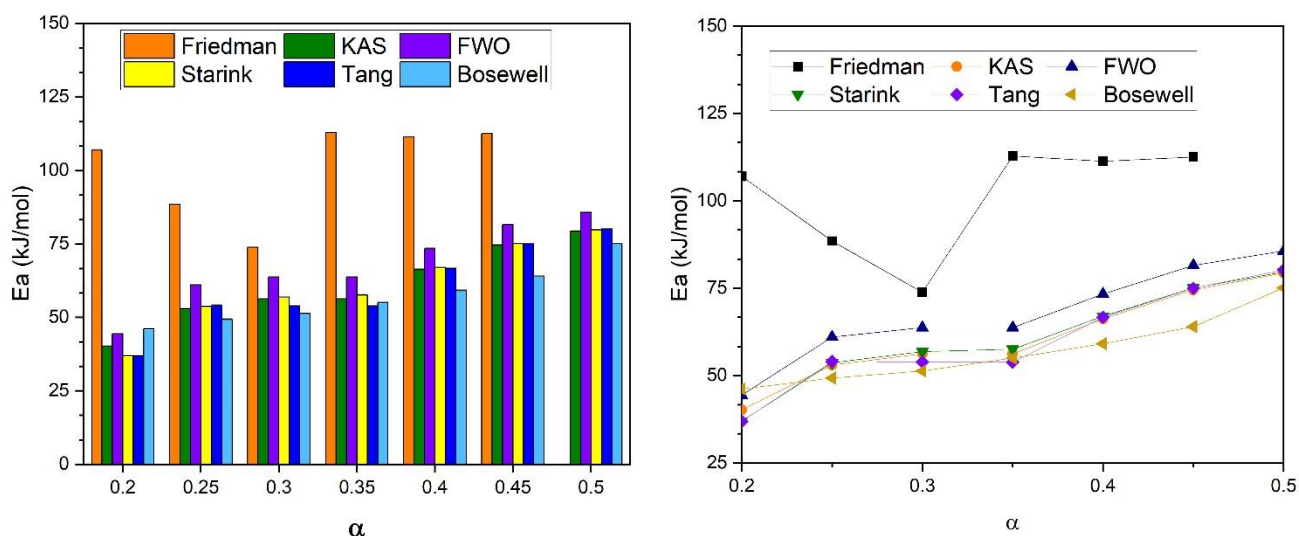


Figure 5.20 (a): Comparison of Activation Energies and (b) Evolution trend of Activation Energies obtained using Friedman, KAS, FWO, Starink, Tang and Bosewell method for WPCB pyrolysis

The values of Ea are displayed in Figure 5.20 (a). Figures 5.20 (b) display the development of Ea collectively for Friedman, KAS, FWO, Starink, Tang and Bosewell methods respectively. As can be seen, in Friedman method, the Ea values increase from 107 kJ/mol ($\alpha = 0.2$) to 112.53 kJ/mol linearly ($\alpha = 0.45$). For Friedman method, values of activation energy for $\alpha > 0.45$ are unreliable. In case of KAS method, Ea values linearly increase from 40.22 kJ/mol ($\alpha = 0.2$) to 79.33 kJ/mol linearly ($\alpha = 0.5$). In case of FWO method, Ea values increase from 44.42 kJ/mol ($\alpha = 0.2$) to 85.66 kJ/mol ($\alpha = 0.5$). In case of Starink, Tang and Bosewell methods, the trends resemble that of FWO methods but the values are closely distributed (Figure 5.20b). For Starink method, Ea values increase from 36.94 kJ/mol ($\alpha = 0.2$) to 79.66 kJ/mol linearly ($\alpha = 0.5$). For Tang method, Ea values increase from 36.92 kJ/mol ($\alpha = 0.2$) to 80.18 kJ/mol exponentially ($\alpha = 0.5$). Bosewell method follows the same trend as well with Ea values in the range of 46.15 kJ/mol ($\alpha = 0.2$) to 75.08 ($\alpha = 0.5$) kJ/mol. The exponential increase of activation energy is illustrative of the large assortment of bonds and the multiphasic nature of its conversion corresponding to consecutive reactions (Carrier et al. 2016). The differences in the values might be caused by the heterogeneity of the WPCBs and equipment noise. The average Ea values have been determined as 101.01, 60.83, 67.63, 60.96, 60.08 and 57.15 kJ/mol for Friedman, KAS, FWO, Starink, Tang and Bosewell methods respectively.

Table 5.8: The Kinetic Parameters determined using Friedman, KAS, FWO, Tang, Starink and Bosewell method for FR-4 WPCB Pyrolysis

α	Friedman		KAS		FWO		STARINK		TANG		BOSEWELL	
	Ea (kJ/mol)	R ²	Ea (kJ/mol)	R ²	Ea (kJ/mol)	R ²	Ea (kJ/mol)	R ²	Ea (kJ/mol)	R ²	Ea (kJ/mol)	R ²
0.2	107	0.99	40.22	0.92	44.42	0.95	36.94	0.92	36.92	0.92	46.15	0.92
0.25	88.5	1	53.03	0.93	61.02	0.95	53.66	0.93	54.05	0.93	49.31	0.9
0.3	73.86	0.98	56.23	0.97	63.72	0.98	56.87	0.97	53.85	0.97	51.3	0.91
0.35	112.78	0.99	56.23	0.97	63.72	0.98	57.56	0.97	53.85	0.97	55.04	0.92
0.4	111.35	0.98	66.23	0.95	73.35	0.96	66.99	0.95	66.66	0.95	59.12	0.92
0.45	112.53	0.9	74.53	0.96	81.52	0.97	75.07	0.96	75.02	0.96	64.02	0.94
0.5	-	-	79.33	0.91	85.66	0.95	79.66	0.92	80.18	0.91	75.08	0.95

5.3.5 Distribution of Activation Energies (DAEM)

5.3.5.1 DAEM of FR-2 PCBs

The relationship between $E\alpha$ and α could be obtained by plotting α against corresponding $E\alpha$ values as shown in Figure 5.21. The values for $f(E)$ have been calculated from the activation energy values obtained using the Miura-maki method. For VPCB, the pattern is a right skewed Gaussian pattern whereas for WPCB, it is a left skewed Gaussian pattern. It is not essential to follow the Gaussian distribution pattern. It is interesting that the skewness of both distributions is reverse of each other. This can be attributed to the presence of several Rare Earth Elements (REE) and their catalytic effect. The peak values of $f(E)$ i.e., 0.0085 and 0.0178 at activation energy 95.78 kJ/mol and 42.09 kJ/mol for FR-2 VPCB and WPCB respectively. Further investigation on this front is required.

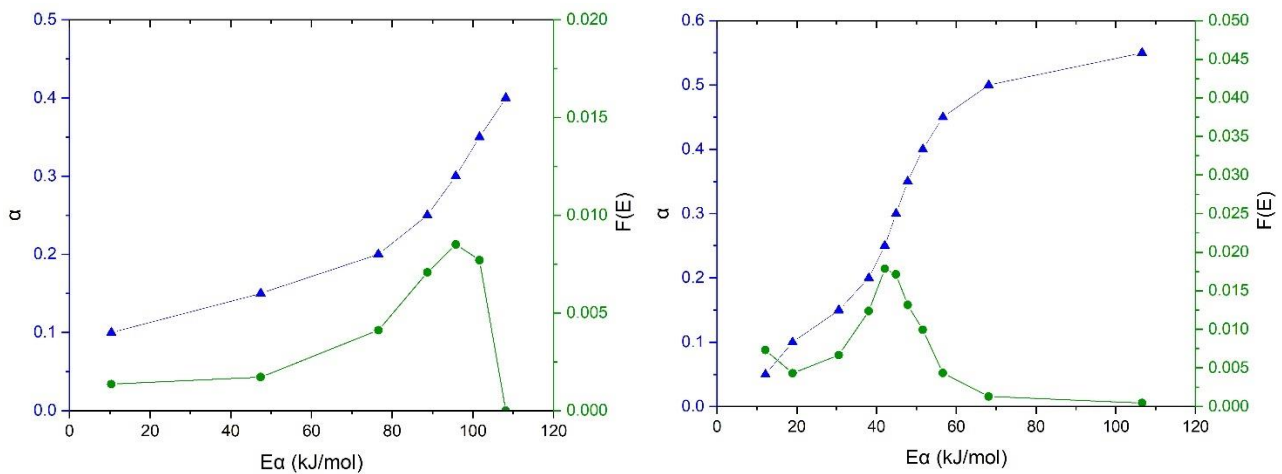


Figure 5.21: Distribution of Activation Energy of FR-2 VPCB and WPCB Pyrolysis

5.3.5.2 DAEM of FR-4 PCBs

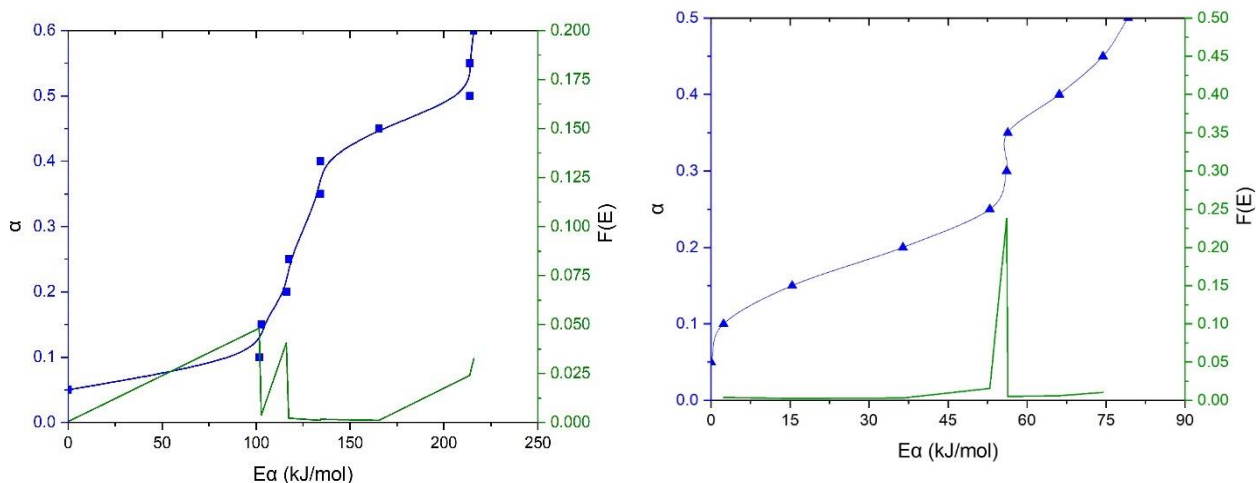


Figure 5.22: Distribution of Activation Energy of FR-4 VPCB and WPCB Pyrolysis

The relationship between $E\alpha$ and α could be obtained by plotting α against corresponding $E\alpha$ values as shown in Figure 5.21. The values for $f(E)$ have been calculated from the activation energy values obtained using the Miura-maki method. For FR4 VPCB, multiple peaks can be observed, which dictates that the activation energies may not be following a singular pattern whereas for FR4 WPCB, it is following a Gaussian pattern. It is interesting that the distributions are different. This can be attributed to the presence of in-situ metals and their catalytic effect. The peak values of $f(E)$ i.e., 0.0085 and 0.0178 at activation energy 101.7 and 116.12 kJ/mol FR-4 VPCB and whereas for FR-4 WPCB peak value of $f(E)$ i.e., 0.238 at activation energy 56.15 kJ/mol.

5.3.6. Compensation Effect

5.3.6.1 FR-2 PCBs

Determination of kinetics is often affected by two major disruptive factors – i) Instrumental Error and ii) mathematical impedance from the methods employed. Variations obtained in the values of the kinetic parameters, can be expressed according to the compensation effect (Collett and Rand 1980). The compensation effect is the apparent linear relationship of the $\ln A$ and Activation Energy (E_a) values obtained during kinetic analysis (Narayan & Antal 1996). In other words, it is the interdependence of the apparent activation energy and frequency factor for a set of related rate processes, such as in heterogeneous reactions (Galwey 1997; Junior et al. 2014). This method has been verified in multiple pyrolysis literature in the past (Zsako 1976; Collett and Rand 1980; Narayan & Antal 1996; Galwey 1997; Junior et al. 2014; Mianowski et al. 2021; Mumbach et al. 2022). The widely implemented way is to plot $\ln(A)$ vs Activation Energy (E_a) and then fitting those data points into a linear relationship. The relationship is obtained in the form $\ln(A) = aE_a + b$. The stronger the relationship, better the reliability of the data points (Cafiero et al. 2014).

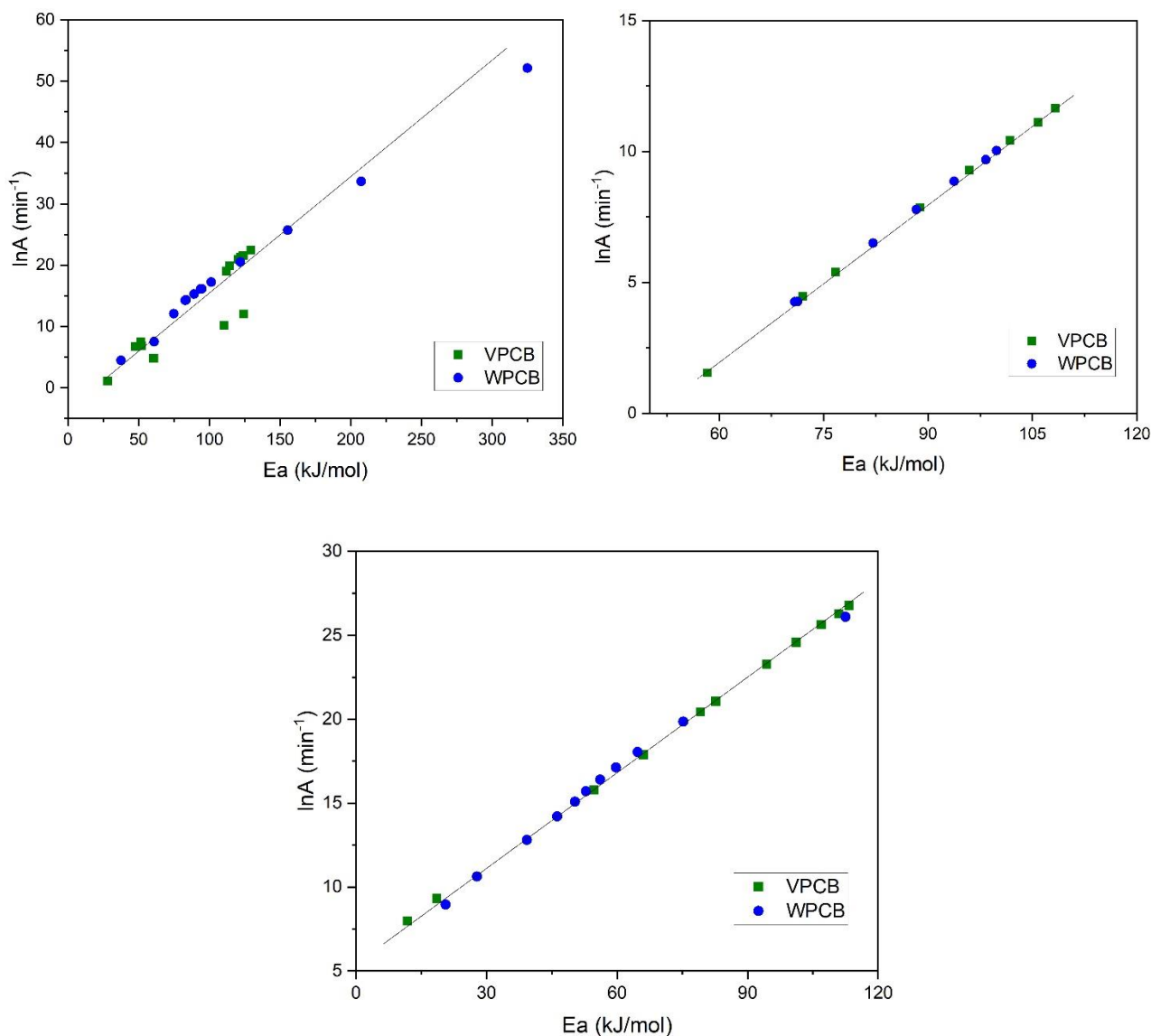


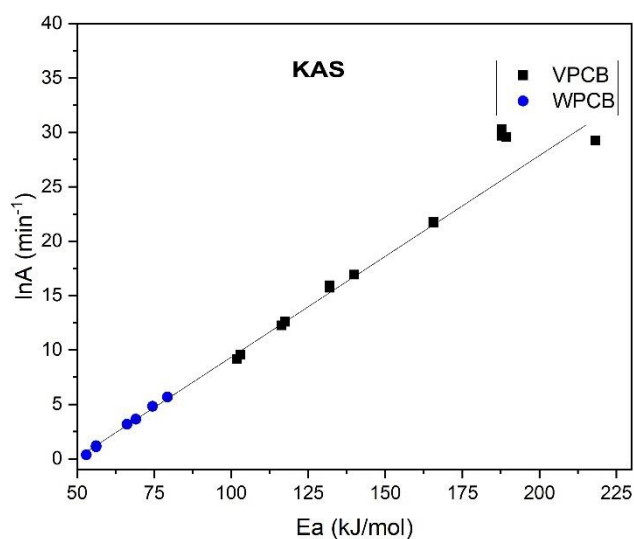
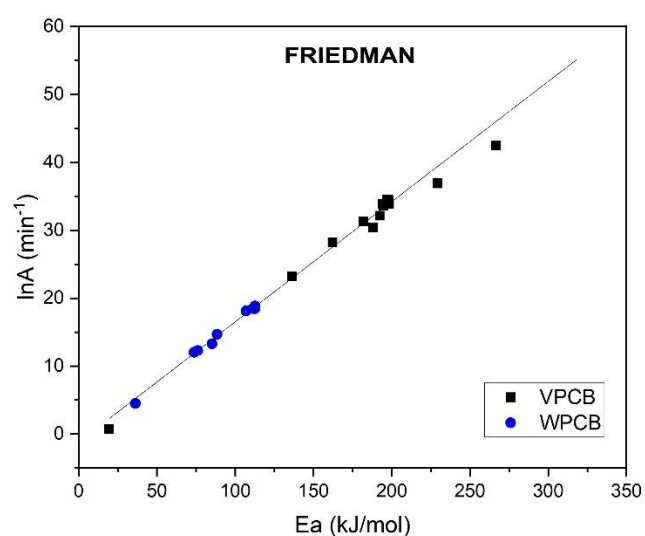
Figure 5.23: Compensation Effect of FR-2 PCBs using Arrhenius Parameters obtained from (a) Friedman method (b) KAS method and (c) FWO method

As illustrated in figure 5.23, it is clear that compensation effect exists for FR-2 PCB pyrolysis for Friedman, KAS and FWO method respectively. In case of Friedman method, despite a few outliers, the obtained points align to a linear relationship. This confirms the acceptability of the values obtained from the Friedman method. On the other hand, for KAS method all the data points align perfectly to a linear relationship. Similar clarity exists in case of FWO method as well. However, they are not a differentiator for identification of the best model.

Table 5.9: The values of compensation effect for FR-2 WPCB Pyrolysis

FRIEDMAN				KAS				FWO			
VPCB		WPCB		VPCB		WPCB		VPCB		WPCB	
Ea	lnA	Ea	lnA	Ea	lnA	Ea	lnA	Ea	lnA	Ea	lnA
kJ/mol	min ⁻¹	kJ/mol	min ⁻¹	kJ/mol	min ⁻¹	kJ/mol	min ⁻¹	kJ/mol	min ⁻¹	kJ/mol	min ⁻¹
28.03	1.14	37.64	4.5	58.24	1.56	70.86	4.27	11.85	7.98	20.59	8.96
47.57	6.73	61.08	7.56	72	4.47	71.27	4.27	18.54	9.32	27.82	10.63
51.52	7.47	74.89	12.1	76.68	5.4	82.1	6.51	54.69	15.81	39.28	12.82
52.01	6.84	83	14.29	88.84	7.87	88.34	7.79	66.07	17.9	46.24	14.22
60.66	4.87	83.59	14.33	95.92	9.29	93.76	8.87	79.19	20.44	50.35	15.09
110.36	10.23	89.31	15.32	101.81	10.44	98.33	9.7	82.67	21.07	52.88	15.72
112.22	19.07	93.95	16.12	105.82	11.12	99.84	10.04	94.37	23.29	56.12	16.4
114.33	19.9	94.74	16.15	108.3	11.67			101.16	24.59	59.75	17.13
120.31	21	101.34	17.24	-	-	-	-	106.93	25.64	64.73	18.05
121.86	21.34	121.91	20.53	-	-	-	-	110.96	26.29	75.24	19.86
124	21.61	155.39	25.71	-	-	-	-	113.33	26.78	112.54	26.11
124.23	12.05	207.43	33.67	-	-	-	-	-	-	-	-
129.54	22.5	325.01	52.13	-	-	-	-	-	-	-	-

5.3.6.2 FR-4 PCBs



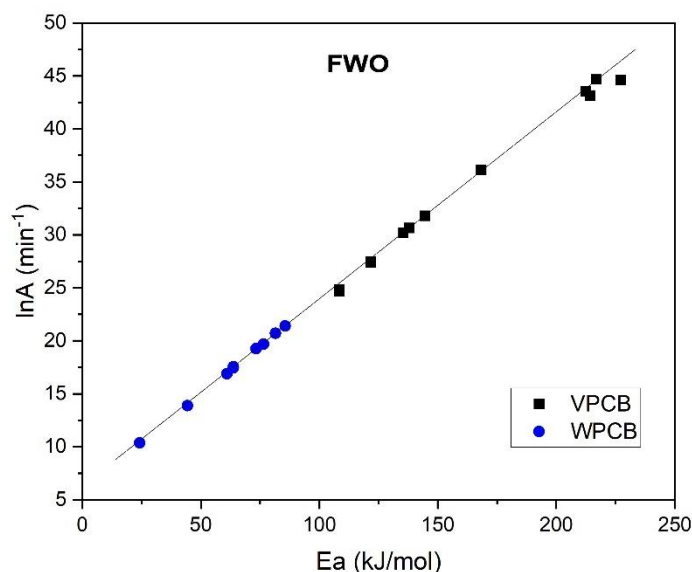


Figure 5.24: Compensation Effect of FR4 PCBs using Arrhenius Parameters obtained from (a) Friedman method (b) KAS method and (c) FWO method

As illustrated in figure 5.24, it is clear that compensation effect exists for FR4 PCB pyrolysis for Friedman, KAS and FWO method respectively. In case of Friedman method, despite a few outliers, the obtained points align to a linear relationship. This confirms the acceptability of the values obtained from the Friedman method. On the other hand, all the data points align perfectly to a linear relationship. In case of FWO method, there are a couple of outliers, but the points align to a linear relationship as well.

Table 5.10: The values of compensation effect for FR-4 WPCB Pyrolysis

FRIEDMAN				KAS				FWO			
VPCB		WPCB		VPCB		WPCB		VPCB		WPCB	
Ea	lnA	Ea	lnA	Ea	lnA	Ea	lnA	Ea	lnA	Ea	lnA
kJ/mol	min ⁻¹	kJ/mol	min ⁻¹	kJ/mol	min ⁻¹	kJ/mol	min ⁻¹	kJ/mol	min ⁻¹	kJ/mol	min ⁻¹
19.3	0.73	36.376	4.48	101.85	9.2	53.03	0.37	108.47	24.69	24.24	10.36
136.35	23.25	76.157	12.3	102.89	9.56	56.23	1.1	108.47	24.85	44.42	13.88
162.19	28.22	106.993	18.09	116.28	12.27	56.23	1.2	121.6	27.39	61.02	16.89
181.84	31.29	88.495	14.66	117.52	12.6	66.23	3.18	121.6	27.49	63.72	17.45
197.09	34.55	73.86	12.01	139.95	16.93	74.53	4.81	144.63	31.8	63.72	17.56
194.15	33.87	112.772	18.82	131.84	15.96	79.33	5.69	138.01	30.65	73.35	19.25
198.04	34.44	111.35	18.47	131.84	15.72	69.08	3.63	135.43	30.19	81.52	20.7
194.88	33.64	112.522	18.43	165.63	21.75	-	-	168.3	36.16	85.66	21.4
198.44	33.84	85.252	13.29	187.71	30.32	-	-	216.94	44.68	76.49	19.7
192.37	32.14	-	-	187.71	29.7	-	-	212.53	43.52	-	-
187.99	30.42	-	-	189.31	29.6	-	-	214.34	43.16	-	-
229.26	36.91	-	-	218.25	29.26	-	-	227.11	44.61	-	-

5.3.7. Determination of Reaction Mechanism Function

5.3.7.1 FR-2 PCBs

The catalytic effect of the in-situ metals has been identified in our primary kinetic analysis. The catalytic effect of the in-situ metals on the pyrolysis mechanism has been determined using the Šesták-Berggren model (Šesták and Berggren 1971). Previously the Šesták-Berggren model has been implemented to derive the pyrolysis mechanism for glass-fibre reinforced PCBs (Gao et al. 2021). This model is not affected by the hypothetical mechanism functions, thereby preventing any inherent inaccuracies. Hence, this model was suitable for investigating the pyrolysis of behaviour of printed circuit boards. The fitting results of the Šesták-Berggren model for FR-2 VPCB and WPCB are presented in Table 5.11.

Table 5.11: Fitting Results of the Šesták-Berggren model

β (K/min)	VPCB					WPCB				
	n	m	p	lnA	R ²	n	m	p	lnA	R ²
10	-46.8	131.21	-125.66	9.15	0.96	-54.24	147.5	-142.25	9.32	0.96
20	-30.51	86.37	-82.82	6.25	0.92	-61.62	162.35	-157.48	9.55	0.95
30	-44.86	124.29	-119.66	9.07	0.97	-53.4	144.16	-139.14	10	0.99
Average	-40.73	113.95	-109.38	8.16		-54.42	147.5	-146.29	9.62	

As can be seen, the regression co-efficient (R²) was greater than 0.95, which affirms that the validity of the results. For FR-2 VPCB, the value of lnA ranges between 6.243 – 9.1434, whereas for WPCB it ranges between 9.3125 – 9.9998. The fitting parameters i.e., n, m and p of the Šesták-Berggren model were found to be dependent of the heating rate. Hence, the average values of the said parameters were used. The mechanism equations for VPCB (Eq. 5.1) and WPCB (Eq. 5.2) are concluded as follows –

$$\frac{d\alpha}{dt} = 3.46 \times 10^3 \left[(1 - \alpha)^{-40.72} \alpha^{113.95} (-\ln(1 - \alpha))^{-109.38} \right] \exp\left(-\frac{107.93 \text{ kJ/mol}}{RT}\right) \quad (5.1)$$

$$\frac{d\alpha}{dt} = 1.5 \times 10^4 \left[(1 - \alpha)^{-56.41} \alpha^{147.49} (-\ln(1 - \alpha))^{-146.28} \right] \exp\left(-\frac{111.68 \text{ kJ/mol}}{RT}\right) \quad (5.2)$$

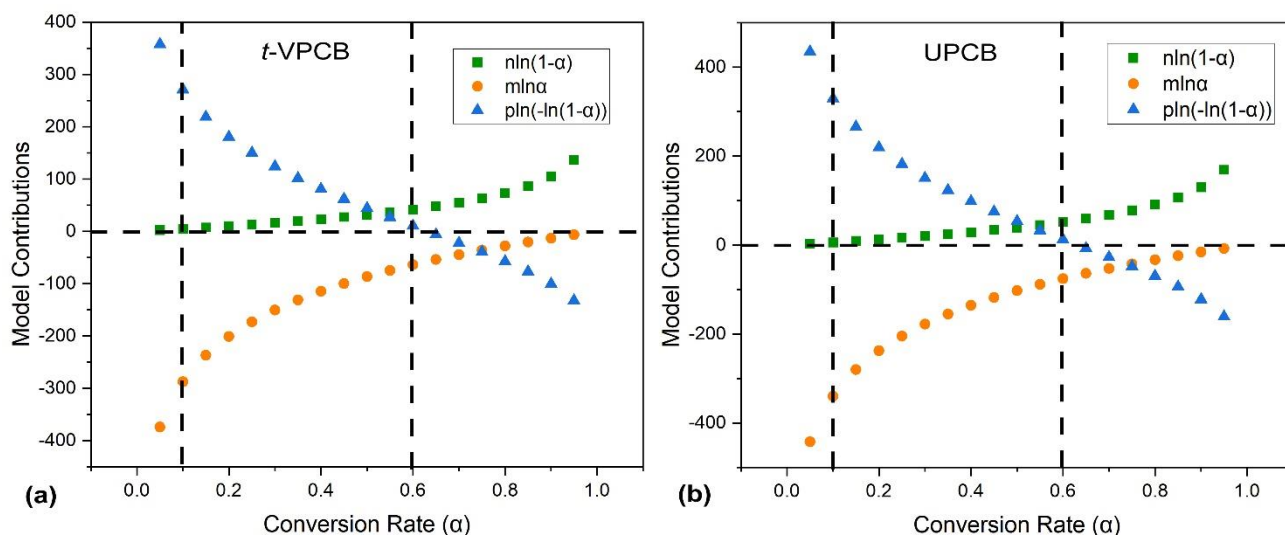


Figure 5.25: Contribution analysis of interface reaction ($n\ln(1-\alpha)$), diffusion ($m\ln\alpha$), and nucleation reaction ($p\ln(-\ln(1-\alpha))$) to pyrolysis of (a) VPCB and (b) WPCB

The mechanism function indicated the catalytic effect of multiple metals on WPCB. In VPCB only Cu is present, hence the effect of Cu is only visible in that case. The Frequency factor for VPCB is in the range of 10^3 whereas for WPCB it is in the range of 10^4 . Frequency factor is associated to the complexity and reactivity of the feedstock. Higher frequency factor indicates more complex reactions occurring. The analysis contributions of Šesták-Berggren model on pyrolysis revealed further insight on the mechanism of the reaction (Figure 5.25). From the Figures 5.25a and 5.25b, it is evident that in both cases, while the terms $(1-\alpha)^n$, $[-\ln(1-\alpha)]^p$ representing phase boundary reaction and nucleation reaction mechanism respectively are positive, the term α^m , representing diffusion reaction mechanism is negative in nature. Positive values of these terms signify the facilitation of the PCB pyrolysis reaction with time. Negative values, on the other hand, signifies the suppression of the reaction. From figure 5.25, the contribution of the model terms is demonstrated for VPCB and WPCB pyrolysis respectively.

In the preliminary stage of pyrolysis ($\alpha < 0.1$), values of the term $p\ln[-\ln(1-\alpha)]$ are quite large and positive, indicating that the nucleation reaction promotes the pyrolysis process. On the other hand, negative values of $m\ln\alpha$ demonstrates that diffusion reaction inhibits pyrolysis process and is the rate controlling step. The values of $n\ln(1-\alpha)$ are positive but not large. This is due to the presence of copper and other metals in PCBs that facilitate the phase boundary reactions. In the midway of pyrolysis ($0.6 < \alpha < 0.1$), the values of $p\ln[-\ln(1-\alpha)]$ gradually decreases which demonstrates that the contribution of nucleation reactions diminish as the pyrolysis progresses. Whereas, values of $m\ln\alpha$ increases with the progression of reaction and the nature still remains negative. This again indicates the rate determining

nature of the diffusion reaction mechanism. The values of $\ln(1-\alpha)$ increases a little which is attributed to the catalytic effect of the in-situ metals which are getting exposed due to the ablation of substrate polymer with the progression of pyrolysis. This ensures that the metals promote phase boundary reaction in PCB pyrolysis process. Only $\ln(1-\alpha)$ remains positive in the final stage of pyrolysis ($\alpha>0.6$) process, suggesting that the phase boundary reaction is the only factor promoting pyrolysis reactions during this period. Values of $m\ln\alpha$ approaches zero and $p\ln[-\ln(1-\alpha)]$ becomes negative due to the exhaustion of substrate.

5.3.7.2 FR-4 PCBs

Šesták-Berggren model has been implemented for investigating the pyrolysis of behaviour of FR-4 printed circuit boards (Šesták and Berggren 1971). The fitting results of the Šesták-Berggren model for FR-4 VPCB and WPCB are presented in Table 5.12.

Table 5.12: Fitting Results of the Šesták-Berggren model

β (K/min)	VPCB					WPCB				
	n	m	p	lnA	R ²	n	m	p	lnA	R ²
10	-41.38	116.92	-111.96	7.87	0.94	-104.15	270.14	-262.45	15.25	0.98
20	-14.58	46.69	-44.13	3.88	0.92	-158.66	394.25	-385.6	18.98	0.92
30	-33.15	91.98	-88.93	5.62	0.9	-101.67	265.65	-257.45	17.2	0.96
Average	-29.7	85.2	-81.67	5.79		-121.49	310.02	-301.83	17.14	

As can be seen, the regression co-efficient (R²) was greater than 0.9, which affirms that the validity of the results. For FR-4 VPCB, the value of lnA ranges between 3.8738 – 7.8693, whereas for FR-4 WPCB it ranges between 15.2458 – 18.9709. The fitting parameters i.e., n, m and p of the Šesták-Berggren model were found to be dependent of the heating rate. Hence, the average values of the said parameters were used. The mechanism equations for FR-4 VPCB (Eq. 5.3) and WPCB (Eq. 5.4) are concluded as follows –

$$\frac{d\alpha}{dt} = 3.25 \times 10^2 \left[(1 - \alpha)^{-29.69} \alpha^{85.19} (-\ln(1 - \alpha))^{-81.67} \right] \exp\left(-\frac{150.99 \text{ kJ/mol}}{RT}\right) \quad (5.3)$$

$$\frac{d\alpha}{dt} = 2.77 \times 10^4 \left[(1 - \alpha)^{-121.49} \alpha^{310.01} (-\ln(1 - \alpha))^{-17.14} \right] \exp\left(-\frac{58.48 \text{ kJ/mol}}{RT}\right) \quad (5.4)$$

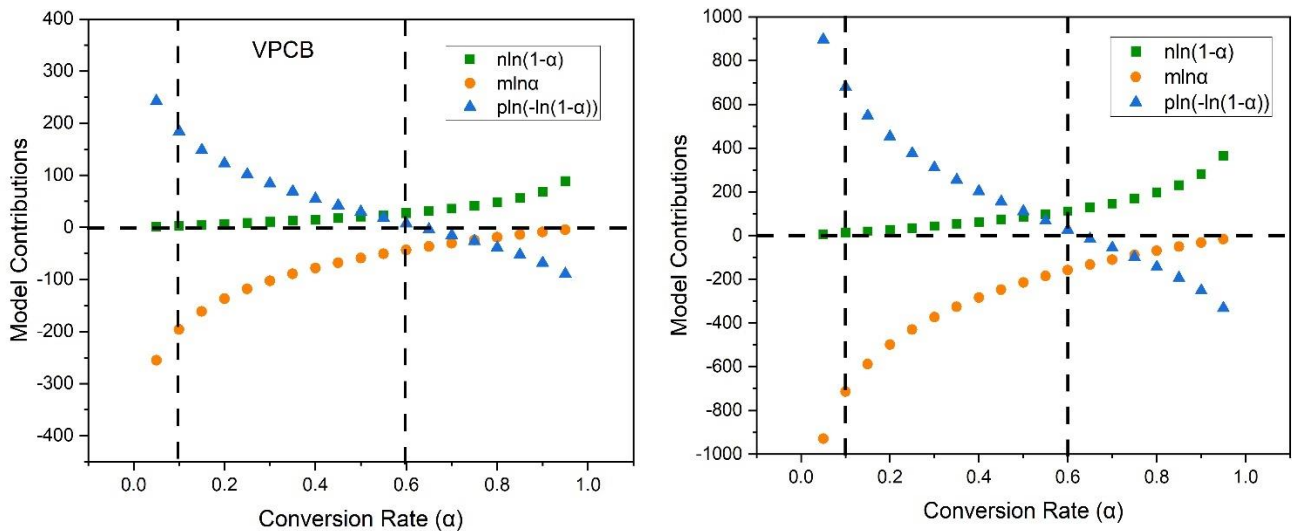


Figure 5.26: Contribution analysis of interface reaction ($n\ln(1-\alpha)$), diffusion ($m\ln\alpha$), and nucleation reaction ($p\ln(-\ln(1-\alpha))$) to pyrolysis of (a) VPCB and (b) WPCB

The mechanism function indicated the catalytic effect of multiple metals on WPCB. In VPCB, only Cu is present in majority, hence the effect of Cu is only visible in that case. The Frequency factor for VPCB is in the range of 10^2 whereas for WPCB it is in the range of 10^4 . Frequency factor is associated to the complexity and reactivity of the feedstock. Higher frequency factor indicates more complex reactions occurring. The analysis contributions of Šesták-Berggren model on pyrolysis revealed further insight on the mechanism of the reaction (Figure 5.26). From the Figures 5.26 a and b, it is evident that in both cases, while the terms $(1-\alpha)^n$, $[-\ln(1-\alpha)]^p$ representing phase boundary reaction and nucleation reaction mechanism respectively are positive, the term, α^m , representing diffusion reaction mechanism is negative in nature. Positive values of these terms signify the facilitation of the PCB pyrolysis reaction with time. Negative values, on the other hand, signifies the suppression of the reaction. From figure 5.26, the contribution of the model terms is demonstrated for FR-4 VPCB and WPCB pyrolysis respectively.

In the preliminary stage of pyrolysis ($\alpha < 0.1$), values of the term $p\ln[-\ln(1-\alpha)]$ are quite large and positive, indicating that the nucleation reaction promotes the pyrolysis process. On the other hand, negative values of $m\ln\alpha$ demonstrates that diffusion reaction inhibits pyrolysis process and is the rate controlling step. The values of $n\ln(1-\alpha)$ are positive but not large. This is due to the presence of copper and other metals in PCBs that facilitate the phase boundary reactions. In the midway of pyrolysis ($0.6 < \alpha < 0.1$), the values of $p\ln[-\ln(1-\alpha)]$ gradually decreases which demonstrates that the contribution of nucleation reactions diminish as the pyrolysis progresses. Whereas, values of $m\ln\alpha$ increases with the progression of reaction and the nature still remains negative. This again indicates the rate determining

nature of the diffusion reaction mechanism. The values of $\ln(1-\alpha)$ increases a little which is attributed to the catalytic effect of the in-situ metals which are getting exposed due to the ablation of substrate polymer with the progression of pyrolysis. This ensures that the metals promote phase boundary reaction in PCB pyrolysis process. Only $\ln(1-\alpha)$ remains positive in the final stage of pyrolysis ($\alpha>0.6$) process, suggesting that the phase boundary reaction is the only factor promoting pyrolysis reactions during this period. Values of $m\ln\alpha$ approaches zero and $\ln[-\ln(1-\alpha)]$ becomes negative due to the exhaustion of substrate.

5.3.8. Determination of Pre-exponential Factor & Thermodynamic Triplets

5.3.8.1 FR-2 PCBs

The pre-exponential factor or the frequency factor and thermodynamic triplets at three heating rates have been estimated as per equation 4.34 – 4.36. Results at $\beta=10$, $\beta=20$ and 30 K/min are shown in Tables 5.13 – 5.15. The results indicates that there is very small effect of heating rate on the thermodynamic triplets.

Table 5.13: Thermodynamic Triplets and Pre-exponential Factors for FR2 VPCB and WPCB at $\beta=10$ K/min

α	VPCB					WPCB				
	$T\alpha$ (K)	A (s^{-1})	ΔH (kJ/mol)	ΔG (kJ/mol)	ΔS (J/mol)	$T\alpha$ (K)	A (s^{-1})	ΔH (kJ/mol)	ΔG (kJ/mol)	ΔS (J/mol)
0.1	495.27	1.02E+02	47.41	189.11	-219.36	555.65	2.86E+04	70.27	182.09	-180.08
0.15	582.09	5.52E+07	109.49	180.95	-110.62	590.42	3.00E+06	89.83	176.92	-140.24
0.2	606.73	5.29E+08	116.82	176.32	-92.11	605.94	2.21E+06	84.27	173.12	-143.08
0.25	617.48	5.43E+08	115.18	174.63	-92.04	613.28	9.49E+05	77.9	171.36	-150.51
0.3	625.28	1.21E+09	118.8	174.01	-85.47	618.32	1.04E+06	78.44	171.45	-149.76
0.35	632.34	3.46E+09	124.28	173.89	-76.80	623.46	6.78E+06	88.77	171.74	-133.61
0.4	639.4	1.2E+08	106.9	174.67	-104.90	629.35	2.37E+07	96.1	172.39	-122.84
0.45	647	3.67E+02	42.19	178.31	-210.71	636.38	7.90E+08	116.62	174.11	-92.58
0.5	658.46	3.42E+02	46.54	183.13	-211.44	647.75	5.54E+11	150.01	176.54	-42.72
0.55	687.05	2.04E-01	7.99	184.76	-273.62	670.92	4.00E+15	201.85	176.59	40.68
0.6	720.1	5.70E-03	-10.77	185.52	-303.85	705.98	3.31E+25	319.14	171.33	238.02
0.65	755.42	5.92E-03	-9.15	187.23	-303.99	738.9	1.37E+03	54.94	184.61	-208.81
0.7	804.36	1.62E-03	-15.96	187.79	-315.40	788.75	4.84E-24	-261.22	196.53	-737.10
0.75	857.27	1.40E-03	-16.7	188.27	-317.27	827.93	4.84E-17	-176.93	194.44	-598.00
0.8	914.96	1.58E-02	-4.7	187.73	-297.86	879.21	9.21E-13	-125.26	193.54	-513.35
0.85	969.88	2.08E+01	19.97	186.59	-257.93	944.35	2.02E-08	-72.94	192.65	-427.66
0.9	1019.19	8.12E+02	52.18	187.13	-208.90	1027.57	2.97E-07	-57.96	193.85	-405.47
0.95	1081.52	9.95E+06	101.37	186.19	-131.31	1145.04	9.5E-08	-64.72	194.19	-416.92

Table 5.14: Thermodynamic Triplets and Pre-exponential Factors for FR2 VPCB and WPCB at $\beta=20\text{K/min}$

α	VPCB					WPCB				
	T α (K)	A (s ⁻¹)	ΔH (kJ/mol)	ΔG (kJ/mol)	ΔS (J/mol)	T α (K)	A (s ⁻¹)	ΔH (kJ/mol)	ΔG (kJ/mol)	ΔS (J/mol)
0.1	546.25	2.38E-01	10.38	189.57	-2.70E+02	557.85	3.43E+01	329.97	184.75	-2.37E+02
0.15	610.04	7.23E+02	46.45	181.98	-2.04E+02	591.85	5.19E+04	699.61	181.64	-1.74E+02
0.2	626.8	1.27E+08	109.12	178.22	-1.04E+02	616.25	5.06E+06	896.15	176.25	-1.35E+02
0.25	635.88	6.68E+08	116.58	176.6	-9.05E+01	626.63	2.59E+06	840.91	174.51	-1.41E+02
0.3	642.71	5.93E+08	114.97	175.7	-9.16E+01	633.95	1.04E+06	777.2	173.2	-1.49E+02
0.35	648.5	1.29E+09	118.61	175.1	-8.52E+01	639.5	1.19E+06	782.64	173.05	-1.48E+02
0.4	653.71	3.76E+09	124.1	174.75	-7.64E+01	644.92	7.60E+06	885.87	173.22	-1.32E+02
0.45	658.63	1.65E+08	106.74	174.66	-1.02E+02	650.88	2.46E+07	959.2	174.13	-1.22E+02
0.5	663.38	1.09E+03	42.06	175.78	-2.02E+02	658.25	8.16E+08	1164.36	175.4	-9.20E+01
0.55	668.8	1.30E+03	46.45	179.24	-2.00E+02	668.79	2.36E+11	1498.29	177.64	-4.34E+01
0.6	679	5.44E-01	8.06	183.81	-2.65E+02	688.29	2.32E+15	2017.04	179	3.54E+01
0.65	701.42	1.73E-02	-10.62	184.34	-2.94E+02	722.8	1.00E+25	3189.94	174.28	2.26E+02
0.7	725.58	2.30E-02	-8.91	184.67	-2.92E+02	753.25	3.67E+03	548.14	182.44	-1.99E+02
0.75	751.29	6.80E-03	-15.52	184.99	-3.02E+02	779.13	6.39E-23	-2611.36	193.64	-7.09E+02
0.8	778.35	5.98E-03	-16.05	185.4	-3.04E+02	806.8	3.49E-16	-1767.54	192.75	-5.76E+02
0.85	807.5	3.40E-02	-3.81	188.31	-2.90E+02	846.63	5.43E-12	-1249.82	191.64	-4.94E+02
0.9	857.59	1.73E+00	20.9	191.76	-2.58E+02	891.71	5.89E-08	-724.95	193.28	-4.15E+02
0.95	953.84	4.43E+02	52.73	193.81	-2.13E+02	976.04	7.82E-07	-575.3	194.69	-3.93E+02

Table 5.15: Thermodynamic Triplets and Pre-exponential Factors for FR2 VPCB and WPCB at $\beta=30\text{K/min}$

α	VPCB					WPCB				
	T α (K)	A (s ⁻¹)	ΔH	ΔG	ΔS	T α (K)	A (s ⁻¹)	ΔH	ΔG	ΔS
			(kJ/mol)	(kJ/mol)	(J/mol)			(kJ/mol)	(kJ/mol)	(J/mol)
0.1	532	2.72E-01	10.49	189.96	-2.69E+02	645.38	7.27E+01	32.27	179	-2.24E+02
0.15	613.19	7.06E+02	46.42	182.97	-2.05E+02	666.07	1.99E+05	69.35	173.14	-1.58E+02
0.2	636.19	1.35E+08	109.04	178.35	-1.04E+02	673.13	1.31E+07	89.15	170.21	-1.24E+02
0.25	646.19	7.05E+08	116.49	176.71	-9.03E+01	677.25	5.98E+06	83.68	169.04	-1.30E+02
0.3	653.63	6.09E+08	114.87	175.96	-9.16E+01	680.57	2.08E+06	77.34	168.47	-1.39E+02
0.35	660.13	1.24E+09	118.51	175.69	-8.57E+01	683.56	2.18E+06	77.9	168.82	-1.39E+02
0.4	666.32	3.32E+09	124	175.79	-7.77E+01	686.75	1.41E+07	88.24	169.02	-1.23E+02
0.45	672.63	1.07E+08	106.63	177.52	-1.06E+02	690.06	4.67E+07	95.6	169.87	-1.13E+02
0.5	681.25	3.69E+02	41.91	182.61	-2.11E+02	693.93	1.56E+09	116.14	171.34	-8.43E+01
0.55	702.82	6.01E+02	46.17	184.35	-2.07E+02	699	4.39E+11	149.58	174.12	-3.75E+01
0.6	732.32	4.18E-01	7.62	186.37	-2.68E+02	707.44	3.39E+15	201.55	177.41	3.69E+01
0.65	774.82	1.23E-02	-11.23	187.44	-2.98E+02	722.88	7.69E+24	319	177.66	2.16E+02
0.7	826.38	1.67E-02	-9.74	187.66	-2.96E+02	739.06	7.55E+03	54.94	177.16	-1.87E+02
0.75	880	5.16E-03	-16.59	187.76	-3.06E+02	753.82	4.41E-22	-260.93	177.83	-6.70E+02
0.8	934.63	5.19E-03	-17.35	187.44	-3.07E+02	770.5	1.78E-15	-176.46	179.62	-5.44E+02
0.85	986.13	4.41E-02	-5.29	188.05	-2.90E+02	793.69	1.83E-11	-124.55	181.4	-4.67E+02
0.9	1043.63	3.65E+00	19.35	188.67	-2.54E+02	825.82	1.30E-07	-71.95	185.97	-3.94E+02
0.95	1108	1.11E+03	51.44	189.61	-2.07E+02	900.25	1.17E-06	-56.9	189.69	-3.76E+02

The frequency factor (A) is a vital kinetic parameter, and its importance is unswervingly associated to the complexity and reactivity of the feedstock. For VPCB & WPCB, the values of A have been found in the range of 10^7 to 10^9 s⁻¹ with α at 0.15–0.4 and 10^4 to 10^{15} s⁻¹ with α at 0.15–0.55 respectively. The

pre-exponential factor for the first-order reaction can vary from 10^4 to 10^{18} s^{-1} . Therefore, the decomposition process of FR2 VPCB could be empirically classified as a first-order reaction (Maia et al. 2016). For VPCB in the range $0.4 < \alpha < 0.9$ and for WPCB $\alpha > 0.6$; the R^2 values are not reliable as the values of A varied between 10^{-3} to 10^2 s^{-1} and 10^{-24} to 10^3 s^{-1} respectively. These lower factors indicates either a surface reaction or the formation of a tight complex, where the reaction is independent of surface area (Turmanova et al. 2008).

Change in enthalpy (ΔH) is a state function, replicates the heat absorbed or liberated at a constant pressure (Ali et al. 2021). In the early conversion zone ($\alpha < 0.4$) more energy is required for pyrolysis of VPCB than WPCB to dissociate the bonds of phenolic compounds. Whereas for $0.4 < \alpha < 0.6$; more energy is required for WPCB pyrolysis compared to VPCB. The difference between the activation energy (E_a) and enthalpy (ΔH) values reveals the reaction feasibility. The lower the difference, the higher is the achievability of the reaction (Musellim et al. 2018). For VPCB, it is observed that the difference between values of E and ΔH at each conversion point ($\sim 3\text{--}5 \text{ kJ/mol}$) is very small. This is due to the energy difference between the activated complex and the reagent (Kaur et al. 2018). The lesser energy variance enhances the activation complex formation (Vlaev et al. 3003). The small difference between E_a and ΔH values state that additional energy ($\sim 5 \text{ kJ/mol}$) is required to favour product formation (Mehmood et al. 2017). For WPCBs the difference in activation energy and enthalpies are in the range of $4.2 - 5.8 \text{ kJ/mol}$. This indicates that pyrolysis of VPCB is easier to be achieved.

Gibbs free energy (ΔG) determines the increase in energy altogether which is appropriate to the reactants to initiate an activated complex. The advanced value of ΔG signifies less favourable reactions (Mian et al. 2019). The ΔG values for VPCB are in the range $173 - 190 \text{ kJ/mol}$ whereas for WPCB it is in the range of $171 - 196 \text{ kJ/mol}$. VPCB depicts overall higher values of ΔG than that of WPCB in the early conversion range ($\alpha < 0.45$).

Entropy (ΔS) is a measure of chaos in the system. Positive values of ΔS ensures reaction feasibility. For VPCB, ΔS have negative values throughout the whole conversion range. For $0.1 < \alpha < 0.4$, the ΔS values increases and then decreases till $\alpha = 0.75$ and again increases. The increase in entropy in the early conversion zone ensures better reaction and thermodynamic feasibility. This is in line with the findings from the master plot kinetics. For WPCB, ΔS have negative values till $\alpha = 0.5$ and positive values have been found at conversion degrees greater than 0.5. The degree of chaos in the products are lesser than the raw feedstock is confirmed by the negative ΔS values. Additionally, it is confirmed that the sample status is close to its thermodynamic equilibrium. Therefore, the sample shows lower reactivity

developing less favourable environment for the activated complex formation (Maia et al. 2016; Kaur et al. 2018). On the other hand, elevated ΔS values indicates elevated product reactivity. As a result, at $\alpha < 0.55$, pyrolysis products of WPCB are much more stable compared to VPCB pyro-products. Overall, the thermodynamic triplets disclose that the existence of *in-situ* metals in WPCB triggers an advanced reaction scope, confirming the catalytic outcome of metals on WPCB pyrolysis.

5.3.8.2 FR-4 PCBs

The pre-exponential factor or the frequency factor and thermodynamic triplets at three heating rates have been estimated as per equation 4.34 – 4.36. Results at $\beta=10$, $\beta=20$ and 30 K/min are shown in Tables 5.16 – 5.18. The results indicates that there is very small effect of heating rate on the thermodynamic triplets.

Table 5.16: Thermodynamic Triplets and Pre-exponential Factors for FR4 VPCB and WPCB at $\beta=10\text{K/min}$

α	VPCB					WPCB				
	$T\alpha$ (K)	A (s^{-1})	ΔH (kJ/mol)	ΔG (kJ/mol)	ΔS (J/mol)	$T\alpha$ (K)	A (s^{-1})	ΔH (kJ/mol)	ΔG (kJ/mol)	ΔS (J/mol)
0.1	629.58	1.76E+09	131.11	184.7	-7.93E+01	451.67	3.91E+00	32.63	191.79	-2.41E+02
0.15	639.39	2.7E+11	156.87	183.46	-3.93E+01	547.78	1.05E+04	71.61	189.08	-1.78E+02
0.2	645.73	1.04E+13	176.47	183.47	-1.04E+01	597.53	7.11E+06	102.03	184.87	-1.25E+02
0.25	651.17	1.75E+14	191.67	183.55	1.20E+01	617.71	5.64E+05	83.36	180	-1.46E+02
0.3	656.06	1.07E+14	188.7	183.22	8.10E+00	626.48	5.59E+04	68.66	177.8	-1.65E+02
0.35	660.77	2.25E+14	192.54	183.12	1.39E+01	632.65	3.95E+07	107.52	181.42	-1.12E+02
0.4	665.25	1.2E+14	189.35	183.37	8.85E+00	643.05	3.63E+07	106.01	180.45	-1.13E+02
0.45	670.06	5.78E+13	186.28	184.25	3.00E+00	651.78	4.36E+07	107.11	180.64	-1.11E+02
0.5	675.87	2.81E+13	184.84	186.75	-2.82E+00	660.78	1.08E+05	73.45	179.33	-1.60E+02
0.55	685.21	2.98E+13	188.28	189.95	-2.47E+00	668.82	1.76E+01	27.04	179.92	-2.31E+02
0.6	701.69	1.39E+14	196.71	190.24	9.57E+00	679.55	5.96E-04	-27.81	180.53	-3.15E+02
0.65	717.94	1.27E+18	248.34	192.93	8.20E+01	694.42	9.43E-03	-8.19	185.42	-2.93E+02
0.7	735.69	2.28E+23	317.98	197.65	1.78E+02	728.61	3.46E-01	12.36	186.86	-2.64E+02
0.75	760.21	1.96E+22	304.07	197.14	1.58E+02	769.84	5.14E+03	64.44	187.62	-1.86E+02
0.8	785.08	3.45E+34	468.46	210.06	3.82E+02	808.55	2.35E-03	-16.74	185.29	-3.06E+02
0.85	859.44	2.01E-16	-179.67	184.77	-5.39E+02	842.88	1.05E-02	-7.49	186.79	-2.94E+02
0.9	974.98	9.32E-11	-105.87	189.35	-4.37E+02	886.65	9.01E-01	18.05	188.72	-2.58E+02
0.95	1124.25	2.38E-09	-89.48	189.56	-4.13E+02	943.28	1.60E+00	20.42	188.46	-2.54E+02

Table 5.17: Thermodynamic Triplets and Pre-exponential Factors for FR2 VPCB and WPCB at $\beta=20\text{K/min}$

α	VPCB					WPCB				
	$T\alpha$ (K)	A (s^{-1})	ΔH (kJ/mol)	ΔG (kJ/mol)	ΔS (J/mol)	$T\alpha$ (K)	A (s^{-1})	ΔH (kJ/mol)	ΔG (kJ/mol)	ΔS (J/mol)
0.1	647	3.18E+09	130962.1	182678.6	-75.65	645.59	20.43	31008.03	186792.1	-224.04
0.15	655.21	5.14E+11	156733.8	180489.8	-34.75	652.59	60713.86	70730.66	182490.2	-160.73
0.2	660	2.04E+13	176348.3	179865.5	-5.15	657.67	23371963	101525	180512.1	-113.6
0.25	663.84	3.27E+14	191564.2	179815.5	17.19	662.67	1067151	82984.81	179027.1	-138.13
0.3	667.34	1.97E+14	188600.3	179663.4	13.08	668.17	94319.19	68304.78	177765.7	-157.43
0.35	670.8	3.73E+14	192454.1	180029.9	18.18	673.96	80818850	107167.8	179451.5	-103.96
0.4	674.42	1.9E+14	189264.7	180593.8	12.69	680.38	61794509	105692.8	179509.3	-106.16
0.45	678.5	8.8E+13	186204.5	181807.5	6.44	686.88	70955611	106811	179919.6	-105.15
0.5	683.67	4.28E+13	184773.1	184394.7	0.56	695.34	173212	73158.77	179495	-152.93

0.55	692	4.12E+13	188220.6	188116.2	0.16	709.46	34.76	26695.77	180080	-220.59
0.6	708.05	1.8E+14	196650.6	188567.5	11.83	739.63	0.01	-28301.1	181032.8	-301.06
0.65	724.67	1.77E+18	248283.7	189644.1	85.78	797.17	0.03	-9036.21	184979.5	-279.03
0.7	739.88	3.17E+23	317945	192770.5	183.1	872.55	0.69	11160.37	187512	-253.62
0.75	758.17	2.09E+22	304083.1	194041	160.96	920.09	4008.77	63181.55	192145.5	-185.47
0.8	783	5.48E+34	468477.3	201020.5	391.21	932.84	0.01	-17765.7	190069.4	-298.9
0.85	818.71	7.08E-16	-179331	186717.5	-535.42	1025.13	0.02	-9002.61	191456.8	-288.29
0.9	911.67	2.16E-10	-105336	191874.2	-434.73	1118.34	2.03	16113.92	188566.1	-248.02
0.95	1068.88	3.94E-09	-89012	193504.2	-413.24	1196.55	3.58	18305.42	188275.2	-244.45

Table 5.18: Thermodynamic Triplets and Pre-exponential Factors for FR2 VPCB and WPCB at $\beta=30\text{K}/\text{min}$

α	VPCB						WPCB				
	$T\alpha$ (K)	A (s^{-1})	ΔH (kJ/mol)	ΔG (kJ/mol)	ΔS (J/mol)	$T\alpha$ (K)	A (s^{-1})	ΔH (kJ/mol)	ΔG (kJ/mol)	ΔS (J/mol)	
0.1	666.07	3.28E+09	130803.6	185147.4	-77.75	614.38	1.07E+02	31.27	186.26	-2.20E+02	
0.15	673.13	4.8E+11	156584.8	182017.4	-36.39	654.07	1.66E+05	70.72	183.12	-1.60E+02	
0.2	677.25	1.75E+13	176204.8	180762.7	-6.53	667.07	4.02E+07	101.45	181.85	-1.14E+02	
0.25	680.57	2.68E+14	191425.1	180154.3	16.13	674.07	1.89E+06	82.9	181.24	-1.40E+02	
0.3	683.56	1.52E+14	188465.4	180530.6	11.36	680.32	1.45E+05	68.21	181.62	-1.61E+02	
0.35	686.75	2.85E+14	192321.5	180745.2	16.57	685.94	1.08E+08	107.07	181.84	-1.06E+02	
0.4	690.06	1.42E+14	189134.7	181653.6	10.71	691.44	7.27E+07	105.61	182.75	-1.10E+02	
0.45	693.93	6.42E+13	186076.2	183223.2	4.09	697.07	6.78E+07	106.73	184.33	-1.10E+02	
0.5	699	3.04E+13	184645.6	186185	-2.21	703.07	1.30E+05	73.1	187.31	-1.62E+02	
0.55	707.44	3.04E+13	188092.3	189695	-2.3	710.44	2.57E+01	26.69	190.84	-2.33E+02	
0.6	722.88	1.27E+14	196527.3	189967	9.39	722.57	2.10E-03	-28.16	191.11	-3.12E+02	
0.65	739.06	1.03E+18	248164.1	189433.2	84.03	745.44	6.73E-02	-8.61	190.58	-2.83E+02	
0.7	753.82	1.49E+23	317829.1	190143.9	182.67	785.07	2.10E+00	11.89	191.29	-2.55E+02	
0.75	770.5	1.01E+22	303980.6	192058.9	160.12	837.69	1.18E+04	63.87	193.22	-1.84E+02	
0.8	793.69	1.46E+34	468388.4	193953.8	392.62	916.07	8.42E-03	-17.63	195.12	-3.03E+02	
0.85	825.82	2.58E-15	-179390	198835.9	-541.1	1022.44	1.86E-02	-8.99	200.03	-2.97E+02	
0.9	900.25	5.04E-10	-105241	202803.2	-440.7	1148.69	7.87E-01	15.87	204.02	-2.68E+02	
0.95	1047.56	7.36E-09	-88834.8	204851	-420.16	1208.75	8.99E-01	18.21	206.08	-2.67E+02	

The pre-exponential factor, also known as the frequency factor (A) is an important kinetic parameter. The importance of the frequency factor is largely associated to the complexity and reactivity of the feedstock. For VPCB, the values of the frequency factor are in the range of 10^9 to 10^{14} s^{-1} with α at 0.15–0.65. For a first-order reaction, the value of A can fluctuate in the range of 10^4 to 10^{18} s^{-1} . Thus, the pyrolysis process of FR4 VPCB could be empirically categorised as first-order process (Turmanova et al. 2008; Maia and de Morais, 2016). For $0.65 < \alpha < 0.95$, the R^2 values are not reliable and the value of the frequency factor was found in the range 10^{-11} to 10^{23} s^{-1} . These broad range of the frequency factor indicates multiple reactions occurring. It could also mean that a tight complex is formed where the reaction is not a function of surface area (Turmanova et al. 2008). These findings are in line with our master plot analysis for FR4 VPCB.

In case of FR4 WPCBs, the values of A have been found in a comparatively lower range i.e., 10^5 to 10^7 s^{-1} with α at 0.2–0.55. With the same argument as VPCB, the thermal decomposition of FR4 WPCB can be classified as first order reaction. For $\alpha < 0.2$; values of A are in the range of 10^{-1} to 10^2 s^{-1} . Again, for $\alpha > 0.6$; the values of A vary between 10^{-2} to 10^4 s^{-1} . These lower values of A can be accredited to either surface reactions or the formation of the complex during the reaction (Turmanova et al. 2008). These findings are in line with our master plot analysis for FR4 VPCB. These incredibly smaller values of A for WPCBs can be attributed to the catalytic effect of the in-situ metals and material heterogeneity.

Change in enthalpy (ΔH) is a state function that is equivalent to the heat evolved or absorbed at a constant pressure (Huang et al. 2015). In the early conversion zone i.e., $0.1 < \alpha \leq 0.4$; energy required for pyrolysis of VPCB is higher than WPCB. In the range $0.4 < \alpha < 0.6$; energy required for WPCB pyrolysis increases then decreases compared to the early conversion zone. But for VPCB the energy requirement reduces by less than 2.5%. This low energy requirement in WPCBs could be due to the catalytic effect of the metals present in WPCBs. In case of WPCB, for $\alpha > 0.6$; few negative values of ΔH are observed. This indicates exothermic reactions occurring at those α values. The difference of the values of activation energy (E_a) and enthalpy (ΔH) is an indicator of the reaction feasibility. A lower difference value indicates higher feasibility of the reaction (Müsellim et al., 2018). For VPCB, it is observed that the difference between values of E and ΔH at each conversion point is in the range of 2.7 – 10.24 kJ/mol. Whereas for WPCBs this difference is in the range of 3.17 – 8.19 kJ/mol. This small deviation is because of the energy difference between the activated complex and the reagent (Kaur et al., 2018). The formation of active complex is enhanced by the smaller deviation value of E and ΔH (Vlaev et al., 2007). It also states that supplementary energy ($\sim 10 \text{ kJ/mol}$) is required to favour product formation (Mehmood et al., 2017). This indicates that pyrolysis of WPCB is easier to be achieved.

Changes in Gibbs free energy (ΔG) demonstrates the total energy enhancement of the system. ΔG allows assessing the level of contortion and changes in heat stream associated with the system. The

progressive values of ΔG indicates less favourable reactions (Mian et al. 2019). For VPCBs, ΔG values are in the range 183 – 210 kJ/mol whereas for WPCB it is in the range of 177 – 191 kJ/mol. VPCB depicts overall higher values of ΔG than that of WPCB in the early conversion range ($\alpha < 0.45$). This indicates that pyrolysis of WPCB is more favourable than VPCB.

Entropy (ΔS) is a measure of randomness or chaos in the system. A process is spontaneous when change in entropy is positive. For VPCB, negative values have been observed for ΔS till $\alpha = 0.25$. Thereafter positive values were obtained till $\alpha = 0.5$. Again, positive values were obtained in the range $0.65 \leq \alpha \leq 0.85$. The positive values of ΔS indicates better reaction and thermodynamic feasibility. WPCBs have negative values of ΔS throughout the whole conversion range. For $0.1 < \alpha < 0.4$, the ΔS values increases and then decreases till $\alpha = 0.65$ and then again increases till $\alpha = 0.8$. The increase in entropy in the initial stage confirms improved reaction and thermodynamic spontaneity. This is in line with the findings from the master plot kinetics. Additionally, the findings from figure 7 and 8 are also validated through thermodynamics. The negative ΔS values confirms that the degree of randomness in the pyrolysis products are lesser than the raw feedstock. It is also confirmed that the sample is close to its thermodynamic equilibrium. As a result, the reactivity of sample becomes low that creates a less favourable atmosphere for the formation of activated complex (Kaur et al., 2018; Maia and de Moraes, 2016; Müsellim et al., 2018). Conversely, higher values of ΔS indicates higher product reactivity. As a result, at $\alpha > 0.25$, pyrolysis products of VPCB are much more stable compared to the pyrolysis products of WPCB. The catalytic effect of several in-situ metal in FR4 WPCB may have something to do with the product instability. Whereas, VPCB being less heterogeneous could achieve thermodynamic spontaneity. Overall, the thermodynamic triplets disclose that the existence of *in-situ* metals in WPCB triggers an advanced reaction scope, confirming the catalytic outcome of metals on WPCB pyrolysis.

5.3.9. Product Distribution

5.3.9.1 FR-2 PCBs

The mass distribution of FR-2 VPCB and WPCB pyrolysis over the temperature range of 623 – 973K is depicted in Figure 5.27 a & b. The solid residue yield was about 51 – 55% and 53 – 57% up to 673K for VPCB and WPCB respectively. The yield reduces to 31 – 47% and 30 – 43% in 773 – 973K zone for VPCB and WPCB respectively. This is obvious as up to 673K, the major reaction contribution was based on degradation of polymeric part which led to formation of char. Whereas beyond 673K, as the temperature increases, it facilitates further degradation of the char which incur further weight loss. Minor anomaly in solid yield is observed at 873K for WPCB pyrolysis only. The oil yield was found to reduce with temperature. Up to 673K, the oil yield was 28 – 31% and 26 – 30% for VPCB and WPCB respectively. Beyond 673K, the yield of oil reduces further. This is due to the secondary cracking of the volatile products formed during pyrolysis reactions for both VPCB and WPCB pyrolysis. However, at 973K the oil yield increases for WPCB pyrolysis. These anomalies are due to the catalytic effect of the in-situ metals present in PCBs. The yield of gas increases with temperature. This can be explained by the probability of occurrence of secondary cracking of oil at higher temperature.

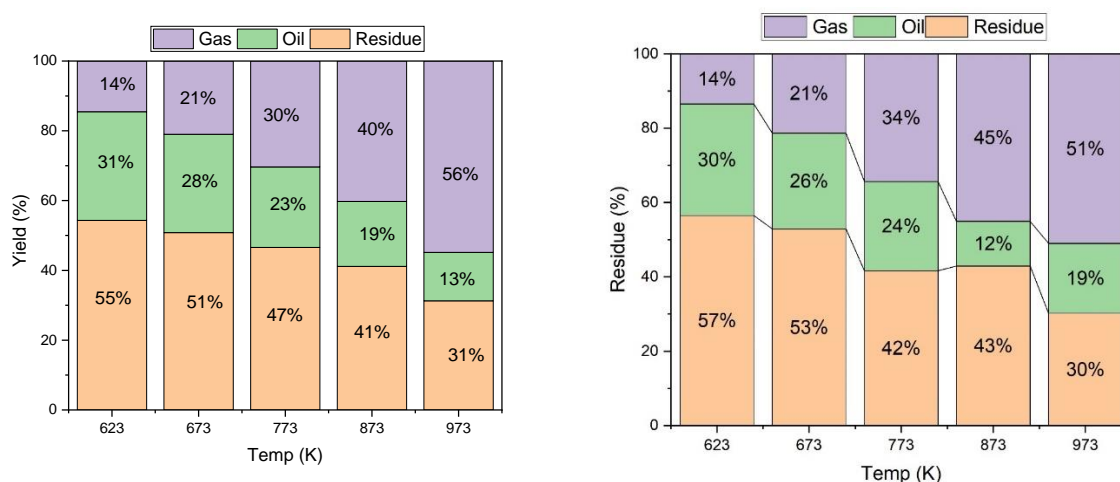


Figure 5.27: Product Distribution of (a) FR-2 VPCB and (b) WPCB pyrolysis

5.3.9.2 FR-4 PCBs

The mass distribution of FR-4 VPCB and WPCB pyrolysis over the temperature range of 623 – 973K is depicted in Figure 5.28 a & b. The solid residue yield was about 70 - 75% and 79 – 84% up to 773K for VPCB and WPCB respectively. The solid residue yield reduces to 65% and 74% in the 873K - 973K zone for FR-4 VPCB and WPCB respectively. This is obvious as up to 773K, the major reaction contribution was based on degradation of polymeric part which led to formation of char. Whereas

beyond 773K, as the temperature increases, it facilitates further degradation of the char which facilitate further weight loss. The oil yield was found to reduce with temperature. For FR-4 VPCB, the oil yield reduced to 7% from 15% i.e., it almost reduced by 50%. Whereas for FR-4 WPCB the oil yield reduced to 6% from 13%. Beyond 673K, the yield of oil reduces rapidly due to the secondary cracking of the volatile products formed during pyrolysis reactions for both FR-4 VPCB and WPCB pyrolysis. The yield of gas increases with temperature. This can be explained by the probability of occurrence of secondary cracking of oil at higher temperature.

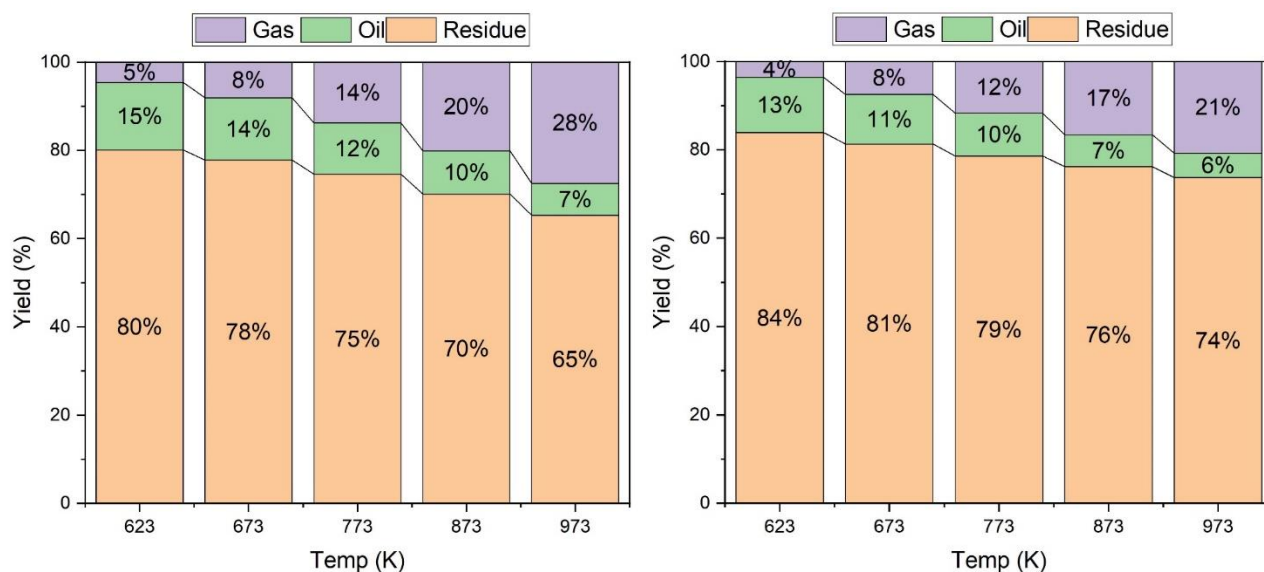


Figure 5.28: Product Distribution of (a) FR-4 VPCB and (b) WPCB pyrolysis

5.3.10 Product Recovery from mixed WPCB pyrolysis

5.3.10.1 Recovery of Pyro-oil

The condenser and the auxiliary condensing units have been used to capture the volatiles. Pyro-oil was recovered successfully by using the condensing arrangement. It was found that the yield of pyro-oil is inversely proportional to the nitrogen flow rate. The lowest flow rate of nitrogen was found to give the highest yield of pyro-oil as it increases the contact time of the gaseous outflow from the reactor in the condensing arrangement which allows enough time for the necessary heat transport to occur in order to condense the volatiles. Figure 5.29 (a) shows the pyro-oil recovered from the combination of 90% FR2 and 10% FR4 PCB and Figure 5.29 (b) shows the pyro-oil recovered from combination of 90% FR4 and 10% FR2 PCB. The Higher Heating value (HHV) of FR-2 WPCB pyro-oil were calculated to be 31.79 MJ/kg, whereas the HHV of FR-4 WPCB pyro-oil was found to be 19.65 MJ/kg. HHV of for Rice-husk derived pyro-oil; Saw Dust derived pyro-oil and Plastic derived pyro-oil are 14.95 MJ/kg, 19.46 MJ/kg and 43 MJ/kg respectively (Ferdinand et al. 2012). Hence, FR-2 WPCB pyro-oil

offers a calorific value which is higher than biomass derived pyro-oil but less than plastic-derived pyro-oil. Whereas, the HHV of FR-4 WPCB pyro-oil is marginally higher than Saw Dust pyro-oil.

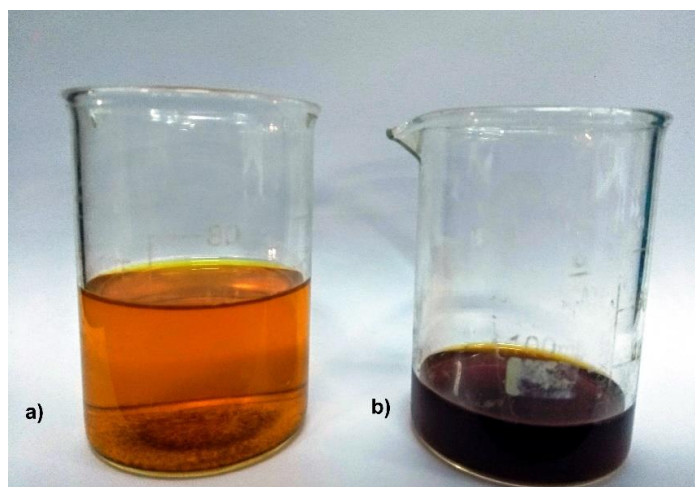


Figure 5.29 (a): Pyro-oil recovered from 90% FR2 and 10% FR4 PCB combination feedstock and (b): 90% FR4 and 10% FR2 PCB combination feedstock.

The polymer part is higher in the FR2 type PCBs compared to FR4 type PCBs. The expected yield of oil is higher when fraction of FR-2 PCB is higher in the FR-2 – FR-4 feed mixture used. The predominant contribution of FR-2 in the generation of pyro-oil can be justified by its presence of higher proportion of polymer in this PCB compared to FR-4 PCB. Figure 5.30 depicts the variation of pyro-oil yield with different percentage of FR-2. It is clear from the figure that at 30% FR-2 (rest FR-4 PCB) the oil yield is highest and lowest at the reverse configuration. The results lack uniformity due to irregular distribution of polymer and metals in the samples as heterogeneity of waste PCB is a big issue worldwide.

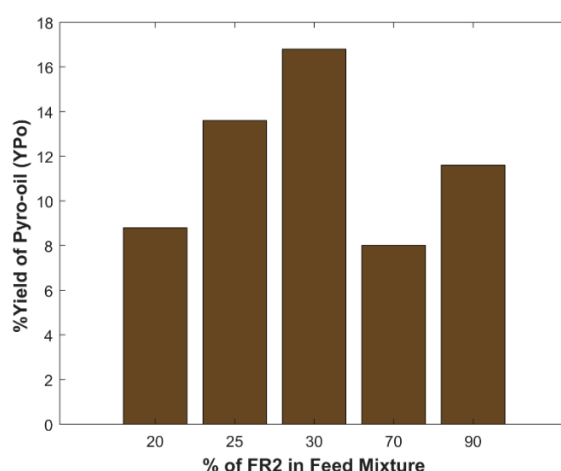


Figure 5.30: Variation of pyro-oil yield with different percentage of FR-2 WPCB in a mixture of FR2 and FR4

5.3.10.2 Recovery of Metals

The residue from the pyrolysis was found to be mixture of metal, glass fibre fabric and carbonaceous materials. The metals recovered contained primarily copper and lead which is present in the linings of the printed circuit boards and solder respectively.

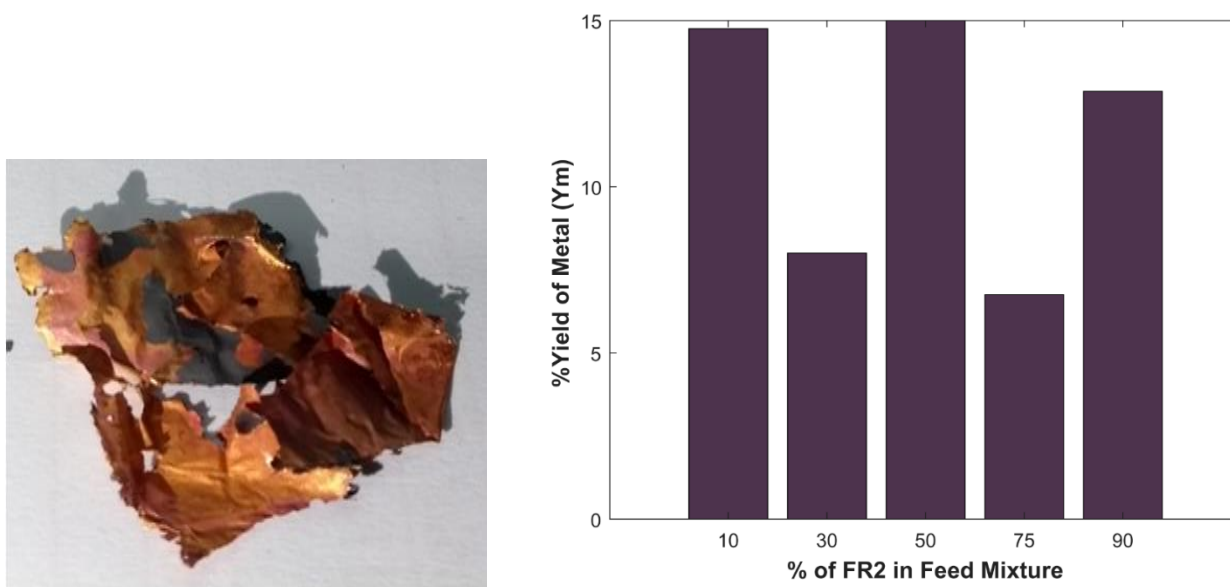


Figure 5.31: (a)Copper recovered via Pyrolysis of mixed WPCB and (b) Variation of yield of metals with different percentage of FR4 PCB

Figure 5.31 (b) depicts the variation of yield of metals with different percentage of FR4 type PCB. The highest yield was found at 50% FR4 PCB followed by 90%. The lowest yield found at 25% FR4 type PCB. Given the fact that the samples were waste PCBs and heterogeneous, the metal yield varied in a non-uniform manner. This effect of heterogeneity could have been eliminated if the ground e-waste were used as feed. As the grinding/milling involves investment of energy, this step has been avoided during the pre-processing of feed of pyrolysis.

5.3.10.3 Recovery of Char and Glass Fibre

The pyro-char was found to be crispy in nature. The glass fibre fabric can be separated manually with ease from the remaining mixture as they are quite bigger (dimensionally) compared to the metal part. The glass fibre was often found to be laden with carbon particles. After combustion, the recovered glass-fibres were found to be quite crispy and may be used as a partial replacement or fillers in composites (Figure 5.32 a).

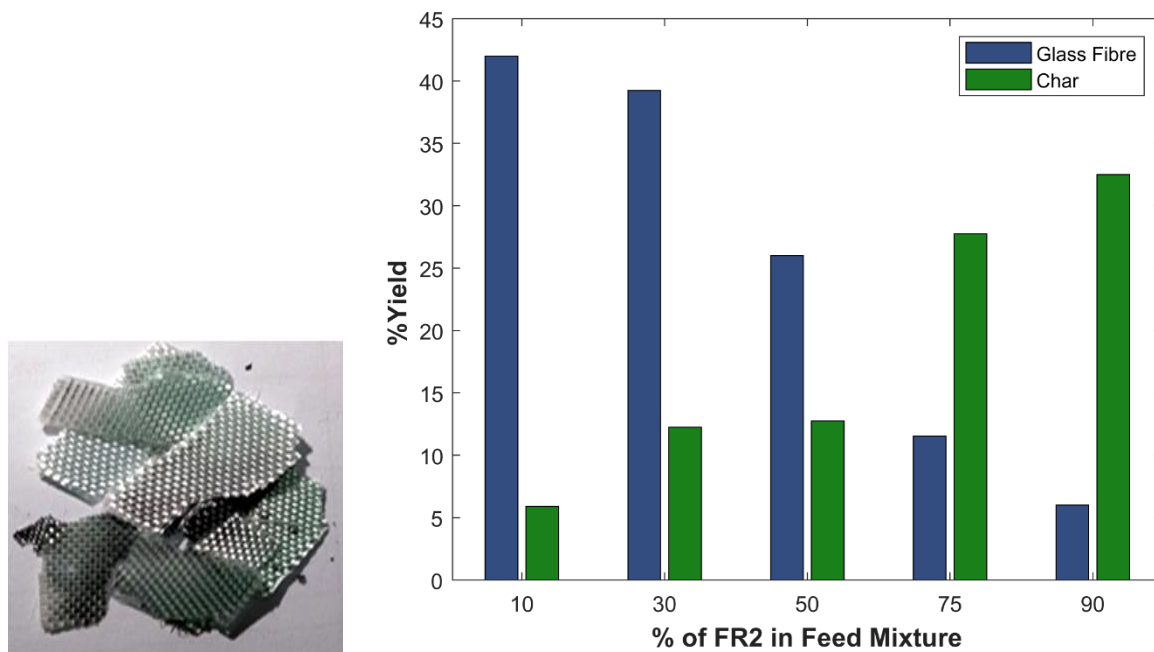


Figure 5.32 (a): Recovered Glass Fibre from PCB and (b) Yield of glass fibre and char

Figure 5.32 (b) depicts the yield of glass fibre and char. It has been observed that with 10% of FR-2 PCB in the feed mixture (i.e., highest mass fraction of FR-4 PCBs), the yield of glass fibre is highest, i.e., ~43%. Yield of glass fibre gradually decreases with the increase in percentage of FR-2 type PCB in the feed mixture with the lowest yield of ~7% at 90% FR-2 PCB in the feed. The reverse result is found in the case of yield of char. The char yield increases with the increase in percentage of FR-2 PCB. It is easily justifiable that content of carbonaceous (polymer) part is higher in FR-2 PCB, in comparison to FR-4.

5.3.11. Characterizations of Pyro-products

5.3.11.1 FESEM and EDX analysis of FR-2 PCBs

The Field Emission Scanning Electron Microscope (FESEM) images shown in figures 5.33(a) and (b) illustrate the FR-2 VPCB raw samples i.e., before pyrolysis and after pyrolysis (pyro-char). Similarly, figures 5.34(a) and (b) present the FESEM images of the FR-2 WPCB raw samples and their corresponding pyro-char samples. The images reveal the surface morphology of the respective samples. As can be seen, the surface of the FR-2 VPCB raw sample is not smooth and contains multiple layers. Whereas the surface of the FR-2 WPCB raw sample contains lots of folds and layers. In addition, some small pores can be noticed which is absent in case of FR-2 VPCB raw samples. The presence of folds and layers could be due to the flakiness of the sample (Li et al. 2007). The pyro-char of FR-2 VPCB (magnification at 2400 x) clearly shows the development of micropores on the surface.

Some cracks are also noticeable which indicates the presence of interconnected channels. In case of FR-2 WPCB pyro-char (magnification at 5000 x) the presence of pores of variable size, possibly distributed as network. Primary investigation revealed that the pores are in the microporous range. EDX analysis (table 5.19) shows that bromine is not present in the FR-2 VPCB pyro-char but bromine is present in FR-2 WPCB pyro-char. Tin, copper, silicon and iron are the available metals in majority. Whereas Silver, Titanium, cadmium and Nickel are present in trace level. These characteristics ensures the possible applicability of FR-2 VPCB and WPCB pyro-char in adsorbent manufacturing for wastewater treatment. Previous studies have reported the usage of the non-metallic fraction char as adsorbent for removal of heavy metals and dye from wastewater (Hadi et al. 2014; Kan et al. 2015).

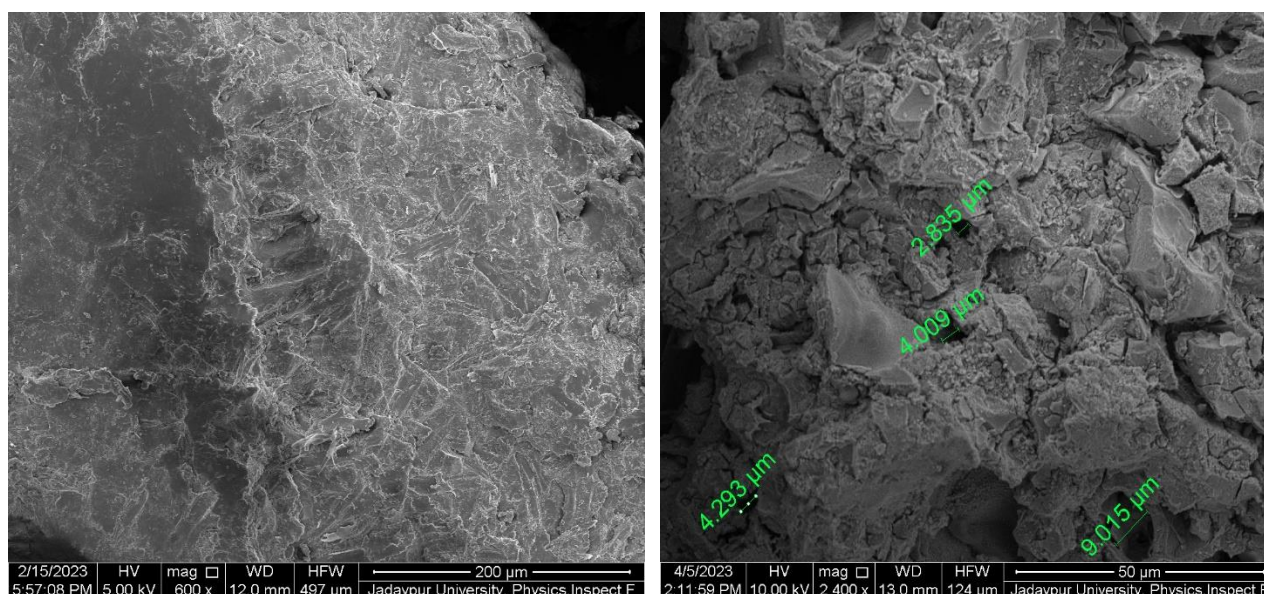


Figure 5.33: FESEM images of FR-2 VPCB (a) before pyrolysis and (b) after pyrolysis

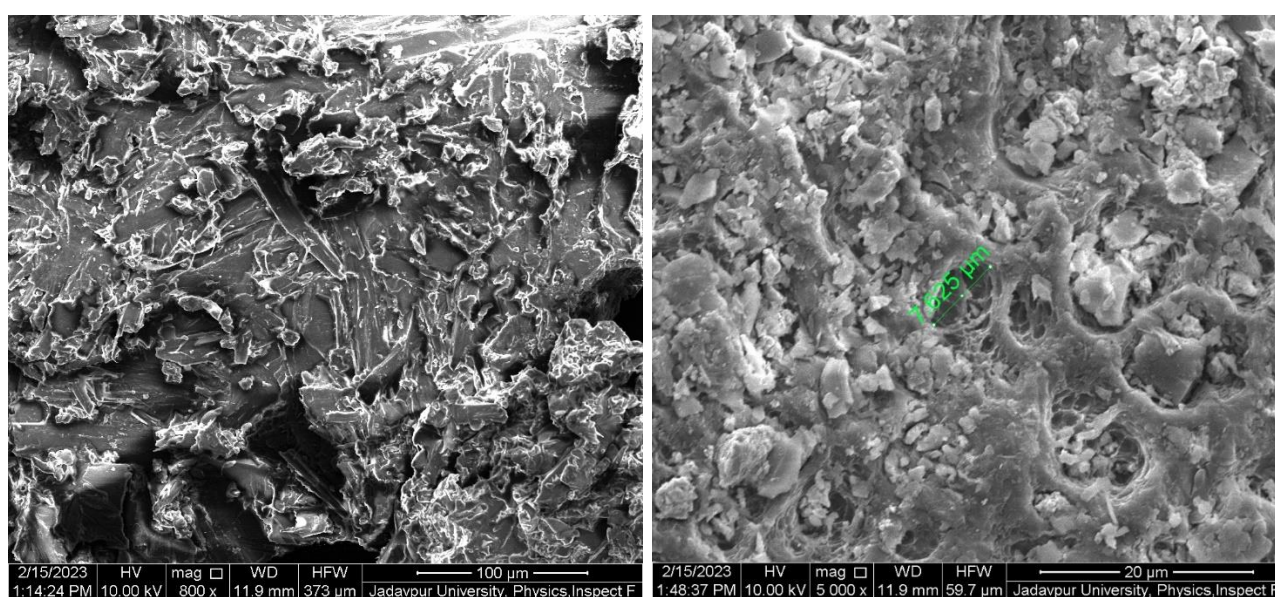


Figure 5.34: FESEM images of FR-2 WPCB (a) before pyrolysis and (b) after pyrolysis

Table 5.19: Metal content mapping of FR-2 VPCB and WPCB before and after pyrolysis

	FR-2 VPCB RAW		FR-2 VPCB Pyro-Char		FR-2 WPCB RAW		FR-2 WPCB Pyro-Char
Metals	Weight (%)	Metals	Weight (%)	Metals	Weight (%)	Metals	Weight (%)
Bromine	12.12	Silicon	7.55	Bromine	4.32	Tin	10.99
Chlorine	7.86	Copper	0.29	Phosphorus	3.47	Bromine	6.79
Gold	7.15			Gold	2.39	Lead	3.91
Tin	1.19			Silicon	1.58	Silicon	2.89
Silver	0.86			Silver	0.7	Gold	2.12
Cadmium	0.78			Tin	0.41	Iron	1.86
Copper	0.61			Copper	0.35	Copper	1.1
Titanium	0.11			Cadmium	0.3	Chlorine	1.07
Silicon	0.1			Arsenic	0.1	Arsenic	0.61
				Nickel	0.09	Silver	0.49
				Iron	0.04	Titanium	0.25
						Nickel	0.11

5.3.11.2 FESEM and EDX analysis of FR-4 PCBs

The Field Emission Scanning Electron Microscope (FESEM) images shown in figures 5.35(a) and (b) illustrate the FR-4 VPCB raw samples before pyrolysis and after pyrolysis (pyro-char). Similarly, figures 5.36 (a) and (b) present the FESEM images of the FR-4 WPCB raw samples and pyro-char respectively. The images reveal the surface morphology of the respective samples. The pyro-char was found to be very fragile and crispy in nature. As can be seen, the surface of both FR-4 VPCB and WPCB raw sample is not smooth and contains multiple layers. The pyro-char of FR-4 VPCB (magnification at 10000 x) clearly shows the development of pores in the nanomaterial range on the surface. Hence, FR-4 VPCB char could be a suitable precursor for development of nanomaterials. In case of FR-4 WPCB pyro-char (magnification at 0000 x) the presence of pores of variable size can be seen, possibly in form of interconnected networks. EDX analysis (Table 5.20) shows that bromine is present in the pyro-char as well as in raw materials. Silicon, Tin, aluminium and copper are the available metals in majority. Whereas Platinum, Titanium, Iron and Nickel are present in trace level. These characteristics ensures the possible applicability of FR-4 VPCB and WPCB pyro-char in adsorbent manufacturing for wastewater treatment. Previous studies have reported the usage of the non-metallic fraction char as adsorbent for removal of heavy metals and dye from wastewater (Hadi et al. 2014; Kan et al. 2015).

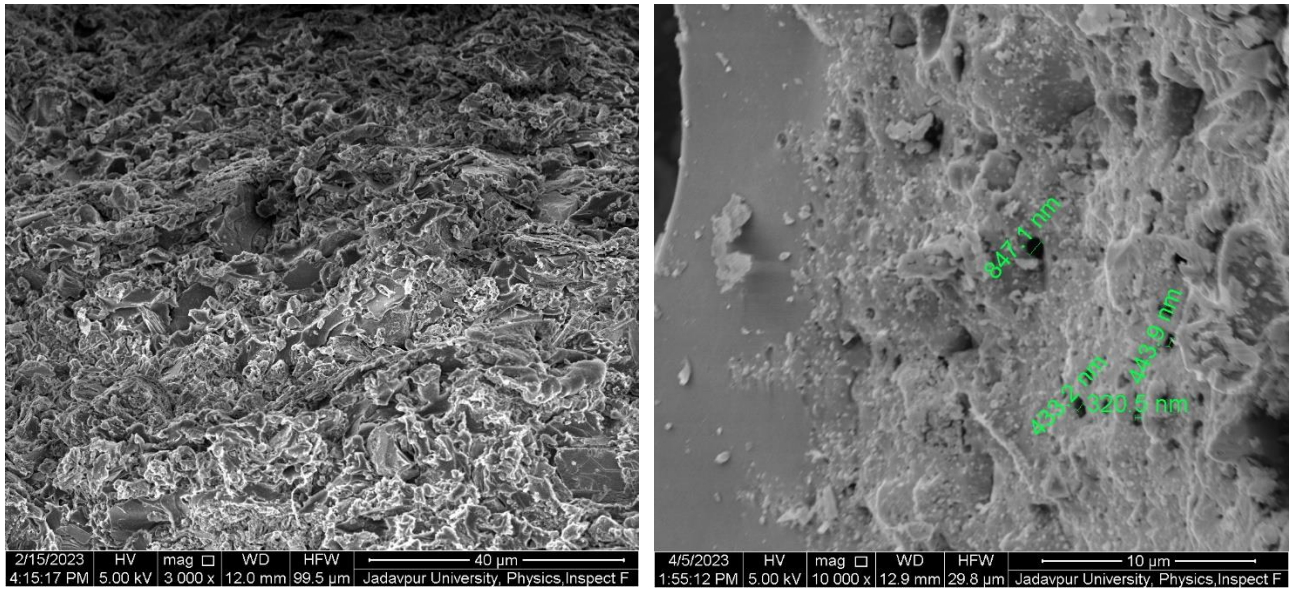


Figure 5.35: FESEM images of FR-4 VPCB (a) before pyrolysis and (b) after pyrolysis

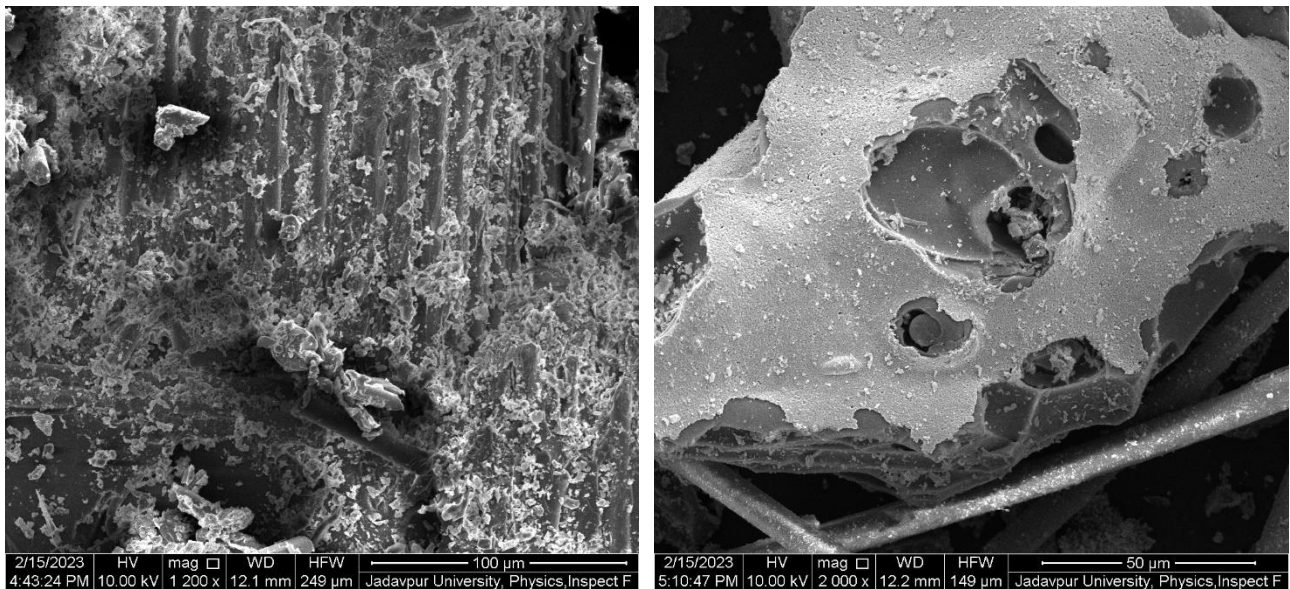


Figure 5.36: FESEM images of FR-4 WPCB (a) before pyrolysis and (b) after pyrolysis

Table 5.20: Metal content mapping of FR-4 VPCB and WPCB before and after pyrolysis

	FR-4 VPCB RAW		FR-4 VPCB Char		FR-4 WPCB RAW		FR-4 WPCB Char
Metals	Weight (%)	Metals	Weight (%)	Metals	Weight (%)	Metals	Weight (%)
Silicon	17.68	Magnesium	0.34	Silicon	16.44	Tin	42.7
Tin	12.37	Nickel	0.63	Calcium	14.66	Bromine	20.12
Aluminium	5.53	Titanium	0.69	Bromine	5.98	Copper	7.07
Gold	3.41	Tin	1.32	Aluminium	3.36	Lead	5.32
Bromine	1.42	Sulfur	1.46	Gold	2.17	Gold	3.3

Copper	0.39	Aluminium	1.9	Lead	1.18	Silicon	0.78
Platinum	0.32	Calcium	1.94	Iron	0.85	Platinum	0.59
Titanium	0.12	Iron	2.03	Titanium	0.57	Arsenic	0.58
Iron	0.04	Lead	2.25	Copper	0.5	Titanium	0.21
Chlorine	0.01	Silicon	4.88	Nickel	0.07	Cadmium	0.16
		Barium	5.55	Cobalt	0.04	Chlorine	0.09
		Copper	5.59			Cobalt	0.08
		Bromine	7.08			Nickel	0.03

5.3.11.3 FESEM and EDX analysis of mixed WPCBs

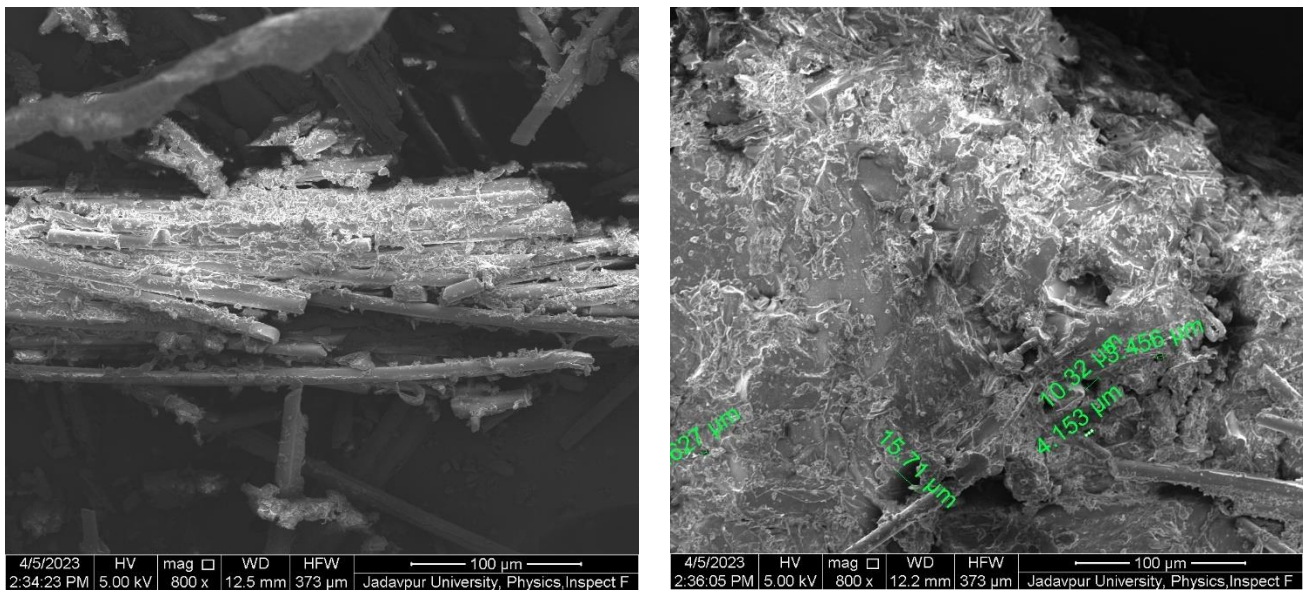


Figure 5.37: FESEM images of mixed WPCB sample before pyrolysis

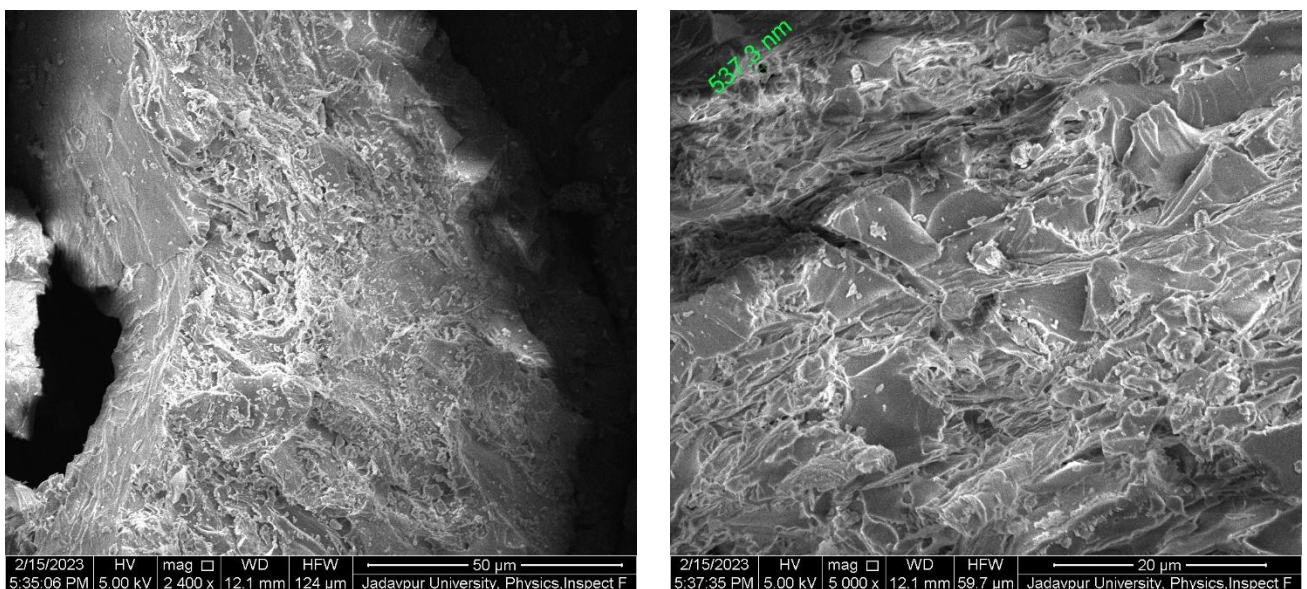


Figure 5.38: FESEM images of mixed WPCB sample after pyrolysis

The Field Emission Scanning Electron Microscope (FESEM) images of mixed WPCB samples are presented in figures 5.37 and 5.38, showing the samples before and after pyrolysis, respectively. The images reveal the surface morphology of the mixed WPCB raw and pyro-char. As can be seen, the surface is not smooth and contains multiple layers. The rod like structures is there due to the presence of glass fibres in the sample. Further magnification (at 800 x) reveals the presence of micropores on the surface of raw material. It can be seen that there are multiple potholes. The presence of folds and layers could be due to the flakiness of the char. Some pores have been identified on the surface of the char. They are in the microporous range. EDX analysis (Table 5.21) shows that bromine is not present in the pyro-char. Tin, cadmium and silver are the available metals in majority. Whereas Tantalum, Titanium, Silicon, Iron, Copper and Nickel are present in trace level. These characteristics ensures the possible applicability of mixed WPCB pyro-char in adsorbent manufacturing for wastewater treatment. However, the residual metals need to be removed before that.

Table 5.21: EDX results of mixed WPCB raw and Pyro-char

Mixed WPCB RAW		Mixed WPCB Pyro-char	
Metals	Weight (%)	Metals	Weight (%)
Bromine	4.22	Tin	2.93
Silicon	2.96	Silver	1.96
Phosphorus	2.93	Cadmium	1.26
Calcium	2.29	Chlorine	1.09
Lead	1.33	Tantalum	0.82
Tantalum	0.82	Titanium	0.74
Tin	0.56	Silicon	0.48
Iron	0.47	Iron	0.48
Sulfur	0.45	Copper	0.06
Silver	0.18	Nickel	0.05
Titanium	0.14		
Copper	0.13		
Cadmium	0.08		

5.3.11.4 XRD analysis of FR-2 PCBs

The XRD analysis is intended for identification of crystal structures. Figure 5.36 (a) & (b) shows the XRD spectra of FR-2 VPCB raw samples and FR-2 VPCB pyro-char respectively. In figure 5.36(a), the broad diffraction peak around 16° is due to the presence of quartz crystals (Shen et al. 2017). The peak at 22.55° has been identified as Cadmium Tin Fluoride (CdSnF₆) (ICSD: 01-073-2437). The diffraction peaks at 43.44°, 50.6° and 74.25° can be attributed to copper (ICSD: 01-073-1326). This is evident as FR-2 VPCBs contain a lot of copper which is clearly visible. Figure 5.36 (b), illustrates the XRD diffraction spectra of FR-2 VPCB pyro-char. It is clearly visible from the figure that there are

very few noticeable sharp peaks, which indicates the amorphous nature of the pyro-char. The peak at 20.86° can be attributed to amorphous SiO_2 (ICSD: 01-082-1570). Peaks at 43.33° and 50.52° can be ascribed to copper (ICSD: 01-085-1326).

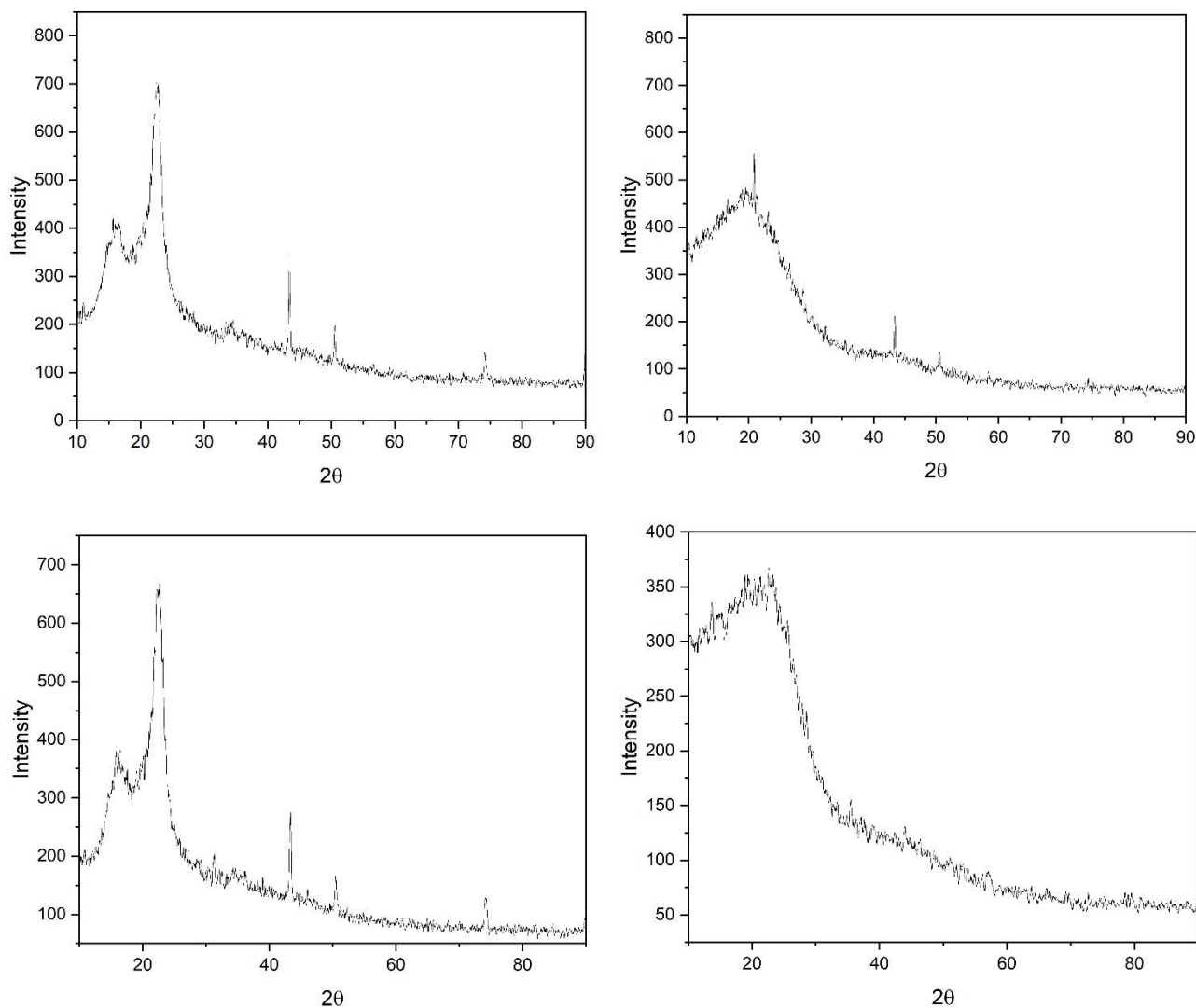


Figure 5.39: XRD Spectra of (a) FR-2 VPCB Raw; (b) FR-2 VPCB Pyro-Char, (c) FR-2 WPCB Raw and (d) FR-2 WPCB Pyro-Char

Figure 5.39 (c) shows the XRD spectra of FR-2 WPCB raw samples. The broad diffraction peak around 15° is due to the presence of quartz crystals (Shen et al. 2017). The peak at 22.45° has been identified as Barium Silicate ($\text{Ba}_2\text{Si}_4\text{O}_{10}$) (ICSD: 01-071-0797). The diffraction peaks at 43.39° , 50.46° and 74.19° are attributed to copper (ICSD: 00-004-0836). This is quite obvious as copper linings are present in the WPCBs and it can be easily seen by naked human eye. Figure 5.39(d), represents the XRD diffraction spectra of FR-2 WPCB pyro-char. As can be seen the structure doesn't contain any

noticeable sharp peaks, which indicates the amorphous nature of the pyro-char. The broad hump around 20° can be attributed to amorphous SiO_2 .

5.3.11.5 XRD analysis of FR-4 PCBs

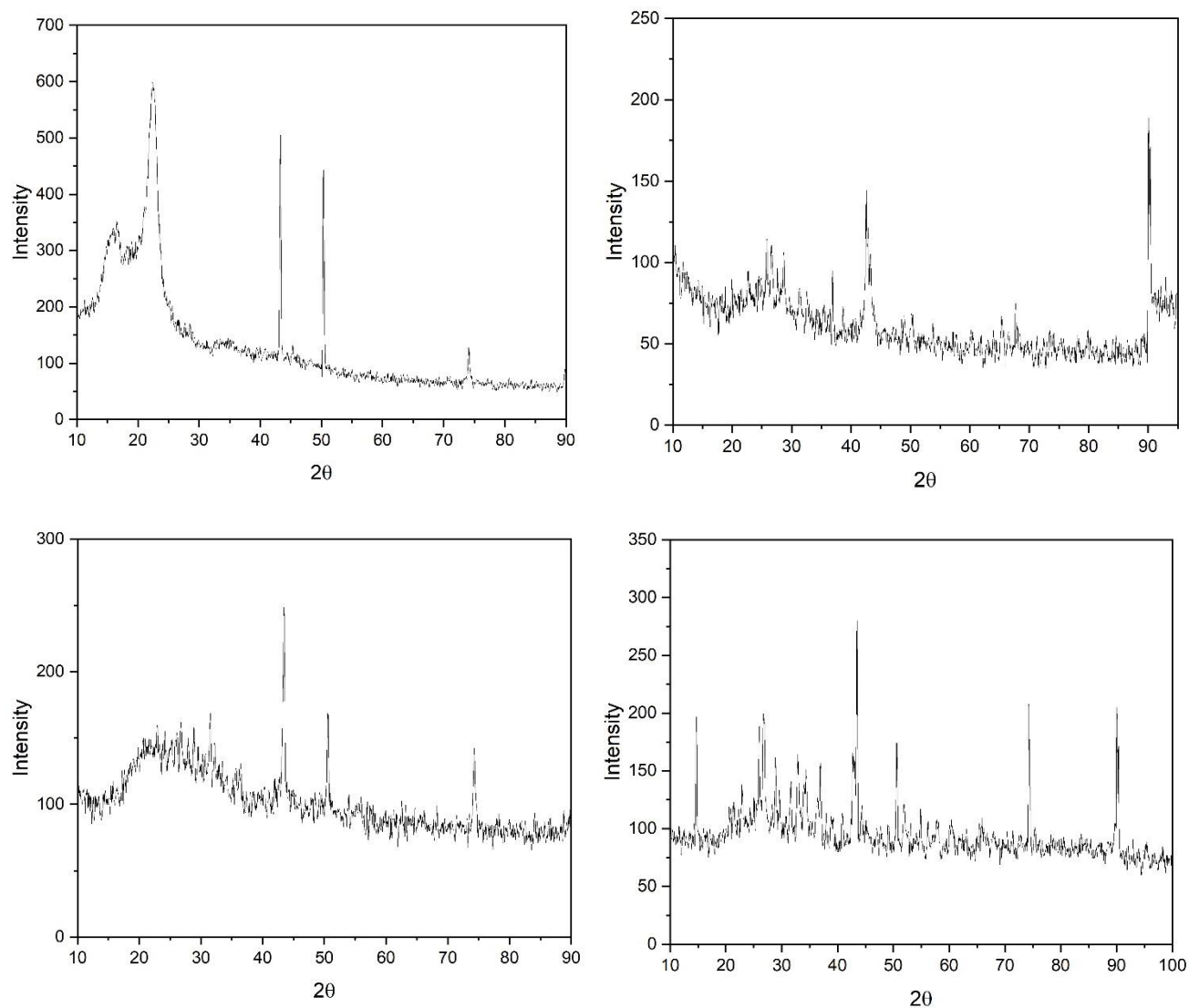


Figure 5.40: XRD Spectra of (a) FR-4 VPCB Raw; (b) FR-4 VPCB Pyro Char, (c) FR-4 WPCB Raw and (d) FR-4 WPCB pyro-char

Figure 5.40 (a) & (b) shows the XRD spectra of FR-4 VPCB raw samples and FR-4 VPCB pyro-char respectively. In figure 5.40(a), the broad diffraction peak around 16° is due to the presence of quartz crystals (Shen et al. 2017). The peak at 18.98° has been identified as Barium Silicate ($\text{Ba}_2\text{Si}_4\text{O}_{10}$) (ICSD: 01-071-0797). The diffraction peaks at 43.3° , 50.3° and 74.1° can be attributed to copper (ICSD: 01-073-1326). This is evident as FR-4 VPCBs contain a lot of copper. Figure 5.40 (b), illustrates the XRD diffraction spectra of FR-4 VPCB pyro-char. It is clearly noticeable that there are

very few sharp peaks, which indicates the amorphous nature of the pyro-char but it also confirms the presence of metals in the char. The peak around 25° can be attributed to Lead silicate oxide (ICSD: 01-075-2276). Peaks at 42.81° and 43.28° are attributed to Nickel Zinc Oxide (ICSD: 01-075-0273) and Iron Nitride (ICSD: 01-075-2131) respectively.

In figure (5.40c) the broad peak around 25° can be attributed to the presence of SiO_2 (Shen et. al 2017). The presence of this peak is evident as FR-4 WPCB's contain glass fibre. Peaks at 43.45° & 50.52° are due to the presence of Cu (ICSD:01-089-2838). Another peak appeared at 74.29° which has been identified as Iron nitride (ICSD:01-075-2129). A few peaks have appeared in the FR-4 WPCB char (Figure 5.40d). Peak at 14.37° was identified as Aluminium Fluoride (ICSD: 01-084-1672). Peak around 26° has been identified as quartz (ICSD: 01-085-0795). Peak at 43.49° has been identified as chromium (ICSD: 01-088-2323) whereas peak at 74.29° is due to copper (ICSD: 01-089-2838).

5.3.11.6 XRD analysis of mixed WPCBs

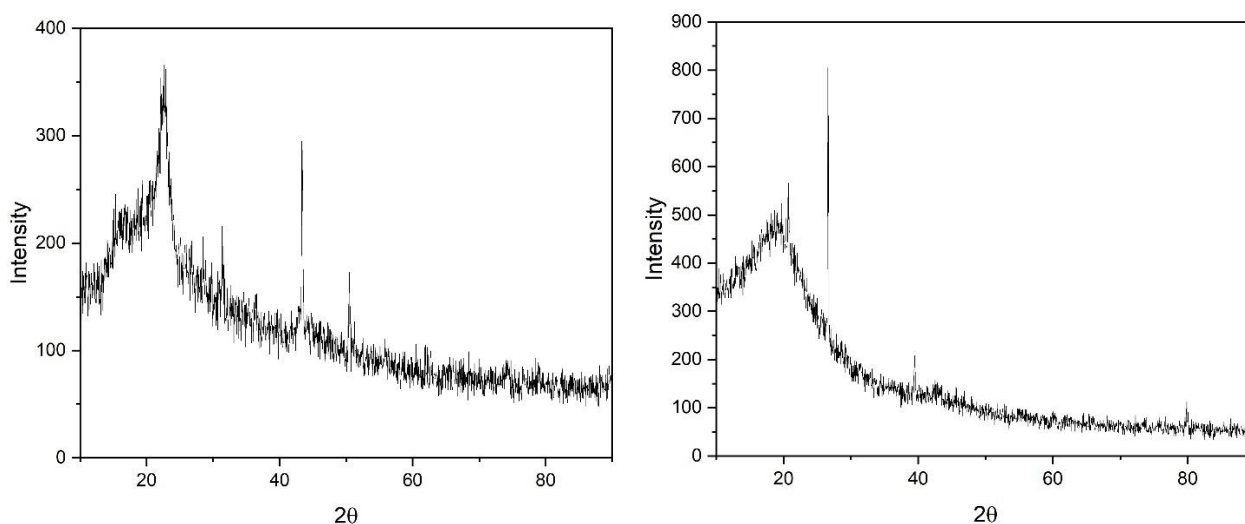


Figure 5.41: XRD Spectra of (a) mixed WPCB Raw and (b) mixed WPCB Pyro Char

Figure 5.41 (a) & (b) shows the XRD spectra of mixed WPCB raw samples and pyro-char respectively. In figure 5.41 (a), the broad peak around 20° can be attributed to quartz crystals. Peaks at 31.36° , 50.49° & 51.26° has been identified as SiO_2 in the form of cristobalite (ICSD :01-089-3606 & 01-082-1232). The SiO_2 peak at 61.92° has been identified as ferrierite (ICSD:01-082-1396). Cu was found at about 43.37° (ICSD: 01-089-2838), Peak around 30° was identified as magnesium silicate in the form of forsterite (ICSD: 01-089-5130).

In case of pyro-char (figure 5.38 b), the broad peak of quartz at about 22° . SiO_2 crystals were identified at around 26.61° & 79.85° (ICSD: 01-088-2487). A peak of copper titanium (CuTi_2) was identified at

about 40° (ICSD:01-072-2403). The peaks at about 37° & 53° can be attributed to ferrous oxide (ICSD:01-089-7047).

5.3.11.7 FTIR Analysis of FR-2 PCBs

FTIR spectra of FR2 VPCB & WPCB, before and after pyrolysis are presented in figure 5.42 (a-b) and figure 5.42 (c-d) respectively. A structural similarity with IR spectra of phenolic resin is observed with figure 5.42 (a) and (c) (Wang et al. 2021). In both VPCB and WPCB raw samples, the peaks are found in the similar region. The presence of the strong broad peak at 3338 and 3332 cm^{-1} in figure 5.42 (a) and (c) affirms the presence of phenol in raw PCB. The peaks within $2800 - 2900\text{ cm}^{-1}$ are assigned to methyl or methylene groups present in the raw material. Peaks at 2157 cm^{-1} ($\text{C}\equiv\text{N}$ stretch) confirms the presence of Acrylonitrile butadiene styrene (ABS). Identical peaks at 1735 , 1457 and 1219 cm^{-1} are obtained for both raw-PCB. These are attributed to $\text{C}=\text{O}$ stretch, $\text{C}-\text{H}$ bend and $\text{C}-\text{N}$ stretching which amplifies the presence of esters, methyl/methylene groups and amines.

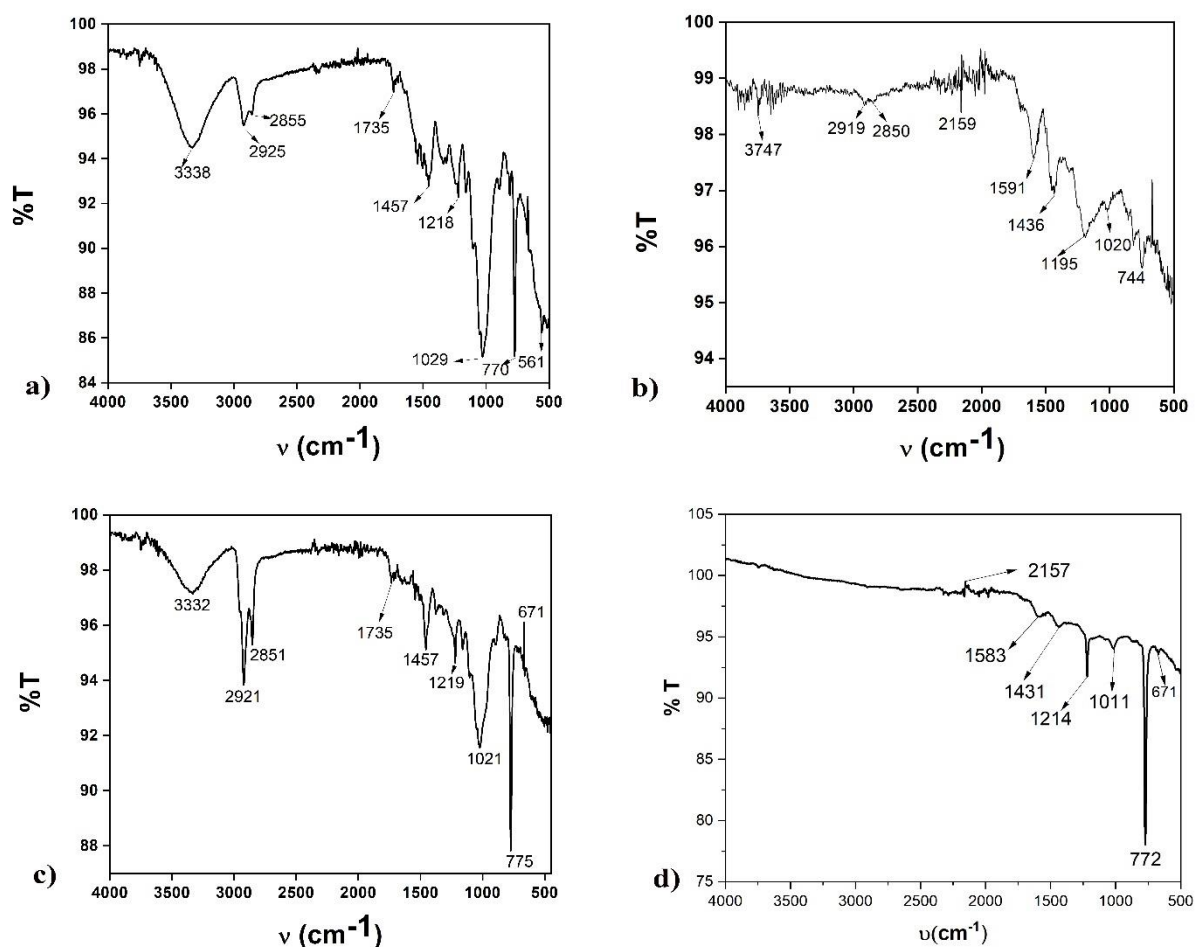


Figure 5.42: IR spectra of (a) Ground FR2 VPCB before pyrolysis; (b) FR2 VPCB char (after pyrolysis); (c) Ground FR2 WPCB before pyrolysis and (d) FR2 WPCB char (after pyrolysis).

The peaks at 1029 and 1021 cm^{-1} represents C–O stretching which could be alcohols, ethers or esters. The peaks around 770 cm^{-1} are important. They represent aromatic mono, para, meta, and ortho-substituted components or halides. The peaks at 671 cm^{-1} and 561 cm^{-1} confirm the presence of bromine in both PCBs as this range is attributed to C-Br stretching. The two major peaks around 3330 and 2920 cm^{-1} confirm the presence of TBBPA, which are the characteristic peaks (Xia et al. 2021). Peaks around 1600, 1300, 1050 and 770 cm^{-1} confirm the presence of TBBPA (Li et al. 2020). In VPCB-char, identified peaks at 3747, 2919 and 2850 cm^{-1} affirm the presence of free OH and methyl or methylene bonds. The WPCB-char doesn't contain any peak in the 4000 – 2200 cm^{-1} regions. Peak at 2159 cm^{-1} and 2157 cm^{-1} ($\text{C}\equiv\text{N}$ stretch) confirms the presence of ABS in PCB char. The peaks within 1600 – 1400 cm^{-1} in both chars represent vibration in aromatics. The 1250 – 750 cm^{-1} range represent the C–O stretching and aromatic mono, para, meta, and ortho-substituted components. This affirms the retention of aromatics, amines and some aliphatic compound in the char. One must note the absence of bromine in the char of both PCBs, rather they are present in the pyro-oil. Additionally, the absence of peaks in 4000 – 2200 cm^{-1} region of WPCB can be accredited to catalytic effect of metals presents in the WCPB. Details of FTIR spectra of FR2 VPCB and WPCB raw sample, char and oil are presented in Table 4.

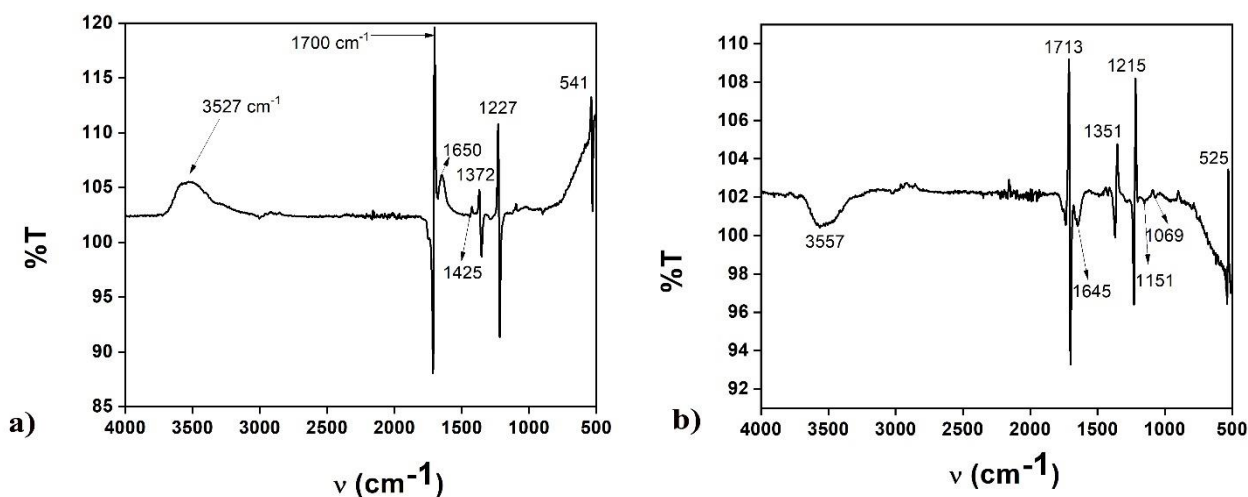


Figure 5.43: IR spectra of Pyro-oil recovered from (a) FR2 VPCB pyrolysis and (b) FR2 WPCB pyrolysis

The broad peaks at 3527 and 3557 cm^{-1} confirm the presence of phenols in both pyro-oils (Figure 5.43). The large peaks at 1700 and 1713 cm^{-1} in VPCB and WPCB oils respectively affirms the

presence of conjugated acids. Aromatics are present in both pyro-oils affirmed by peaks within 1600 – 1400 cm^{-1} . The OH vibration of phenol and phenol derivatives (1372 and 1351 cm^{-1}) reaffirms it. The bands between 1390 and 1220 cm^{-1} are present always when phenolic compounds are analysed (Zhou and Qiu 2010). Peaks at 1151 and 1069 cm^{-1} of WPCB pyro-oil are attributed to C–O stretching which marks the possibility of presence of alcohols, ethers, esters, carboxylic acid etc in pyro-oil. The peaks at 541 and 525 cm^{-1} affirms the migration of bromine in pyro-oil. Characteristic peaks around 1650, 1350, 1230 and 550 cm^{-1} suggest that Bisphenol A is a possible pyrolysis product (Ullah et al. 2016).

Table 5.22: FTIR spectra analysis of FR2 VPCB Raw, Char and Oil

FR2 VPCB RAW			FR2 VPCB CHAR			FR2 VPCB OIL		
Frequency	Bond	Interpretation	Frequency	Bond	Interpretation	Frequency	Bond	Interpretation
3338	O–H Stretching	vibration in hydroxyl group in phenols or alcohols (s,b)	3747	O-H stretching	Free OH (medium, sharp)	3527	O–H Stretching	vibration in hydroxyl group in phenols or alcohols (s,b)
2925	C–H stretch	Methyl or methylene group (m)	2919	C–H stretch	Methyl or methylene group (m)	1700	C=O stretch	Conjugated acid (s)
2855	C-H stretching	Methyl or methylene group (m)	2850	C–H stretch	Alkane (m)	1650	C=C stretching (in-ring)	vibration in aromatics group
1735	C=O stretch	Esters	2159	C≡N stretch	Acrylonitrile butadiene styrene (ABS) (s)	1425	C=C stretching (in-ring)	vibration in aromatics group
2157	C≡N stretch	Acrylonitrile butadiene styrene (ABS) (s)	1591	C=C stretching (in-ring)	vibration in aromatics group	1372	O–H Stretching	vibration in phenols or phenol derivatives
1457	C–H bend	Alkanes (m) Methyl/Methylene Group						
1218	C–N Stretching	Amines (s)	1436	C=C stretching (in-ring)	vibration in aromatics group	1225	C–N Stretching	Amine (s)
1029	C-F Stretching Or C-O Stretching	Fluoro compound (s) Or Alcohols, ethers, esters, carboxylic acids, anhydrides (s)	1195	C–O Stretching	Ether or tertiary alcohols (s)	541	C-Br stretching	Halide (s)
770	C–Cl stretching	Aromatic mono, para, meta, and ortho-substituted components	1020	C-F Stretching Or	Fluoro compound (s) Or Alcohols, ethers, esters, carboxylic			

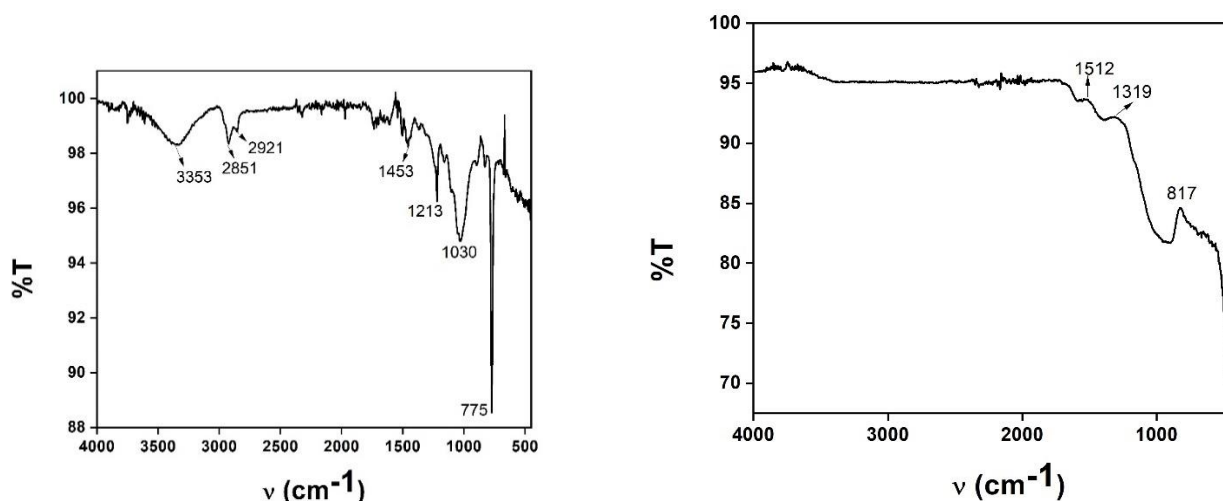
561	C-Br stretching	Halide (s)	744	C-O stretching C-Cl stretching	acids, anhydrides (s) Aromatic mono, para, meta, and ortho-substituted components
-----	-----------------	------------	-----	-----------------------------------	--------------------------------------------------------------------------------------

Table 5.23: FTIR Spectra of FR2 WPCB Raw, Char and Oil

FR2 WPCB RAW			FR2 WPCB CHAR			FR2 WPCB OIL		
Frequency	Bond	Interpretation	Frequency	Bond	Interpretation	Frequency	Bond	Interpretation
3332	O-H Stretching	vibration in hydroxyl group in phenols or alcohols (s,b)	2157	C≡N stretch	Acrylonitrile butadiene styrene (ABS) (s)	3557	O-H Stretching	vibration in hydroxyl group in phenols or alcohols (s,b)
2921	C-H stretch	Methyl or methylene group (m)	1583	C=C stretch (in-ring)	vibration in aromatics group	1713	C=O stretch	Conjugated acid (s)
2851	C-H stretching	Methyl or methylene group (m)	1431	C=C stretch (in-ring)	vibration in aromatics group	1645	C=C stretch (in-ring)	vibration in aromatics group
2153	C≡N stretch	Acrylonitrile butadiene styrene (ABS) (s)	1214	C-O Stretching	Ether or tertiary alcohols (s)	1351	O-H Stretching	vibration in phenols or phenol derivatives
1457	C-H bend	Alkanes (m) Methyl/Methylene Group	1011	C-F Stretching Or C-O Stretching	Fluoro compound (s) Or Alcohols, ethers, esters, carboxylic acids, anhydrides (s)	1215	C-N Stretching	Amine (s)
1219	C-N Stretching	Amine (s)	772	C-Cl stretching	Aromatic mono, para, meta, and ortho-substituted components	1151	C-O Stretching	Aliphatic Ether (s)
1021	C-F Stretching Or C-O Stretching	Fluoro compound (s) Or Alcohols, ethers, esters, carboxylic acids, anhydrides (s)				1069	C-F Stretching Or C-O Stretching	Fluoro compound (s) Or Alcohols, ethers, esters, carboxylic acids, anhydrides (s)
775	C-Cl stretching	Aromatic mono, para, meta, and ortho-substituted components				525	C-Br stretching	Halide (s)
671	C-Br stretching	Halide (s)						

5.3.11.8 FTIR Analysis of FR-4 PCBs

FTIR spectra of FR4 VPCB & WPCB, before and after pyrolysis are presented in figure 5.44 (a -b) and figure 5.44 (c - d) respectively. A structural similarity with IR spectra of epoxy resin is observed with figure 5.44 (a) and (c) (Wang et al. 2021). In both VPCB and WPCB raw samples, the peaks are found in the similar region. The presence of the strong broad peak at 3353 and 3369 cm^{-1} in figure 5.44 (a) and (c) affirms the presence of phenol in raw PCB. The peaks within 2800 – 2900 cm^{-1} are assigned to methyl or methylene groups present in the raw material. No peaks were found in the range of 2100 cm^{-1} ($\text{C}\equiv\text{N}$ stretch) which confirms the absence of Acrylonitrile butadiene styrene (ABS) in FR-4 PCBs. Identical peaks around 1700 - 1750, 1400-1500 and 1210 -1230 cm^{-1} are obtained for both raw-PCB. These are attributed to $\text{C}=\text{O}$ stretch, $\text{C}-\text{H}$ bend and $\text{C}-\text{N}$ stretching which amplifies the presence of esters, methyl/methylene groups and amines. The peaks at 1030 and 1013 cm^{-1} represents $\text{C}-\text{O}$ stretching which could be alcohols, ethers or esters. The peaks at 775 and 765 cm^{-1} are important. They represent aromatic mono, para, meta, and ortho-substituted components or halides. These peaks could be due to the presence of chlorine (as identified by EDX) in both PCBs as well. The two major peaks around 3350 and 2900 cm^{-1} confirm the presence of TBBPA, which are the characteristic peaks (Xia et al. 2021). Peaks around 1600, 1300, 1050 and 770 cm^{-1} confirm the presence of TBBPA in both FR-4 VPCB and WPCB as well (Li et al. 2020).



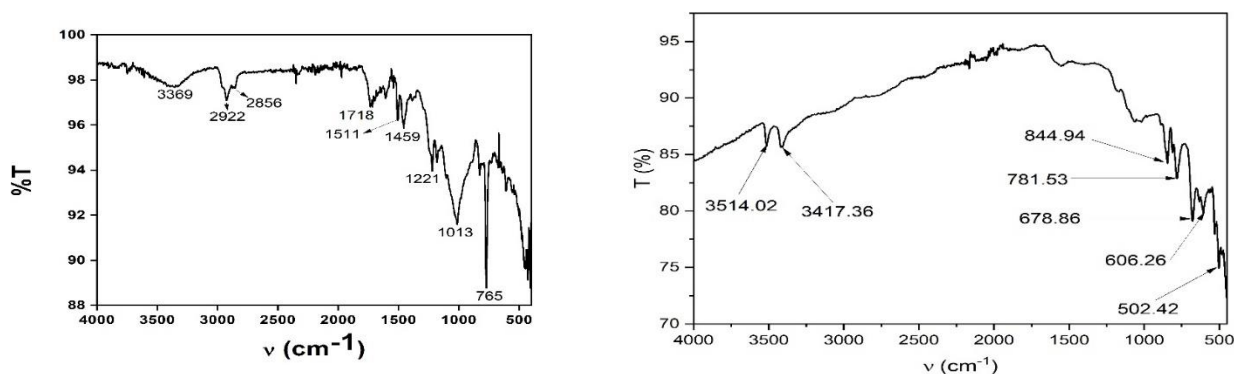


Figure 5.44: IR spectra of (a) FR4 VPCB before pyrolysis; (b) FR4 VPCB char (after pyrolysis); (c) FR4 WPCB before pyrolysis and (d) FR4 WPCB char (after pyrolysis).

In VPCB-char, the peaks of TBBPA and Phenolic OH has not been identified, which confirms complete decomposition of phenols and TBBPA. The identified peak at 1512 and 1319 cm⁻¹ represent vibration in aromatics. Peak at 817 cm⁻¹ affirms the presence of halides. The WPCB-char contain two peaks in the 3400 – 3550 cm⁻¹ regions, which affirms that full decomposition of phenolic has not taken place in this case. No peaks have been found within 1600 – 1400 cm⁻¹. This affirms the retention of aromatics, amines and some aliphatic compound in the pyro-oil. Some peaks have been obtained in the range of 500 – 800 cm⁻¹ regions of WPCB can be accredited to the presence of bromine and chlorine. Details of FTIR spectra of FR4 VPCB and WPCB raw sample, char and oil are presented in Table 5.24.

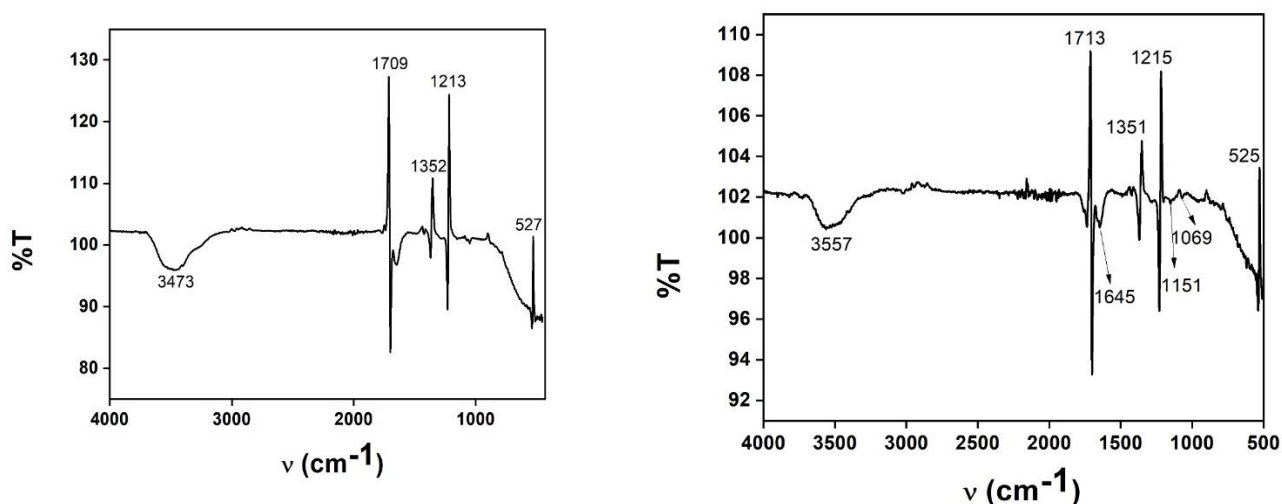


Figure 5.45: IR spectra of Pyro-oil recovered from (a) FR4 VPCB pyrolysis and (b) FR4 WPCB pyrolysis

The broad peaks at 3473 and 3557 cm⁻¹ confirm the presence of phenols in both FR-4 VPCB and WPCB pyro-oils (Figure 5.45). The large peaks at 1709 and 1713 cm⁻¹ in FR-4 VPCB and WPCB oils

respectively affirms the presence of conjugated acids. Aromatics are present in both pyro-oils affirmed by peaks within $1600 - 1300 \text{ cm}^{-1}$. The OH vibration of phenol and phenol derivatives (1352 and 1351 cm^{-1}) reaffirms it. The bands between 1390 and 1220 cm^{-1} are present always when phenolic compounds are analysed (Zhou and Qiu 2010). Peaks at 1151 and 1069 cm^{-1} of FR-4 WPCB pyro-oil are attributed to C–O stretching which marks the possibility of presence of alcohols, ethers, esters, carboxylic acid etc in pyro-oil. The peaks at 527 and 525 cm^{-1} affirms the migration of bromine in pyro-oil. Characteristic peaks around 1709 , 1350 , 1210 and 550 cm^{-1} suggest that Bisphenol A is a possible pyrolysis product (Ullah et al. 2016).

Table 5.24: FTIR spectra analysis of FR4 VPCB Raw, Char and Oil

FR4 VPCB RAW			FR4 VPCB CHAR			FR4 VPCB OIL		
Frequency	Bond	Interpretation	Frequency	Bond	Interpretation	Frequency	Bond	Interpretation
3353	O–H Stretching	vibration in hydroxyl group in phenols or alcohols (s,b)	1512	C=C stretch (in-ring)	vibration in aromatics group	3473	O–H Stretching	vibration in hydroxyl group in phenols or alcohols (s,b)
2921	C–H stretch	Methyl or methylene group (m)	1319	C=C stretch (in-ring)	vibration in aromatics group	1709	C=O stretch	Conjugated acid (s)
2851	C–H stretching	Methyl or methylene group (m)	817	C–Cl stretching	Aromatic mono, para, meta, and ortho-substituted components	1352	O–H Stretching	vibration in phenols or phenol derivatives
1720	C=O stretch	Esters						
1453	C–H bend	Alkanes (m) Methyl/Methylene Group				1213	C–N Stretching	Amine (s)
1213	C–N Stretching	Amines (s)						
1030	C–F Stretching Or C–O Stretching	Fluoro compound (s) Or Alcohols, ethers, esters, carboxylic acids, anhydrides (s)						
775	C–Cl stretching	Aromatic mono, para, meta, and ortho-substituted components						

Table 5.25: FTIR Spectra of FR4 WPCB Raw, Char and Oil

FR4 WPCB RAW			FR4 WPCB CHAR			FR4 WPCB OIL		
Frequency	Bond	Interpretation	Frequency	Bond	Interpretation	Frequency	Bond	Interpretation
3369	O-H Stretching	vibration in hydroxyl group in phenols or alcohols (s,b)	3514, 3417	O-H Stretching	vibration in hydroxyl group in phenols or alcohols (s,b)	3557	O-H Stretching	vibration in hydroxyl group in phenols or alcohols (s,b)
2922	C-H stretch	Methyl or methylene group (m)	844.94, 781.53	C-Cl stretching	Aromatic mono, para, meta, and ortho-substituted components	1713	C=O stretch	Conjugated acid (s)
2856	C-H stretching	Methyl or methylene group (m)	678, 606, 502	C-Br stretching	Halide (s)	1645	C=C stretch (in-ring)	vibration in aromatics group
1718	C=O stretch	Esters				1351	O-H Stretching	vibration in phenols or phenol derivatives
1459	C-H bend	Alkanes (m) Methyl/Methylene Group				1215	C-N Stretching	Amine (s)
1221	C-N Stretching	Amine (s)				1151	C-O Stretching	Aliphatic Ether (s)
1013	C-F Stretching Or C-O Stretching	Fluoro compound (s) Or Alcohols, ethers, esters, carboxylic acids, anhydrides (s)				1069	C-F Stretching Or C-O Stretching	Fluoro compound (s) Or Alcohols, ethers, esters, carboxylic acids, anhydrides (s)
765	C-Cl stretching	Aromatic mono, para, meta, and ortho-substituted components				525	C-Br stretching	Halide (s)
621	C-Br stretching	Halide (s)						

5.3.11.9 FTIR Analysis of mixed PCBs

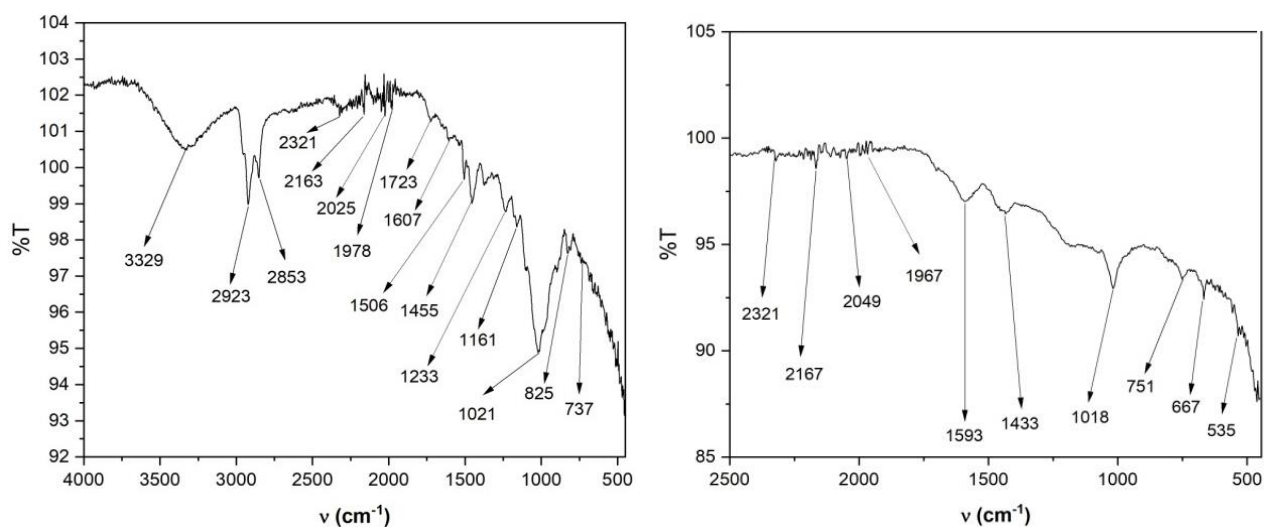


Figure 5.46: IR spectra of (a) FR4 VPCB before pyrolysis; (b) FR4 VPCB char (after pyrolysis); (c) FR4 WPCB before pyrolysis and (d) FR4 WPCB char (after pyrolysis).

FTIR spectra of mixed WPCB, before and after pyrolysis are presented in figure 5.46 (a) and (b). A structural similarity with IR spectra of FR-2 and FR-4 WPCB are observed (Wang et al. 2021). In both mixed WPCB raw samples, the presence of the strong broad peak at 3329 cm⁻¹ affirms the presence of phenol in raw PCB. The peaks within 2800 – 2900 cm⁻¹ are assigned to methyl or methylene groups present in the raw material. Peak at 2321 cm⁻¹ (C≡N stretch) confirms the presence of Acrylonitrile butadiene styrene (ABS). The peak at 2163 cm⁻¹ presents (–C≡C–) stretch alkynes. Peaks at 1723, 1607, 1506, 1455, 1233 and 1161 cm⁻¹ are attributed to C=O stretch, C=C alkane, N–O asymmetric stretch nitro compounds, C–H bend and C–N stretching which amplifies the presence of esters, methyl/methylene groups and amines. The peak at 1021 cm⁻¹ represents C–O stretching which could be alcohols, ethers or esters. The peaks around 770 cm⁻¹ are important. They represent aromatic mono, para, meta, and ortho-substituted components or halides. The two major peaks at 3329 and 2923cm⁻¹ confirm the presence of TBBPA, which are the characteristic peaks (Xia et al. 2021). Peaks around 1600, 1300, 1050 and 770 cm⁻¹ confirm the presence of TBBPA (Li et al. 2020).

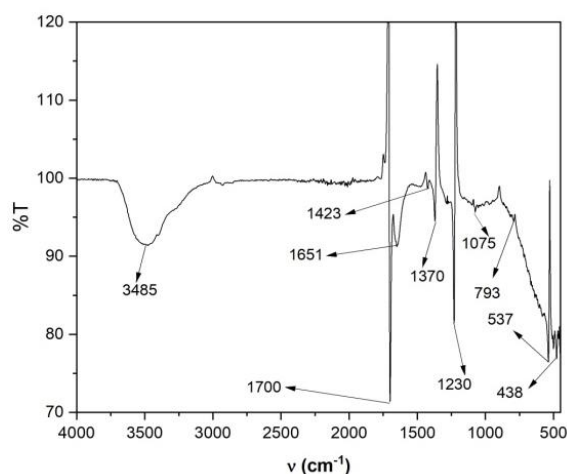


Figure 5.47: IR spectra of Pyro-oil recovered from mixed WPCB pyrolysis

FTIR spectra of Pyro-oil recovered from mixed WPCB pyrolysis is shown in figure 5.47. The broad peak at 3485 cm^{-1} confirms the presence of phenols in both pyro-oils (Figure 5.47). The large peak at 1700 cm^{-1} (similar to FR-2 VPCB) affirms the presence of conjugated acids. Aromatics are present in the pyro-oils as affirmed by peaks within $1600 - 1400\text{ cm}^{-1}$. The OH vibration of phenol and phenol derivatives (1370 cm^{-1}) reaffirms it. The bands between 1390 and 1220 cm^{-1} are present always when phenolic compounds are analysed (Zhou and Qiu 2010). Peak at 1075 cm^{-1} of WPCB pyro-oil are attributed to C–O stretching which marks the possibility of presence of alcohols, ethers, esters, carboxylic acid etc in pyro-oil. The peak at 537 cm^{-1} affirms the migration of bromine in pyro-oil. Characteristic peaks around 1651 , 1370 , 1230 and 537 cm^{-1} suggest that Bisphenol A is a possible pyrolysis product (Ullah et al. 2016).

Table 5.26: FTIR spectra analysis of Mixed WPCB Raw, Char and Oil

Mixed WPCB RAW			Mixed WPCB CHAR			Mixed WPCB OIL		
Frequency	Bond	Interpretation	Frequency	Bond	Interpretation	Frequency	Bond	Interpretation
3329	O–H Stretching	vibration in hydroxyl group in phenols or alcohols (s,b)	2321, 2167	C≡N stretch	Acrylonitrile butadiene styrene (ABS) (s)	3485	O–H Stretching	vibration in hydroxyl group in phenols or alcohols (s,b)
2923	C–H stretch	Methyl or methylene group (m)	2049, 1967	X=C=Y	Allenes, Ketenes, Isocyanates, Isothiocyanates	1700	C=O stretching	Conjugated acid (s)
2853	C–H stretching	Methyl or methylene group (m)	1593	C=C stretch	vibration in aromatics group	1651	C=C stretching	vibration in aromatics group

1723	C=O stretch	Esters	1433	(in-ring) C=C stretch	vibration in aromatics group	1423	h (in-ring) C=C stretch	vibration in aromatics group
2321, 2163	C≡N stretch	Acrylonitrile butadiene styrene (ABS) (s)	1020	(in-ring) C-F stretching	Fluoro compound (s) Or Alcohols, ethers, esters, carboxylic acids, anhydrides (s)	1370	h (in-ring) O-H stretching	vibration in phenols or phenol derivatives
1455	C-H bend	Alkanes (m) Methyl/Methylene Group		Or C-O stretching				
1233	C-N stretching	Amines (s)				1230	C-N stretching	Amine (s)
1021	C-F stretching	Fluoro compound (s) Or Alcohols, ethers, esters, carboxylic acids, anhydrides (s)				1075	C-F stretching	Fluoro compound (s) Or Alcohols, ethers, esters, carboxylic acids, anhydrides (s)
825, 737	C-Cl stretching	Aromatic mono, para, meta, and ortho-substituted components				793	C-Cl stretching	Aromatic mono, para, meta, and ortho-substituted components
						537	C-Br stretching	Halide (s)

5.3.11.10 ¹H NMR Results of FR-2 PCBs

¹H NMR spectra of VPCB and WPCB pyro-oils are shown in Figure 5.48 (a) and (b). The resonances between 6 – 8 ppm are associated with aromatic structures. The broad peak in 4 – 5 ppm range is of the DMSO-d₆. Resonances in 4 – 6 ppm are assigned to phenolic proton. Their peaks may overlap with that of the solvent and hence may be covered by the latter. Peaks in the 1 – 3 ppm range confirm the presence of aliphatic protons. In case of VPCB, the aliphatic peaks are moderately stronger than WPCB ones. Most aromatic hydrogens occur in 6.5-7.5 ppm range, suggesting aromatic species are predominantly phenolic, which is in line with the FTIR results.

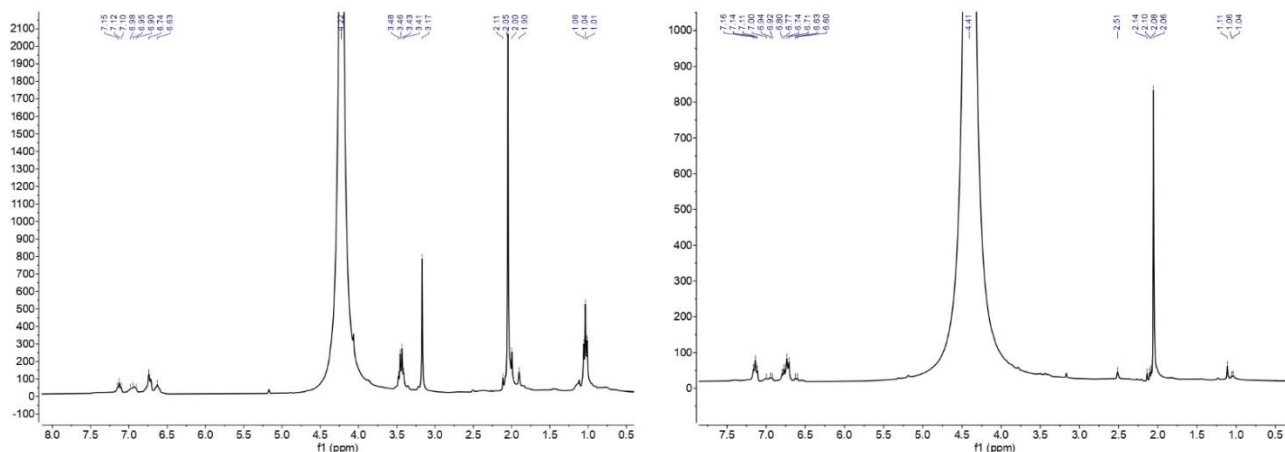


Figure 5.48: ^1H NMR spectra of (a) VPCB Pyro-oil and (b) WPCB Pyro-oil

5.3.11.11 ^1H NMR Results of FR-4 PCBs

^1H NMR spectra of FR-4 VPCB and WPCB pyro-oils are shown in Figure 5.49 (a) and (b). The resonances between 6 – 8 ppm are associated with aromatic structures. Resonances in 4 – 6 ppm are assigned to phenolic proton. Peaks in the 1 – 3 ppm range confirm the presence of aliphatic protons. In case of VPCB, the aliphatic peaks are moderately stronger than WPCB ones. Most aromatic hydrogens occur in 6.5-7.5 ppm range, suggesting aromatic species are predominantly phenolic, which is in line with the FTIR results.

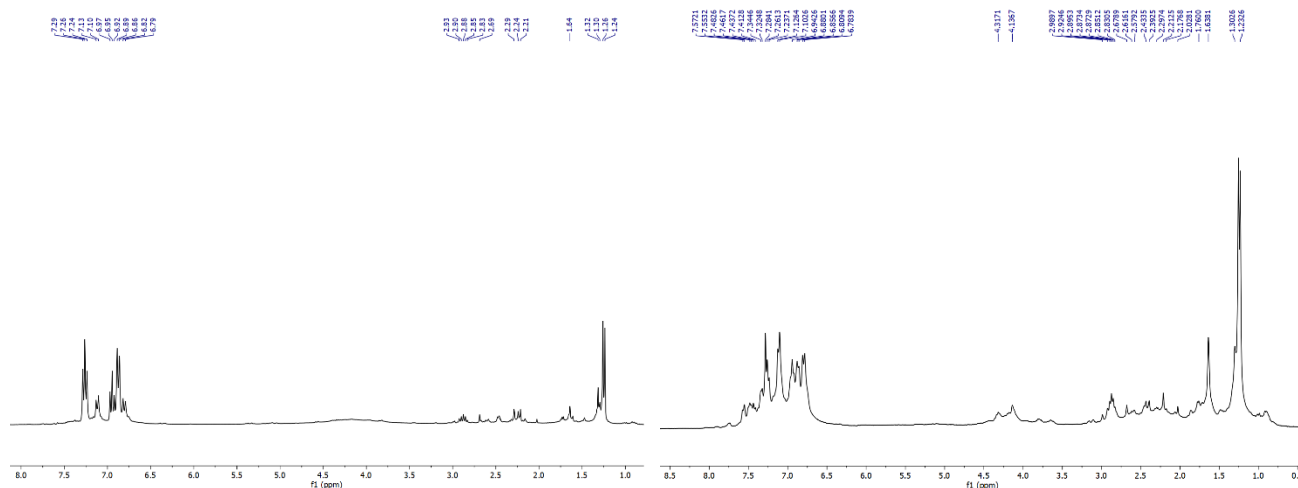


Figure 5.49: ^1H NMR spectra of (a) VPCB Pyro-oil and (b) WPCB Pyro-oil

5.3.11.12 ^1H NMR Results of mixed WPCBs pyro-oil

^1H NMR spectra of mixed WPCB pyro-oil is shown in Figure 5.50. The resonances between 1 – 3 ppm are associated with aliphatic structures. The peaks in 4 – 6 ppm range are assigned to phenolic proton. Peaks in the 6 – 8 ppm range confirm the presence of aromatic protons.

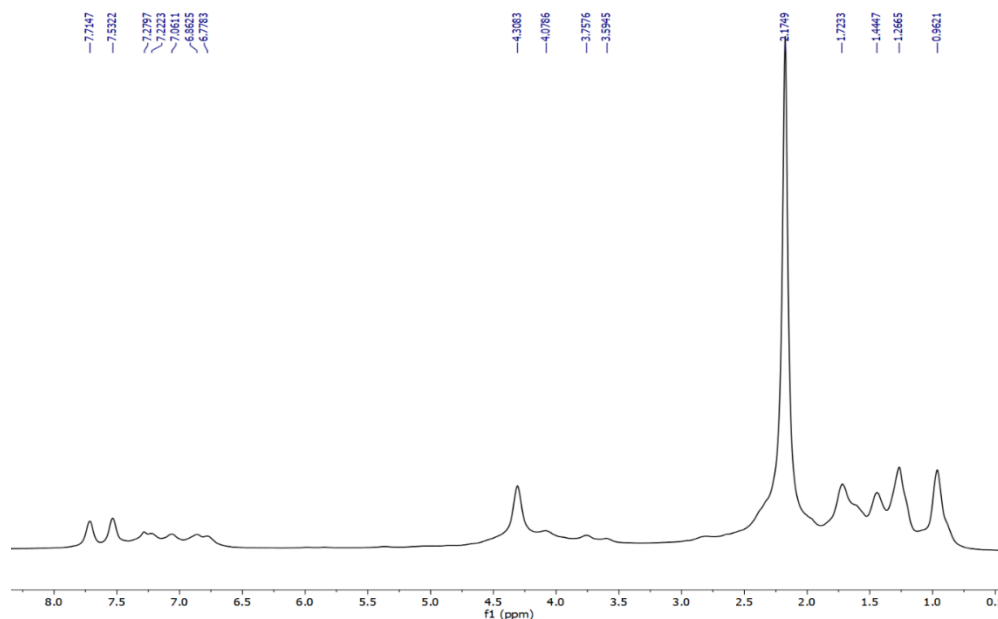


Figure 5.50: ^1H NMR spectra of mixed WPCB Pyro-oil

5.3.11.13 GC-MS analysis of FR-2 WPCBs

Characterization of pyro-oil was obtained through Gas Chromatograph/Mass Spectrometer (GC/MS) analysis. The compounds present in pyro-oil obtained using pyrolysis of WPCB at 623K is presented in Table 5.27. The table provides the list of compounds with their retention times and RSI values. From the table it is clear that, WPCB pyro-oil contains compounds like phenols, cresols, benzene derivatives, furan, furfural, acid, oxime, ketones, aldehydes, amine, amides, pyridine, pyrimidine and alcohols with aromatic and aliphatic properties. These findings are in line with previously published studies (Kim et al. 2015; Gao et al. 2018; Poddar et al. 2015).

The presence of benzene derivatives and phenolic compounds assures that aromatics are present in the oil, which was identified in FTIR analysis as well. The occurrence of Methyl 6-bromo-5-oxohexanoate confirms the migration of bromine to the pyro-oil. This phenomenon has been previously reported as well (Ma et al. 2016). This finding is also supported by the FTIR analysis. It is quite compelling that the chemicals identified from pyro-oil may be suitable for oil-based resin production as developed by others (Grause et al. 2008; Gao et al. 2018; Gao and Xu 2019). This makes pyrolysis of PCBs hugely attractive as it can be used as a feedstock for production of valuable chemicals.

Table 5.27: Composition of FR-2 WPCB Oil determined via Pyrolysis

SI No.	RT	NAME	RSI	MW
Alcohols				
1	7.12	2-Hexyl-1-octanol	898	214.39
2	8.84	2-Dodecanol	916	186.33
3	10.51	2-ethyl-1-Hexanol	877	130.23
Aldehydes/Ketones				
4	6.69	2-Hexanone	878	100.16
5	9.31	4-hydroxy-4methyl-2-Pentanone	863	116.16
6	15.09	2-heptadecenal	856	252.4
7	15.25	3-heptadecenal	880	252.4
Alkanes/Alkenes/Alkynes				
8	7.49	Dodecane	931	170.33
9	8.1	2,4-Nonadiyne	888	124.22
10	9.41	tetradecane	919	198.39
11	14.61	2-methyl decane	883	156.31
12	18.18	1,2-cyclooctadiene	873	108.18
Amines/Amides				
13	3.29	Acetamide	907	59.07
14	3.69	N-formyl-N-methyl-Formamide	977	87.08
15	6.59	Tolycaine	906	278.35
16	14.23	2,3-dimethylamphetamine	882	163.26
17	21.91	3-methyl amphetamine	904	149.24
Carboxylic Acids				
18	6.46	Ethaneperoxoic acid	886	92.05
19	10.26	Acetic Acid	923	60.05
20	20.42	2-napthuric acid	874	172.18
Ethers/Esters				
21	6.9	3-propoxy-1-propane	966	100.16
22	10.09	2,4,6-cycloheptatrien-1-yl methyl ether	804	91.13
23	21.13	Methyl 6-bromo-5-oxohexanoate	947	223.06
Heterocyclic Organic Compounds				
24	9.02	2,4-dimethyl Pyridine	890	107.15
25	9.99	Furfural	864	96.08
26	10.43	3-Furaldehyde	937	96.08
27	10.88	Benzofuran	835	118.1
28	12.01	2-methyl-Benzofuran	901	132.16
29	12.35	3-methyl-2-(2-oxopropyl)furan	915	138.16
30	16.98	5-methyl-pyrimidine	797	94.11
31	24.72	Dibutyl phthalate	902	278.34
Phenolic Compound				
32	8.46	1-ethyl-3methyl-benzene [m-ethyl toluene]	889	120.19

33	9.84	1,3-bis(1,1-dimethylethyl)-Benzene	845	190.33
34	10.66	1-phenyl-1-pentyn-4-ol	833	160.21
35	11.09	4-ethyl-3-methyl phenol [m-cresol]	924	136.19
36	11.15	thiophene-2-ol, benzoate	842	204.25
37	12.96	5,8-dihydro-1-naphthalenol	846	146.19
38	16.14	1-phenyl-1-nonanol	914	220.35
39	17.23	Phenol	880	94.11
40	18.38	2-ethyl-6-methyl phenol	853	136.19
41	18.99	1-phenyl-1-decanol	903	234.38
Oximes				
42	2.02	2-(aminooxy)-Propanoic acid	970	105.09
43	3.54	Acetaldoxime	965	59.07
44	8.36	O-decyl-Hydroxylamine	894	173.3
Miscellaneous				
45	7.29	Aminoacetonitrile	914	56.07
46	9.92	10-Heneicosene (c,t)	896	294.6
47	11.31	Ethyl Boronic Acid	823	73.89

5.3.11.14 GC-MS analysis of FR-4 WPCBs

The compounds present in pyro-oil obtained using pyrolysis of WPCB at 623K is presented in Table 5.28. The table provides the list of compounds with their retention times and RSI values. From the table it is clear that, FR-4 WPCB pyro-oil contains compounds like phenols, cresols, benzene derivatives, furan, ketones, amides, pyridine etc with aromatic and aliphatic properties. These findings are in line with previously published studies (Kim et al. 2015; Gao et al. 2018).

The presence of benzene derivatives and phenolic compounds assures that aromatics are present in the oil, which was identified in FTIR analysis as well. The occurrence of 3-Methyl-2-(2oxopropyl)-furan confirms the presence of furan in pyro-oil. The present array of compounds makes pyrolysis oil of PCBs hugely attractive as it can be used as a feedstock for production of valuable chemicals.

Table 5.28: Composition of FR-4 WPCB Oil determined via Pyrolysis

SI No.	RT	NAME	RSI	MW
Amines/Amides				
1	2.02	1,2Propanediamine, N,N'dimethyl, (S)- Ethylamine	984	102.18
2	2.57	N Dimethylaminomethyl-tert.-butyl-isopropylphosphine	932	189.28
3	3.74	N-methyl-Formamide	930	87.08
4	6.62	Tolycaine	904	278.35
Alkanes/Alkenes/Alkynes				
5	9.41	Tetradecane	835	198.39
Heterocyclic Organic Compound				

6	7.71	Pyridine	902	79.1
7	11.91	Benzofuran, 2-methyl	859	132.16
8	12.72	3-Methyl-2-(2oxopropyl)-furan	937	138.16
9	15.06	Naphthalene, 1,2,3,4tetrahydro 1,1,6trimethyl	883	174.28
Halides				
10	16.82	2-bromo phenol	799	173.01
Phenolic Compounds				
11	13.4	1Naphthalenol, 5,8dihydro	856	146.19
12	16.15	1-Phenyl-1-nonanol	906	144.26
13	17.2	Phenol	912	94.11
14	18.03	p-cresol	902	108.14
15	18.45	Picein	890	298.29
16	24.58	Allyldimethylphenylsilane	811	176.34
Oximes				
17	3.25	Acetaldoxime	943	59.07
Ketones				
18	6.72	2-Hexanone	855	100.16
Sulfonyl Compound				
19	7.13	2,2Dimethylpropyl 2,2dimethylpropanesulfinyl sulfone	959	254.4
Nitro Compounds				
20	7.54	Benzene, (1nitroethyl)	917	151.16

5.3.11.15 GC-MS analysis of mixed WPCB pyro-oil

The compounds present in pyro-oil obtained using pyrolysis of mixed WPCB at 623K is presented in Table 5.29. The table provides the list of compounds with their retention times and RSI values. Pyro-oil obtained from mixed WPCB pyrolysis contain compounds like phenols, cresols, benzene derivatives, formate, ketones, aldehydes, amine, amides, acetates and alcohols with aromatic and aliphatic properties. The presence of benzene derivatives and phenolic compounds assures that aromatics are present in the oil, which was identified in FTIR analysis as well. The occurrence of chlorine and hydrogen bromide confirms the presence of halogens in the raw material. This phenomenon has been previously reported as well (Ma et al. 2016). This finding is also supported by the FTIR analysis. In contrast to the pyro-oils obtained from typical plastic waste sources such as polyethylene, polypropylene, and polystyrene, recent studies have revealed a notable predominance of long-chain saturated and unsaturated aliphatic compounds ($C_4 - C_{30}$). A few identified products include 1-Butene; 1-Pentene, 2-methyl-; 1-tetradecene; 1-Nonadecene; 1,19-Eicosadiene; 1-Undecene; 1-Hexacosene etc. Phenol and phenolic derivatives were observed infrequently, except notably in the case of polystyrene, while heterocyclic compounds were detected across all three plastic

samples (Qin et al. 2018; Zhang et al. 2021). This suggests that pyro-oil derived from typical plastic waste exhibits a lower concentration of aromatic compounds compared to pyro-oil obtained from waste printed circuit boards (WPCB). These findings make the mixed WPCB pyro-oil hugely attractive for production of valuable chemicals and further upgradation.

Table 5.29: Composition of mixed WPCB Oil determined via Pyrolysis

Sl. No.	Retention Time	Compound Name	RSI Value	MW
Alkanes/Alkenes/Alkynes				
1.	3.78	1,2-Butadiene	787	54.09
2.	4.14	1-Methylcyclopropene	811	56.1
3.	4.8	2-Butene	775	56.11
4.	6.05	1-Buten-3-yne	761	54.09
5.	7.44	3-Methylheptyl acetate	821	69.7
6.	9.15	1,1,1-trifluoro Propane	929	107.1
7.	17.08	3-Hexyne, 2-methyl	963	149.3
8.	21.72	2-chloro-1-buten-3-one	914	96.1
Alcohols/Ethers/Aldehydes/Ketones				
9.	3.32	2-Pentanol, formate	926	104.1
10.	6.67	2,2,2-Trifluoroethyl methyl ester	894	156.2
11.	7.35	2-methyl-6-methylene-octa-1,7-dien-3-ol	937	184.3
12.	7.4	3-Dodecen-1-ol, (Z)-	856	158.2
13.	7.53	2-Pentanol, formate	905	179.2
14.	8.96	Carbamic acid, hydroxy-, ethyl ester	880	89.1
15.	9.22	Acetamidoacetaldehyde	866	254.4
16.	10.54	3-Heptadecenal	857	118.1
17.	15.14	Phenylacetaldehyde	883	145
18.	15.44	4-Heptanal	886	146.2
19.	17.38	2,6,10,14-Tetramethylpentadecan-2-ol	897	94
Amines/Amides				
20.	5.89	2-Aminocynoacetamide	810	102.1
21.	8.29	N,N-bis(methylsulfonyl)hydroxylamine	879	91.1
22.	18.19	2,3-Dimethylamphetamine	904	152
Halides				
23.	6.51	Hydrogen bromide	919	134.1
24.	8.71	Phosphonic difluoride	844	94.07
25.	11.6	Nitrogen trifluoride	956	143.8
26.	12.16	Bromine Azide	942	134.18
27.	13.82	Chlorine	975	114.19
Organometallic Compounds				
28.	2.03	Arsine	886	77.95
29.	10.46	Dimethyl selenide	767	108.5
30.	18.38	Silane, (bromomethyl)-	950	160.3
31.	20.07	Methyl trimethylsilyl carbonate	934	77.95
Nitrile and Nitro Compound				
32.	4.3	1-Propanamine, 3-nitro-	801	89.1
33.	4.5	2-Propen-1-amine, N-nitro	979	86.1

34.	4.59	Propane, 2-methyl-1 nitro-	892	103.1
35.	5.94	2-Propenenitrile	877	53.06
36.	6.11	1-Propanamine, 3-nitro-	906	80.91
37.	16.42	Trifluoromethyl peroxy-nitrate	999	84.16
Miscellaneous				
38.	3.03	2(5H)-Furanone	834	96.1
39.	4.24	Aziridine, 1-(methoxymethyl)-	914	87.1
40.	7.22	2,7-Octadiene-1,6-diol, 2,6-dimethyl-, (E)-	931	152.2
41.	7.71	Pentaborane	814	96.9
42.	10.82	Methanol, chloro-, acetate	894	71
43.	11.31	Acetic acid, hydroxy-, propyl ester	973	124.2
44.	12.02	4-Cyclopropylnorcarane	900	70.9
45.	16.83	Pentyl glycolate	945	270.5
46.	18.85	Trivinylphosphine Oxide	932	114.5

References

- Alves, J. L. F., da Silva, J. C. G., da Silva Filho, V. F., Alves, R. F., de Araujo Galdino, W. V., & De Sena, R. F. (2019). Kinetics and thermodynamics parameters evaluation of pyrolysis of invasive aquatic macrophytes to determine their bioenergy potentials. *Biomass and bioenergy*, 121, 28-40.
- Anca-Couce, A., Berger, A., & Zobel, N. (2014). How to determine consistent biomass pyrolysis kinetics in a parallel reaction scheme. *Fuel*, 123, 230-240.
- Bandyopadhyay, S., Chowdhury, R., & Biswas, G. K. (1999). Thermal deactivation studies of coconut shell pyrolysis. *The Canadian Journal of Chemical Engineering*, 77(5), 1028-1036.
- Barontini, F., Marsanich, K., Petarca, L., & Cozzani, V. (2005). Thermal degradation and decomposition products of electronic boards containing BFRs. *Industrial & engineering chemistry research*, 44(12), 4186-4199.
- Carrier, M., Auret, L., Bridgwater, A., & Knoetze, J. H. (2016). Using apparent activation energy as a reactivity criterion for biomass pyrolysis. *Energy & Fuels*, 30(10), 7834-7841.
- Cheng, S., Qiao, Y., Huang, J., Wang, W., Wang, Z., Yu, Y., & Xu, M. (2019). Effects of Ca and Na acetates on nitrogen transformation during sewage sludge pyrolysis. *Proceedings of the Combustion Institute*, 37(3), 2715-2722.
- Collett, G. W., & Rand, B. (1980). Thermogravimetric investigation of the pyrolysis of pitch materials. A compensation effect and variation in kinetic parameters with heating rate. *Thermochimica Acta*, 41(2), 153-165.
- Cortés, A. M., & Bridgwater, A. V. (2015). Kinetic study of the pyrolysis of miscanthus and its acid hydrolysis residue by thermogravimetric analysis. *Fuel Processing Technology*, 138, 184-193.
- Evangelopoulos, P., Kantarelis, E., & Yang, W. (2015). Investigation of the thermal decomposition of printed circuit boards (PCBs) via thermogravimetric analysis (TGA) and analytical pyrolysis (Py-GC/MS). *Journal of Analytical and Applied Pyrolysis*, 115, 337-343.
- Galwey, A. K. (1997). Compensation behaviour recognized in literature reports of selected heterogeneous catalytic reactions: aspects of the comparative analyses and significance of published kinetic data. *Thermochimica acta*, 294(2), 205-219.
- Galwey, A. K. (2004). Is the science of thermal analysis kinetics based on solid foundations?: A literature appraisal. *Thermochimica Acta*, 413(1-2), 139-183.

- Hadi, P., Ning, C., Ouyang, W., Lin, C. S. K., Hui, C. W., & McKay, G. (2014). Conversion of an aluminosilicate-based waste material to high-value efficient adsorbent. *Chemical Engineering Journal*, 256, 415-420.
- Hao, J., Wang, H., Chen, S., Cai, B., Ge, L., & Xia, W. (2014). Pyrolysis characteristics of the mixture of printed circuit board scraps and coal powder. *Waste Management*, 34(10), 1763-1769.
- Hossain, R., Nekouei, R. K., Al Mahmood, A., & Sahajwalla, V. (2022). Value-added fabrication of NiO-doped CuO nanoflakes from waste flexible printed circuit board for advanced photocatalytic application. *Scientific Reports*, 12(1), 12171.
- Kan, Y., Yue, Q., Kong, J., Gao, B., & Li, Q. (2015). The application of activated carbon produced from waste printed circuit boards (PCBs) by H₃PO₄ and steam activation for the removal of malachite green. *Chemical Engineering Journal*, 260, 541-549.
- Kaur, R., Gera, P., Jha, M. K., & Bhaskar, T. (2018). Pyrolysis kinetics and thermodynamic parameters of castor (*Ricinus communis*) residue using thermogravimetric analysis. *Bioresource technology*, 250, 422-428
- Kaya, M. (2016). Recovery of metals and nonmetals from electronic waste by physical and chemical recycling processes. *Waste management*, 57, 64-90.
- Lever, T., Haines, P., Rouquerol, J., Charsley, E. L., Van Eckeren, P., & Burlett, D. J. (2014). ICTAC nomenclature of thermal analysis (IUPAC Recommendations 2014). *Pure and Applied Chemistry*, 86(4), 545-553.
- Liu, J., Jiang, Q., Wang, H., Li, J., & Zhang, W. (2021). Catalytic effect and mechanism of in-situ metals on pyrolysis of FR4 printed circuit boards: Insights from kinetics and products. *Chemosphere*, 280, 130804.
- Liu, W., Xu, J., Han, J., Jiao, F., Qin, W., & Li, Z. (2019). Kinetic and mechanism studies on pyrolysis of printed circuit boards in the absence and presence of copper. *ACS Sustainable Chemistry & Engineering*, 7(2), 1879-1889.
- Maia, A. A. D., & de Morais, L. C. (2016). Kinetic parameters of red pepper waste as biomass to solid biofuel. *Bioresource Technology*, 204, 157-163.
- Mehmood, M. A., Ye, G., Luo, H., Liu, C., Malik, S., Afzal, I., ... & Ahmad, M. S. (2017). Pyrolysis and kinetic analyses of Camel grass (*Cymbopogon schoenanthus*) for bioenergy. *Bioresource technology*, 228, 18-24.

- Mian, I., Li, X., Jian, Y., Dacres, O. D., Zhong, M., Liu, J. & Rahman, N. (2019). Kinetic study of biomass pellet pyrolysis by using distributed activation energy model and Coats Redfern methods and their comparison. *Bioresource technology*, 294, 122099.
- Mianowski, A., Radko, T., & Siudyga, T. (2021). Kinetic compensation effect of isoconversional methods. *Reaction Kinetics, Mechanisms and Catalysis*, 132(1), 37-58.
- Müsellim, E., Tahir, M. H., Ahmad, M. S., & Ceylan, S. (2018). Thermokinetic and TG/DSC-FTIR study of pea waste biomass pyrolysis. *Applied Thermal Engineering*, 137, 54-61.
- Narayan, R., & Antal, M. J. (1996). Thermal lag, fusion, and the compensation effect during biomass pyrolysis. *Industrial & engineering chemistry research*, 35(5), 1711-1721.
- Poddar, S., De, S., & Chowdhury, R. (2015). Catalytic pyrolysis of lignocellulosic bio-packaging (jute) waste—kinetics using lumped and DAE (distributed activation energy) models and pyro-oil characterization. *RSC advances*, 5(120), 98934-98945.
- Qin, L., Han, J., Zhao, B., Wang, Y., Chen, W., & Xing, F. (2018). Thermal degradation of medical plastic waste by in-situ FTIR, TG-MS and TG-GC/MS coupled analyses. *Journal of analytical and applied pyrolysis*, 136, 132-145.
- Rautela, R., Arya, S., Vishwakarma, S., Lee, J., Kim, K. H., & Kumar, S. (2021). E-waste management and its effects on the environment and human health. *Science of The Total Environment*, 145623.
- Sarkar, A., Mondal, B., & Chowdhury, R. (2014). Mathematical modeling of a semibatch pyrolyser for sesame oil cake. *Industrial & Engineering Chemistry Research*, 53(51), 19671-19680.
- Song, H., Liu, G., & Wu, J. (2016). Pyrolysis characteristics and kinetics of low rank coals by distributed activation energy model. *Energy Conversion and Management*, 126, 1037-1046.
- Trick, K. A., & Saliba, T. E. (1995). Mechanisms of the pyrolysis of phenolic resin in a carbon/phenolic composite. *Carbon*, 33(11), 1509-1515.
- Turmanova, S. C., Genieva, S. D., Dimitrova, A. S., & Vlaev, L. T. (2008). Non-isothermal degradation kinetics of filled with rice husk ash polypropylene composites. *Express Polymer Letters*, 2(2), 133-146.
- Vlaev, L. T., Markovska, I. G., & Lyubchev, L. A. (2003). Non-isothermal kinetics of pyrolysis of rice husk. *Thermochimica acta*, 406(1-2), 1-7.

- Vyazovkin, S., Burnham, A. K., Criado, J. M., Pérez-Maqueda, L. A., Popescu, C., & Sbirrazzuoli, N. (2011). ICTAC Kinetics Committee recommendations for performing kinetic computations on thermal analysis data. *Thermochimica acta*, 520(1-2), 1-19.
- Wang, D., Ding, J., Wang, B., Zhuang, Y., & Huang, Z. (2021). Synthesis and Thermal Degradation Study of Polyhedral Oligomeric Silsesquioxane (POSS) Modified Phenolic Resin. *Polymers*, 13(8), 1182.
- Wu, W., Cai, J., & Liu, R. (2013). Isoconversional kinetic analysis of distributed activation energy model processes for pyrolysis of solid fuels. *Industrial & Engineering Chemistry Research*, 52(40), 14376-14383.
- Yao, Z., Xiong, J., Yu, S., Su, W., Wu, W., Tang, J., & Wu, D. (2020). Kinetic study on the slow pyrolysis of nonmetal fraction of waste printed circuit boards (NMF-WPCBs). *Waste Management & Research*, 38(8), 903-910.
- Zhang, Y., Fu, Z., Wang, W., Ji, G., Zhao, M., & Li, A. (2021). Kinetics, product evolution, and mechanism for the pyrolysis of typical plastic waste. *ACS Sustainable Chemistry & Engineering*, 10(1), 91-103.

CHAPTER-6

**OPTIMIZATION OF MIXED
WASTE PRINTED CIRCUIT
BOARDS (WPCB) PYROLYSIS**

CHAPTER – 6

6.1 Background

As detailed in chapter 6 and 7, the analysis of pyrolysis of FR-2 and FR-4 PCB with kinetics and product distribution indicates the potential of resource recovery from both FR-2 and FR-4 type PCBs. However, it is understandable that in reality an e-waste recycling plant will be dealing a heterogeneous batch of mixed PCBs. It is essential to address this issue of heterogeneity while valorising maximum materials out of WPCBs. This chapter is focused on *Studies on pyrolytic valorisation of mixed Waste Printed Circuit Board with product characterization and optimization*. The chapter encompasses the following objectives described in **Chapter 3** under aim 3 –

- Development of experiment matrix using Design of Experiments (DoE) methodology.
- Experimental investigation on mixed waste PCBs pyrolysis in semi-batch pyrolyzer for product recovery
- Optimization of mixed WPCB pyrolysis using Response Surface Methodology (RSM) and Genetic Programming (GP).

6.2 Experimental

The mixed PCBs were subjected to pyrolysis in a pre-heated furnace using the fixed bed reactor. The pyrolysis temperature was chosen based on the TGA results of individual waste PCBs, as discussed in Chapter 5 and those obtained for mixed PCBs, mixed in the ratio of 1:1. Nitrogen flow was introduced to maintain an inert atmosphere and to provide necessary residence time for the volatiles to condense in the condensing units. The volatiles were passed through a bulb type condenser followed by two auxiliary condensing units. Pyro-oil was recovered from the condenser and the auxiliary units after the experiment by rinsing with acetone. The non-condensable portion was scrubbed with water and NaOH solution before it was vented out. The solid residues were collected after cooling down the reactor to the room temperature and weighed in a precision weighing balance. The residues were crushed and sieved to recover the carbonaceous part. The glass fibres were found to be laden with carbon particles and they were inseparable. To recover the glass fibre, the pyrolyzed glass fibres were subjected to combustion at a temperature of 773 K which removed the carbon particles. The total mass of char was determined by summing up 1) the mass of free char and 2) that associated with glass fibre. The mass of the second part of char was determined by the difference of mass of (Glass fibre+ Char) and carbon-free glass fibre after combustion. The yield of pyro-oil, % recovery of glass fibre and

metal+glass fibre and yield of pyro-char were determined by Equation 4.39-4.42 using the values of collected mass of the corresponding product (pyro-oil, glass fibre, metal+glass fibre and pyro-char) and initial mass of feed PCBs. The experiments were conducted with the aim to maximize metal + glass fibre recovery and pyro oil yield with respect to input parameters, namely, pyrolysis time (30-60min); percentage of FR4 in FR2-FR4 mixture (10-90%) and nitrogen flow rate (1-2Lpm). The set of experimental parameters was decided using the Design of Experiments (DOE) criteria of Box-Behnken Design of Response Surface Methodology (RSM), as represented in Table 8.1. A quadratic model was developed and the optimization of the response variables was done using Design Expert 13 software.

6.3 TGA analysis of Mixed WPCB

Figure 6.1 depicts the TGA-DTG curves for mixed WPCB. It is clear from the plot that the pyrolysis of mixed PCB occurs in three phases over the temperature range of 310 – 1173K. The weight loss from 310K till 400K is less than 5%. In this region the moisture is removed.

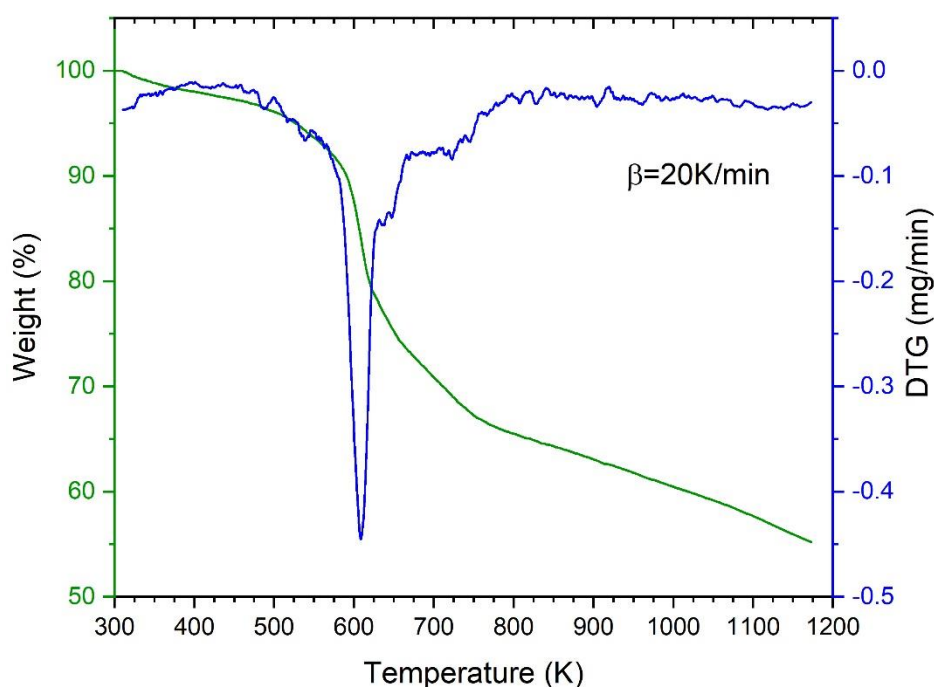


Figure 6.1: TGA-DTG plot of mixed WPCB at 20K per min heating rate

Then the actual pyrolysis starts as a steep fall in the weight loss curve is observed within the range of 400K – 623K. Almost 22% weight loss is observed during this range. From 623K – 800K, a further weight loss of 13% is observed. 800K onwards the curve follows an exponential profile culminating to total weight loss of 55.2%, which is the slow pyrolysis range. It has been found from the DTG curve that peak temperature is 608K. Since, we observed the maximum

weight loss during the range of 400 – 623K range, we chose 623K as our proper temperature of operation, which is in line with published articles (Chen et al. 2021).

6.4 Optimization of mixed WPCB pyrolysis

It is important to optimise the reaction conditions for the maximum recovery of resources. Two methods were explored for this purpose. The first method is a statistical method known as Response Surface Methodology (RSM) and the second method is an evolutionary method known as Genetic Programming (GP). Both of these methods produce data-driven model that describes the output parameters behaviour.

6.5.1 Methodology

6.5.1.1 Response surface methodology (RSM)

The aim of response surface methodology (RSM) is to optimize the output response and also to determine the optimum values of input variables (Raychaudhuri and Behera 2020). Response surface design employs second-order model and is symmetrical. Box–Behnken design (BBD) of RSM represents second order design and is a mathematical technique to formulate different sets of experimental designs, develop 3-D models and evaluate the effect of input variables on output response variables. The maximum and minimum values of input variables are designated as +1 and –1 levels respectively. The design ensures spherical experimental domain. The number of design points increases at the same rate as the number of polynomial coefficients when the spherical arrangement of BBD levels is followed. The number of experiments (N) is defined as follows:

$$N = 2k(k - 1) + C_0 \quad (6.1)$$

Where, k = number of variables ; C_0 = number of centre points

Evaluation of fitness of predictive model with the experimental values of output responses is conducted by ANOVA (Analysis of variables).

Using Design Expert 13.0.5 software, BBD has been used to correlate response variables, metal + glass fibre recovery and pyro oil yield with (A) pyrolysis time (30-60min); (B) percentage of FR4 in FR2-FR4 mixture (10-90%); (C) nitrogen flow rate (1-2Lpm). Under this study, a second order polynomial response surface model have been attempted and the equation (6.2) is expressed below:

$$Y_i = \alpha_{0i} + \alpha_{1i}A + \alpha_{2i}B + \alpha_{3i}C + \alpha_{12i}AB + \alpha_{13i}AC + \alpha_{23i}BC + \alpha_{11i}A^2 + \alpha_{22i}B^2 + \alpha_{33i}C^2 \quad (6.2)$$

Where,

$$Y_i = \text{ith response variable, where, } i=1,2 \quad (6.3)$$

$$Y_1 = \% \text{ Metal + Glass Fibre Recovery}; Y_2 = \% \text{ Yield of Pyro – oil} \quad (6.4)$$

$$\mathbf{A} = \text{pyrolysis time}; \mathbf{B} = \text{percentage of FR4 in FR2 – FR4 mixture (10 – 90\%)}; \mathbf{C} = \text{nitrogen flow rate} \quad (6.6)$$

The Box-Behnken statistical design requires 17 experimental runs, including five replicates at the central points. For the present case, the set of experimental parameters using the DOE of BBD method has been represented in Table 6.1.

Table 8.1: Experimental Set following DOE of BBD Method

Run	Time (min)	% FR4 WPCB in a mixture of FR-2 & FR-4 WPCB (wt %)	N₂ gas Flowrate (lpm)
1	45	50	1.5
2	30	90	1.5
3	30	10	1.5
4	45	90	1
5	30	50	1
6	60	50	1
7	45	10	1
8	30	50	2
9	45	50	1.5
10	60	90	1.5
11	45	50	1.5
12	45	90	2
13	60	10	1.5
14	60	50	2
15	45	50	1.5
16	45	10	2
17	45	50	1.5

Based on the TGA analysis, it was found that major mass loss occurs at 615 -623K range. In addition to that, experimental outputs of individual PCBs (FR2 and FR4), described in Chapter 4, indicates that maximum resource recovery is possible at 623K. Hence, the temperature of pyrolysis for optimization studies of mixed PCB has been chosen as 623K.

6.5.1.2 Genetic Programming (GP)

Genetic Programming (GP) was introduced by Koza in 1992 as an of the Genetic Algorithm (GA) approach (Koza 1992; Koza and Poli 1994). GP has been found to be extremely beneficial for a variety of applications in engineering and science (Koza and Rice 1992; Kandpal et al. 2013; Kiadehi et al. 2020). GP is a biologically inspired evolutionary algorithm that has its roots in genetic algorithms. GP adopts genetic operations to evolve its population which is based on the Darwinian principle (Azarhoosh et al. 2014). The main steps of a GP include “*initiation of the population (generation 0), evolution (through reproduction, crossover and mutation), model ranking (based on their fitness value that includes an analysis of root mean square error (RMSE) of the model, its complexity etc.) and creation of the next generation. This process continues from one generation to the next until a stopping criterion is satisfied.*”

A GP-based software, namely genetic modelling system (GeMS) has been developed by National University of Singapore. This software has been widely used for the determination of algebraic, dynamic and state space models (Tun and Lakshminarayanan 2004; Kandpal et al. 2010; Kandpal et al. 2013). GP has been previously applied to optimize systems evolving from chemical engineering and its allied fields (Rahmani et al. 2020; Wang et al. 2020; Sivapragasm et al. 2021). GP has also been employed by researchers for optimization of processes like pyrolysis and gasification (Zhang et al. 2021; Marzban et al. 2022). Hence, it is understandable that using GP-based software package such as GeMS enhances the predictability of models obtained from RSM. GeMS software has been used to develop GP-based models for both % metal + glass fibre recovery pyrooil yield with respect to the same input parameters using the experimental outputs of experimental runs conducted following the DOE of BBD method, as represented in Table 6.1.

Table 6.2: Parameter for GP analysis

GP Parameter	Parameter Value
number of generations	75
population size	100
maximum number of identical chromosomes	3
maximum length of chromosomes	10
maximum number of parameters in the model	7
normal length of chromosome	10
probability of mutation	0.5
probability of crossover	0.5
probability of reproduction	0.05

In GP, there are several tuning parameters that impact the modelling results. In this study, the following settings, as represented in Table 6.2, have been employed. The tournament selection technique is used to pick an individual from a population of individuals for crossover, mutation, or reproduction with the mentioned probabilities. The tournament size is three, which means that three individuals are picked at random from the population. Based on fitness the best one is chosen for genetic operation.

6.6 Results and Discussion

6.6.1 Response surface model and ANOVA

Table 6.3 illustrates the experimental values of metal+glass fibre (wt%), pyro-oil (wt %), glass fibre (wt%) and pyro-char (wt%) recovered via pyrolysis of mixed WPCB obtained via 17 experiments conducted using the combination of input parameters revealed via the design of experiments protocol of BBD method.

Table 6.3: BBD matrix of three input process variables and their corresponding experimental outputs of metal+glass fibre recovery and pyro-oil yield.

R un	Time (A) (min)	% FR4 WPCB in a mixture of FR-2 & FR-4 WPCB (B) (wt %)	N₂ gas Flowrate (C) (lpm)	Metal + Glass Fibre Recovery (%)	Pyro-oil Yield (%)
1	45	50	1.5	70.68	61
2	30	90	1.5	72.38	19.37
3	30	10	1.5	53.47	76.12
4	45	90	1	74.92	24.65
5	30	50	1	63.03	53
6	60	50	1	65.97	59
7	45	10	1	53.8	74.73
8	30	50	2	66.64	61
9	45	50	1.5	67.9	58
10	60	90	1.5	69.73	26.41
11	45	50	1.5	71.27	60
12	45	90	2	71.31	22.89
13	60	10	1.5	60.57	70.54
14	60	50	2	71.77	62
15	45	50	1.5	71.27	62
16	45	10	2	63.87	75.42
17	45	50	1.5	68.91	63

6.6.1.1 Metal + glass fibre recovery

The ANOVA of the response surface quadratic model for % recovery of metal + glass fibre is represented in Table 6.4

Table 6.4: ANOVA and the summary statistics of quadratic model for yield of metal+glass fibre

Source	Sum of Squares	df	Mean Square	F-value	p-value
Model	608.14	9	67.57	39.28	< 0.0001
A-Time	19.59	1	19.59	11.39	0.0118
B-% FR4	400.87	1	400.87	233.03	< 0.0001
C-N2 Flow	31.48	1	31.48	18.30	0.0037
AB	23.77	1	23.77	13.81	0.0075
AC	1.20	1	1.20	0.6970	0.4314
BC	46.79	1	46.79	27.20	0.0012
A ²	27.28	1	27.28	15.86	0.0053
B ²	49.33	1	49.33	28.68	0.0011
C ²	1.56	1	1.56	0.9048	0.3732
Residual	12.04	7	1.72		
Lack of Fit	2.76	3	0.9186	0.3957	0.7639
Pure Error	9.29	4	2.32		
Cor Total	620.18	16			
Summary statics of the quadratic model:					
Std. Dev.: 1.31; Mean: 66.91; C.V. %: 1.96; R-Squared: 0.9806; Adj R-Squared: 0.9556; Pred R-Squared: 0.9055; Adeq Precision: 21.0464					

The ANOVA of the quadratic model has been used to examine the validity of the competence of the model in terms of prediction based on p-value (Table 6.4). The model terms having a p-value lesser than 0.0500 have been considered to be significant. According to this, the p-values of the terms A, B, C, AB, BC, A², B² bear significance in the present quadratic model. The F-value of the model is 39.28 and corresponding p-value is <0.0001. This affirms that the model is significant. According to ANOVA “There is only a 0.01% chance that a "Model F-Value" this large could occur due to noise”.

The quadratic model equation (Equation 6.7) has been suggested by RSM to best explain the % yield of metal+glass fibre as a function of (A) pyrolysis time (30-60min); (B) percentage of FR4 in FR2-FR4 mixture (10-90%); (C) nitrogen flow rate (1-2Lpm).

$$\mathbf{Metal + Glass Fibre Recovery = 70.01 + 1.56A + 7.08B + 1.98C - 2.44AB + 0.5475AC - 3.42BC - 2.55A^2 - 3.42B^2 - 0.6080C^2} \quad (6.7)$$

Incorporating only the significant terms, the model equation reduces to the form:

$$\mathbf{Metal + Glass fibre Recovery = 70.01 + 1.56A + 7.08B + 1.98C - 2.44AB - 3.42BC - 2.55A^2 - 3.42B^2} \quad (6.8)$$

The value of the correlation coefficient (R^2) is 0.9806 which indicates that variance close to unity and is statistically acceptable. It further confirms that the model presented by equation (6.8) is valid. This also demonstrates the model's excellent fitness to the experimental data and prediction accuracy. The values of adjusted and predicted R^2 have been calculated to be 0.9556 and 0.9055 respectively. The difference is less than 0.2 which highlights that they are in a reasonable agreement. This echoes in the correlation plot of actual vs. predicted data (figure 6.2a). The figure clearly depicts an overall converging pattern with very few outliers.

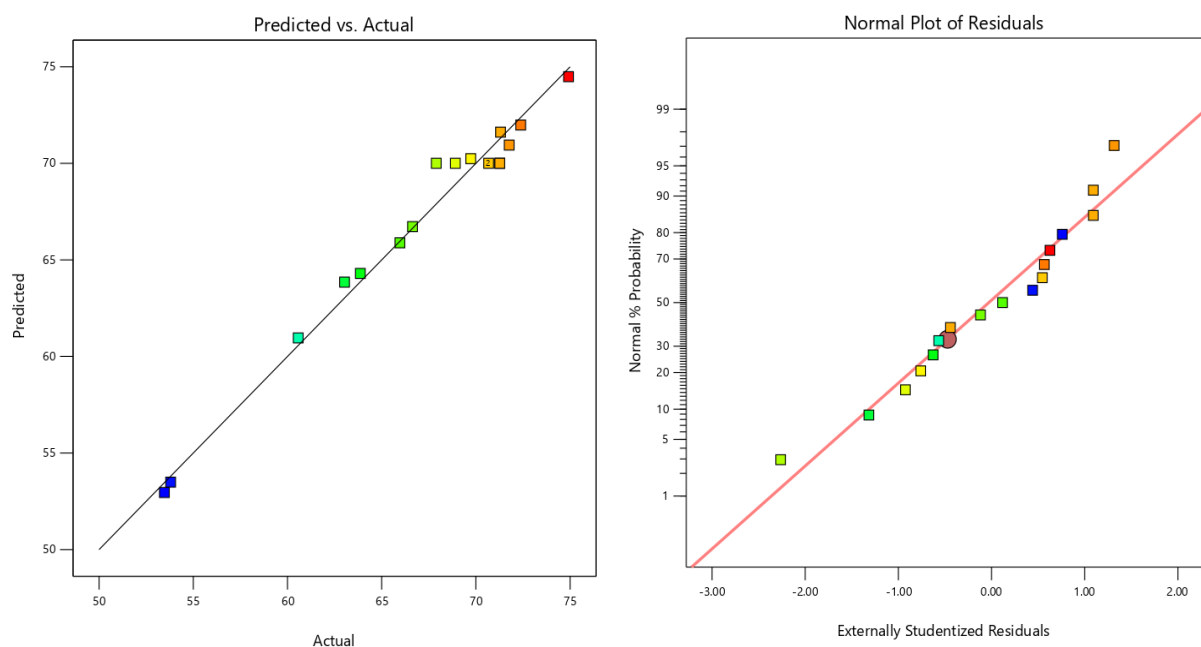


Figure 6.2: Plot of (a) predicted vs. actual response and (b) normal % probability vs. externally studentized residuals.

Analysis of the adequacy of the model has also been assessed through the plot of normal % of probability versus the externally studentized residuals (figure 6.2b). The correlation between the normal probability and internally studentized residuals has been observed to be linear having low deviation ensuring high degree of agreement. The ‘signal-to-noise ratio’ quantifies how the response fluctuates with respect to the nominal or goal value under various noise conditions. It compares the projected value range at each design point to the average prediction error. Ratios higher than 4 signify sufficient model discrimination. Hence, the benchmark value is 4. The value of adequate precision for the present model is calculated to be 21.40 which is almost 5.4 times higher than the benchmark value. Altogether, the ANOVA results corroborate the statistical significance of the quadratic model developed for the metal + glass fibre recovery from mixed WPCB pyrolysis.

6.6.1.2 Effect of individual variables on metal+glass fibre recovery: perturbation analysis

The results of ANOVA identifies that the input variable (B) has significant effect on the response of the system. However, it is natural that the impacts of all three components will differ significantly. The perturbation plot has been used to investigate this variation. A steep curve suggests strong sensitivity, whereas a flat curve shows a less influence on system response.

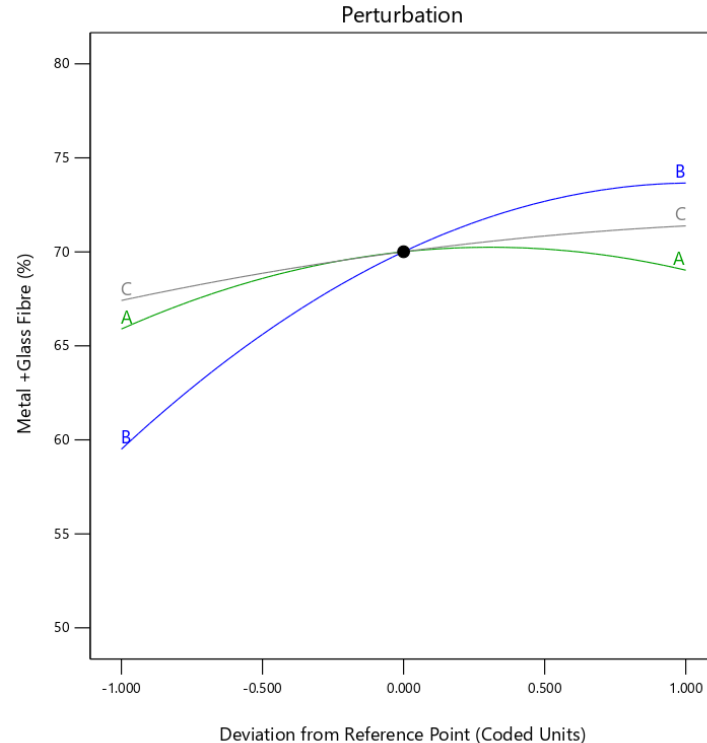


Figure 6.3: Perturbation plot showing the effect of three process variables on the response metal+glass fibre recovery

The perturbation plot, depicted in Figure 6.3 shows that all three input variables are having significant effects on metal+glass fibre recovery. As can be apprehended from the curves of the three input variables (A, B, C) the response metal+glass fibre recovery will be more sensitive towards variations in the values of B, i.e., % FR4 in FR2-FR4 mixture than A (pyrolysis time) and C (nitrogen flow rate).

6.6.1.3. Effect of process variables on metal+glass fibre recovery: response surface plots

The overall influence of the independent process factors on metal + glass fibre recovery was determined using response surface plot analysis. These plots provide a direct visual representation of the interacting effects of two process factors on system response. Figure 6.4 (a-c) shows the 3D surface diagrams and the corresponding 2D contour plots. The effects of simultaneous variation of two input parameters on the system response are visible in these plots. The values of the third variable are maintained constant to their central value for each pair of process variables participating in interaction at any moment.

Figure 6.4 (a) shows the 3D surface plot of interactive effect of time and %FR-4 WPCB in a mixture of FR-2 and FR-4 WPCB, at a constant N₂ flowrate of 1.5 lpm. It was observed that %metal + glass fibre recovery increases with the increase in the %FR-4 WPCB in a mixture of FR-2 and FR-4 WPCB. Metal + glass fibre recovery is observed to be the maximum at 60 minutes following an increasing pattern with time.

The surface plot (Figure 6.4 b) obtained from the variation of time and N₂ flowrate at 50 %FR-4 WPCB in a mixture of FR-2 and FR-4 WPCB exhibits a rather linear relationship. Metal + glass fibre recovery reaches the highest value at the highest flow rate of nitrogen while the effect of time is not much visible. Figure 6.4 (c) shows the 3D surface plot of interactive effect of N₂flow rate and %FR-4 WPCB in a mixture of FR-2 and FR-4 WPCB at time = 45 min. As can be noticed from the figure, metal + glass fibre recovery is the highest with the combination of 10% FR-2 and 90% FR-4 WPCB while the metal + glass fibre recovery increases with increase in N₂ flowrate. From the overall analysis of the perturbation plots and the 3D surface plots it can be conferred that %FR-4 WPCB in a mixture of FR-2 and FR-4 WPCB is the most significant parameter with respect to the maximization of metal + glass fibre recovery.

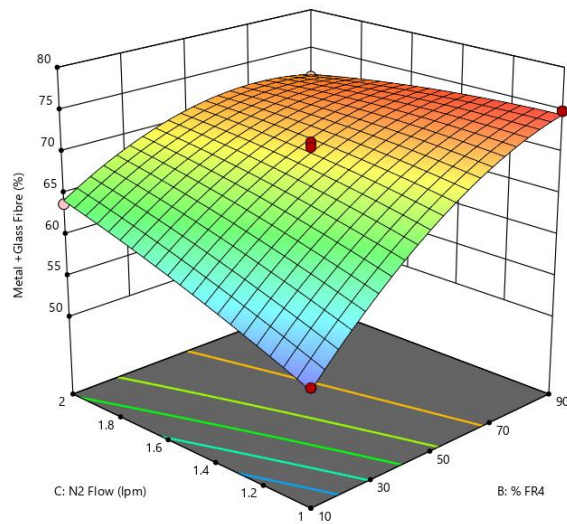
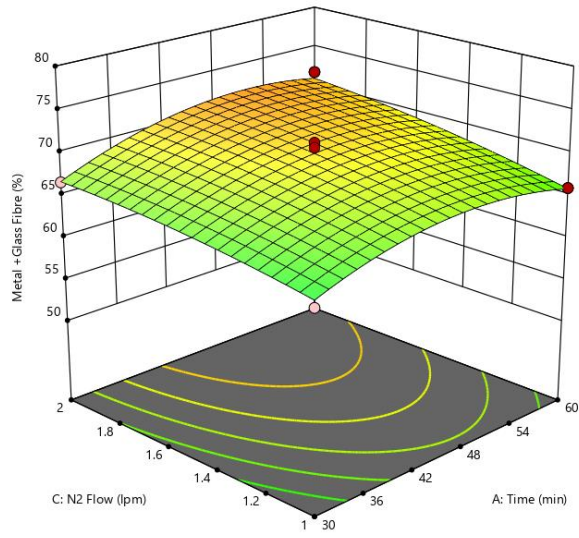
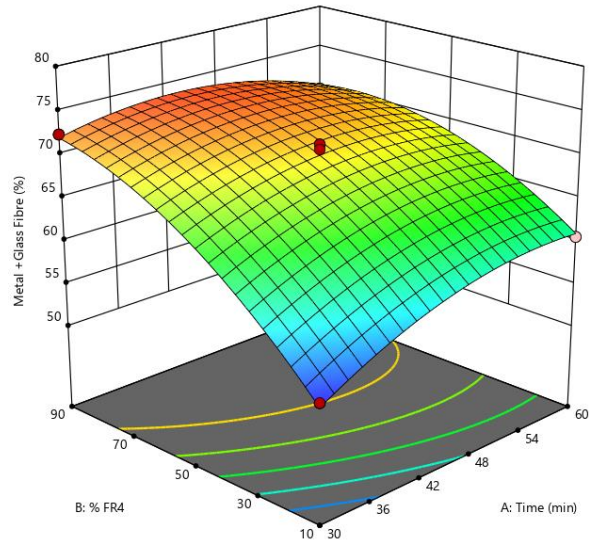


Figure 6.4: 3D surface plot of metal + glass fibre recovery (a) effect of time and %FR-4 WPCB in a mixture of FR-2 and FR-4 WPCB, (b) effect of time and N₂ Flowrate and (c) effect of N₂ Flowrate and %FR-4 WPCB in a mixture of FR-2 and FR-4 WPCB

The pattern of iso-response lines formed in contour plots by the interaction of two independent variables are found to be in accord with the patterns observed in their corresponding surface plots. Therefore, based on the overall statistical analysis, it can be inferred that %FR-4 WPCB in a mixture of FR-2 and FR-4 WPCB is the most significant factor for increasing metal+glass fibre recovery via pyrolysis of mixed WPCB. The optimum operating condition for maximum metal+glass fibre recovery is time= 60 min, %FR-4 WPCB in a mixture of FR-2 and FR-4 WPCB = 90% and N₂ flowrate = 2lpm.

6.6.1.4 Pyro Oil Yield

The ANOVA of the response surface quadratic model for yield of pyro-oil is represented in Table 6.5

Table 6.5: ANOVA and the summary statistics of quadratic model for yield of pyro-oil

Source	Sum of Squares	df	Mean Square	F-value	p-value
Model	5781.61	9	642.40	120.81	< 0.0001
A-Time	8.95	1	8.95	1.68	0.2357
B-% FR4	5176.02	1	5176.02	973.43	< 0.0001
C-N2 Flow	12.33	1	12.33	2.32	0.1717
AB	39.82	1	39.82	7.49	0.0291
AC	6.25	1	6.25	1.18	0.3142
BC	1.50	1	1.50	0.2822	0.6117
A ²	11.90	1	11.90	2.24	0.1783
B ²	510.28	1	510.28	95.97	< 0.0001
C ²	0.5725	1	0.5725	0.1077	0.7524
Residual	37.22	7	5.32		
Lack of Fit	22.42	3	7.47	2.02	0.2536
Pure Error	14.80	4	3.70		
Cor Total	5818.83	16			
Summary statics of the quadratic model:					
Std. Dev.: 2.31; Mean: 54.65; C.V. %: 4.22; R-Squared: 0.9936; Adj R-Squared: 0.9854; Pred R-Squared: 0.9344; Adeq Precision: 32.94					

The ANOVA of the quadratic model has been used to examine the validity of the competence of the model in terms of prediction based on p-value (Table 6.5). The model terms having a p-value

lesser than 0.0500 have been considered to be significant. According to this, the p-values of the terms B, AB, B² are the significant terms in the present quadratic model. The F-value of the model is 120.81 and corresponding p-value is <0.0001. This affirms that the model is significant. According to ANOVA “There is only a 0.01% chance that a "Model F-Value" this large could occur due to noise”.

The quadratic model equation (Equation 6.9) has been suggested by RSM to best explain the % yield of pyro-oil as a function of (A) pyrolysis time (30-60min); (B) percentage of FR4 in FR2-FR4 mixture (10-90%); (C) nitrogen flow rate (1-2Lpm).

$$\text{Pyro - oil Yield} = 60.80 + 1.06A + 25.44B + 1.24C - 3.16AB - 1.25AC + 0.6125BC - 1.68A^2 - 11.01B^2 - 0.3687C^2 \quad (6.9)$$

Incorporating only the significant terms, the model equation reduces to the form:

$$\text{Pyro - oil Yield} = 60.80 + 25.44B - 3.16AB - 11.01B^2 \quad (6.10)$$

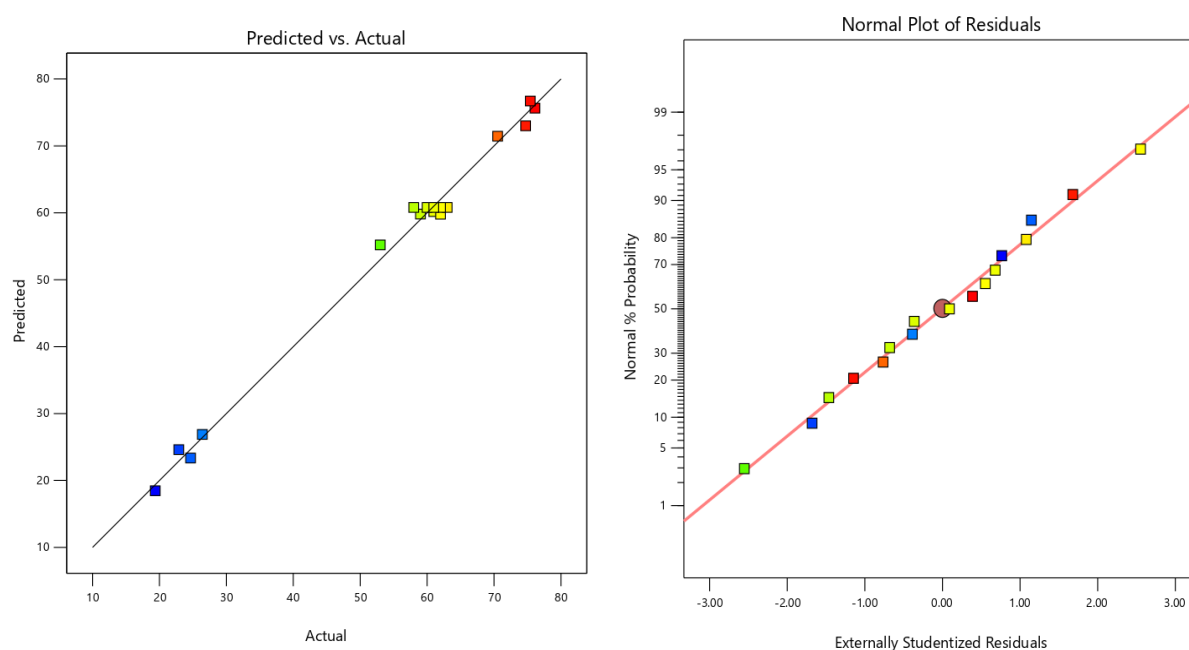


Figure 6.5: Plot of (a) predicted vs. actual response and (b) normal % probability vs. externally studentized residuals for pyro-oil recovery

The value of the correlation coefficient (R²) is 0.9936 which indicates that variance is close to unity. It further assures that the model represented by equation (6.10) is valid. This also demonstrates the model's excellent fitness to the experimental data and prediction accuracy. The values of adjusted and predicted R² have been calculated to be 0.9854 and 0.9344 respectively.

The difference is less than 0.2 which depicts that they are in a realistic agreement. This can be ratified from the plot of actual vs. predicted data (figure 6.5a). The figure clearly depicts an overall converging pattern. Analysis of the adequacy of the model has also been evaluated through the plot of normal % of probability versus the externally studentized residuals (figure 6.5b). The correlation between the normal probability and externally studentized residuals has been observed to be linear having minor deviations that ensures higher degree of agreement. The ‘signal to noise ratio’ is measured by the “Adequate precision”, the desirable value for which is more than the benchmark value 4. The value of adequate precision for the present model is calculated to be 32.94 which is nearly 8.3 times higher than the benchmark value. Altogether, the ANOVA results corroborate the statistical significance of the quadratic model developed for the pyro-oil recovery from mixed WPCB pyrolysis.

6.6.1.5 Effect of individual variables on pyro-oil yield: perturbation analysis

The results of ANOVA identified that the input variables A and B have significant effects on the response of the system. However, it is only expected that the effects of the three factors will vary significantly. The perturbation plot has been used to investigate these fluctuations.

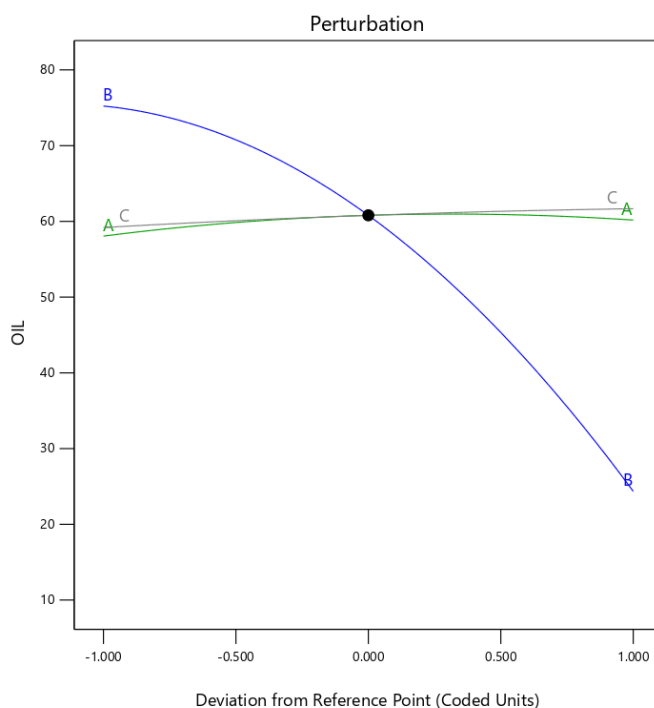


Figure 6.6: Perturbation plot showing the effect of three process variables on the response Pyro-oil yield

The perturbation plot has been depicted in Figure 6.6. The perturbation plot shows that all three variables are having significant effects on the yield of pyro-oil. As can be understood from the curves of the three input variables (A, B, C) the response yield of pyro-oil will be more sensitive

towards variations in the values of B, i.e., % FR4 in FR2-FR4 mixture than C i.e., nitrogen flow rate and A (pyrolysis time).

6.6.1.6. Effect of process variables on pyro-oil recovery: response surface plots

The overall influence of the independent process factors on metal + glass fibre recovery was determined using response surface plot analysis. These plots provide a direct visual representation of the interacting effects of two process factors on system response. Figure 8.11 (a-c) shows the 3D surface diagrams and the corresponding 2D contour plots. The effects of simultaneous variation of two input parameters on the system response are visible in these plots. The values of the third variable are maintained constant to their central value for each pair of process variables participating in interaction at any moment.

Figure 6.7 (a) shows the 3D surface plot of interactive effect of time and %FR-4 WPCB in a mixture of FR-2 and FR-4 WPCB, at a constant N₂ flowrate of 1.5 lpm. It was observed that pyro-oil yield increases with the decrease in the %FR-4 WPCB in a mixture of FR-2 and FR-4 WPCB. Maximum pyro-oil yield has been observed at 30 minutes whereas time had minor effect on the yield.

The surface plot (Figure 6.7 b) obtained from the variation of time and nitrogen flowrate at 50 %FR-4 WPCB in a mixture of FR-2 and FR-4 WPCB exhibits a linear relationship. Pyro-oil yield reaches the highest value at the highest flow rate of nitrogen while the effect of time is not much significant. Figure 6.7 (c) shows the 3D surface plot of interactive effect of nitrogen flow rate and %FR-4 WPCB in a mixture of FR-2 and FR-4 WPCB at time = 45 min. As can be noticed from the figure, pyro-oil yield is the highest with the combination of 90% FR-2 and 10% FR-4 WPCB while the effect of nitrogen flowrate on pyro-oil yield is not significant. From the overall analysis of the perturbation plots and the 3D surface plots it can be conferred that %FR-4 WPCB in a mixture of FR-2 and FR-4 WPCB is the most significant parameter with respect to the maximization of pyro-oil yield.

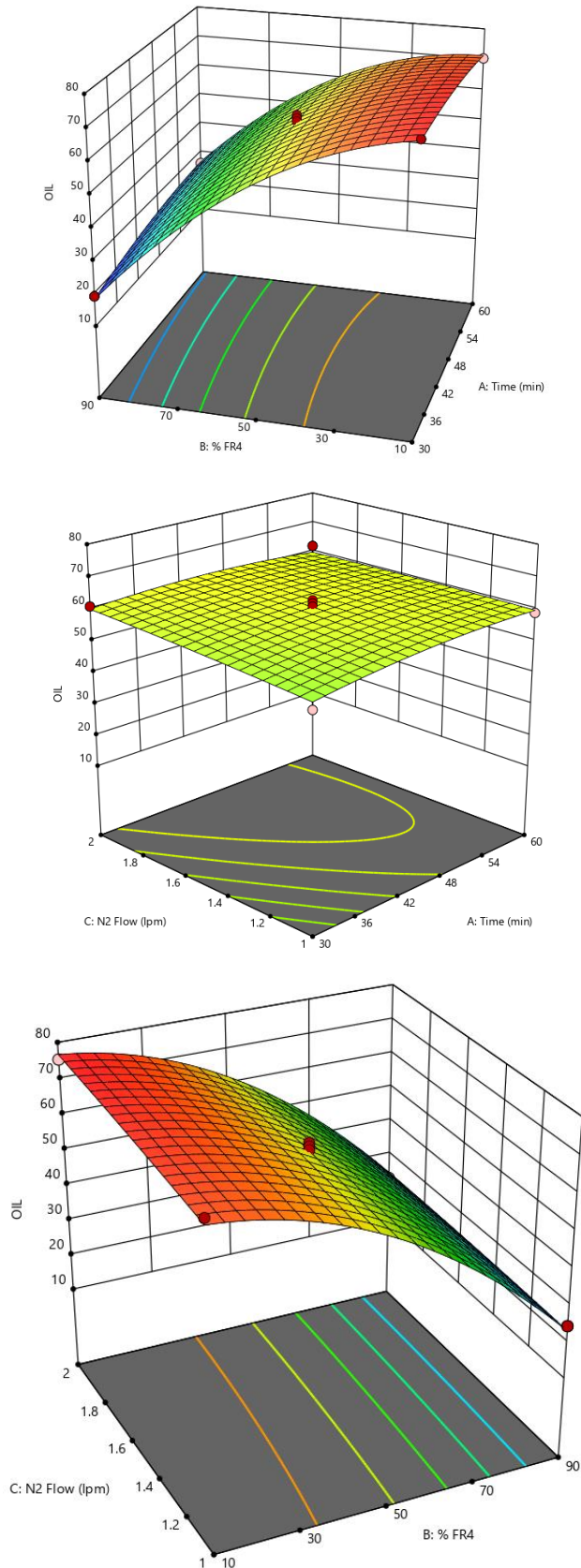


Figure 6.7: 3D surface plot of pyro-oil recovery (a) effect of time and %FR-4 WPCB in a mixture of FR-2 and FR-4 WPCB, (b) effect of time and N₂ Flowrate and (c) effect of N₂ Flowrate and %FR-4 WPCB in a mixture of FR-2 and FR-4 WPCB

The pattern of iso-response lines formed in contour plots by the interaction of two independent variables are found to be in well agreement with the patterns observed in their respective surface plots. Therefore, based on the overall statistical analysis, it can be inferred that %FR-4 WPCB in a mixture of FR-2 and FR-4 WPCB and nitrogen flowrate are the two most significant factors for increasing pyro-oil yield via pyrolysis of mixed WPCB. The optimum operating condition for maximum metal+glass fibre recovery is time= 30 min, %FR-4 WPCB in a mixture of FR-2 and FR-4 WPCB = 10% and N₂flowrate = 1.5lpm.

Table 6.6 Maximum Yield of Metal+Glass Fibre and Pyro-oil at optimal conditions

Optimum condition for	Time (A)	% FR4 WPCB in a mixture of FR-2 & FR-4 WPCB (B)	N ₂ gas Flowrate (C)	Metal + Glass Fibre Recovery	Pyro-oil Yield
	(min)	(wt %)	(lpm)	(%)	(%)
% Metal + Glass Fibre Recovery	60	90	1.5	69.73	26.41
%Pyro-oil Yield	30	10	1.5	53.47	76.12

The maximum yield of Metal+glass fibre and pyro-oil has been presented in table 6.6. As can be seen, metal + glass fibre recovery is 69.73% at the optimum combination predicted by RSM. Whereas the yield of pyro-oil is 76.12% at the optimum combinations.

6.6.2 Genetic Programming (GP)

6.6.2.1 Metal + glass fibre recovery

Following the GP parameters, represented in Table 6.2, the predicted model by GP to best explain the metal + glass fibre recovery as a function of (A) pyrolysis time (30-60min); (B) percentage of FR4 in FR2-FR4 mixture (10-90%); (C) nitrogen flow rate (1-2Lpm) is as follows:

$$\text{Metal + Glass fibre Recovery} = [C + \{1.968 \times 10^{-3} \cdot (A-B)^2\} + 0.8178 \cdot B] + \{[-1.27 \times 10^{-2} \cdot (A-C)^2\} + 1.226 \cdot A] + \{[-4.10 \times 10^{-3} \cdot (20.35 \cdot C + B)^2\} + 15.25 \cdot C \quad (6.11)$$

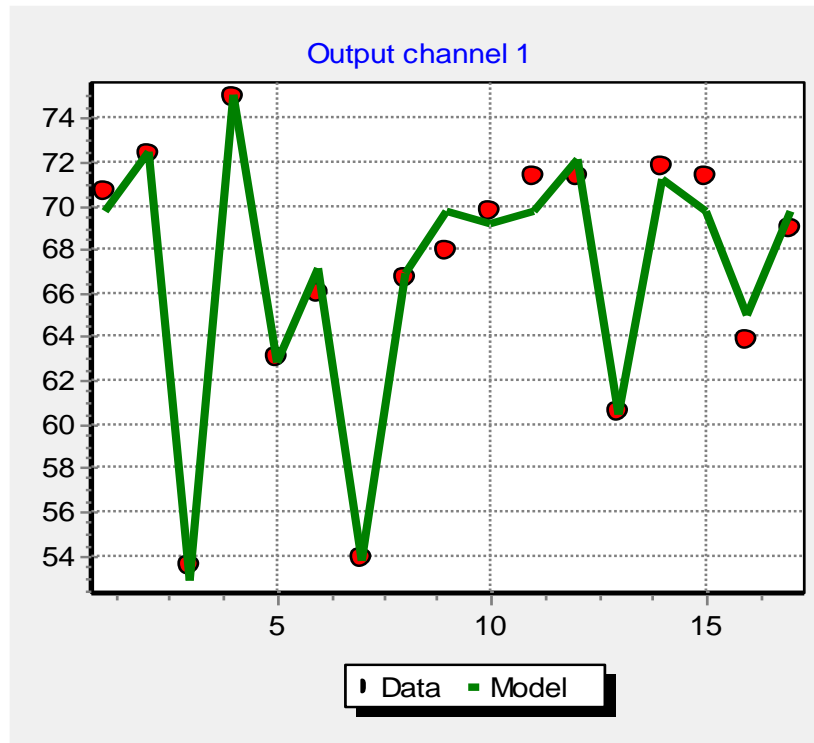


Figure 6.7: Model Fitting using GP for Metal + glass fibre recovery

The representative model fitting plot for metal + glass fibre recovery is shown in figure 6.8. The model suggests that A, B, C, AB, AC, BC, A², B² and C² are the significant factors and A is not significant. The desired RSME value should be as low as possible as well as the complexity. The RMSE value in this case is 0.869 and the complexity is 14.59. This suggests that the model is a good fit and can be used to describe the behaviour of the system for metal + glass fibre recovery.

6.6.2.2 Pyro-oil Yield

Similar to the metal + glass fibre recovery case, GP-based model for pyro-oil recovery using the experimental outputs for the combination of input design matrix generated using the Box-Behnken Design has been developed. The tuning parameters are detailed in table 6.2. The predicted model for pyro-oil yield by GP is presented below –

$$\text{Pyro – oil Yield} = 3.66 \times 10^{-5} [C - \{(A+B) \cdot B^2\} + \{(C + 0.1991 \cdot A) + (1.135 \cdot B + C)\}] \quad (6.12)$$

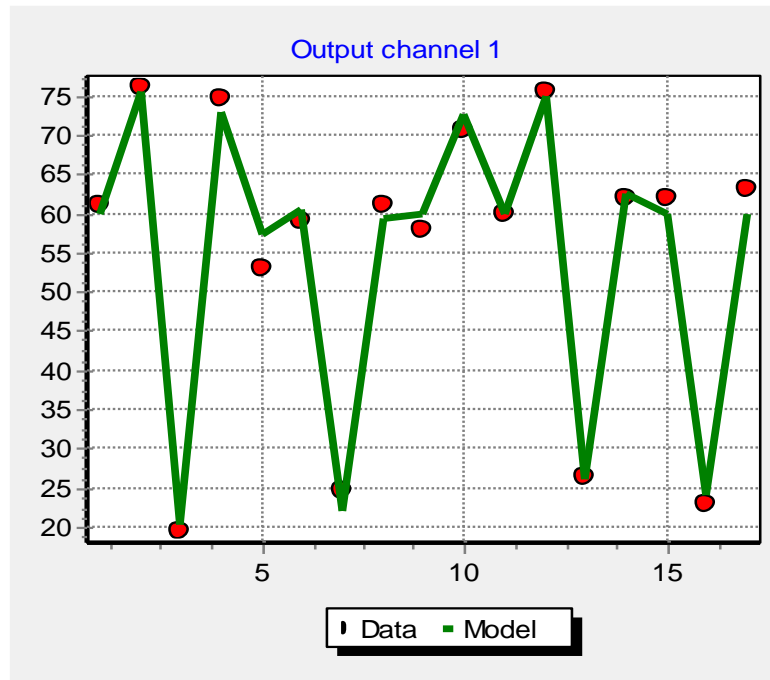


Figure 6.9: Model Fitting using GP for Pyro-oil recovery

The representative model fitting plot is shown in figure 6.9. The model suggests that A, B, C and B^2 are the significant factors. The desired RSME value should be as low as possible as well as the complexity. The RMSE value in this case is 0.186 and the complexity is 12.21. This suggest that the model is a good fit and can be used to describe the behaviour of the system for pyro-oil recovery.

6.6.3 Model Critique

In this study two methods have been employed, namely Response Surface Methodology (RSM) and Genetic Programming (GP), to maximize metal + glass fibre recovery and pyro oil yield of mixed WPCB pyrolysis as a function of (A) pyrolysis time, (B) percentage of FR-4 in FR2-FR4 mixture and (C) nitrogen flow rate. In case of metal + glass fibre recovery, it has been predicted by the RSM model (Eq. 6.8) correctly that (B) percentage of FR-4 in FR2-FR4 mixture is the most significant input parameter. The same has been reconfirmed by the evolutionary method of GP. As detailed in chapter 5, FR-2 and FR-4 WPCBs have different compositions. FR-2 WPCBs are rich in polymer while FR-4 PCBs are rich in metal and glass fibre. The effect of process parameters on a mixed WPCB sample containing FR-2 & FR-4 WPCB in different proportions for material recovery via pyrolysis is visible on metal + glass fibre recovery and pyro oil yield. During the pyrolysis process a mixed WPCB mixture containing higher amount of FR2 WPCB yield high amount of pyro-oil and a good amount of metal can be recovered. In this case the amount of glass fibre recovered will be low. On the other hand, if the mixture contains high

amount of FR-4 WPCB, the yield of pyro-oil will be low but metal and glass fibre recovery will be higher. In addition to that, it has been predicted by GP (Eq. 6.11) that the increase in the nitrogen flow rate enhances metal + glass fibre recovery. This can be justified by the fact that high flow rate of nitrogen helps in removing the volatiles and hence suppresses the secondary pyrolysis in gas phase and supports the primary pyrolysis of polymers intermingled with the metal. As a consequence, the chance of removal of polymer from metal increases. Overall effect of increase in N_2 flow rate is thus reflected in higher metal + glass fibre recovery. The presence of the interaction term 'BC' which is the interaction of (B) percentage of FR-4 in FR2-FR4 mixture and (C) nitrogen flow rate, in both the models, also reconfirms the role of nitrogen flow rate. The input parameter (A) pyrolysis time has been predicted to be insignificant by both RSM and GP.

In case of pyro-oil yield, it has been predicted by the RSM model (Eq. 6.10) that (A) pyrolysis time and (B) percentage of FR-4 in FR2-FR4 mixture are the two most significant parameters. This is true because the longer WPCB samples are exposed to pyrolysis process, the higher is the yield of pyro oil. Surprisingly the RSM method predicts that the nitrogen flow rate is insignificant. But the perturbation analysis identifies (C) nitrogen flow rate as a sensitive parameter. The interaction term 'AC' which is the interaction of (A) pyrolysis time and (C) nitrogen flow rate with a positive co-efficient, also affirms that (C) nitrogen flow rate does affect the pyro-oil yield indirectly. In case of GP, it has been predicted by the model (Eq. 6.8) that all three input parameters are significant, which is in not in agreement to the RSM findings.

References

- Raychaudhuri, A., & Behera, M. (2020). Review of the process optimization in microbial fuel cell using design of experiment methodology. *Journal of Hazardous, Toxic, and Radioactive Waste*, 24(3), 04020013.
- Kandpal, M., Kalyan, C. M., & Samavedham, L. (2013). Genetic programming-based approach to elucidate biochemical interaction networks from data. *IET systems biology*, 7(1), 18-25.
- Kiadehi, A. D., Taghizadeh, M., Azarhoosh, M. J., & Aghaeinejad-Meybodi, A. (2020). Hydrogen production using ethylene glycol steam reforming in a micro-reformer: experimental analysis, multivariate polynomial regression and genetic programming modeling approaches. *Journal of the Taiwan Institute of Chemical Engineers*, 112, 20-33.
- Koza, J. R. (1994). *Genetic programming II* (Vol. 17). Cambridge: MIT press.
- Kandpal, M., Chakravarthy, K. M., & Lakshminarayanan, S. (2010, July). A genetic programming based methodology for variable interaction determination in multivariate dynamical systems. In *Proceedings of the 2010 International Conference on Modelling, Identification and Control* (pp. 173-178). IEEE.
- Alviso, D., Artana, G., & Duriez, T. (2020). Prediction of biodiesel physico-chemical properties from its fatty acid composition using genetic programming. *Fuel*, 264, 116844.
- Marzban, N., Libra, J. A., Hosseini, S. H., Fischer, M. G., & Rotter, V. S. (2022). Experimental evaluation and application of genetic programming to develop predictive correlations for hydrochar higher heating value and yield to optimize the energy content. *Journal of Environmental Chemical Engineering*, 10(6), 108880.
- Zhang, Y., Ji, Y., & Qian, H. (2021). Progress in thermodynamic simulation and system optimization of pyrolysis and gasification of biomass. *Green Chemical Engineering*, 2(3), 266-283.
- Tun, K., & Lakshminarayanan, S. (2004). Identification of Algebraic and State Space Models Using Genetic Programming. *IFAC Proceedings Volumes*, 37(9), 311-316.
- Chen, Y., Liang, S., Xiao, K., Hu, J., Hou, H., Liu, B., Deng, H. & Yang, J. (2021). A cost-effective strategy for metal recovery from waste printed circuit boards via crushing pretreatment combined with pyrolysis: Effects of particle size and pyrolysis temperature. *Journal of Cleaner Production*, 280, 124505.

Koza, J. R. (1992, December). Evolution of subsumption using genetic programming. In *Proceedings of the first European conference on artificial life* (pp. 110-119). Cambridge, MA, USA: MIT Press.

CHAPTER-7

**STEAM GASIFICATION AIDED
PYROLYSIS OF WASTE
PRINTED CIRCUIT BOARDS
(WPCB)**

CHAPTER – 7

7.1 Background

Steam gasification aided pyrolysis is a non-conventional thermochemical process for the generation of gaseous fuel (syn-gas) as well as recovery of metal mixture, glass fibre and char (Zhang et al. 2012; Li et al. 2022). As identified in the research gap, very few literatures exist on gasification aided pyrolysis of WPCB (Zhang et al. 2012; Zhang et al. 2013; Li et al. 2022; Sahu and Vairakannu 2023; Yao et al. 2023). Previous researchers recommended steam gasification aided pyrolysis, whereby pyro-gas is further converted by steam, CO₂ etc. to generate product gas of syngas quality (Khaobang et al. 2022; Li et al. 2022; Sahu and Vairakannu 2023). The primary aim to utilise steam gasification aided pyrolysis is to upgrade the gas composition while facilitating metal recovery. These are the basic advantages for steam gasification aided pyrolysis.

- i. The steam gasification aided pyrolysis process facilitates further cracking of products evolved as the part of primary pyrolysis reactions compared to conventional pyrolysis. It also promotes further reaction with the carbonaceous char particles ($C + H_2O \leftrightarrow CO + H_2$) leading to the production of more gaseous fraction compared to conventional pyrolysis.
- ii. The steam gasification aided pyrolysis process increases the hydrocarbon content in the pyrolysis gas products and reduce harmful gases.
- iii. Due to the steam reforming and water-gas shift reactions, the decomposition of the organic matter (i.e., the polymer part) is higher compared to conventional pyrolysis that increases the metal content in solid phase products thereby creating higher economic value for smelting enterprises.
- iv. The steam gasification aided pyrolysis process reduces the bromine elements in solid-phase products.

Hence research intervention in this direction is important and timely. This chapter is focused on experimental “*Studies on steam gasification aided pyrolysis of individual Printed Circuit Board (FR2 and FR4)*”. The chapter encompasses the following objectives –

- Experimental investigation on gasification aided pyrolysis using FR-2 WPCB
- Experimental investigation on gasification aided pyrolysis using FR-4 WPCB.
- Characterization of gasification aided pyrolysis char.

7.2 Experimental

WPCBs were subjected to steam gasification aided pyrolysis in a pre-heated furnace using the fixed bed reactor (Figure 4.3) at different temperature over the range of 823 – 1073 K. For each WPCB and mixed PCBs (1:1 mixture of FR2 and FR4), 5g sample was fed to the reactor at the beginning. Steam and nitrogen were introduced at a rate of 0.5 lpm each to facilitate the steam gasification aided pyrolysis reactions. Experiments were carried out for 60 minutes. The volatile products were passed through series of condensers, one continuous bulb type condenser and two batch mode condensers, using constant temperature water of 283K as the cooling fluid in each case. The condensable volatiles were collected as liquid product and the non-condensable volatiles were collected as gaseous product. The gas was collected in a Tedlar bag for analysis using the Gas chromatograph, described in Chapter 4. The solid residues were collected after cooling down the reactor to the room temperature and weighed in a precision weighing balance, to determine the weight loss. The residues were crushed and sieved to separate the metals from the char.

7.3 Results and Discussion

Figure 7.1 (a) shows the residue obtained from steam gasification aided pyrolysis of FR-2 and FR-4 WPCBs. The yield of solid residue via steam gasification aided pyrolysis of FR-4 PCB is shown in figure 7.1 (b). The heterogeneous distribution of metals and polymer in PCBs is reflected through the non-uniform pattern shown in these figures.



Figure 7.1: Solid Residue of (a) FR-2 and (b) FR-4 WPCB steam gasification

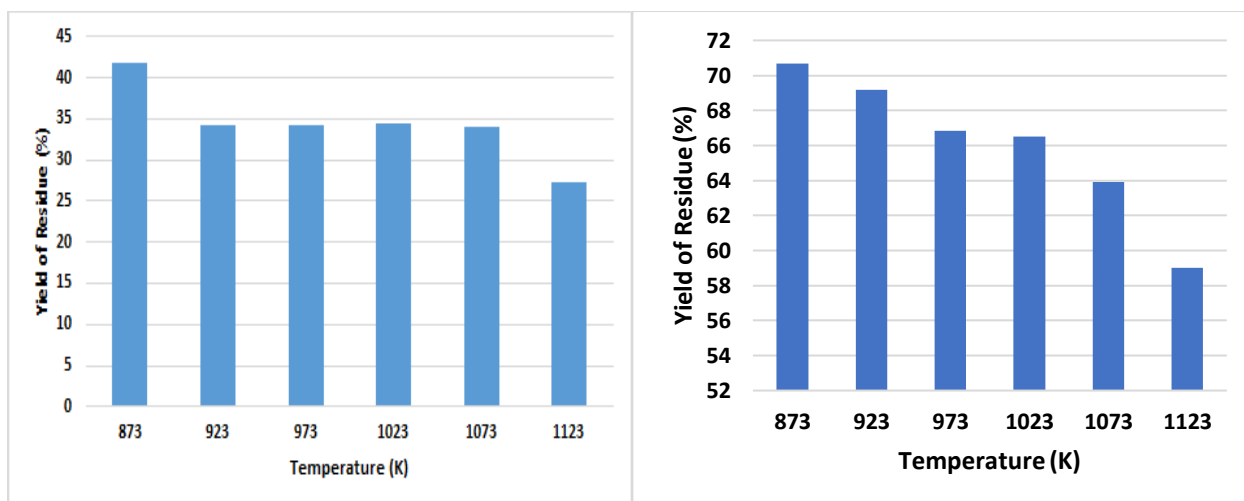


Figure 7.2: Yield of Solid Residue of (a) FR-2 and (b) FR-4WPCB steam gasification aided pyrolysis

Table 7.1: Data for the yield of solid residue of FR-2 and FR-4 and Mixed WPCB steam gasification aided pyrolysis

	FR-2 WPCB	FR-4 WPCB
Temperature (K)	Yield of Solid Residue (wt %)	Yield of Solid Residue (wt %)
873	41.81	70.69
923	34.16	69.16
973	34.26	66.84
1023	34.41	66.5
1073	34	63.91
1123	27.25	59

As can be seen from figure 7.2, with increasing temperature, the yield of residue decreases. In case of FR-2 WPCB, there is not much change in yield of solids in the range of 923 - 1073K. But in case of FR-4 WPCB, there is a decreasing trend in the same temperature range. However, in the temperature range of 973 – 1023K the yield is almost same. Actually, with the increase in temperature thermal decomposition of polymers through pyrolysis is expected to increase. Moreover, in presence of steam, reforming reaction of char is also expected to occur. Maximum decomposition is also expected to reach a maximum at a temperature, 973K for FR4 and 923K for FR2 in this case, beyond which no more decomposition of solid is expected. All these facts can justify the present observations. The composition of gaseous products at 873K, as analysed by the Gas chromatograph is presented in table 7.2.

Table 7.2: Syn-gas Composition obtained from Steam gasification aided pyrolysis of FR-2 and FR-4 WPCB

	FR-2 WPCB				FR-4 WPCB			
Temperature (K)	H ₂ (v/v %)	CO (v/v %)	CO ₂ (v/v %)	Others	H ₂ (v/v %)	CO (v/v %)	CO ₂ (v/v %)	Others
873	46.32	48.3	<1	5.37	37.03	38.37	<1	24.5
923	45.97	40.18	<1	13.84	36.59	36.78	<1	26.62
973	45.78	39.72	<1	14.49	33.38	33.51	<1	33.1
1023	45.66	39.42	<1	14.91	33.26	33.37	<1	33.36
1073	43.19	33.41	<1	23.39	29.51	29.55	<1	40.93
1123	43.19	33.41	<1	23.39	29.18	29.23	<1	41.58

7.4 Characterizations of Steam Gasification aided Pyrolysis Char

7.4.1 FESEM and EDX analysis

The Field Emission Scanning Electron Microscope (FESEM) images are displayed in figure 7.3 (a – d) for FR-2 WPCB raw samples, FR-2 WPCB steam gasification aided pyrolysis char, FR-4 WPCB raw samples and FR-4WPCB steam gasification aided pyrolysis char respectively. The images reveal the surface morphology of the respective samples. As can be seen, the surface of the FR-2 WPCB raw sample is not smooth and contains lots of folds and layers. In case of FR-2 WPCB steam gasification aided pyrolysis char (magnification at 5000 x) the presence of pores of variable size, possibly distributed as network, can be seen. Primary investigation reveals that the pores are in the microporous range. These characteristics ensure the possible applicability of FR-2 WPCB steam gasification aided pyrolysis char as adsorbent for wastewater treatment.

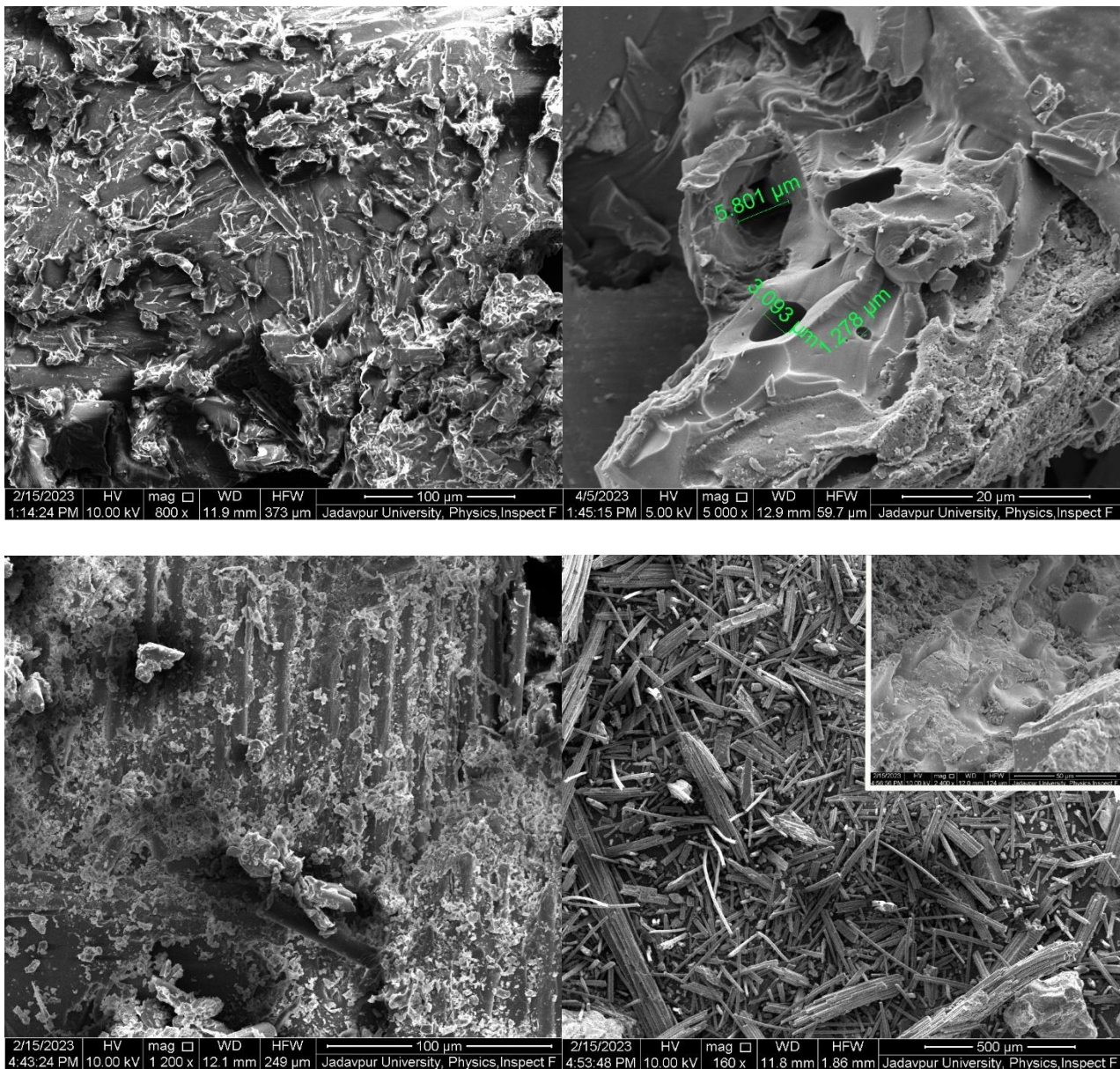


Figure 7.3: FESEM images of (a) FR-2WPCB Raw; (b) FR-2WPCB Steam gasification aided pyrolysis char, (c) FR-4 WPCB Raw and (d) FR-4 WPCB Steam gasification aided pyrolysis char

The surface of the FR-4 WPCB raw samples are rough and grid like structures can be seen. These are due to the presence of the glass fibre in the raw samples. Although some folds and layers can be observed, no pores have been found on the surface of FR-4 WPCB samples. In case of FR-4 WPCB steam gasification aided pyrolysis char, the rod-like structure obtained are due to the glass fibre. This affirms that glass fibre retains the shape after the steam gasification aided pyrolysis process. This finding is in accord with the findings of Sahu and Vairakannu (2023). At higher magnification (2400x), shown inset of figure 7.3(d) teeth like structure can be seen. It confirms that the steam gasification aided pyrolysis process significantly modifies the surface of the FR-4 WPCB samples. This signifies

that FR-4 WPCB steam gasification aided pyrolysis char could be considered as a precursor for developing tailored carbonaceous materials (Benega et al. 2021).

The metal content mapping of FR-2 and FR-4 WPCB before and after steam gasification aided pyrolysis has been carried out using EDX (Table 7.3). The analysis reveals that FR-2 WPCBs contains bromine and phosphorus, which is mainly due to the presence of phosphate based and brominated flame retardants (Grause et al. 2008; Kumagai et al. 2017). It also contains silicon, tin, copper, nickel, iron etc. It may be noted that post gasification, bromine and phosphorus are not found in the residue, while concentration of some of the metals have increased. Bromine is also found in FR-4 WPCB samples, a part of which is found in the steam gasification aided pyrolysis char as well. Other metals found in FR-4 WPCB before and after steam gasification aided pyrolysis include copper, iron, titanium and aluminium.

Table 7.3: Metal content mapping of FR-2 and FR-4 WPCB before and after gasification

	FR-2WPCB RAW		FR-2WPCB Gasif-Char		FR-4 WPCB RAW		FR-4 WPCB Gasif-Char
Metals	Weight (%)	Metals	Weight (%)	Metals	Weight (%)	Metals	Weight (%)
Bromine	4.32	Aluminium	5.22	Silicon	16.44	Silicon	19.52
Phosphorus	3.47	Silicon	0.84	Calcium	14.66	Tin	13.66
Silicon	1.58	Iron	0.83	Bromine	5.98	Aluminium	5.42
Silver	0.7	Tin	0.62	Aluminium	3.36	Copper	1.13
Tin	0.41	Copper	0.5	Lead	1.18	Lead	0.48
Copper	0.35	Lead	0.19	Iron	0.85	Titanium	0.46
Cadmium	0.3	Titanium	0.11	Titanium	0.57	Bromine	0.45
Arsenic	0.1	Platinum	0.07	Copper	0.5	Iron	0.38
Nickel	0.09	Lead	0.19	Nickel	0.07	Platinum	0.07
Iron	0.04			Cobalt	0.04		

7.4.2 XRD analysis

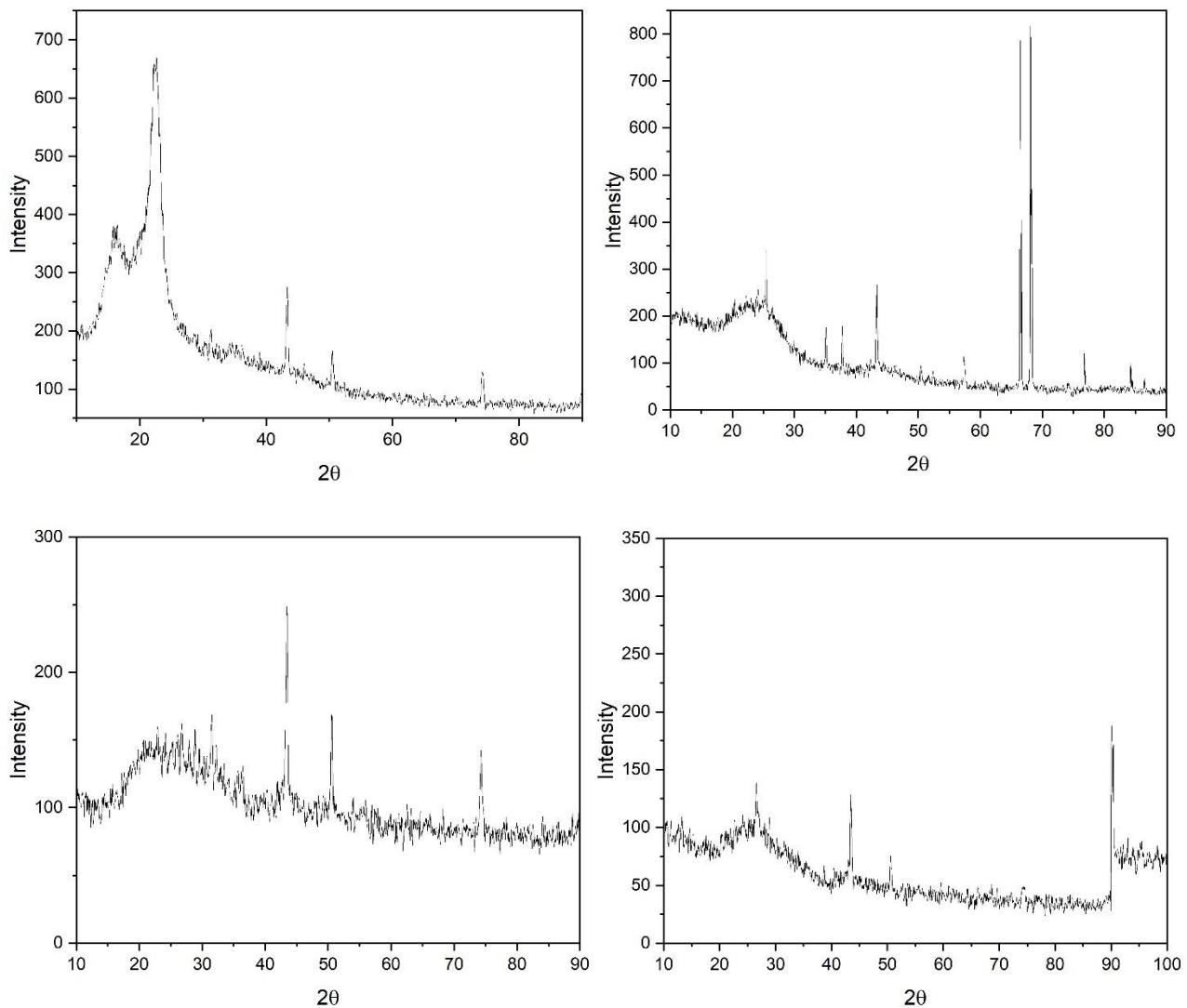


Figure 7.4: XRD Spectra of (a) FR-2WPCB Raw; (b) FR-2WPCB Steam gasification aided pyrolysis Char, (c) FR-4 WPCB Raw and (d) FR-4 WPCB Steam gasification aided pyrolysis char

The XRD analysis is intended for identification of crystal structures. Figure 7.4 (a) & (b) shows the XRD spectra of FR-2 WPCB raw samples and FR-2 WPCB steam gasification aided pyrolysis char respectively. In figure 7.4 (a), the broad diffraction peak around 15° is due to the presence of quartz crystals (Shen et al. 2017). The peak at 22.45° has been identified as Barium Silicate (ICSD: 01-071-0797). The diffraction peaks at 43.39°, 50.46° and 74.19° are attributed to copper (ICSD: 00-004-0836). This is quite obvious as copper linings are present in the WPCBs and it can be easily seen by naked human eye. In case of steam gasification aided pyrolysis char (figure 7.4 b), the broad peak of quartz at about 25° and Cu peaks about 43°, 50° are still present but a few new peaks have appeared. Peaks of Sn have appeared at around 35° and 84°. Peaks at about 37° and 53° are attributed to Al and

Pb. The peak at about 76° is due to Cu_2O (ICSD: 65-3288) which confirms that due to the steam gasification aided pyrolysis reactions, Cu is converted to Cu_2O . Peaks at 57.36° , 66.45° and 68.12° was identified as Al_2O_3 (ICSD: 01-076-0144).

In figure(7.4c) the broad peak around 25° can be attributed to the presence of SiO_2 (Shen et.al 2017). The presence of this peak is evident as FR-4 WPCBs contain glass fibre. Peaks at 43.45° & 50.52° are due to the presence of Cu (ICSD:01-089-2838). Another peak appears at 74.29° which has been identified as Iron nitride (ICSD:01-075-2129). In case of FR-4 WPCB steam gasification aided pyrolysis char peaks of Cu at around 43° remains as it is. The Iron nitride peak appeared at around 50° Peak for quartz crystal appeared at 26.5° (ICSD: 01-084-1780). This reconfirms the conversion of amorphous silicon into SiO_2 due to the steam gasification aided pyrolysis process.

7.4.3 FTIR Analysis

FTIR spectra of FR-2 and FR-4 WPCB, before and after steam gasification aided pyrolysis are presented in figure 7.5 (a) and 14(b) respectively. In both FR-2 and FR-4 WPCB gasification, the peaks are found in the similar region. The presence of the strong broad peak at 3425 and 3437 cm^{-1} (figure 14) affirms the presence of phenolic OH which is still present after gasification. In FR-2 WPCB steam gasification aided pyrolysis char, the presence of the peak at 1569 cm^{-1} can be attributed to the presence of primary amines. Peak at 1079 cm^{-1} can be accredited to C–N stretching which amplifies the presence of amines. The peaks at 1019 cm^{-1} and 1027 cm^{-1} found in FR-2 and FR-4 WPCB steam gasification aided pyrolysis chars respectively, represent C–O stretching which could be alcohols, ethers or esters.

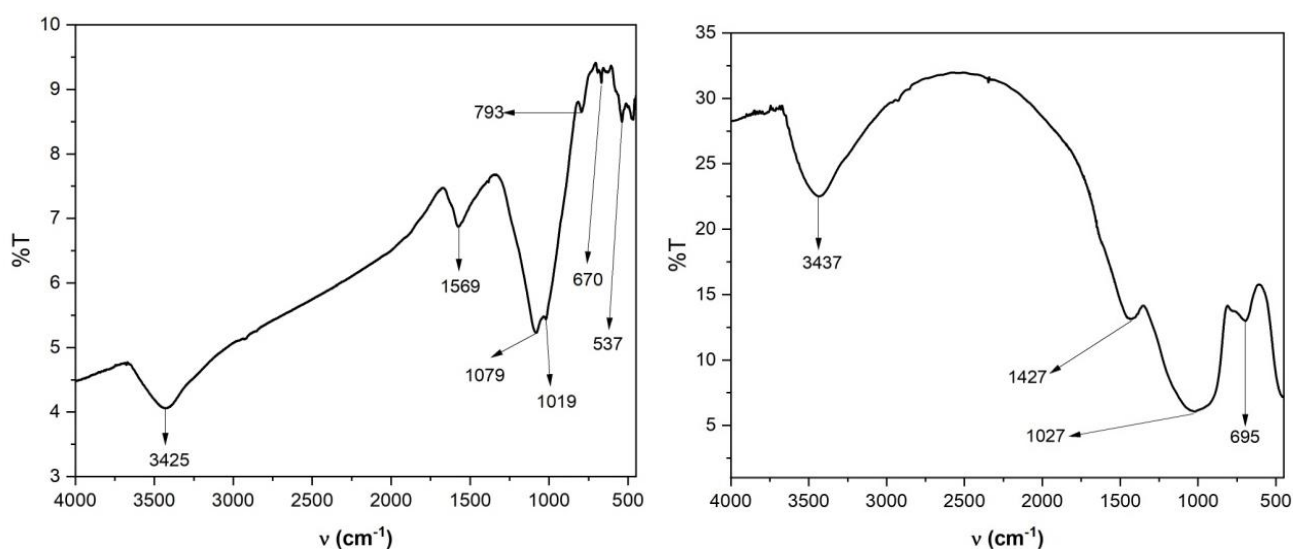


Figure 7.5: IR spectra of (a) FR-2 WPCB and (b) FR-4 WPCB steam gasification aided pyrolysis char

The peak around 793 cm^{-1} present in FR-2 WPCB char, is important. It represents aromatic mono, para-, meta-, and ortho- substituted component or halides. The peaks at 695 cm^{-1} and 537 cm^{-1} confirm the presence of bromine in both PCBs as this range is attributed to C-Br stretching. Details of FTIR spectra of FTIR spectra analysis of FR-2 and FR-4 WPCB Steam gasification aided pyrolysis char are presented in Table 7.4.

Table 7.4: FTIR spectra analysis of FR-2 and FR-4 WPCB Steam Gasification aided Pyrolysis Char

FR-2 WPCB Steam gasification aided Pyrolysis Char			FR-4 WPCB Steam Gasification aided Pyrolysis Char		
Frequency	Bond	Interpretation	Frequency	Bond	Interpretation
3425	O-H Stretching	vibration in hydroxyl group in phenols or alcohols (s,b)	3437	O-H stretching	vibration in hydroxyl group in phenols or alcohols (s,b)
1569	N-H bend	1° amines	1427	C=C stretch (in-ring)	vibration in aromatics group
1079	C-N Stretching	aliphatic amines	1027	Alcohols, ethers, esters, carboxylic acids, anhydrides	Alcohols, ethers, esters, carboxylic acids, anhydrides
1019	C-O Stretching	Alcohols, ethers, esters, carboxylic acids, anhydrides	695	C-Br stretching	Halide (s)
793	C-Cl stretching	Aromatic mono, para, meta, and ortho-substituted components			
670, 537	C-Br stretching	Halide (s)			

References

- Benega, M. A. G., Silva, W. M., Schnitzler, M. C., Andrade, R. J. E., & Ribeiro, H. (2021). Improvements in thermal and mechanical properties of composites based on epoxy-carbon nanomaterials-A brief landscape. *Polymer testing*, 98, 107180.
- Grause, G., Furusawa, M., Okuwaki, A., & Yoshioka, T. (2008). Pyrolysis of tetrabromobisphenol-A containing paper laminated printed circuit boards. *Chemosphere*, 71(5), 872-878.
- Khaobang, C., Sarabhorn, P., Siripaiboon, C., Scala, F., & Areeprasert, C. (2022). Pilot-scale combined pyrolysis and decoupling biomass gasification for energy and metal recovery from discarded printed circuit board and waste cable. *Energy*, 245, 123268.
- Kumagai, S., Grause, G., Kameda, T., & Yoshioka, T. (2017). Thermal decomposition of tetrabromobisphenol-A containing printed circuit boards in the presence of calcium hydroxide. *Journal of Material Cycles and Waste Management*, 19, 282-293.
- Li, C., Xia, H., Liu, C., & Zeng, K. (2022). Steam steam gasification aided pyrolysisassisted pyrolysis directional de bromination of waste printed circuit boards and comprehensive utilization of products. *Journal of Cleaner Production*, 366, 132979.
- Rai, C., Bhui, B., & Prabu, V. (2022). Techno-economic analysis of e-waste based chemical looping reformer as hydrogen generator with co-generation of metals, electricity and syngas. *International Journal of Hydrogen Energy*, 47(21), 11177-11189.
- Sahu, P., & Vairakannu, P. (2023). CO2 based co-steam gasification aided pyrolysisof printed circuit board with high ash coal. *Energy*, 263, 125977.
- Shen, Y., Chen, X., Ge, X., & Chen, M. (2018). Thermochemical treatment of non-metallic residues from waste printed circuit board: Pyrolysis vs. combustion. *Journal of Cleaner Production*, 176, 1045-1053.
- Yao, Z., Reinmüller, M., Ortuño, N., Zhou, H., Jin, M., Liu, J., & Luque, R. (2023). Thermochemical conversion of waste printed circuit boards: Thermal behavior, reaction kinetics, pollutant evolution and corresponding controlling strategies. *Progress in Energy and Combustion Science*, 97, 101086.
- Zhang, S., Yoshikawa, K., Nakagome, H., & Kamo, T. (2012). Steam steam gasification aided pyrolysisof epoxy circuit board in the presence of carbonates. *Journal of Material Cycles and Waste Management*, 14, 294-300.
- Zhang, S., Yoshikawa, K., Nakagome, H., & Kamo, T. (2013). Kinetics of the steam steam gasification aided pyrolysisof a phenolic circuit board in the presence of carbonates. *Applied energy*, 101, 815-821.

CHAPTER-8

**MREW FRAMEWORK AND
PROCESS MODELING USING
ASPEN**

CHAPTER – 8

8.1 BACKGROUND

Urban mining essentially focuses on recovery of resources from the urban stockpiles and putting them back into the value chain. In urban mining, the concept of landfill mining extends to the reclamation process of elements and compounds from the anthropogenic stockpiles (Baccini and Brunner 2012). E-waste is a mine for several resources, and it can be a source for supply of secondary raw materials to different industries. While the primary resources are depleting, metals from e-waste could be an important source and Metal Recovery from E-waste (MREW) could be a potential opportunity of metal recovery from secondary resources (Xavier et al. 2023). High content of base metal (Fe, Cu, Al, Pb and Ni) and precious metal (Ag, Au, Pt and Pd) present in e-waste makes it a potential source of secondary resources for metal recovery (Chakraborty et al. 2022). Hence, urban mining has become almost synonymous with the extraction of metals from e-waste as the metal concentration is comparatively high compared to ores (Murthy & Ramakrishna 2022; Cossu 2015).

MREW is a lucrative business as well as a very popular area of research. Different conventional techniques like physical processing, pyro-metallurgical processing, hydro-metallurgical and bio-metallurgical processing have been in implementation for metal recovery. Physical or mechanical recycling of e-waste is considered as a pre-treatment process. Metal rich fraction evolving from the pre-treatment are subjected to pyro-metallurgical, hydro-metallurgical and bio-metallurgical processing for selective recovery of metals. However, very few study have taken a holistic approach to address MREW technologies and bringing them under one umbrella. This chapter is focused on *Development of working framework featuring pyrolysis and gasification as pre-treatment processes* with the following objectives –

- Conceptualization of Material Recovery from E-waste (MREW) using pyrolysis and gasification as pre-treatment processes for printed circuit boards.
- Development of MREW plant layout with detailed input and output.

8.2 Methodology

Firstly, inferences from experimental outputs were organised along with brainstorming to coin the term Material Recovery from E-waste (MREW). Thereafter, case study organizations were visited and their process operations were understood and reviewed thoroughly. Based on the findings, three conceptual frameworks were developed for integrated

MREW facility. Then a generalized comparative analysis of the three scenarios were carried out from the principles of Life Cycle Assessment (LCA).

8.3 Case Studies

8.3.1 Case Study Organization A:

Location: Karnataka, India

Capacity: Full recycling capacity of 10 ton/day but currently handling 6 ton /day

Land Area: 1.5 acres of land with 25,000 sq. ft. closed area & 60, 000 sq. ft. of open area

No. of Employees: 100 (50 men + 50 women).

Profitability trend (last five years): High.

This organization is one of the oldest e-waste recycling plants in India. The objective of this unit is to convert e-waste into beneficial raw materials (metals, plastics, glass etc.) by implementing simple, cost effective, indigenous, environment friendly technologies suitable for Indian conditions. Its products and services include e-waste collection, dismantling, processing, recycling; metal, plastic, glass and different other recycled products; gold recovery from printed circuit board strips etc.

This company provides the necessary logistics for collection of different types of e-waste through e-auction or direct purchase. The collected e-waste coming from the collection centres and other sources in the facility is recorded in the data entry book in terms of its weight, source and data entry records. All the e-waste is first checked for any radioactive materials before being taken in to the dismantling line/area. Different streams are segregated at the first level before actual pre-processing. The collected e-waste first undergoes manual dismantling. Trained employees with safety equipments uses basic toolkits such as hot air gun, screw driver etc. to efficiently dismantle the e-waste. Separate work tables are allocated for each person. Air suction duct is present in each table which prevents any kind of particulate emission during dismantling. The dismantled parts are further segregated and dismantled into various streams. This facilitates easier operation and efficient processing. The resulting streams are fed to respective machineries for resource recovery and recycling. The basic dismantling results into metal rich parts, printed circuit boards, plastics, wires and CRT. These streams (except CRT and wires) go through mechanical size reduction performed by Shear-shredder and hammer mills. Then density separation is carried out to separate metals and non-metals. Sister

companies and other 3rd party industries are in contractual practice for metal recovery and other component recycling.

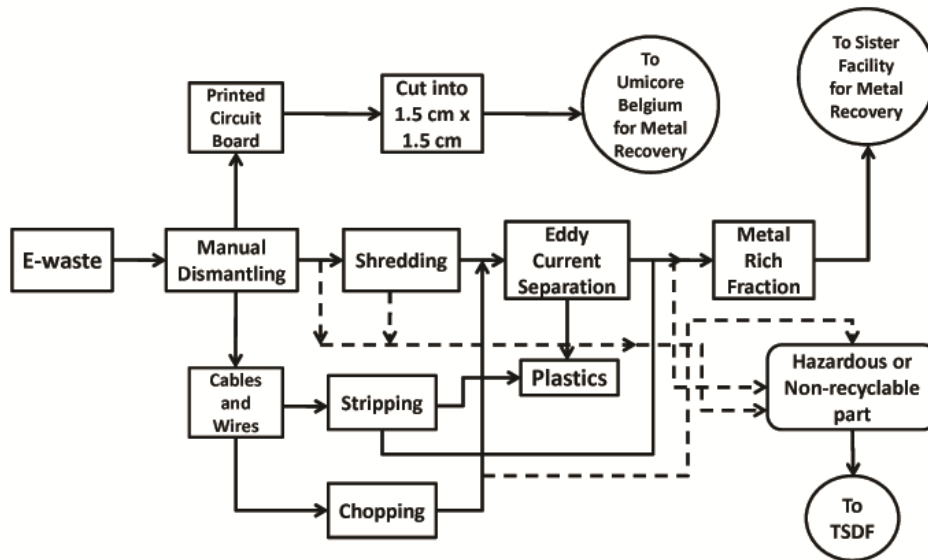


Figure 8.1: Process of E-waste Recycling in Indian Unit

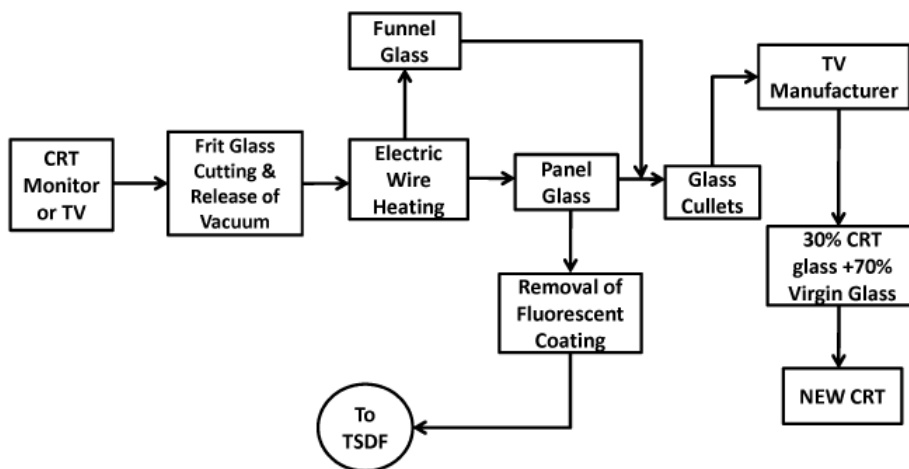


Figure 8.2: Process for CRT recycling in Indian Unit

The company have developed their own process for CRT recycling. The composition and hazardous characteristics of the panel and the funnel glass are different. The recyclability of waste CRTs are substantially increased when the panel and funnel glass are separated and sold to manufacturers. These scraps then can be recycled to produce new panel and funnel glass. Electric wire heating method is used to cut CRT into two halves. This separation also facilitates removal of hazardous fluorescent colour coating from the surface of the panel glass.

Vacuum-suction method is employed for this purpose. The glass is recycled by one of the leading TV manufacturers which uses 30% of the waste glass and rest virgin glass for manufacturing the TV glass panel. For wires, their indigenous stripping machine strips of the metal from the polymer coating. For cables with higher diameter, ranging from 2 mm to 10mm, are manually fed in the inlet holes from one end and longitudinally chopped pieces are collected from the other end, which are further manually segregated and sent to eddy current separator for separation of metals and non-metals.

The company is also associated in a social project where they have employed informal waste collectors and they buy waste printed circuit board (PCB) and other e-waste from them. These PCBs are shredded to 1.5" X-1.5" size for smelting. It exports shredded circuit boards and components for copper smelting to Umicore Precious Melting Refining, Belgium with the approval from Ministry of Environment and Forests. All together it can be commented that this e-waste recycling plant cares about the society and environment and is working for the cleaner environment.

8.3.2 Case Study Organization B:

Location: Beijing, China

Capacity: 10,000 tons/year

Land Area: 1.5 acres of land with 25,000 sq. ft. closed area & 60, 000 sq. ft. of open area

No. of Employees: 120

Profitability trend (last five years): High.

This organization is a model e-waste recycling plant for the city of Beijing, China. The unit provides waste dismantling, recycling service and disassembling e-waste as main competitive products. The company has specialized management team with professional knowledge in this sector committed to quality, honesty and value in e-waste recycling.

In the processing there are manual and semiautomatic sorting, dismantling in the e-waste recycling plant. Then the preprocessed material is sent to the processing stage. The material hence recovered are then reprocessed if required. They have separate line for refrigerators and degassing unit for safe removal of coolants. Then they are coarsely shredded and further crushed before subjecting to magnetic separation and eddy current separation for separation of metal and non-metals. Waste television sets are treated separately to take out the

CRTs. The vacuum tube is cut out first. Then the glass panel and the funnel are separated out. The hazardous substances are removed before crushing the glass.

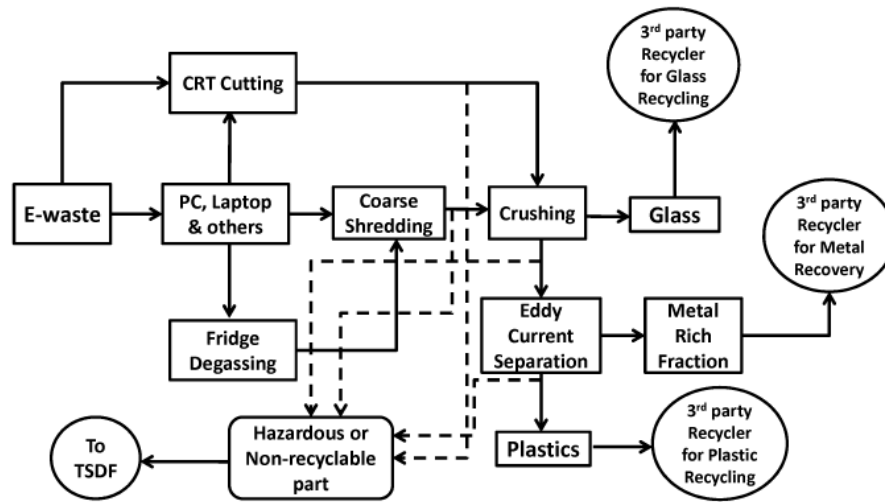


Figure 8.3: Process for e-waste recycling in Chinese Unit

8.4 The Concept of MREW

8.4.1 Description of MREW Facility

A schematic diagram of the MREW facility is presented in Fig.8.4. The operations regime of the MREW facility have outlined by a dotted boundary line. The material flows are depicted through the black arrows. E-waste is collected by different collectors, collection drives etc and/or deposited directly in the respective collection centre. The collected e-waste is then dispatched to the MREW facility. The purview of the MREW facility starts as soon as the e-waste enters the facility. Different categories of e-waste are processed in their respective processing lines. The Cathode Ray Tubes (CRT) passes through the CRT cutting unit where it is separated into panel and funnel glass. In this process line, the fluorescent coatings are collected and stored for disposal in a Treatment Storage and Disposal Facility (TSDF). White goods such as refrigerators, AC, incubators etc are dismantled in a separate process line, followed by the degassing of compressors. Any other type of e-waste including mobile, small household electronics, laptop, computer (excluding the monitor), are dismantled to separate out the printed circuit boards (PCB) and remaining materials. Similarly, the PCBs from white goods and CRTs are also separated. After dismantling, the resulting streams containing metals and plastics as well as the PCBs are then subjected to mechanical recycling. The recovered glass is stored separately for further processing and recycling. Two fractions evolve from this process – a) Rich in metals and b) Rich in plastics and others. The size reduced PCBs are

mixture of polymer, metal and woven glass fibre. They are either pyrolyzed at a temperature less than 623 K or they can be gasified using steam as a gasification agent at 873K, both as a pre-treatment step towards material recovery. The pyrolysis process yields pyro-oil and pyro-gas which have certain market value. Whereas, gasification process yields syn-gas and solid residue containing char, metal mixture and glass fibre. The pyro-gas and syn-gas produced in the pyrolysis and gasification process respectively can be utilised in the process itself for supplying energy to the process. The solid residues from both pyrolysis and steam gasification of PCB can be separated with mild mechanical processing which produces char, glass fibre and metals. The metal rich fractions (other than PCBs) obtained from mechanical processes are then handled by the MREW technologies. Metal fraction recovered from the above process is then treated by the MREW technologies (Pyro-, Hydro- and Bio-metallurgical technologies) for metal recovery.

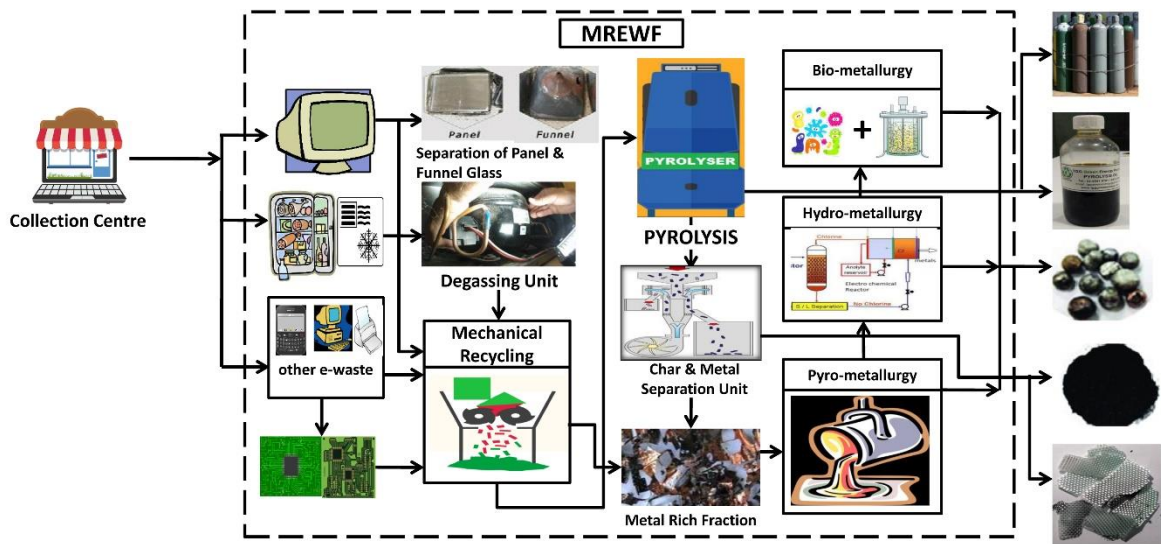


Fig. 8.4: Schematic Diagram of MREW Facility

8.4.2 Three Scopes of MREW

Three conceptual frameworks for MREW have been developed represented in Figure 8.5 – 8.7. In option 1, the metallurgical processes of pyro, hydro and bio categories are preceded by pre-treatment operations consisting only of mechanical and gravimetric types. On the other hand, the pre-treatment step is a combination of mechanical size reduction and two thermo-chemical processes namely pyrolysis (option – 2) and steam gasification aided pyrolysis (option – 3) along with post separation step for isolating metal rich solids from the char residues. As per the requirement of all unit operations and chemical processes the input energy and the material resources have been clearly shown across the system boundaries. Similarly, the output streams;

including metals, glass, plastic, oil, gas etc. whichever applicable have been clearly indicated. The possible emissions of carbon dioxide from different processes and unit operations incurred due to the usage of grid energy originally generated in coal or oil or natural gas-based power plants as well as transportation has been indicated.

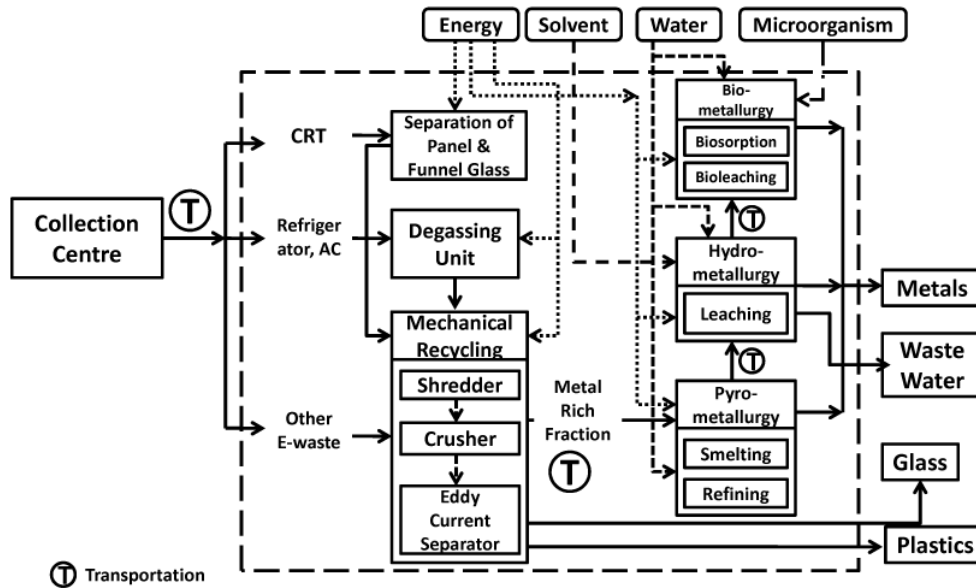


Figure 8.5: Conceptual Framework with conventional mechanical pre-treatment followed by metallurgical processing for MREW (Option-1)

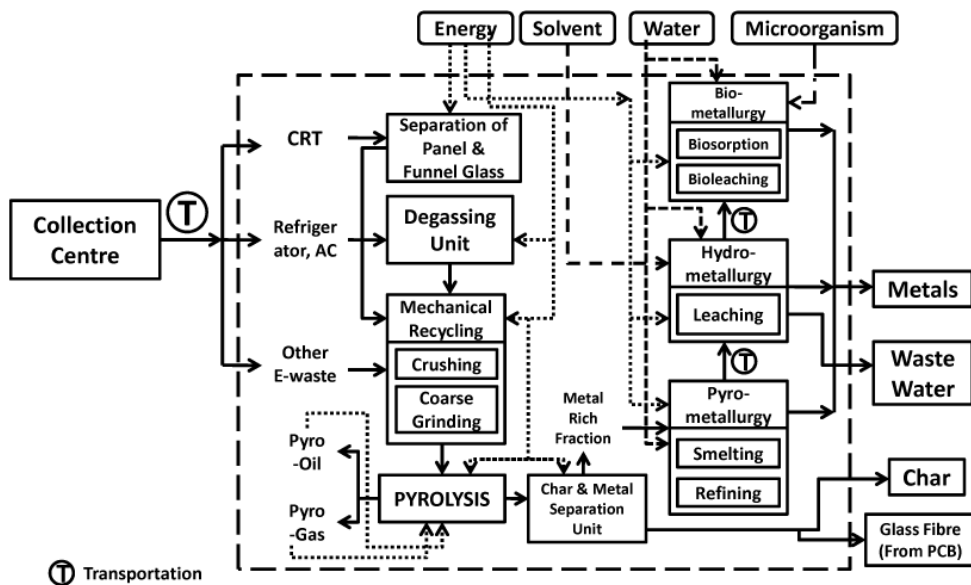


Figure 8.6: Conceptual Framework with light mechanical recycling and pyrolysis as pre-treatment followed by metallurgical processing for MREW (Option-2)

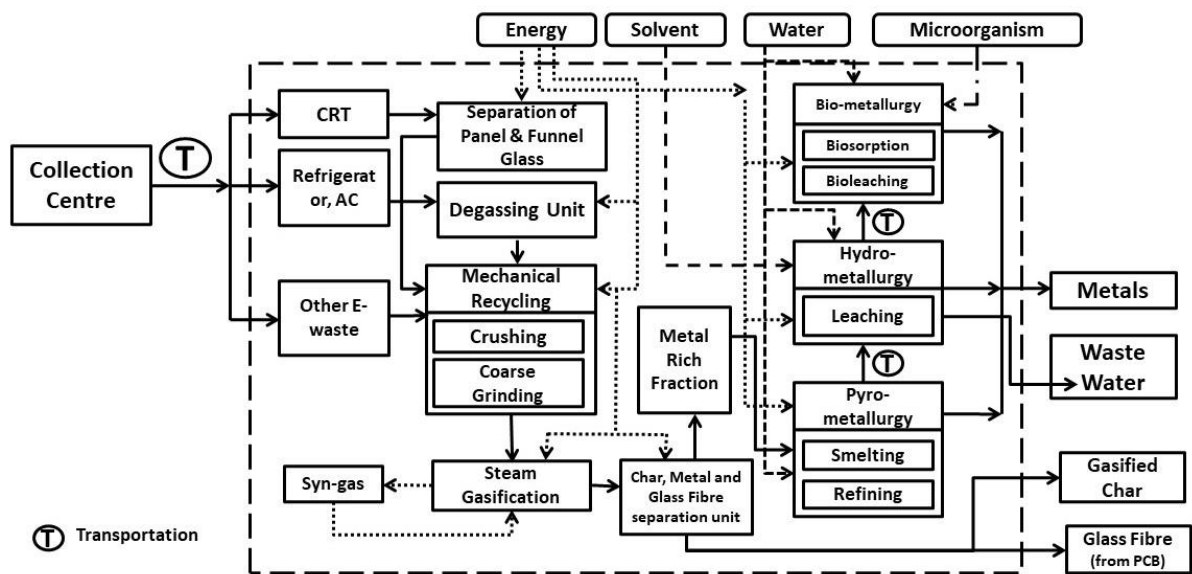


Figure 8.7: Conceptual Framework with light mechanical recycling and gasification aided pyrolysis as pre-treatment followed by metallurgical processing for MREW (Option-3)

LCA could not be performed due to lack of reliable data and accurate values of energy consumption, requisite material resources and so on. However, analysis of three scenarios from the principles of LCA reveals the following points.

- i) Consumption of energy and in turn the depletion of fossil fuel is expected to be less in the pre-treatment process involving option 2 since it requires less severity of size reduction. As a consequence, the carbon dioxide emission is also low in option 2. However, in option 3 it might increase as steam gasification aided pyrolysis process occur at a higher temperature.
- ii) In option 2 & 3, both pyrolysis and gasification aided pyrolysis process require energy which can be supplied from the liquid and gaseous products generated in the respective processes. The char resulting from these processes may be utilized for waste water treatment after activation (Andooz et al. 2022).
- iii) Hydro-metallurgical processing and electro-chemical refining is expected to have significant water footprint as both the processes generate waste water. Hydro-metallurgical processes use chemical solvents which contribute to COD of the waste water generated. As a result, the possible contributions will be in the impact category of eutrophication, acidification, marine and freshwater ecotoxicity, human toxicity and water depletion.

Recycling of the chemicals is a good option to reduce environmental impacts (Iannicelli-Zubiani et al. 2017).

- iv) Bio-metallurgical processes are expected to have similar impacts as different chemicals are required for preparation of the media for the culture and some waste water will be generated. But the magnitude of the impact is expected to be very less as it employs microorganism and toxic material generated during the process is limited (Xavier et al. 2023).
- v) The activated carbon used in waste water treatment may be manufactured from pyro-char and gasification aided pyrolysis char.
- vi) Usage of activated carbon prepared from waste biomass or any other waste materials instead of activated carbon prepared from virgin materials is encouraged. This will have some positive impact on the environment (Zhu et al. 2022).
- vii) Substantial amount of emission is associated with transportation of e-waste from collection centres to the recycling facility. It will be always preferred to have the collection centres in close vicinity of the recycling centre (Hannan et al. 2020).
- viii) As found from the case studies, after mechanical recycling it is send to sister companies or third-party facilities for processing and recovery of metals (Ghosh et al. 2016). This will increase the consumption of the fuel and ultimately will contribute to climate change and fossil fuel depletion.
- ix) It is suggested that if the collection rate is substantially high then such processing facilities to be established in close vicinity or adjacent to the existing facility. This will reduce emissions due to transportation. However, if the rate of collection is not worthy by volume, then it is better to use existing facility as new land acquisition will also have some adverse effects on the environment. Another factor, to be kept in mind that, any unit carrying out dry operations can be setup at the out skirts of any urban area as a centralized facility. If the unit to be established is for dry processing as well as metallurgical processing of e-waste, a decentralized facility will be preferred in the industrial zone.

8.5 Process Modelling

As detailed in the previous sections, Material Recovery from E-waste (MREW) is a key component towards realizing a sustainable e-waste valorisation. The MREW facility proposed in the previous chapter, can be a platform towards development of sustainable resource recovery schemes from e-waste. Both pyrolysis and gasification aided pyrolysis has been proposed as pre-treatment processes supported by the experimental findings. From chemical

engineering point of view, it is essential to perform process modelling for better understanding of the process.

8.6 Process Modelling Methods

Process modelling was carried out using the ASPEN PLUS v10 process simulator. ASPEN PLUS is one of the most used commercial process simulators in chemical engineering. ASPEN PLUS does not contain a pre-designed model for pyrolysis and gasification aided pyrolysis; hence combination of different blocks has been used. Pyrolysis has been carried out using R-yield block whereas gasification aided pyrolysis has been carried out using CSTR block with established kinetics.

Below are the assumptions made for the development of the model:

- The pyrolysis simulation model prepared with Aspen PLUS is a stationary and isothermal model that uses the sequential-modular calculation technique.
- Uniformity of temperature and pressure in the reactor.
- All the gas components were considered to be ideal.

In the software, MIXCINC has been set as the global flow class of the simulation. This is used when both conventional and unconventional solids are present. The unconventional components are not present in the Aspen Plus database and are modelled through proximate and ultimate analysis. Enthalpy and density are the only properties calculated for unconventional components and are made from empirical correlations. The specific property methods for enthalpy and density are chosen for this simulation are the HCOALGEN method and the DCOALIGT method: both are based on proximate and ultimate analysis. PCBs are considered unconventional solids as they are not present in the ASPEN database.

8.7 Simulation model of Mixed PCB Pyrolysis

Mixed PCB pyrolysis simulation has been carried out by simulating FR-2 and FR-4 WPCB pyrolysis in equal amount and then combining them together. The simulation flowsheet is presented in figure 8.8. Printed Circuit Board is a heterogeneous mixture of materials. it is not available as a conventional material in the Aspen Plus database; hence a WPCB Stream was created using a mixer with the following input streams. FR-2 WPCB contains polymers and metals. A typical composition of FR-2 WPCB used in experiments has been used to create FR-2 PCB in Aspen. FR-4 WPCB stream was created using a mixer block .FR-4 WPCB contains

polymers, metals and glass fibres. A typical composition of FR-4 PCB recovered from desktop computer in experiments has been used to create FR-4 PCB in Aspen. The proximate and ultimate analysis results obtained in our experiments, has been used in the simulation. The details are presented in table 8.1

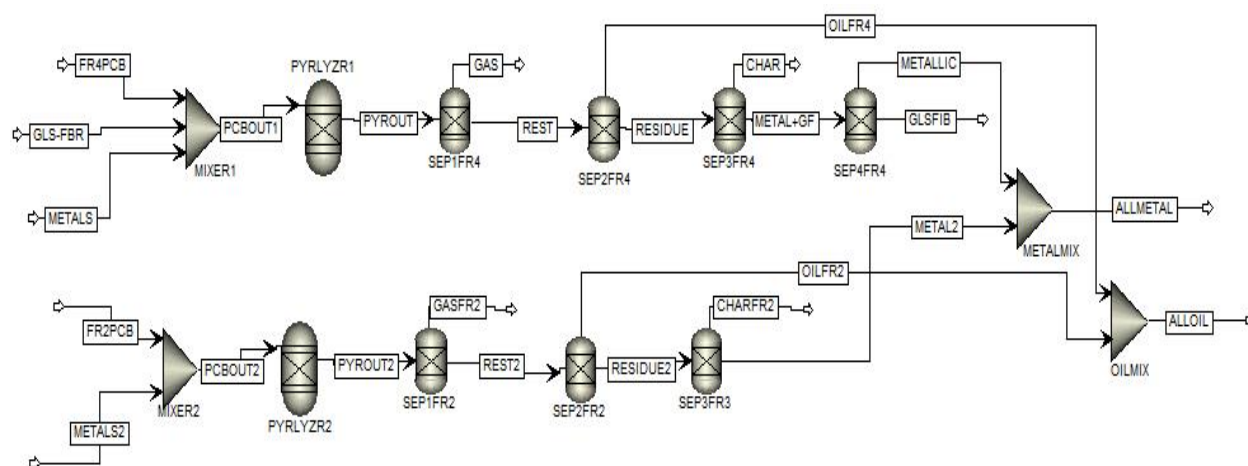


Figure 8.8: Aspen Plus Simulation of mixed WPCB pyrolysis and product separation

Table 8.1 Proximate and Ultimate analysis of FR-2 and FR-4 WPCB

Sample	Moisture	Volatiles	Ash	Fixed Carbon	Carbon	Hydrogen	Nitrogen	Sulphur
FR-2 VPCB	1.27	24.8	25.3	48.2	49.73	4.289	3.39	0.366
FR-2 WPCB	2	21.30	33	43.70	42	6.3	1.7	0.266
FR-4 VPCB	1.5	25.32	69.5	3.68	42.54	3.823	0.15	0.216
FR-4 WPCB	0.50	24.25	73.2	2.05	24.83	0.412	0.58	0.325

In case of FR-2 WPCB, NPCB, which is the non-metallic fraction of the printed circuit board was used as one of the input Streams for creating PCB. This is a non-conventional stream (NC-Solid). Proximate and ultimate analysis of FR-2 PCB was given as input for the NC-Solid stream. METALS stream includes all the metals which is considered as CI-Solid stream. The input PCB flow rate was taken as 100 kg/hr. Pyrolysis was carried out using the R-Yield reactor block to mimic a Pyrolyzer (PYRLYZR). The pyrolyzer is operated at 623K. The output from the pyrolyzer (PYROUT) is fed to a separator block (SEP1), where Pyro-gas (GAS) is separated. The residue from the SEP1 (REST) is fed to a second separator block (SEP2) where Pyro-oil (PYROOIL) is separated, and the solid residue (RESIDUE) is fed to a third separator block (SEP3) where char and metals are finally separated.

Similar to FR-2 WPCB, polymer fraction of the PCB (NPCB) was used as one of the input streams for creating FR-4 WPCB. This is a non-conventional stream (NC-Solid). Proximate and ultimate analysis of FR-4 PCB was given as input for the NC-Solid stream. METALS stream includes all the metals considered as CI-Solid stream. The non-metal portion which is the glass fibre (GLS-FBR) was introduced for preparation of PCB as a mixed stream. The input FR-4 PCB flow rate was set as 100 kg/hr. Pyrolysis was carried out using the R-Yield reactor block to mimic a Pyrolyzer (PYRLYZR). The output from the pyrolyzer (PYROUT) is fed to a separator block (SEP1), where Pyro-gas (GAS) is separated. The residue from the SEP1 (REST) is fed to second separator block (SEP2) where Oil (PYROOIL) is separated, and the bottom product (RESIDUE) is fed to a third separator block (SEP3) where char is separated. The mixture of metal and glass fibres (METAL+GF) is again sent to a separator block (SEP4), where metals (METALLIC) are separated, and components of glass fibres are sent to a mixer (B1) to finally obtain the glass fibre (GLSFBR).

8.8 Simulation model of Mixed PCB Gasification aided pyrolysis

Simulation of mixed PCB gasification aided pyrolysis has been carried out by simulating FR-2 and FR-4 WPCB gasification aided pyrolysis in equal amount and then combining them together. The simulation flowsheet is presented in figure 8.9.

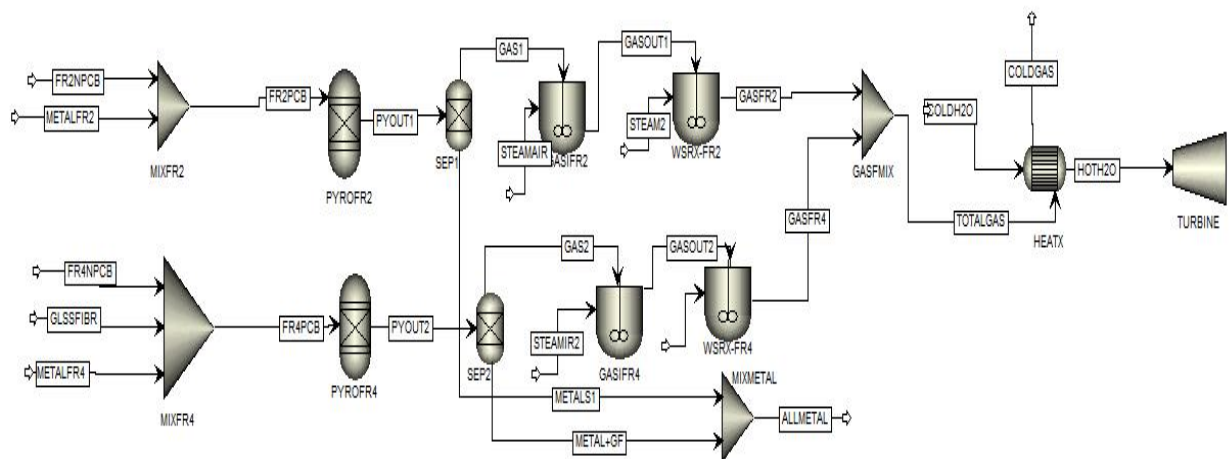


Figure 8.9: Aspen Plus Simulation of mixed WPCB Gasification aided pyrolysis and product separation

Process modelling of mixed WPCB gasification aided pyrolysis has been carried as shown in the figure 8.9. FR-2 and FR-4 WPCB stream is created using a mixer block that contains polymers, metals and glass fibres. Composition of FR-2 and FR-4 WPCB are same that is used in mixed WPCB pyrolysis simulation. The polymer fraction of the printed circuit board

(NPCB) was used as a non-conventional input stream (NC-Solid). Proximate and ultimate analysis of both type WPCB was given as input for the NC-Solid stream. METALS stream includes all the Metals which is considered as CI-Solid stream. The non-metal portion which is the glass fibre (GLSSFIBR) has been introduced for preparation of PCB as a mixed stream. Since pyrolysis occurs in the beginning of the gasification process, the pyrolysis step was simulated first as described in section 8.7 using R-Yield block. The pyrolyzer is operated at 623K. Two major equations of gasification aided pyrolysis along with the established kinetics has been used in this case (Table 8.2). For ease of operation the two steps were simulated in two separate gasification blocks using R-CSTR module. The gasifiers are operated at in the temperature range of 800 – 1200K. Metals has been separated out before gasification to avoid any error. All metals recovered are then mixed in a mixer that yield total metal (ALLMETAL). The generated syn-gas is then passed through a heat exchanger (HEATX) followed by a steam turbine (TURBINE) that generates electricity from the heat recovered from the syn-gas.

Table 8.2: Rate constants for gasification reactions

Reaction name	Equation	Rate constant	Source
Steam gasification reaction	$C + H_2O \xrightarrow{K_1} CO + H_2$	$K_1 = 1.272 \times m_s T \times C_{H_2O} e^{\frac{-188270.5}{RT}}$	Pati et al. 2020
Water-gas shift reaction	$CO + H_2O \xrightarrow{K_2} CO_2 + H_2$	$K_2 = 7.68 \times 10^{10} \times T \times C_{CO}^{0.5} \times C_{H_2O} e^{\frac{-188270.5}{RT}}$	Pati et al. 2020

8.9 Results and Discussions

8.9.1 Results of simulation of mixed WPCB pyrolysis

The results of mixed WPCB pyrolysis simulations are presented in table 8.3. The simulation process yields nearly 33% glass fibre, 29% metals, 19% pyro-oil, 13% char and 6% gas.

Table 8.3: Simulation results of mixed WPCB Pyrolysis

COMPONENTS	Mixed PCB (Wt %)
Metals	21.48
Glass Fibre	52.16
CO	5.47

CO ₂	0.28
CH ₄	1.27
H ₂	0.61
OIL	10.86
Char	7.91

Table 8.4: Simulation results of mixed WPCB pyrolysis at different temperature

Metal	FR-2 (wt%)	FR-4 (wt%)
Cu	27.32	48.54
Sn	8.16	18.69
Pb	35.76	9.85
Fe	24.79	15.93
Ni	3.01	5.49
Cr	0	1.19
Mo	0.73	0.06
Ag	0.12	0.15
Au	0.06	0.07
Pd	0.09	0.08

8.9.2 Results of simulation of mixed WPCB gasification aided pyrolysis

The results of mixed WPCB gasification aided pyrolysis simulations are presented in table 8.5. Gasification aided pyrolysis simulation has been executed in the temperature range of 1073 – 1473K. As can be seen, the yield of hydrogen is the highest at 1073K and then it decreases by 3% till 1273K. Beyond 1173K, the yield of H₂ begins to saturate. Whereas, the yield of CO increases by almost 17% over the whole temperature range. Although, beyond 1273K, the yield of CO begins to saturate. On the other hand, yield of CO₂ decreases from 1.83% to 1.52% in the temperature zone of 1073 – 1273K, then the yield of CO₂ is saturated which is desirable.

Table 8.5: Simulation results of mixed WPCB gasification aided pyrolysis at different temperature

Syn-gas (Volume%)	Temperature (K)				
	1073	1173	1273	1373	1473
H ₂	43.07	41.12	40.05	39.82	39.76
CO	33.7	44.98	49.08	49.97	50.18
CO ₂	21.42	12.36	9.37	8.72	8.57
CH ₄	1.83	1.57	1.52	1.51	1.51
Energy (kW)	10.31	11.55	12.79	14.03	15.27

As shown in table 8.6, most of the valuable metals can be recovered via gasification aided pyrolysis process including copper, nickel, aluminium, iron etc. The glass fibre can also be recovered through this process.

Table 8.6: ASPEN predicted composition of metal stream from gasification aided pyrolysis

Metals & Glass Fibre	(wt%)
Ni	1.46
Cu	13.17
Fe	6.88
Au	0.02
Ag	0.07
Pb	66.02
Cr	0.15
Mo	0.02
Pd	0.05
Sn	0.48
Al	6.46
Sb	0.42
As	0.55
Zn	1.96
Glass Fibre	2.37

References

- Andooz, A., Eqbalpour, M., Kowsari, E., Ramakrishna, S., & Cheshmeh, Z. A. (2022). A comprehensive review on pyrolysis of E-waste and its sustainability. *Journal of Cleaner Production*, 333, 130191.
- Baccini, P., Brunner, P., 2012. *Metabolism of the Antroposphere: Analysis, Evaluation, Design*. The MIT Press, ISBN 9780262016650.
- Bhandari, G., Gupta, S., Chaudhary, P., Chaudhary, S., & Gangola, S. (2023). Bioleaching: A Sustainable Resource Recovery Strategy for Urban Mining of E-waste. In *Microbial Technology for Sustainable E-waste Management* (pp. 157-175). Cham: Springer International Publishing.
- Chakraborty, S. C., Qamruzzaman, M., Zaman, M. W. U., Alam, M. M., Hossain, M. D., Pramanik, B. K., Nguyen, L.N., Nghiem, L.D., Ahmed, M.F., Zhou, J.L., Mondal, M.I.H, Hossain, M.A., Johir, M.A.H, Ahmed, M.B., Sithi, J.A., Zargar, M. & Moni, M. A. (2022). Metals in e-waste: Occurrence, fate, impacts and remediation technologies. *Process Safety and Environmental Protection*, 162, 230-252.
- Cossu R. and Williams I.D. (2015). Urban mining: Concepts, terminology, challenges. *Waste Management*, 45, 1-3.
- Ghosh, S. K., Roychoudhuri, R., Wath, S. B., Debnath, B., Jayakumar, S., & Maloo, A. (2016). Waste Management in India: E-waste recycling & Bio-methanation-Case studies. *Journal of Solid Waste Technology & Management*, 42(1), p748-759.
- Hannan, M. A., Begum, R. A., Al-Shetwi, A. Q., Ker, P. J., Al Mamun, M. A., Hussain, A., Basri, H. & Mahlia, T. M. I. (2020). Waste collection route optimisation model for linking cost saving and emission reduction to achieve sustainable development goals. *Sustainable Cities and Society*, 62, 102393.
- Murthy, V., & Ramakrishna, S. (2022). A review on global e-waste management: urban mining towards a sustainable future and circular economy. *Sustainability*, 14(2), 647.
- Pati, S., Manna, D., De, S., & Chowdhury, R. (2023). Thermodynamic and phase equilibrium models of syngas generation through gasification. In *Advances in Synthesis Gas: Methods, Technologies and Applications* (pp. 3-42). Elsevier.
- Xavier, L. H., Ottoni, M., & Abreu, L. P. P. (2023). A comprehensive review of urban mining and the value recovery from e-waste materials. *Resources, Conservation and Recycling*, 190, 106840.
- Zhu, X., Labianca, C., He, M., Luo, Z., Wu, C., You, S., & Tsang, D. C. (2022). Life-cycle assessment of pyrolysis processes for sustainable production of biochar from agro-residues. *Bioresource technology*, 127601.

CHAPTER-9
SUPPLY CHAIN KINETICS OF
MREW PLANT

CHAPTER – 9

9.1 BACKGROUND

Industrially, the resource recovery of e-waste is limited to mechanical recycling and in some cases, recovered metal is transported to sister companies or third-party smelters (Khaliq et al. 2014). The management of e-waste is globally handled mostly by informal sectors that further compounds the problem as appropriate technologies are often not used, even when available, either due to lack of resource or intention. This is even more so in developing nations (Widemar et al. 2005; Ghosh et al. 2016). The informal sectors often employ inefficient and rudimentary technologies to extract copper, gold etc. from e-waste (Sengupta et al. 2022). This is one of the primary reasons for non-circularity of materials recovered from the e-waste. This results in an inefficient supply chain which is not a closed loop incumbency, thus affecting business cycles in the longer run. The erratic and uncontrolled use of technology and disposal schemes attribute a strong stochastic element to the e-waste business. Typical examples of this relate to heterogeneous material, hazardous waste disposal, energy efficiency, secondary emissions, recovery efficiency, supply uncertainty, etc.

E-waste plants are prone to operate in uncertainty zone as scrap metal prices are subjective to market volatility and plant sustenance depends on the availability of feedstock (Reuter et al. 2015). The overall operation of an MREW plant is complex structure with numerous major and minor loops leading towards input procurement, product manufacturing, product distribution and waste disposal. There are different types of uncertainties that affects the business individually or collectively. Hence, the key challenge is to collectively consider MREW plant performance in decision making. Additionally, it is vital to study time evolution kinetics of these variables to understand the plant performance. This chapter is focused on *Time Evolution Dynamics of Material Recovery from E-waste (MREW) plant focusing on plant operation and its sustainability* with the following objectives –

- Data collection for model development and validation.
- Development of cost function for MREW supply chain network.
- Evaluation of weight factor and interrelation co-efficient.
- Optimization of cost function and conversion into dynamic system.
- Development of constrained problem.
- Model validation for both unconstrained and constrained scenarios.

9.2 Description of the MREW Supply Chain Network

Supply Chain Networks can be addressed from the perspective of Life Cycle Assessment (LCA) and the range can vary based on the approach taken, such as cradle-to-cradle (Neiro et al. 2016), cradle-to-gate (Westfall et al. 2016), gate-to-gate (Colley et al. 2020) etc. Figure 9.1 illustrates different boundaries of supply chain based on LCA concepts. In this study, we consider a generalized version of an MREW SCN, starting from the consumers, MREW as the internal operations section and ending with the 3rd party recyclers handling the recovered materials from e-waste, translating to a “utilization-to-cradle” model. MR

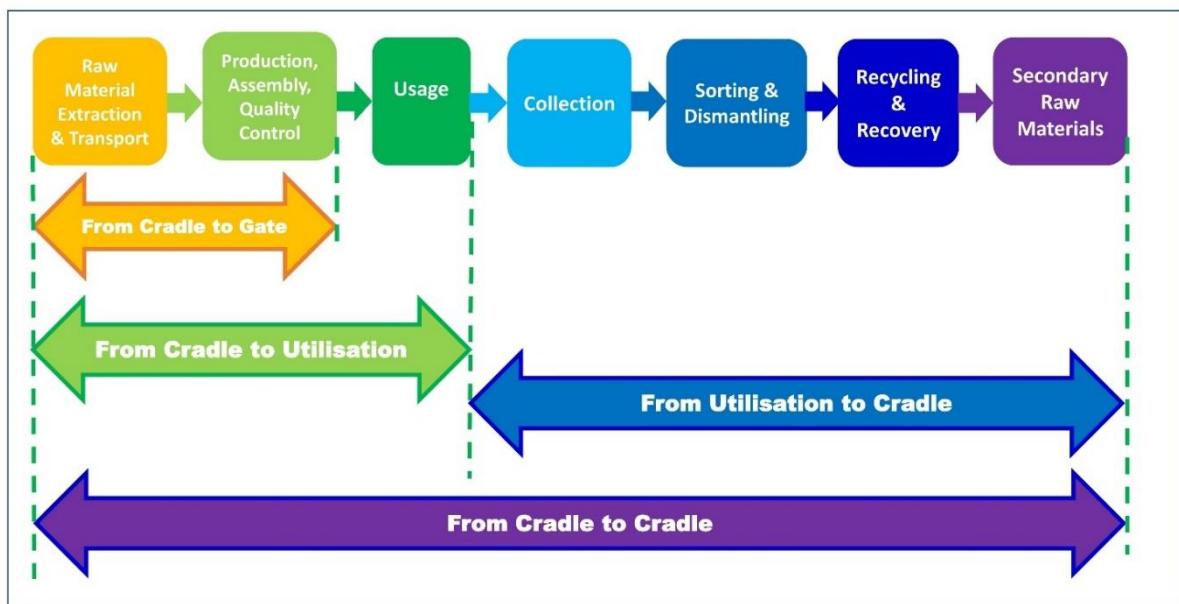


Figure 9.1: Boundaries of Supply Chain based on LCA

Despite the technological advancements and maturity over time, it is imperative to have a very efficient supply chain network to balance the supply and the demand for materials and ensure circular economy. Based on the findings of Ghosh et al. (2016), literature findings, brainstorming and the authors’ experience in visiting several e-waste recycling facilities, a supply chain framework has been developed (Figure 9.2). The framework is intended for urban mining of e-waste considering MREW facility. The supply chain framework can be divided into three parts—the supply side, the internal operations side and the demand side. OEMs, retailers, customers and the technology providers are in the supply side. The informal sector, formal recyclers and the MREW facility are in the internal operations side whereas; third party recyclers, raw material suppliers, reusable product manufacturer and customers of recycled products are in the demand side.

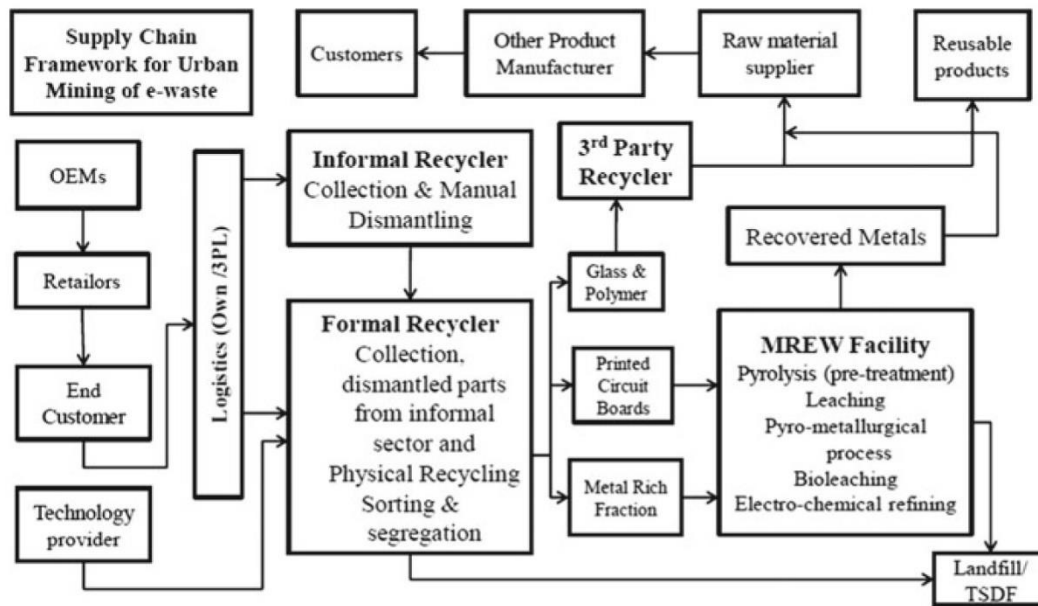


Figure 9.2: Supply chain network for MREW facility

The developed supply chain framework (Figure 9.2) has considered the MREW facility for the recovery of metals from e-waste. The supply side considers the traditional stakeholder flow from OEM to end customers. The logistics for e-waste to recycling facilities has been kept as a choice of the users. To some extent, the door-to-door collection of the informal sector makes it independent of the users. After the collection and dismantling at the primary recycling facilities, the recovered fractions enter the MREW facility. In the MREW, all possible routes of metal recovery have been considered including pyrolysis as a pretreatment process. This is where the urban mining gets a boost. The existence of the dedicated MREW facility for metal recovery is the key and the strongest point here is to ensure the resource recovery. The circularity of resources is ensured by the demand side where the third-party recyclers are involved in recycling the resulting fractions and the recycled product manufacturers convert these into products which can be sold in the market. Some portion of recovered e-waste can be considered as raw materials and these are then supplied to different places by the raw material suppliers, which mean the material re-enters the value chain.

9.3 Methodology

This study adopts the mathematical structure outlined in Chattopadhyay et al. (2020). The current investigation exclusively develops a cost function-based model specifically for the e-waste supply chain network, complementing three uncertainty modules that affect the supply chain sustainability, each weighted by its own individual weight. The uniqueness of the study

is that we have used two popular methods i.e., AHP and PCA and integrated them to develop a new hybrid AHP-PCA method for ranking the uncertainty variables.

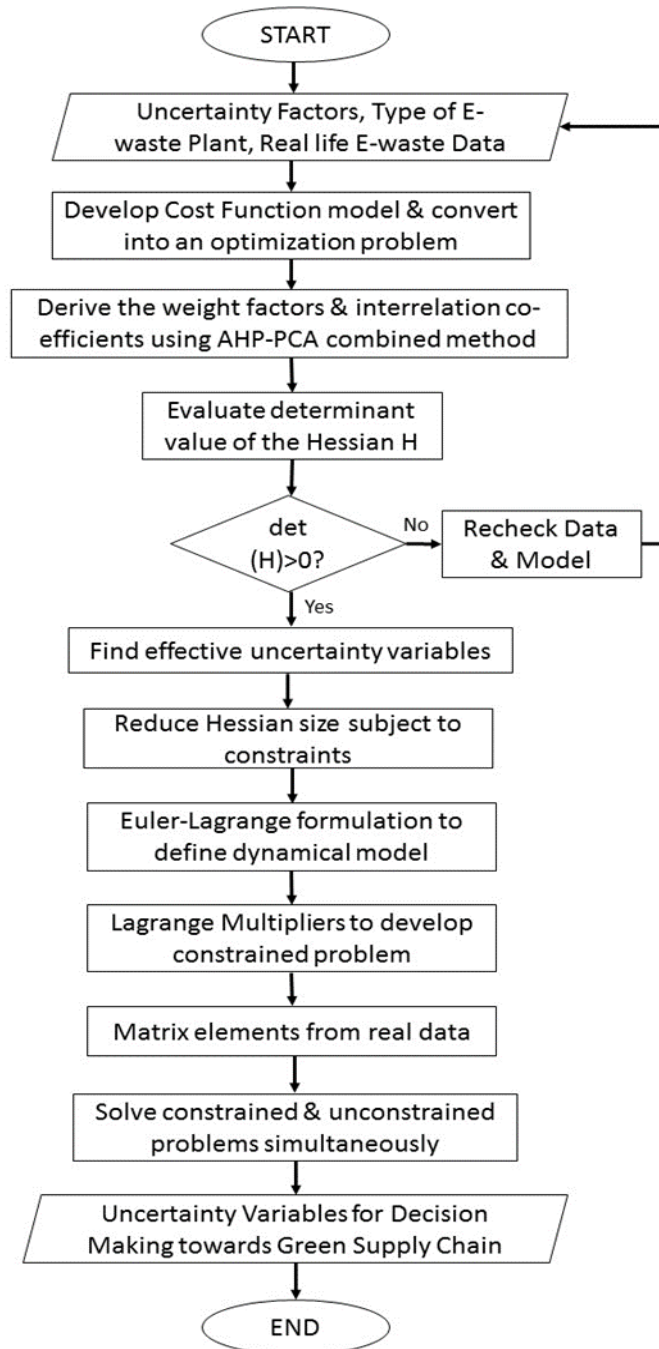


Figure 9.3: Working Flowchart of the problem to solution approach

The hybrid AHP-PCA method uses the best of both the methods. The algorithm is detailed later in section 3.2.3. The developed model is then converted into a dynamic constrained problem with the introduction of a Hamiltonian and Lagrange Multipliers. The set of equations evolved out of this exercise are simultaneously solved for both constrained and unconstrained

cases using MATLAB (bvp4c) with boundary conditions imitating different situations of an e-waste recycling plant. Real life data obtained from an anonymous e-waste recycling plant is used for validation purpose. The overall process is outlined in the form of a flowchart (Figure 9.3).

9.4 Mathematical Modelling

9.4.1 Model Assumptions

The assumptions considered in the model are stated below –

- i) Numbers are recorded on a daily basis, total 300 working days and 10 working hours daily.
- ii) The model is developed considering a Material Recovery from E-waste (MREW) facility.
- iii) Cost of recycled product remains constant over time.
- iv) Unit costs remain constant.
- v) Legislative cost and cost towards disposal of hazardous materials in a TSDF remains constant annually.
- vi) The interdependency of the dependent variables has been assumed to be quadratic order accuracy.

9.4.2. Model Descriptions

The model uses three stochastic ‘forces’ of volatility as inputs, each of which pertain to the MREW SCN derived from the three pillars of sustainability (Chattopadyay et al. 2020). We assume, as suggested by the duality theory of production and cost (McFadden (1978)), a quadratic cost-function based model, where minimization of the cost function kernel defines the time dynamics of the flow (Eq. 1). The structure resembles that of Eulerian mechanics (Goldstein 1964) where the cost function plays the role of a ‘free energy’ potential whose optimized dynamics leads to the paradigmatic Euler-Lagrange model. The quadratic cost function can be decomposed into three components environmental, social, and economic. At each level of decomposition, it could incorporate an uncertain element. The following quadratic cost function can thus be treated as drawn from the duality relations between production and cost underlying the production of the MREW plant we are examining.

$$F = C_{Environmental} + C_{Social} + C_{Economic}, \text{ where} \quad (9.1)$$

F = Cost Function; $C_{Environment}$ = Cost function component for Environmental Uncertainty; C_{Social} = Cost function component for Social Uncertainty; $C_{Economic}$ = Cost function component for Economic Uncertainty.

Now,

$$C_{Environment} = \sum V_{CO_2} f_1 + \sum E_c f_2 + \zeta(\sum W_p f_3 + \sum W_w f_4) \quad (9.2)$$

Where, V_{CO_2} = Volume of CO_2 generated; E_c = Energy Consumption in the processes involved; W_p = Water used due to the processes involved; W_w = Wastewater generated in the process; f_1 = Unit cost for CO_2 recovery; f_2 = Unit cost of energy used; f_3 = Unit cost for water used; f_4 = Unit cost of wastewater treatment

$$C_{Social} = \sum N_1 f_5 + \sum N_3 f_6 \quad (9.3)$$

Where, N_1 = No. of labors; N_3 = No. of awareness activities; f_5 = Salary of one labour; f_6 = Average cost of awareness activity.

$$C_{Economic} = \sum N_4 f_7 - \sum N_5 f_8 - \sum N_7 f_{10} - \sum N_8 f_{11} - \sum N_9 f_{12} \quad (9.4)$$

Where, N_4 = No. of recycled products sold; N_5 = No. of operations involved; N_7 = No. of Logistics involved; N_8 = No. of waste materials being send to Treatment, Storage and Disposal Facility (TSDf); N_9 = No. of Taxes to be paid; f_7 = Revenue earned from product sold; f_8 = Cost of each operation; f_{10} = Cost of logistics; f_{11} = Cost for disposal in TSDf; f_{12} = Cost of Taxes.

The three function modules outlined in Equations (9.2 – 9.4) are derived from the three pillars of sustainability, namely environmental uncertainty (Eq. 9.2); social uncertainty (Eq. 9.3) and economic uncertainty (Eq. 9.4). Each uncertainty function module consists of a linear combination of two or more variables affecting the MREW plant performance, categorized as environmental, social or economic uncertainty respectively. These variables cover a wide range of aspects as they unify the e-waste plant performance as a single component module in the utility-function. Also, socio-economic factors are addressed within the same framework.

Combined with the weight factors (represented by the ϵ_i 's & A_i 's) derived from AHP and combined AHP-PCA method (as detailed later), the cost function takes the form below –

$$F = \epsilon_1(\sum A_1 V_{CO_2} f_1 + \sum A_2 E_c f_2 + \sum \zeta A_3 W_p f_3 + \sum \zeta A_4 W_w f_4) + \epsilon_2(\sum A_5 N_1 f_5 + \sum A_6 N_3 f_6) + \epsilon_3(\sum A_7 N_4 f_7 - \sum A_8 N_5 f_8 - \sum A_9 N_7 f_{10} - \sum A_{10} N_8 f_{11} - \sum A_{11} N_9 f_{12}) \quad (9.5)$$

The interdependencies of the variables are expressed as linear combination of the dependent variables with quadratic accuracy (Nelder 1977). Equations 9.6a – 9.6g represent the mathematical expressions for the interdependency of the variables.

$$V_{CO_2} = V_{CO_2}(N_5, N_7) = a_1 N_5 + a_2 N_7 + a_{12} N_5 N_7 + a'_1 N_5^2 + a'_2 N_7^2 \quad (9.6a)$$

$$E_C = E_C(N_4, N_5) = b_1N_4 + b_2N_5 + b_{12}N_4N_5 + b'_1N_4^2 + b'_2N_5^2 \quad (9.6b)$$

$$W_P = W_P(N_5) = W_P^0 + c_1N_5 + c_2N_5^2 \quad (9.6c)$$

$$W_W = W_W(N_5, W_P) = d_1N_5 + d_2W_P + d_{12}N_5W_P + d'_1N_5^2 + d'_2W_P^2 \quad (9.6d)$$

$$N_3 = N_3(N_4, N_9) = \alpha_1N_4 + \alpha_2N_9 + \alpha_{12}N_4N_9 + \alpha'_1N_4^2 + \alpha'_2N_9^2 \quad (9.6e)$$

$$N_4 = N_4(E_C, N_5) = \beta_1E_C + \beta_2N_5 + \beta_{12}E_CN_5 + \beta'_1E_C^2 + \beta'_2N_5^2 \quad (9.6f)$$

$$N_7 = N_7(V_{CO_2}) = \gamma V_{CO_2} \quad (9.6g)$$

Where, ϵ_i 's = Weigh factor for the three cost functions; A_i 's = Weigh factor for the main parameters ; a_i 's, a_{ij} 's & a'_i 's = Interdependency values for V_{CO_2} ; b_i 's, b_{ij} 's & b'_i 's = Interdependency values for E_C ; c_i 's = Interdependency values for W_P ; d_i 's, d_{ij} 's & d'_i 's = Interdependency values for W_w ; α_i 's, α_{ij} 's & α'_i 's = Interdependency values for N_3 ; β_i 's, β_{ij} 's & β'_i 's = Interdependency values for N_4 ; γ = Interdependency value for N_7 .

9.4.3 Determination of weight factors and Interaction Terms

9.4.3.1 Analytical Hierarchical Process (AHP)

In this study, two exclusive AHP analyses have been carried out similar to Chattopadhyay et al. (2020). However, the structural specifications differ as the present focus is on e-waste SCN. The first AHP (Figure 9.4) model addresses three criteria enumerating the three uncertainties occurring from the three pillars of sustainability; the key (three) variables are linked through eleven criteria nodes.

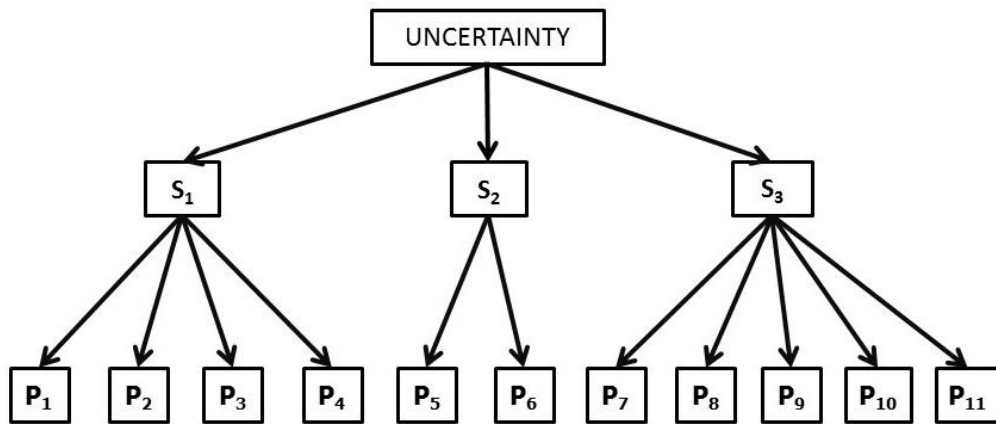


Figure 9.4: AHP model 1 to determine the general alternative rankings. Environmental uncertainty (S₁), Social uncertainty (S₂), Economic uncertainty (S₃) are in the criteria layer. Volume of CO₂ generated (P₁), Energy Consumption in the processes involved (P₂), Water used due to the processes involved (P₃), Wastewater generated in the whole process (P₄) are the alternatives connected to S₁; No. of laborers (P₅), No. of awareness activities (P₆) are the alternatives connected to S₂; No. of recycled products sold (P₇), No. of

operations involved (P_8), No. of logistics involved (P_9), No. of waste materials being send to Treatment, Storage and Disposal Facility (TSDF) (P_{10}), No. of taxes (P_{11}) are the alternatives connected to S_3 .

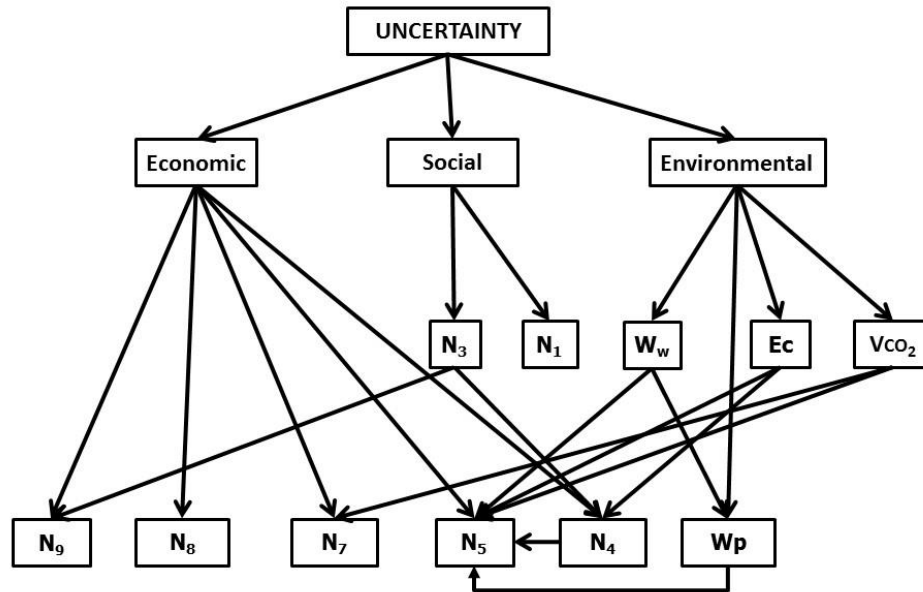


Figure 9.5: Layered AHP model for determination of interrelationship values

The second is a layered AHP (Figure 9.5) that utilizes the same criteria as the first but has two layers of alternatives. The layers are created in such a way that the structure not only connect the alternatives with the criteria but also the individual interdependencies of the alternatives. The first layer of alternatives consists of those variables that have dependencies on the variables in the second layer (function of a function, i.e., a functional). The second AHP is executed to find the interdependencies whereas the first AHP is designed to rank the variables. A registered student version of the commercial software package “Super Decision” is used for the AHP calculations (<http://www.superdecisions.com/>). The determination of compound and square interdependencies follows the methodology of our previous work. The detailed AHP flowchart is outlined below:

9.4.3.2 Multivariate Study - Principal Component Analysis (PCA)

Principal component analysis (PCA) is perhaps the primogenital and one of the well-known multivariate analysis techniques. PCA was first introduced by Pearson (1901) and later developed by Hotelling (1933) independently (Jolliffe 2002). The fundamental idea of PCA is to reduce the dimensionality of a huge data set with interrelated variables, increasing interpretability while retaining maximum information (Jolliffe and Cadima 2016). The

methodology involves transformation of the original dataset to a new set of variables aka the principal components (PCs), which are uncorrelated, and ranked where the top few PCs captures maximum variation present in all the original variables (Jolliffe 2002).

In the context of supply chains, the PCA has been used for a wide range of multivariate analyzes, e.g., damage and fault detection (Pozo and Vidal 2018), hypothesis testing (Pozo and Vidal 2018), constrained PCA- based method development (Takane 2013), Chemometrics (Kundu et al. 2017); radiative transfer computational advancement (Gray 2017), rankings and preferences (da Costa 2015) etc. PCA is also a popular method among supply chain managers for its versatility (Agrawal and Saxena 2018). In this study, PCA has been used as a hybrid method, combined with the AHP analysis in step 1, for further refining the values obtained from the generic AHP, specifically to quantify the interdependencies of the dependent variables as well as to measure their relative positions in the co-efficient matrix. The method is detailed in the following subsection.

9.4.3.3. Hybrid AHP-PCA method

Under the current investigation, a hybrid AHP-PCA method is developed for ranking and finding the interdependencies of the variables of the utility function, the first such approach known. The uniqueness of this method is that it utilizes the best of both, generic ranking (PCA) and interdependency calibration (AHP). The super weighted matrix has been used as input for the PCA. By doing this, the results obtained using AHP are being cross-checked and verified. This method thus unifies Multi Criteria Decision Making (MCDM) with statistical approaches. The working algorithm of this method is given below –

Step 1: Develop the AHP models with ‘m’(here m=3) criteria and ‘n’ alternatives (here n=11) – the linear one for alternative rankings and the layered structure for interdependencies.

Step 2: Input ratings for the pairwise comparison matrix for both regular and layered AHP models to derive the ranking of the alternatives.

Step 3: Record the AHP outputs and the super weighted matrices.

Step 4: Reduce the super weighted matrix obtained from the crown structure AHP into ‘p x p’ matrix (here p=7).

Step 5: Use the ‘p x p’ matrix obtained in step 4 as input and run PCA.

Step 6: Use the principal components as alternative rankings for the variables.

Step 7: Replace infinitesimally small values with zero in the correlation matrix obtained from PCA. In this case, we reduce 25 entries to zero while the matrix dimension changes to 7x6.

Step 8: Find norm of the newly developed correlation matrix.

Step 9: Divide each element of the new correlation matrix by the norm values.

Step 10: Map the matrix developed in step 9 with the matrix in step 4 and derive the interdependency factors by matching the positions.

Step 11: IF, any required values obtained from PCA is zero then use equivalent AHP value. Further normalize it and use the resultant values as weight factors.

For zero entries from the benchmarking table, AHP values are given preference over PCA as with AHP, the rankings are already given using the eigenvalues. We recall F is the cost function. The lambda values are chosen here through the AHP and AHP-PCA analysis. As it was shown in the previous paper (Chattopadhyay (2020)), these are proportional to the epsilon values. The final values of lambda and other weight factors are provided in the supplementary material to this paper. When PCA is reapplied, the less important alternatives i.e., the options with the smallest eigenvalues, were simply converted to zeroes (given no weight) to emphasize the prioritized (data or logic driven) options. In a realistic scenario involving an e-waste supply chain, we may not be allowed to resort to such oversimplification though. This double screening through AHP→PCA filters and ensures that the finally obtained values offer reliable estimates for relative weight and interdependency factors. The compound and square interdependencies are derived using the methodology of Chattopadhyay et al. (2020). The compound interdependencies have been taken as product of concerned co-efficient, e.g., value of a_{23} = value of a_2 x value of a_3 . The squared co-efficient has been taken as square root of the concerned co-efficient. For example, the value of a'_3 = square root of a_3 .

9.4.4 Optimization Algorithm

In order to arrive at an optimal strategy for the SCN, the model cost function (Eq. 5) is optimized (minimized). The resultant Hessian matrix, like an information matrix in statistics, characterizes the general uncertainty scenario of a supply chain network. The optimization mechanism runs through two gateways – (a) Unconstrained Optimization, dealing largely with a hypothetical scenario in which the SCN has unlimited resources in finances, workforce, machinery and equipment and raw material and (b) Constrained Optimization, which portrays a more realistic scenario of a company with limited resources. To arrive at a dynamical formulation of the SCN, we optimize the cost function with a time independent Lagrangian structure using textbook treatment of classical mechanics as in (Goldstein 1964; Hamill 2013). We assume the Lagrangian to be time independent as it is our assumption that we are dealing

with a SCN associated with a SME that is in a stabilized working condition, after going through its teething problems, and not yet ready to grow into a bigger company through a dynamic growth path. Equations (13) and (16) are solved using data obtained from an anonymous Indian Small and Medium Enterprise (SME) company. The following algorithmic flowchart outlines the problem to solution path.

STEP 1: Identify factors imposing uncertainty along the supply chain network & Real-life information.

STEP 2: Develop the Cost Function Model and convert into an optimization problem (Eq. 9.5).

STEP 3: Derive the weight factors & interrelation coefficients using AHP followed by PCA.

STEP 4: Evaluate the first and second derivatives and build the hessian matrix.

STEP 5: Evaluate the determinant value of the Hessian H.

STEP 6: Check for $\det(H) > 0$ (for a cost minimization problem). If yes, then go to step 7, else recheck data and model, go to step 1.

STEP 7: Identify the effective uncertainty variables.

STEP 8: Reduce the uncertainty variables subjected to constraints (Eq. 9.7).

STEP 9: Use the Euler-Lagrange formulation to define dynamical model (Eq. 9.8).

STEP 10: Introduce the Lagrange Multipliers to analyze the constrained problem (Eq. 9.9).

STEP 11: Derive the elements of the matrix using real data.

STEP 12: Identify the boundary conditions.

STEP 13: Solve constrained & unconstrained problems simultaneously.

Independent verification is attained using MATLAB R2021a (bvp4c) to solve the corresponding boundary value problems.

9.5 Unconstrained Problem

We follow the standard method to generate the dynamic path from the steady state equilibrium. We use the free energy F (The total cost of uncertainty) and employ Lagrangian mechanics. The time dependent movements of the cost function modules are expected to satisfy optimum cost function formulation to generate a steady state solution. A perturbation of the SCN will 'kick' the system out of its steady state equilibrium. Then the system will either follow a conservative trajectory towards that steady state (a stable fixed point) or follow a non-conserved dynamics towards an unstable fixed point. To mathematically encapsulate this, we prescribe the multivariate Euler-Lagrange structure (Step 9) (Goldstein 1964; Risken 1996)

$\delta \left(\frac{\partial F}{\partial N_i} \right) = \delta \left(\frac{d}{dt} \frac{\partial F}{\partial \dot{N}_i} \right)$, where F is the Free Energy or cost in our example. The central mathematical outline depicts the optimized (from the cost function) time evolution of the interacting variables defining the income-outcome cost matrix. The perturbed dynamics close to the linearly stable fixed points can then be represented by the following dynamical system:

$$\delta \left(\frac{d}{dt} \begin{bmatrix} \frac{\partial F}{\partial V_{CO_2}} \\ \frac{\partial F}{\partial E_C} \\ \frac{\partial F}{\partial W_P} \\ \frac{\partial F}{\partial W_W} \\ \frac{\partial F}{\partial N_1} \\ \frac{\partial F}{\partial N_3} \\ \frac{\partial F}{\partial N_4} \\ \frac{\partial F}{\partial N_5} \\ \frac{\partial F}{\partial N_7} \\ \frac{\partial F}{\partial N_8} \\ \frac{\partial F}{\partial N_9} \end{bmatrix} \right) = \begin{bmatrix} m_{11} & m_{12} & 0 & m_{14} & 0 & m_{16} & 0 & 0 & 0 & 0 & 0 \\ m_{21} & m_{22} & 0 & m_{24} & 0 & m_{26} & 0 & 0 & 0 & 0 & 0 \\ 0 & 0 & 0 & 0 & 0 & 0 & 0 & 0 & 0 & 0 & 0 \\ m_{41} & m_{42} & 0 & m_{44} & 0 & m_{46} & 0 & 0 & 0 & 0 & 0 \\ 0 & 0 & 0 & 0 & 0 & 0 & 0 & 0 & 0 & 0 & 0 \\ m_{61} & m_{62} & 0 & m_{64} & 0 & m_{66} & 0 & 0 & 0 & 0 & 0 \\ 0 & 0 & 0 & 0 & 0 & 0 & 0 & 0 & 0 & 0 & 0 \\ 0 & 0 & 0 & 0 & 0 & 0 & 0 & 0 & 0 & 0 & 0 \\ 0 & 0 & 0 & 0 & 0 & 0 & 0 & 0 & 0 & 0 & 0 \\ 0 & 0 & 0 & 0 & 0 & 0 & 0 & 0 & 0 & 0 & 0 \\ 0 & 0 & 0 & 0 & 0 & 0 & 0 & 0 & 0 & 0 & 0 \end{bmatrix} \begin{bmatrix} \delta V_{CO_2} \\ \delta E_C \\ \delta W_P \\ \delta W_W \\ \delta N_1 \\ \delta N_3 \\ \delta N_4 \\ \delta N_5 \\ \delta N_7 \\ \delta N_8 \\ \delta N_9 \end{bmatrix} \quad (9.7)$$

Focusing only on the leading dynamic variables of MREW plant performance (V_{CO_2} , E_C , N_3 , N_4), Eq. (9.7) can be easily simplified to

$$\delta \left(\frac{d}{dt} \begin{bmatrix} \frac{\partial F}{\partial V_{CO_2}} \\ \frac{\partial F}{\partial E_C} \\ \frac{\partial F}{\partial N_3} \\ \frac{\partial F}{\partial N_4} \end{bmatrix} \right) = \begin{bmatrix} a_{11} & a_{12} & a_{13} & a_{14} \\ a_{21} & a_{22} & a_{23} & a_{24} \\ a_{31} & a_{32} & a_{33} & a_{34} \\ a_{41} & a_{42} & a_{43} & a_{44} \end{bmatrix} \begin{bmatrix} \delta V_{CO_2} \\ \delta E_C \\ \delta N_3 \\ \delta N_4 \end{bmatrix} \quad (9.8)$$

Rearrangement of equation (9.8) leads to -

$$\frac{d^2}{dt^2} \begin{bmatrix} \rho_1 \delta V_{CO_2} \\ \rho_2 \delta E_C \\ \rho_3 \delta N_3 \\ \rho_4 \delta N_4 \end{bmatrix} = \begin{bmatrix} a_{11} & a_{12} & a_{13} & a_{14} \\ a_{21} & a_{22} & a_{23} & a_{24} \\ a_{31} & a_{32} & a_{33} & a_{34} \\ a_{41} & a_{42} & a_{43} & a_{44} \end{bmatrix} \begin{bmatrix} \delta V_{CO_2} \\ \delta E_C \\ \delta N_3 \\ \delta N_4 \end{bmatrix} \quad (9.9)$$

Here δN_3 , δN_4 , *etc.* represent perturbations of variables N_3 , N_5 , etc. around their equilibrium points, where ‘equilibrium points’ refer to the ‘break even trade situation’. Eq. (9.9) is reminiscent of Newton’s law of motion that describe how fast a system can accelerate or decelerate away from its equilibrium, that ‘break even’ point. In other words, a trajectory away from the equilibrium manifold is indicative of possible bankruptcy and vice versa.

9.6 Constrained Problem

The constrained version of the problem is formulated by introducing Lagrange multipliers (Goldstein 1964; Elton et al. 2009). This helps in solving the optimization problem without explicit parameterization in terms of the constraint (Tur et al. 2009). The values of the individual Lagrange multipliers are considered to be proportional to the epsilon values that replicate the corresponding weightage of the individual uncertainties in the cost function. The Lagrangian ‘ \mathcal{L} ’ is defined as –

$$\mathcal{L} = F - \lambda_1(V_{CO_2}f_1 - V) - \lambda_2(N_1f_5 + N_3f_6 - E) - \lambda_3(N_4f_7 - R) \quad (9.10)$$

where λ_i ’s are the Lagrange multipliers. The realistic system restrictions (constraints) are expressed through the quantities joined with the Lagrange multipliers which we enforce on the system. We impose three constraints on V, E, and R, which we have chosen in consultation with the e-waste recycler, on Eq. (9.10): 1) V, the cost associated with CO₂ emission control; 2) E, the maximum expenditure budget accorded for wages of the labors and employees, and 3) R, the maximum revenue target. Overall, this amounts to suitably recalibrated greener supply chain within viable operation lines.

The constrained version of the problem takes the following form –

$$\delta \left(\frac{d}{dt} \begin{bmatrix} \frac{\partial \mathcal{L}}{\partial V_{CO_2}} \\ \frac{\partial \mathcal{L}}{\partial E_C} \\ \frac{\partial \mathcal{L}}{\partial N_3} \\ \frac{\partial \mathcal{L}}{\partial N_4} \end{bmatrix} \right) = \begin{bmatrix} c_{11} & c_{12} & c_{13} & c_{14} \\ c_{21} & c_{22} & c_{23} & c_{24} \\ c_{31} & c_{32} & c_{33} & c_{34} \\ c_{41} & c_{42} & c_{43} & c_{44} \end{bmatrix} \begin{bmatrix} \delta V_{CO_2} \\ \delta E_C \\ \delta N_3 \\ \delta N_4 \end{bmatrix} \quad (9.11)$$

Rearrangement of Eq. (11) leads to -

$$\frac{d^2}{dt^2} \begin{bmatrix} \omega_1 \delta V_{CO_2} \\ \omega_2 \delta E_C \\ \omega_3 \delta N_3 \\ \omega_4 \delta N_4 \end{bmatrix} = \begin{bmatrix} c_{11} & c_{12} & c_{13} & c_{14} \\ c_{21} & c_{22} & c_{23} & c_{24} \\ c_{31} & c_{32} & c_{33} & c_{34} \\ c_{41} & c_{42} & c_{43} & c_{44} \end{bmatrix} \begin{bmatrix} \delta V_{CO_2} \\ \delta E_C \\ \delta N_3 \\ \delta N_4 \end{bmatrix} \quad (9.12)$$

Equations (9.9) and (9.12) are solved using data obtained from an anonymous multi award winner Indian E-waste recycler company. MATLAB R2019 was used to solve the system of equations concerning the solutions of the corresponding boundary value problems.

9.7 Results & Discussion

Time dynamic behavior of the leading dynamic variables, both for constrained and unconstrained environments, are discussed below. First, we need to have an essence of what the standalone constrained and unconstrained systems represent. In simple parlance, they jointly characterize the dystopian and utopian case scenarios respectively. Both cases are ranked using AHP and hybrid AHP-PCA method and compared. For a real e-waste recycler, the SCN is stochastic and highly sensitive to minor logistic perturbations, technically represented as SCN strategies. Appropriate Initial and Boundary Conditions represent such strategies mathematically in the time varying model that we have here. The initial conditions represent the present scenario and the boundary value or the fixed end point represent a future scenario. This study considers the strategy of decreasing environmental load while increasing the social accountability together with economic profitability. The effect of different ranking methods is explored in the chosen variables both in constrained and unconstrained conditions, separately at intervals of one year, three-year and five-year timelines. The 1-year results replicate immediate effect; whereas the 5-year timer represents long time effect. Thee 3-year results provides an understanding of events at intermediate time scales. This intermediate time scale is strategically important because this provides a clear numerical grasp of the state the company is in at that point and offers scopes of strategizing for the future. The time dynamic behavior of the 4 key variables e.g. carbon dioxide emission volume (V_{CO_2}), energy

consumption (E_C), number of awareness activities (N_3) and product sales (N_4) all rely on the hybrid AHP→PCA ranking method outlined in the preceding sections to identify best performance strategies.

9.7.1 Volume of Carbon Dioxide Emission

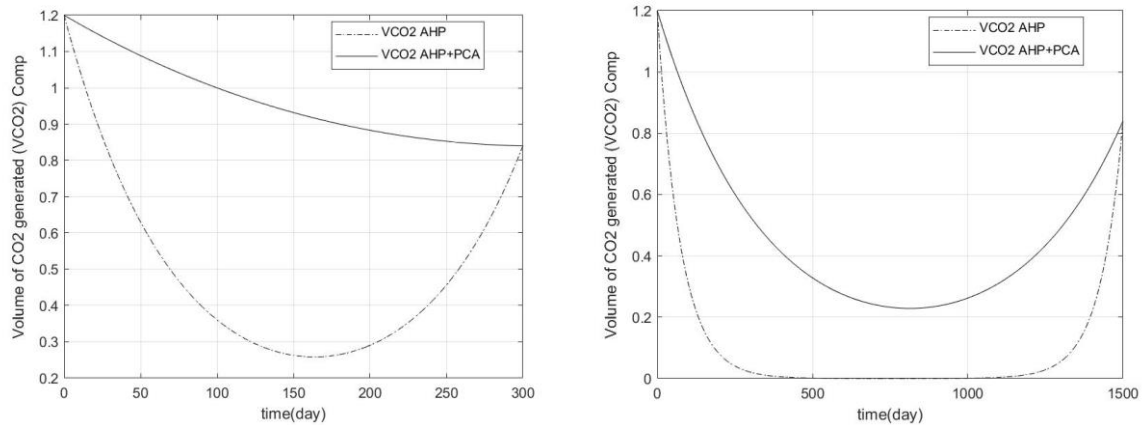


Figure 9.65: Time dependency of V_{CO_2} in constrained environment, using AHP for ranking (dash-dotted line) and hybrid AHP-PCA for ranking (solid line) obtained from simultaneous solution of Eqs. (9.9) and (9.12): (a) 1-year time span; (b) 5-year time span.

Figures 9.6 (a) & (b) compare the time dependence of the volume of CO_2 generated (V_{CO_2}) in a constrained environment respectively for 1 and 5 years. In both cases, two ranking methods are used for comparison – AHP (dash-dotted line) and hybrid AHP-PCA method (solid line). It is clear from the figures that the hybrid AHP-PCA method provides a better ranking than any individual scoring methods (AHP or PCA for us) as the solid-line curves capture the immediate effects much better than the dash-dotted lines. For a 1-year timeline, the AHP results suggest that the carbon dioxide emission will reach minimum within the fifth and the sixth month and rises again before reaching the boundary value whereas the hybrid AHP-PCA results suggest that carbon dioxide emission will smoothly decrease to the targeted value. The AHP curve clearly suggest when to resurrect the strategy change, represented by the point of inflection. Whereas, the AHP-PCA curve suggest that within a year it is quite not possible resurrect a strategy change, rather it is a time period of observation. We find that the hybrid AHP-PCA results are more realistic, as it is practically impossible to run into a record low-emission figure (~79% of the starting value) within 4 months.

In the 5-year timelines, the hybrid AHP-PCA curve identifies the inflection point (the minima) after 2 years and then converges again to its target value. This suggests that in the long term, it

is important to devise a policy change to lower down the emissions, i.e., savings in environmental efforts, combining technological efforts in emission reduction, carbon credits, positive environmental impacts through Corporate Social Responsibility (CSR) and other green activities like greening the supply chain, cleaner production lines and zero waste efforts. Compared to the hybrid AHP-PCA ranked results, the standalone AHP ranked results fail to capture the ‘negative-emission’ characteristic of the curve as the curve flattens to zero after 1st year till towards the end of the fourth year. Unless, there is a very enthusiastic supply chain manager, the AHP results will lead to a happy-face decision of offsetting the carbon footprint in the long run. Hence there may not be a continual improvement, unless it is mentioned in the quality (ISO 9000) and environmental (ISO 14000) policy of the recycling company concerned.

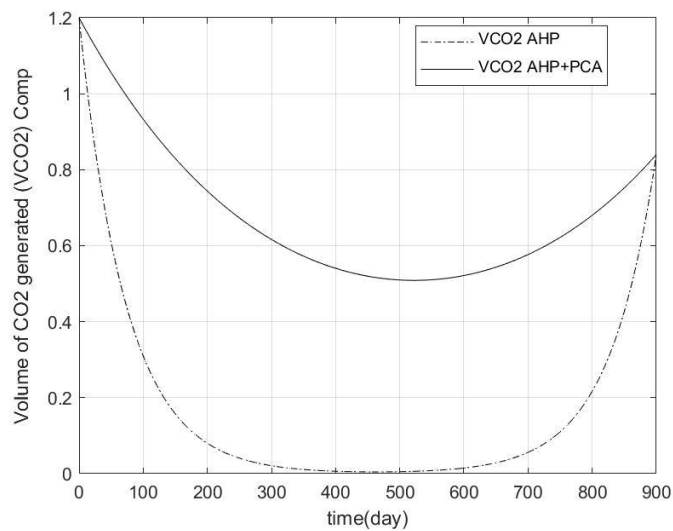


Figure 9.7: Time dependency of V_{CO_2} in constrained environment, using AHP for ranking (dash-dotted line) and hybrid AHP-PCA for ranking (solid line) obtained from simultaneous solution of Eqs. (9.9) and (9.12) in 3-year time span

Figure 9.7 depicts the time dependence of volume of CO₂ generated (V_{CO_2}) in a constrained environment, starting the end of the 3-year year timespan with AHP (dash-dotted line) and hybrid AHP-PCA method (solid line) as the ranking methods. This is an example of hierarchical module training, based on Machine Learning inputs from the hybrid AHP→PCA model. In the unconstrained environment, the solutions are non-convergent indicating an unstable system. The curves resemble the ones with 5-year timelines. However, in this case, the hybrid AHP-PCA curve ensures an “operation-window” within the 400 – 600 days. This indicates that it is possible to achieve further reduction in emission driven by a policy change. Hence, it is quite an intelligent approach to set targets by the 3-year timeline for carbon dioxide

emission, and revise/ tailor as required within the next 2 years' timeline. This will allow the supply chain manager to locate operation windows in a less risk-prone time period enabling short-term strategy enforcement towards better fitted solutions. This also opens up opportunities to explore unconventional and newly developed approaches for pilot studies which is a good way to strengthen the much-required industry-academia bond.

9.7.2 Energy Consumption

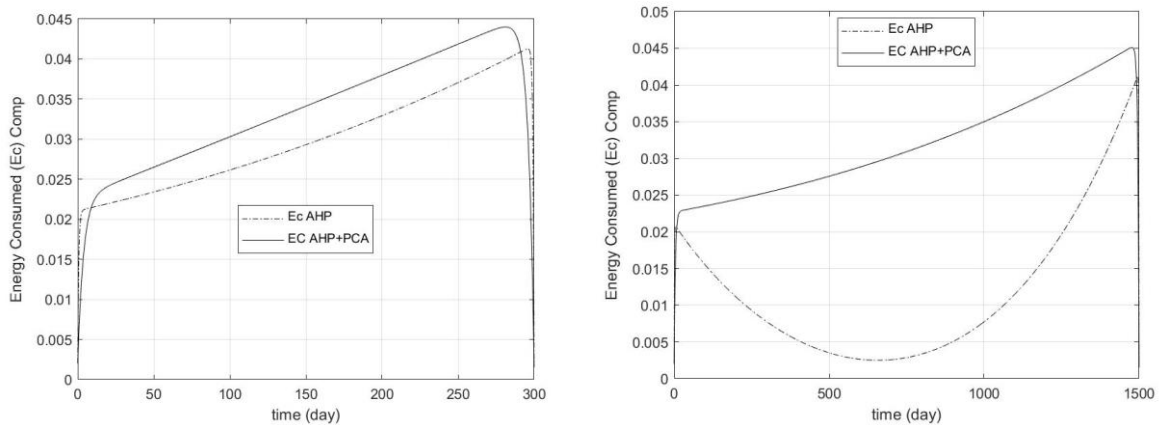


Figure 9.8: Time dependency of E_c in a constrained environment, using AHP for ranking (dash-dotted line) and hybrid AHP-PCA for ranking (solid line) obtained from simultaneous solution of Eqs. (9.9) and (9.12): (a) 1-year time span; (b) 5-year time span.

In the 1-year timeline, the results from both AHP and hybrid AHP-PCA ranking method shows a similar trend. Both the curves increase smoothly only to reach the target value. Figure 9.8(a) suggests increasing energy consumption as we interpret that the mechanical recycling of e-waste is highly energy intensive. In the 5-year timeline (Figure 9.8(b)), the AHP curve has a hyperbola shape. The curve shows a steep fall in the beginning reaching a minimum by the end of the second year, then rising to a higher value (nearly double) by the end of the fifth year. Alternatively, the hybrid AHP-PCA curve shows a similar trend to its 1-year scenario, which is an increasing profile. We interpret that, the system is inherently stochastic and energy consumption is a very critical and sensitive parameter which needs attention. In the long run, the AHP-curve is able to identify an “operation-window” for devising policy changes. In reality, decrease in energy consumption implies an organization heading towards bankruptcy. However, the variations may be attributed to the supply of e-waste or demand uncertainty or even an economically damaging pandemic that shuts off the entire work cycle. As the AHP-PCA curve fails to provide any inflection point, we interpret that the current energy policy in

the e-waste organization needs immediate attention. Again, this behavior could be attributed to the over-estimation of the AHP-PCA method or the under-estimation of AHP.

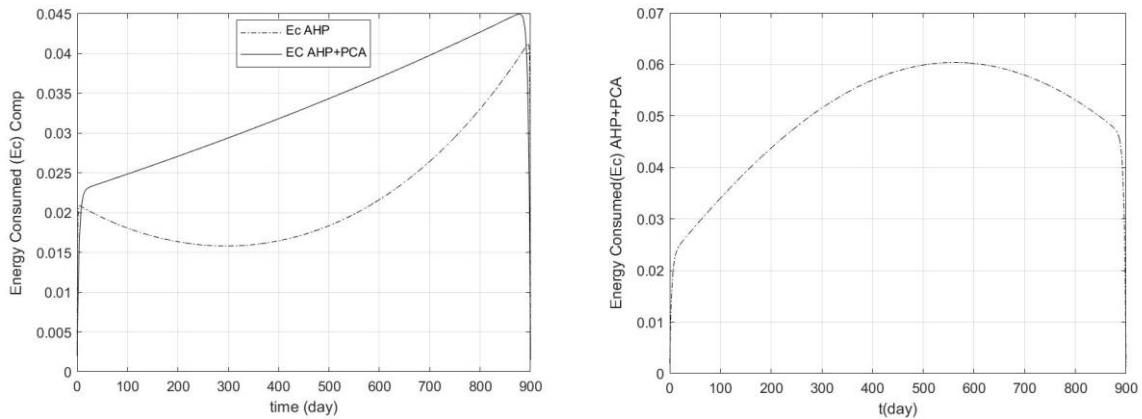


Figure 9.9: Time dependency of E_c : (a) in constrained environment, using AHP for ranking (dash-dotted line) and hybrid AHP-PCA for ranking (solid line) and (b) in unconstrained environment using hybrid AHP-PCA for ranking obtained from simultaneous solution of Eqs. (9.9) and (9.12) in a 3-year timespan

In the constrained environment, the hybrid AHP-PCA ranked curve imitates the 1-year & 5-year AHP ranked curve. This is quite realistic as in reality, the energy consumption of an e-waste recycling plant will increase over time as supply increases, which is an indicator for sustainable business. Alternatively, from mathematical point of view perhaps AHP-PCA method is overestimating the dynamics of the system. On the other hand, the AHP ranked curve (constrained) carries a similar profile to its 5-year appearance. In this case, an operation window within the 200 – 400 days is obtained. Whereas the hybrid AHP-PCA ranked curve in the unconstrained environment exhibits an increasing parabolic profile, which reaches a maximum within 500 – 600 days and then reduces. The sensitivity of this parameter is quite high compared to the other cases; hence such behavior of curves has appeared. However, comparing the results of constrained and unconstrained cases of the hybrid AHP-PCA method, we interpret that there might be a case of over-prediction in the constrained case.

We should also be cautious about the possibility of recurrent over-estimation accruing from our hybrid AHP-PCA ranking method, as have been discussed above. Additionally, both methods are seen to contribute towards parameter sensitivity and are differentially adaptive of the ambient response (AHP is more stable than PCA on this). E-waste recycling facilities performing mechanical recycling operations are highly energy intensive and hence energy consumption is ought to be a critical factor for business sustainability.

9.7.3 Number of Awareness Activities

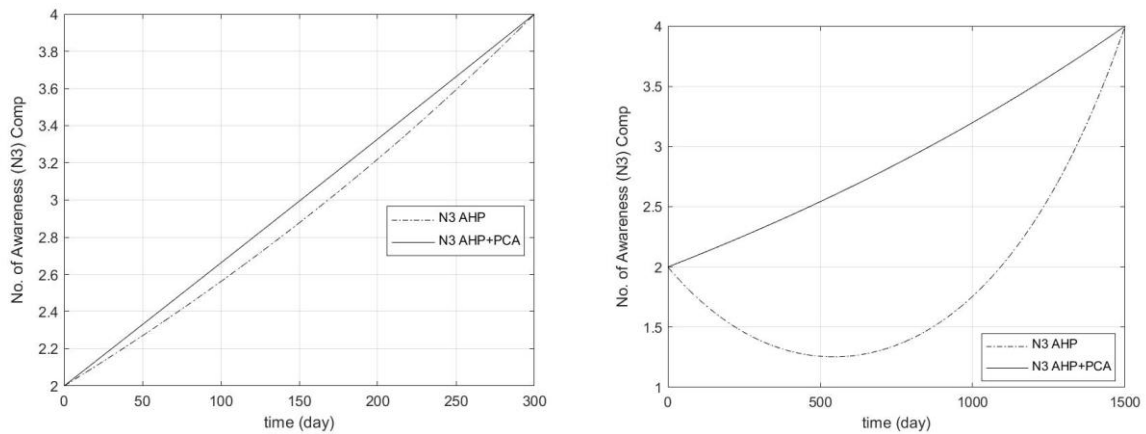


Figure 9.10: Time dependency of N_3 in constrained environment, using AHP for ranking (dash-dotted line) and hybrid AHP-PCA for ranking (solid line) obtained from simultaneous solution of Eqs. (9.9) and (9.12): (a) 1-year time span; (b) 5-year time span

In the developing countries, awareness level of e-waste disposal is a big issue and needs proper attention (Debnath et al. 2015). The level of awareness is proportional to the business of an e-waste recycler. Hence, it is for the best of the recyclers interest, awareness activities need to be taken seriously and as a CSR activity as well. Such practice is also visible among the e-waste recyclers around the globe. Time dependency of number of awareness activities (N_3) in a constrained environment is presented in figures 9.10 (a) & (b), for 1-year and 5-year timespan respectively. The results obtained using standalone AHP as ranking method is in dash-dot lines whereas the results obtained using the hybrid AHP-PCA method is in solid lines.

As shown in the 1-year scenario, both curves depict a smooth increasing profile. While the solid line is almost a straight line, the dash-dotted one is slightly bent in between. Certainly, both curves give an outlook that over time, increase in awareness activities will be helpful. In the long-term scenario (5-year), the dash-dotted curve depicts a minimum around the 500th day and sharply increases to reach the target value. In contrast, the solid line depicts the social responsibility of the recycler with a smoothly increasing curve which helps the social image and eventually increasing the business potential of the recycler. The dash-dot curve implies that the e-waste recycler might struggle to sufficiently increase the number of awareness activities in the initial years but after some time they will eventually gear up to increase the number of awareness activities. The minimum is obtained in the second quarter of the second year which means that is the point, when further decision needs to be taken for higher social

accountability based on company policy and budgets. We interpret that the hybrid AHP-PCA model might be giving the perfect fit as the path shown is more realistic.

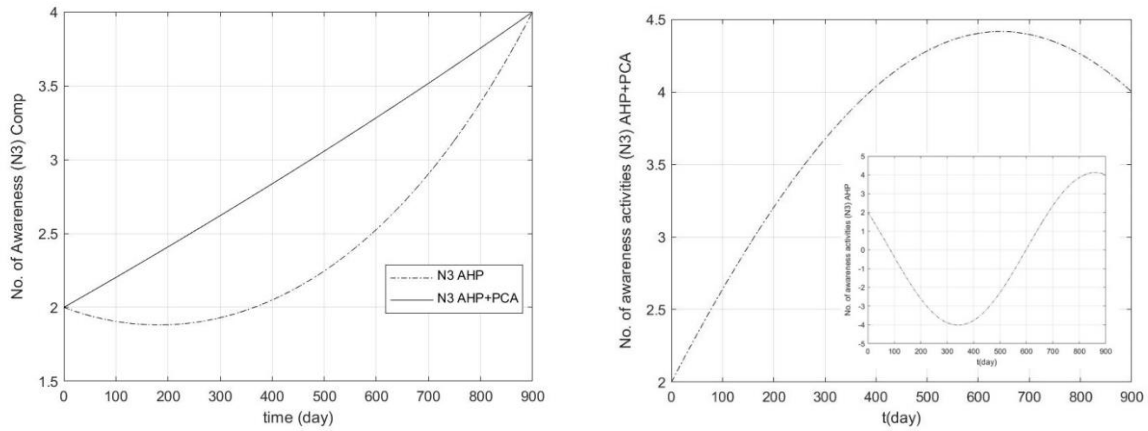


Figure 9.11: Time dependency of N_3 : (a) in constrained environment, using AHP for ranking (dash-dotted line) and hybrid AHP-PCA for ranking (solid line) and (b) in unconstrained environment using hybrid AHP-PCA for ranking and AHP for ranking (provided in the insets) obtained from simultaneous solution of Eqs. (9.9) and (9.12)

In the constrained environment, the solid line exhibits a straight line translating to a realistic scenario. Compared to this, the dash-dotted curve is a repetition of the 5-year scenario and hence needs no further discussion. In the unconstrained environment, AHP ranking method provides a wave like profile however the negative minima is unphysical (as shown in the insets of figure 9.11 b). On the other hand, the hybrid AHP-PCA method of ranking creates a semi-parabolic profile that offer a maximum value (~ 4.5) at 600th day timestamp. This means that in an arbitrage condition, the recycler can keep increasing the awareness activities.

Number of awareness activity (N_3) relates to the social uncertainty contributing to the overall cost function. Positive growth in social aspects is always a good deal and the hybrid AHP-PCA ranking method can predict the realistic trends in both constrained and unconstrained scenarios. On the other hand, the standalone AHP method underpredicts and fails to describe the dynamic system both in constrained and unconstrained scenarios. Our model shows that in this case, the decision making on number of awareness activities is guided by the budget constraint. Despite the fact, that an e-waste recycling facility can survive on its own or operate on break-even mode in an arbitrage condition of continuous supply of e-waste, it is suggested that regular monitoring and cross-validation of existing policy should be carried out for business sustainability.

9.7.4 Recycled Product Sales

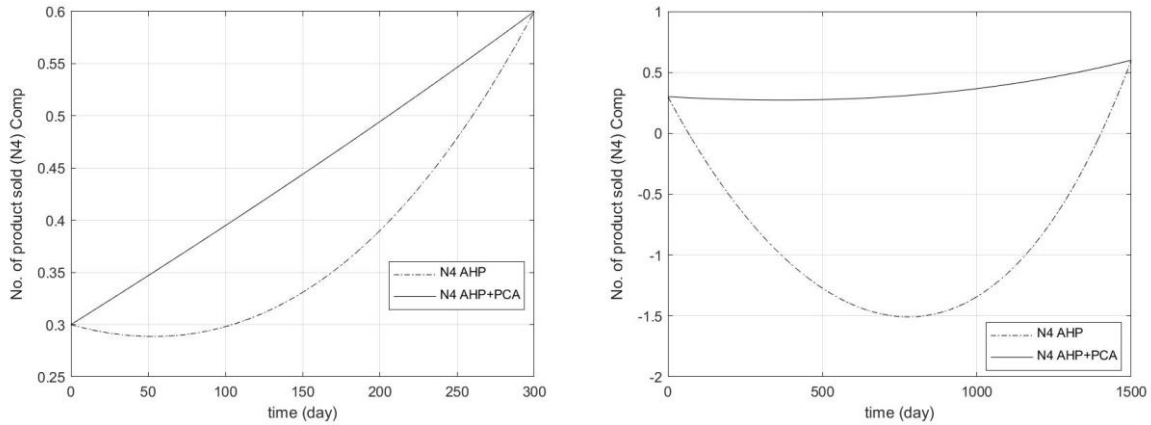


Figure 9.12: Time dependency of N_4 in constrained environment, using AHP for ranking (dash-dotted line) and hybrid AHP-PCA for ranking (solid line) obtained from simultaneous solution of Eqs. (9.9) and (9.12): (a) 1-year time span; (b) 5-year time span

In the 1-year timeline, using AHP (dash-dotted line) as the ranking method predicts that immediately after the beginning, the e-waste plant incurs loss as the curve falls down and starts to peak up after 3 months to reach a target value. This parabolic curve (dash-dotted line) suggests, that in the current scenario the company face some issues in the beginning. On the other hand, using hybrid AHP-PCA ranking method (solid line) dictates a straight line. In the 5-year scenario, the dash-dotted line exhibits a parabolic profile with a minimum at the 750th day timestamp. Clearly, AHP underpredicts the dynamics of the system. In contrast, the solid line demonstrates smooth increasing curve. The market price volatility of recycled products is a major issue; hence it is suggested that both the methods should be tested in the interest of a greener supply chain with a cleaner production line leading to sustainable business.

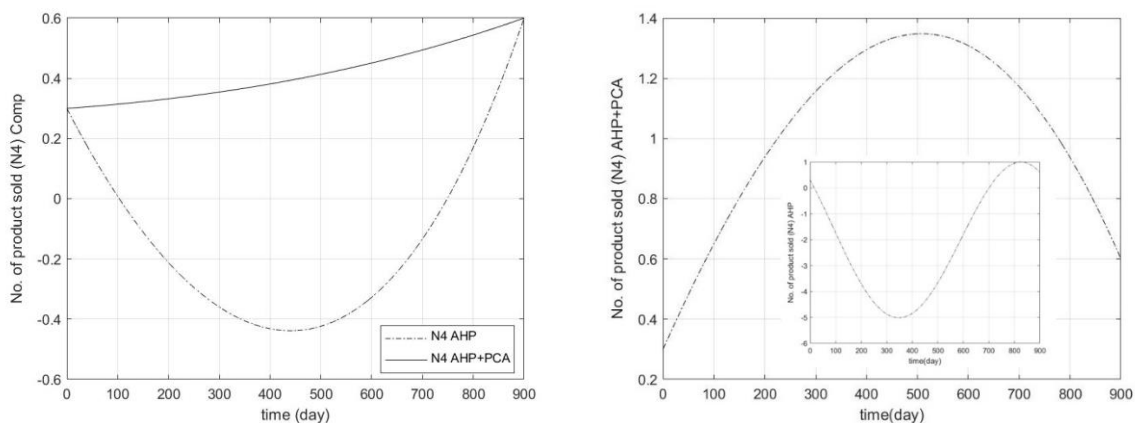


Figure 9.13: Time dependency of N_4 : (a) in constrained environment, using AHP for ranking (dash-dotted line) and hybrid AHP-PCA for ranking (solid line) and (b) in unconstrained environment using hybrid AHP-PCA for ranking and AHP for ranking (provided in the insets) obtained from simultaneous solution of Eqs. (9.9) and (9.12)

The curves in figure 9.13 (a) represents results in the constrained environment using AHP (dash-dotted line) and hybrid AHP-PCA (solid line) for ranking. Both the curves display a similar profile to the 5-yearly results. Hence the interpretation remains unchanged. In the unconstrained scenario, the hybrid AHP-PCA method is able to pull off some interpretable results. The results using AHP ranking method are provided in the insets of figure 9.13 (b). As seen in the previous cases, here also standalone AHP fails to obtain rational results in an unconstrained scenario (figure 9.13b inset). The hybrid AHP-PCA ranked result shows a parabolic curve. This shows the robustness of the hybrid AHP-PCA method as it captures the system dynamics in the unconstrained scenario. The curve profile suggests that even in arbitrage conditions, the company may not have a steady growth profile.

Economic sustainability is the most important of all from the business perspective (Debnath and Ghosh 2019). From that sense, product sold (N_4) is the most important parameter which needs to be nurtured for maximum profit. A greener supply chain network with a sustainable production line is a utopian case but we can always look forward to reach as close as possible to the target values. That is exactly what these boundary conditions have helped us to do. The alluded case gives an outlook of comparison of both the methods, but the choice of boundary conditions lies in the hand of the supply chain manager of the respective plant. For business sustainability, it is suggested that regular monitoring of critical parameters and policy changes at certain intervals (identified through analysis) will help in improving the plant performance and thus greening the supply chain.

References

- Chattopadhyay, A. K., Debnath, B., El-Hassani, R., Ghosh, S. K., & Baidya, R. (2020). Cleaner Production in Optimized Multivariate Networks: Operations Management through a Roll of Dice. *arXiv preprint arXiv:2003.00884*.
- da Costa, J. P. (2015). *Rankings and Preferences: New Results in Weighted Correlation and Weighted Principal Component Analysis with Applications*. Springer.
- Forti V., Baldé C.P., Kuehr R., Bel G. (2020). The Global E-waste Monitor 2020: Quantities, flows and the circular economy potential. United Nations University (UNU)/United Nations Institute for Training and Research (UNITAR) – co-hosted SCYCLE Programme, International Telecommunication Union (ITU) & International Solid Waste Association (ISWA), Bonn/Geneva/Rotterdam.
- Ghosh, S. K., Debnath, B., Baidya, R., De, D., Li, J., Ghosh, S. K., Zheng, L., Awasthi, A.K., Liubarskaia, M.A., Ogola, J.S. and Tavares, A. N. (2016). Waste electrical and electronic equipment management and Basel Convention compliance in Brazil, Russia, India, China and South Africa (BRICS) nations. *Waste Management & Research*, 34(8), 693-707.
- Goldstein, H., 1964. *Classical mechanics*. Reading, Mass.: Addison-Wesley.
- Gray, V. (Ed.). (2017). *Principal Component Analysis: Methods, Applications and Technology*. Nova Science Publishers, Incorporated.
- Khaliq, A., Rhamdhani, M. A., Brooks, G., & Masood, S. (2014). Metal extraction processes for electronic waste and existing industrial routes: a review and Australian perspective. *Resources*, 3(1), 152-179.
- Kundu, M., Kundu, P. K., & Damarla, S. K. (2017). *Chemometric Monitoring: Product Quality Assessment, Process Fault Detection, and Applications*. CRC Press.
- Nelder, J. (1977). A reformulation of linear models. *Journal of the Royal Statistical Society Series A: Statistics in Society*, 140(1), 48-63.
- Polat, L. Ö., Polat, O., & Güngör, A. (2019). Designing Fuzzy Reverse Supply Chain Network For E-Waste. *Economy & Business Journal*, 13(1), 367-375.
- Pozo, F., & Vidal, Y. (2018). Damage and fault detection of structures using principal component analysis and hypothesis testing. In *Advances in Principal Component Analysis* (pp. 137-191). Springer, Singapore.
- Reuter, M. A., van Schaik, A., & Gediga, J. (2015). Simulation-based design for resource efficiency of metal production and recycling systems: Cases-copper production and recycling,

e-waste (LED lamps) and nickel pig iron. *The International Journal of Life Cycle Assessment*, 20, 671-693.

Risken, H., 1996. *The Fokker-Planck Equation*. Springer Berlin Heidelberg.

Sengupta, D., Ilankoon, I. M. S. K., Kang, K. D., & Chong, M. N. (2022). Circular economy and household e-waste management in India: Integration of formal and informal sectors. *Minerals Engineering*, 184, 107661.

Takane, Y. (2013). *Constrained principal component analysis and related techniques*. CRC Press.

Widmer, R., Oswald-Krapf, H., Sinha-Khetriwal, D., Schnellmann, M., & Böni, H. (2005). Global perspectives on e-waste. *Environmental impact assessment review*, 25(5), 436-458.

CHAPTER-10
SUSTAINABILITY ANALYSIS
OF MREW PLANT

CHAPTER – 10

10.1 BACKGROUND

Sustainability analysis of any process requires detailed intervention of the three pillars of sustainability i.e., environment, economic and social. Material recovery from e-waste is a complex process and the heterogeneity of the material makes it even more complex. It is important to consider all three parameters for evaluation and prediction of the sustainability of material recovery processes from e-waste. One important observation from the popular literature is that almost all the assessments of sustainability of e-waste processing are focused on determination of environmental impacts via LCA. The economic and the social aspects have been overlooked in those studies. A few studies have been identified in the social sector but the focus is on the informal sector. This chapter is focused on *Sustainability analysis of MREW plant featuring pyrolysis and gasification aided pyrolysis as alternative green treatment technologies* encompassing the following objectives –

- Life Cycle Analysis (LCA) of FR-2 WPCB and FR-4 WPCB pyrolysis process
- Life Cycle Analysis (LCA) of mixed WPCB steam gasification aided pyrolysis process
- Economic analysis of FR-2 WPCB and FR-4 WPCB pyrolysis plant
- Economic analysis of mixed WPCB steam gasification aided pyrolysis plant
- Social aspects of MREW

10.2 Methodology

10.2.1 LCA Methodology

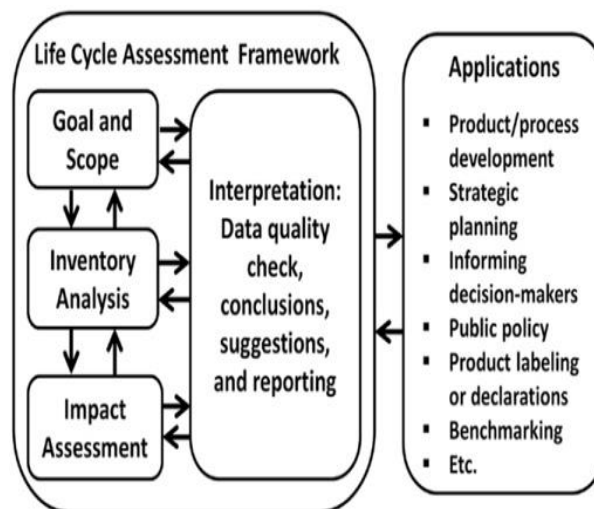


Figure 10.1: LCA Framework according to ISO 14040 series

Based on the principle of environmental life cycle assessment method in accordance to the ISO 14040 series, LCA has been applied using the 4 phases of goal and scope definition, life cycle inventory (LCI), life cycle impact assessment (LCIA), and interpretation (ISO14044, 2006).

10.2.1.1 Goal & Scope Definition

Functional Unit

The goal of this study is to develop LCA model for pyrolysis and gasification based pyrolysis of Waste Printed Circuit Boards. 100 kg of PCB is selected as the functional unit to provide a quantified reference for all other related inputs and outputs. All air, water, and soil emissions, raw materials and energy consumption, and waste disposal are based to this functional unit. The area of LCA has been considered to be Asia.

System Boundary

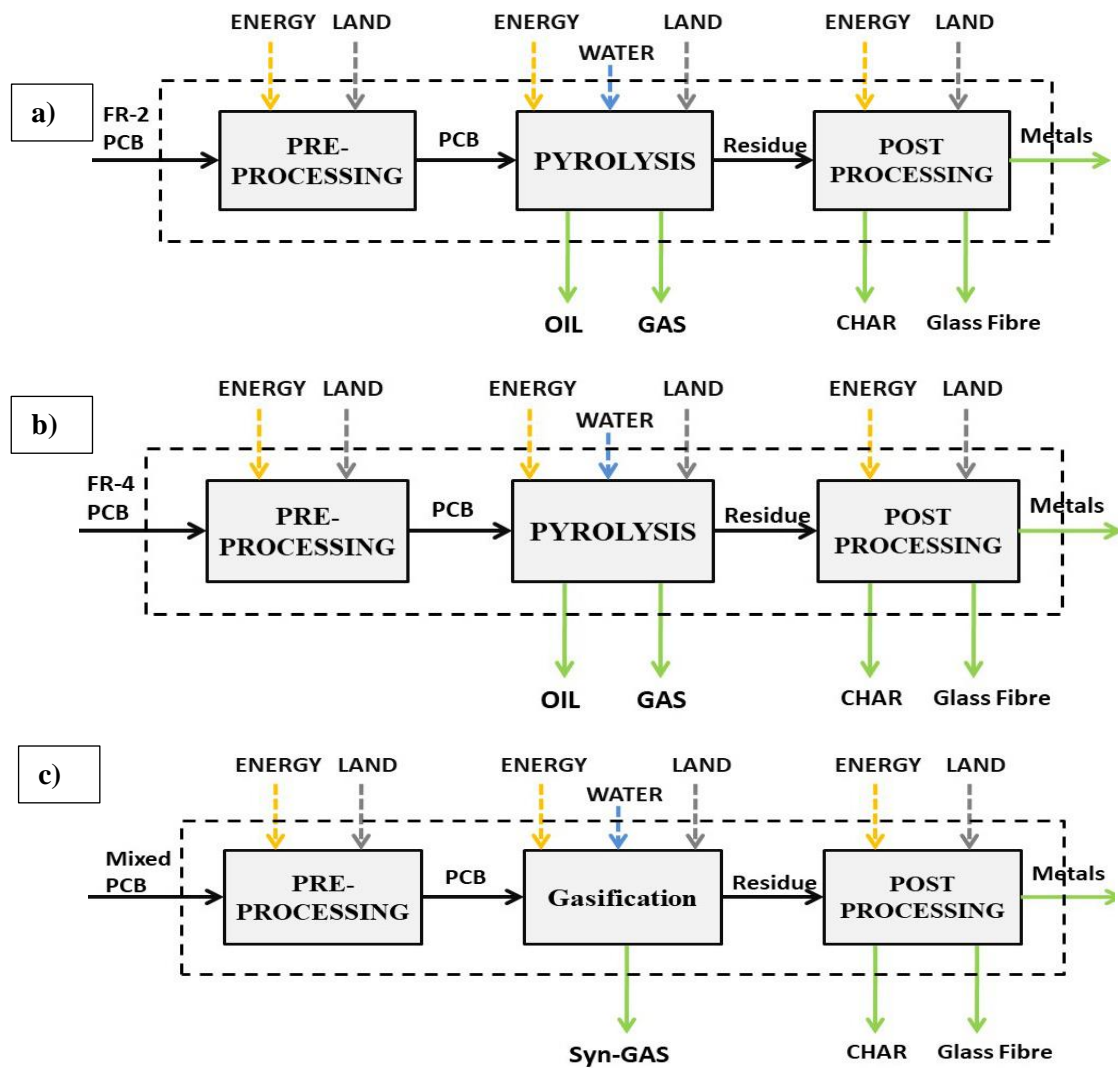


Figure 10.2: System Boundary of LCA (a) of FR-2 WPCB Pyrolysis; (b) FR-4 WPCB Pyrolysis and (c) Mixed WPCB Gasification based pyrolysis

Scenario (a) shows the system boundary of the LCA model for pyrolysis of FR-2 WPCB. The energy, land, water and 100 kg of FR-2 WPCB are considered as the input materials pyro-oil, gas, char and metals are considered as the output of the model. Figure 10.2 (a) shows the system boundary for pyrolysis of FR-2 WPCB. Scenario (b) shows the system boundary of the LCA model for pyrolysis of FR-4 WPCB. The energy, land, water and 100 kg of FR-4 WPCB are considered as the input and pyro-oil, gas, char, glass fibre and metals are considered as the output. Figure 10.b (a) shows the system boundary for pyrolysis of FR-4 WPCB. Scenario (c) shows the system boundary of the LCA model for steam gasification based pyrolysis of mixed WPCB. The energy, land, water and 100 kg of mixed WPCB are considered as the input materials syn-gas, char, glass fibre and metals are considered as the output of the model. Figure 10.2 (c) shows the system boundary for steam gasification-based pyrolysis of mixed WPCB.

10.2.1.2 Life Cycle Inventory Analysis (LCI)

The life cycle inventories are stressors or pollutants causing environmental impacts under various categories. Their analysis is about inlet and outlet mass and energy flow analysis. The inventory analysis is to identify each block of a process life cycle, and to quantify the material and energy inputs and outputs for each of these stages. The inventory analysis includes the following steps, detailed definition of the system, data collection, and allocation and quantification of the environmental burdens. Further, the compositions of streams emitted to water, land and air must be estimated for the assessment of impacts under various categories. This step involves simulation/data collection/modeling of each box. LCIs are established for the present scenario using Asian data based on Ecoinvent 3.1 database. The data for the integrated MREW facilities are based on the findings from chapter 7 – 10. Operational data (i.e., energy, chemicals, raw material, water and wastewater, solid waste, and product) and direct emissions to water, air and soil associated with the considered scenarios are also calculated to generate LCI.

10.2.1.3 Life Cycle Impact Assessment (LCIA)

LCIA aims to evaluate the significance of potential environmental impacts using the results coming out from the LCI phase. The process has been carried out using ReCiPe 2016 Midpoint (H), version 1.13 via the Simapro software version 9.1. ReCiPe 2016 Midpoint method is also the most recent indicator approach available in LCA analysis (Huijbregts et al. 2016). It considers a broad set of 18 midpoint impact categories i.e., human carcinogenic toxicity, human non-carcinogenic toxicity, fine particulate matter formation, ionizing radiation, ozone

formation human health, terrestrial acidification, freshwater eutrophication, terrestrial ecotoxicity, freshwater eco-toxicity, marine eutrophication, marine eco-toxicity, land use, global warming potential, water consumption, fossil resource scarcity, stratospheric ozone depletion, ozone formation terrestrial ecosystems and mineral resource scarcity .

10.2.2 Economic Analysis

The economic analysis has been carried out using in-built Aspen Plus economic analyser. The necessary data have been gathered to perform the economic analysis from various sources including multiple websites, research reports and papers. 20 years of plant life and 1 year of plant commission period has been considered.

10.3 Sustainability Analysis

Sustainability is an essential notion which is necessary at this moment and has to be implemented for a better future (Becker 2011). According to the World Commission on Environment and Development (WCED) report sustainability is defined as (Brundtland 1987) – “*Development that meets the needs of the present without compromising the ability of future generations to meet their own needs.*” Traditional semantics of sustainability is based on three pillars – Environmental, Economic and Social (Brundtland 1987). In this study, all three pillars are explored to assess the sustainability of MREW plants.

10.3.1 Environmental Sustainability

Environmental Sustainability of any process is generally characterised by some factors. These factors are assigned with some scores that dictate the magnitude of impact on the environment. A LCA is arguably the ultimate method to assess environmental sustainability. Material recovery from e-waste is lucrative as well as complex in nature as the metals are present within the solid polymer matrix of the printed circuit boards. To assess the environmental sustainability of the thermo-chemical pre-treatment processes, LCA has been carried out.

10.3.1.1 LCA of FR-2 &FR-4 WPCB pyrolysis process

LCA of WPCB pyrolysis has been carried out considering three major steps – i) Pre-processing/Shredding which reduces the size of the PCB, ii) Pyrolysis where the thermal decomposition takes place and iii) Post-processing which are the steps of material recovery. The major impact categories for FR-2 WPCB pyrolysis are Global Warming, Fossil Resource Scarcity, Ozone formation human health, Ozone formation terrestrial ecosystems and Fine particulate matter formation. Similarly, for FR-4 WPCB, the major impact categories are global

warming, fossils resource scarcity, Ozone formation human health, Ozone formation terrestrial ecosystems, Fine particulate matter formation and water consumption. As can be clearly seen from figure 10.3 & 10.4, the positive impacts of the pre-processing and pyrolysis are offset by the negative impacts in the post-processing stage i.e., when the resource is being recovered after pyrolysis. The overall scheme integrating pyrolysis as the central process has been proved to be “Green” and eco-friendly.

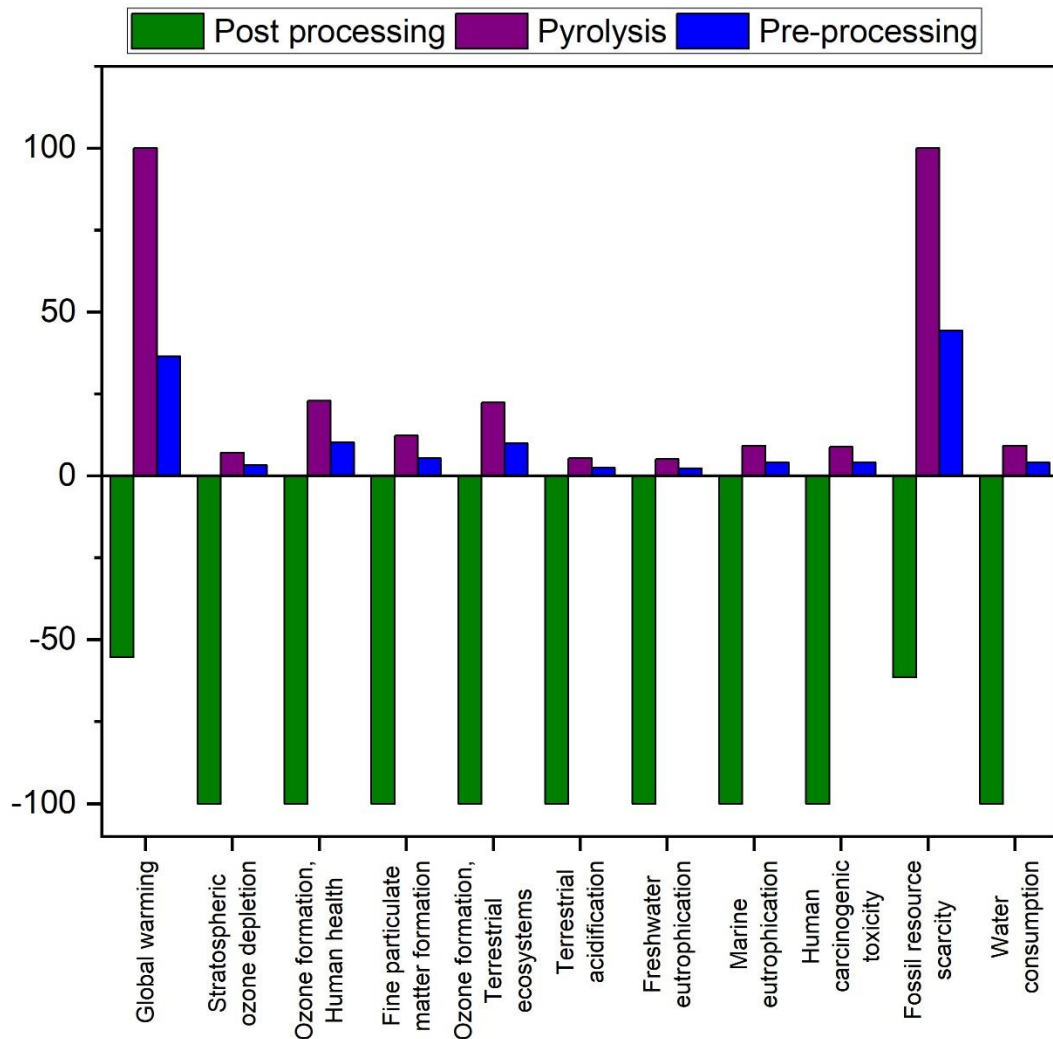


Figure 10.3: LCA midpoint results of FR-2 WPCB pyrolysis

Table 10.1: Midpoint Results of LCA of FR-2 WPCB Pyrolysis

Midpoint Category	Unit	Post processing	Pyrolysis	Pre- processing
Global warming	kg CO ₂ eq	-55	100	36.42
Stratospheric ozone depletion	kg CFC11 eq	-100	7.12	3.17
Ionizing radiation	kBq Co-60 eq	-100	0.67	0.34
Ozone formation, Human health	kg NO _x eq	-100	22.92	10.09
Fine particulate matter formation	kg PM2.5 eq	-100	10.27	5.39
Ozone formation, Terrestrial ecosystems	kg NO _x eq	-100	22.37	9.85
Terrestrial acidification	kg SO ₂ eq	-100	5.32	2.35

Freshwater eutrophication	kg P eq	-100	5.12	2.25
Marine eutrophication	kg N eq	-100	9.25	4.07
Terrestrial ecotoxicity	kg 1,4-DCB	-100	0.21	0.105
Freshwater ecotoxicity	kg 1,4-DCB	-100	0.32	0.19
Marine ecotoxicity	kg 1,4-DCB	-100	0.34	0.19
Human carcinogenic toxicity	kg 1,4-DCB	-100	8.78	3.96
Human non-carcinogenic toxicity	kg 1,4-DCB	-100	0.91	0.42
Land use	m ² a crop eq	-100	2.82	1.24
Mineral resource scarcity	kg Cu eq	-100	0.25	0.15
Fossil resource scarcity	kg oil eq	-61	100	44.27
Water consumption	m ³	-100	9.14	4.05

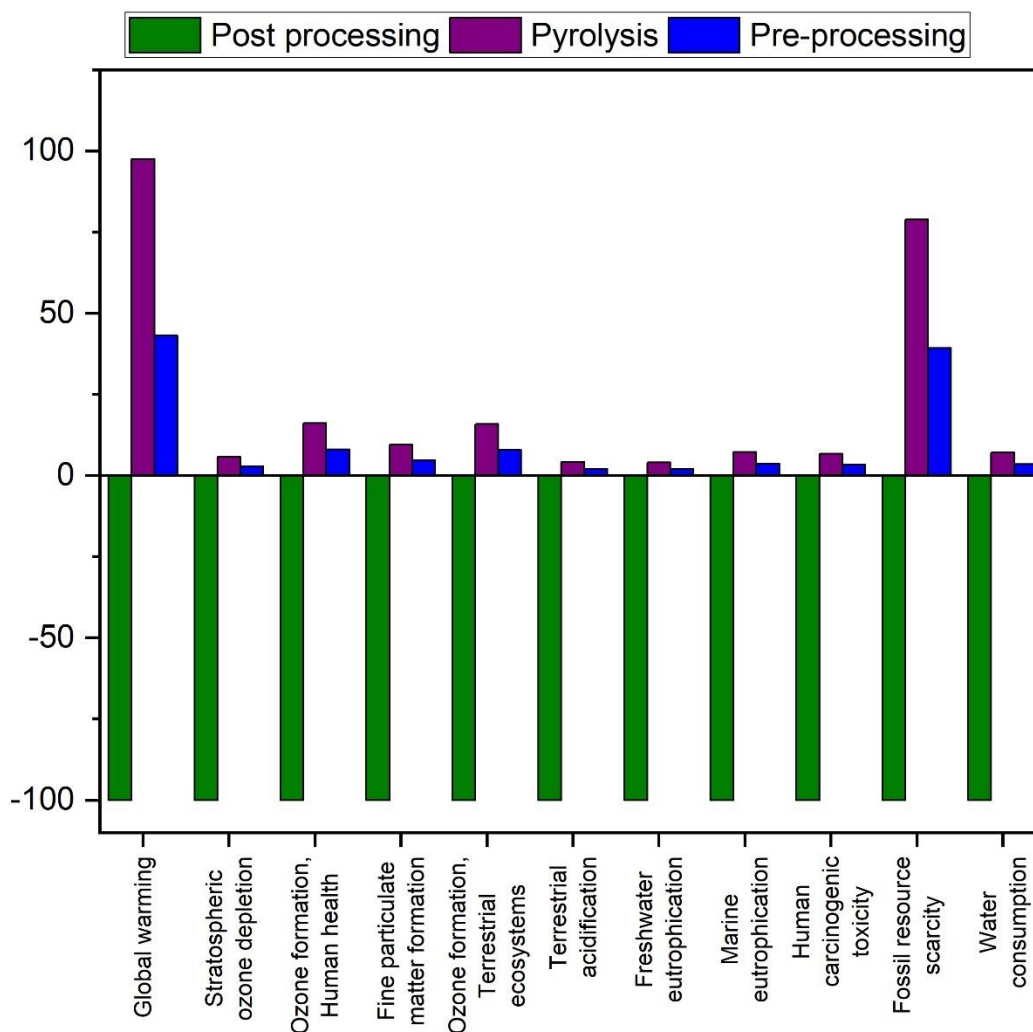


Figure 10.4: LCA midpoint results of FR-4 WPCB pyrolysis

Table 10.2: Midpoint Results of LCA of FR-4 WPCB Pyrolysis

Midpoint Category	Unit	Post processing	Pyrolysis	Pre-processing
Global warming	kg CO ₂ eq	-100	97.49	43.13
Stratospheric ozone depletion	kg CFC11 eq	-100	5.74	2.87
Ionizing radiation	kBq Co-60 eq	-100	0.5	0.27
Ozone formation, Human health	kg NO _x eq	-100	16.06	7.95
Fine particulate matter formation	kg PM _{2.5} eq	-100	9.42	4.66
Ozone formation, Terrestrial ecosystems	kg NO _x eq	-100	15.83	7.84
Terrestrial acidification	kg SO ₂ eq	-100	4.10	2.04

Freshwater eutrophication	kg P eq	-100	4.02	2.00
Marine eutrophication	kg N eq	-100	7.20	3.56
Terrestrial ecotoxicity	kg 1,4-DCB	-100	0.17	0.11
Freshwater ecotoxicity	kg 1,4-DCB	-100	0.26	0.17
Marine ecotoxicity	kg 1,4-DCB	-100	0.27	0.17
Human carcinogenic toxicity	kg 1,4-DCB	-100	6.72	3.40
Human non-carcinogenic toxicity	kg 1,4-DCB	-100	0.72	0.37
Land use	m ² a crop eq	-100	2.29	1.14
Mineral resource scarcity	kg Cu eq	-100	0.19	0.105
Fossil resource scarcity	kg oil eq	-100	78.82	39.17
Water consumption	m ³	-100	7.10	3.54

10.3.1.2 LCA of mixed WPCB steam gasification aided pyrolysis process

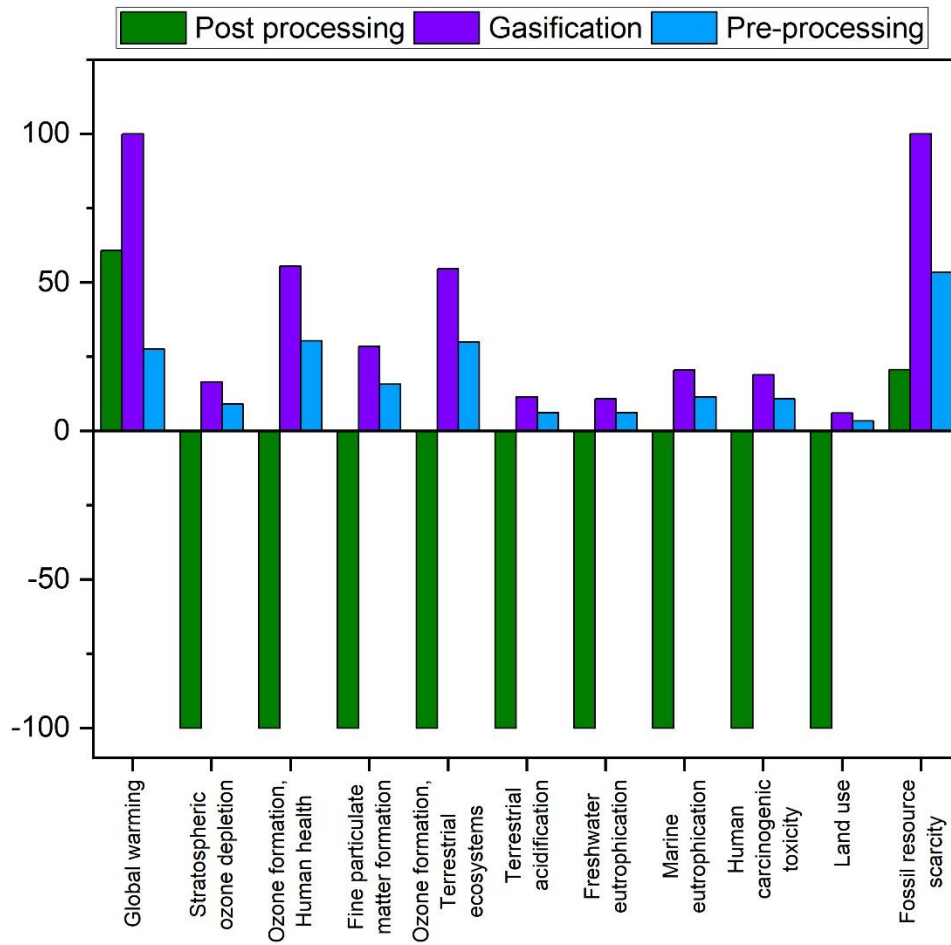


Figure 10.5: LCA midpoint results of mixed WPCB steam gasification aided pyrolysis

Table 10.3: Midpoint Results of LCA of Mixed WPCB steam gasification aided pyrolysis

Midpoint Category	Unit	Post processing	Gasification based pyrolysis	Pre- processing
Global warming	kg CO ₂ eq	60.8299	100	27.56
Stratospheric ozone depletion	kg CFC11 eq	-100	16.47	9.00
Ionizing radiation	kBq Co-60 eq	-100	1.46	0.76
Ozone formation, Human health	kg NO _x eq	-100	55.43	30.38
Fine particulate matter formation	kg PM _{2.5} eq	-100	28.44	15.77
Ozone formation, Terrestrial ecosystems	kg NO _x eq	-100	54.53	29.87
Terrestrial acidification	kg SO ₂ eq	-100	11.42	6.20
Freshwater eutrophication	kg P eq	-100	10.81	6.07
Marine eutrophication	kg N eq	-100	20.55	11.50
Terrestrial ecotoxicity	kg 1,4-DCB	-100	0.51	0.30
Freshwater ecotoxicity	kg 1,4-DCB	-100	0.64	0.48
Marine ecotoxicity	kg 1,4-DCB	-100	0.68	0.49
Human carcinogenic toxicity	kg 1,4-DCB	-100	18.84	10.81
Human non-carcinogenic toxicity	kg 1,4-DCB	-100	1.83	1.06
Land use	m ² a crop eq	-100	5.96	3.38
Mineral resource scarcity	kg Cu eq	-100	0.48	0.35
Fossil resource scarcity	kg oil eq	20.6317	78.81	39.17
Water consumption	m ³	-100	7.10	3.54

LCA of mixed WPCB gasification aided pyrolysis has been carried out considering three major steps – i) Pre-processing/Shredding which reduces the size of the PCB, ii) Gasification based pyrolysis and iii) Postprocessing which are the steps of material recovery and energy recovery. The major impact categories are Global Warming, Fossils resource scarcity, Ozone formation human health, Ozone formation terrestrial ecosystems, fine particulate matter formation, marine eutrophication, human carcinogenic toxicity and water consumption. Similar to pyrolysis, the impacts of the pre-processing and gasification aided pyrolysis are offset by the negative impacts due to resource recovery in the post processing stage. However, in this case, post processing phase also have some positive impact in global warming and fossils resource scarcity category.

10.3.2 Economic Sustainability

Economic sustainability is perhaps the most important aspect of sustainability when it comes to business. From the technological perspective, economical sustainability is there otherwise the e-waste recycling units would have shut down by this time. The most important thing of e-waste valorisation is material recovery. It is nothing but chanting the ‘3R’ mantra once again and it is quite lucrative. E-waste business fostering around the world gets its maximum profit by metal reuse and recycling. To assess the economic sustainability of the thermo-chemical

pre-treatment processes, economic analysis has been carried out using Aspen Plus Economic Analyzer.

Table 10.4: Economic Analysis of FR-2 and FR-4 WPCB Pyrolysis plant

Economic Components	FR-2 WPCB Pyrolysis	FR-4 WPCB Pyrolysis
Total capital cost (USD)	4982010	5068110
Total operating cost (USD/year)	1638830	1368960
Total raw material cost (USD/year)	599469	315504
Total product sales (USD/year)	3704110	785109
Total Utilities cost (USD/year)	66088.2	98983.4
Desired rate of return (Percent/year)	20	20
Payback period (year)	4.86	1.27
Total installed cost (USD)	752000	798500
Pyrolyzer (Equipment cost) (USD)	130200	130200
Other Equipment cost (USD)	257800	295800

The economic analysis has been carried out using in-built Aspen Plus economic analyser. The necessary data have been gathered from experimental outputs to perform the economic analysis. Other remaining data have been obtained from various sources including multiple websites, research reports and papers. 20 years of plant life and 1 year of plant commission period has been considered. The results are listed in table 10.4 & 10.5. As can be seen, total capital cost is nearly \$50 and \$51 million for FR-2 and FR-4 WPCB pyrolysis plant respectively. Total equipment cost is nearly \$3.9 and \$4.3 million and total operating cost is nearly \$14 and \$17 million for FR-2 and FR-4 WPCB pyrolysis plant respectively. The payback period is 4.86 and 1.27 years for FR-2 and FR-4 WPCB respectively.

Table 10.5: Economic Analysis of mixed WPCB steam gasification aided pyrolysis plant

Economic Components	Mixed WPCB Gasification based pyrolysis
Total capital cost (USD)	5961090
Total operating cost (USD/year)	1644520
Total raw material cost (USD/year)	610875
Total product sales (USD/year)	188752
Total Utilities cost (USD/year)	46871.9
Desired rate of return (Percent/year)	20
Payback period (year)	8.54
Total installed cost (USD)	1168300
Gasifier (Equipment cost) (USD)	317600
Other Equipment cost (USD)	107847

Similar to the previous case, the required data have been obtained from experimental outputs. Any further data required have been gathered from websites, research reports and research

articles. In case of gasification based pyrolysis, the economic analysis has been carried out for mixed WPCB. Total capital cost is nearly \$60 million, total equipment cost is nearly \$4.5 million and total operating cost is nearly \$17 million. The desired rate of return is 20% per year and payback period is 8.54 years.

10.3.3 Social Sustainability

Social sustainability of any process is complex enough to go about. The behaviour, mentality and other social indicators change with geographical region. Religion also plays a big role in this case. With respect to the technologies discussed, it is quite hard to predict the social sustainability. The social LCA is the best way to understand the social impact. Social LCA study of e-waste recycling is really scant. Umair et al. (2015) have shed some light in his study on social LCA of informal sectors associated with E-waste recycling. Considering stakeholder classification (United Nations, 2007) and the study of Umair et al. the following (Table 5) sub-categories may be taken into consideration for the formal recycling of e-waste and recovery of metals. Undoubtedly, the industrial implementation of these methods will certainly create job opportunities. The society will also be benefitted with the use of recycled products fuels and the use of green technologies in the industries. Overall, with time and advancement in the technologies, more the products will be commercialized, more it will be socially accepted and we will march toward social sustainability.

Table 10.6: Stakeholder category and sub-categories for social aspects of MREW

Stakeholder Category	Subcategories	References
Worker	Working Hours	Umair et al. 2015
	Child Labour	
	Health and Safety	
	Social Security	
	Wages	
	Equal opportunities/discrimination	
Local community	Safety and health	Umair et al. 2015
	Community engagement	
	Local Employment	
Society	Public contribution to sustainable issues	Umair et al. 2015
	Contribution to economic development	
Governance	Corruption	United Nations 2007
	Crime	
Demographics	Population	United Nations 2007
Education	Education Level	United Nations 2007
	Literacy	
	Awareness	

References

- Becker, C. U. (2012). The role of philosophy for sustainability research. *Sustainability Ethics and Sustainability Research*, Springer, Dordrecht, 127-131.
- Brundtland, G. H. (1987). Report of the World Commission on Environment and Development: Our Common Future. UN Documents. New York.
- Huijbregts, M. A., Steinmann, Z. J., Elshout, P. M., Stam, G., Verones, F., Vieira, M., Zijp, M., Hollander, A., & Van Zelm, R. (2017). ReCiPe2016: a harmonised life cycle impact assessment method at midpoint and endpoint level. *The International Journal of Life Cycle Assessment*, 22, 138-147.
- International Organization for Standardization (ISO). (2006). Environmental management — Life cycle assessment — Requirements and guidelines (ISO Standard No. 14044:2006). <https://www.iso.org/standard/38498.html>
- Umair, S., Björklund, A., & Petersen, E. E. (2015). Social impact assessment of informal recycling of electronic ICT waste in Pakistan using UNEP SETAC guidelines. *Resources, Conservation and Recycling*, 95, 46-57.
- United Nations. Department of Economic. (2007). *Indicators of sustainable development: Guidelines and methodologies*. United Nations Publications.

CHAPTER-11

CONCLUSION

CHAPTER – 11

Resource Recovery from e-waste is a wide area of research encompassing multiple technological approaches and branches. Under the current research, the focus has been on material and fluidic (liquid and gas) fuel recovery from waste printed circuit boards focusing on green processes. The research study can be divided into the following sub-categories –

- i) Kinetic and thermodynamic analysis of pyrolysis of FR-2 and FR-4 type waste printed circuit boards (WPCB) with reaction mechanism and product array characterization.
- ii) Optimization of process parameters of low temperature pyrolysis of mixed WPCB for maximization of non-carbonaceous solid recovery and pyro-oil yield.
- iii) Gasification aided pyrolysis of FR-2 and FR-4 type waste printed circuit boards for upgradation of pyro-gas.
- iv) Development of Material Recovery from E-waste (MREW) framework for sustainable resource recovery using pyrolysis and steam gasification aided pyrolysis as pre-treatment process with process modelling using ASPEN.
- v) Supply chain kinetics of MREW focusing on plant performance.
- vi) Sustainability analysis of MREW plant focusing on three pillars of sustainability i.e., environment, economic and social.

The overall outcomes, at a glance are as follows:

- The TG analysis reveals that pyrolysis of both FR-2 and FR-4 type VPCB and WPCB occurs in three stages. The average activation energy values have been determined as 121.1, 89.26, 94.87, 90.06, 89.89 and 94.46 kJ/mol for Friedman, KAS, FWO, Starink, Tang and Bosewell methods respectively for FR-2 type VPCB pyrolysis. The average activation energy of FR-2 WPCB pyrolysis have been determined as 116.99, 88.94, 64.73, 57.24, 58.93 and 63.52 kJ/mol for Friedman, KAS, FWO, Starink, Tang and Bosewell methods respectively. In case of FR-4 VPCB pyrolysis, the average activation energy has been determined as 194.94, 156.09, 159.79, 156.69, 156.87 and 162.44 kJ/mol for Friedman, KAS, FWO, Starink, Tang and Bosewell methods respectively. For FR-4 WPCB pyrolysis, 101.01, 60.83, 67.63, 60.96, 60.08 and 57.15 kJ/mol have been the values of activation energy determined using Friedman, KAS, FWO, Starink, Tang and Bosewell methods respectively.

- The distribution of activation energies based on Miura-maki method follows a right skewed and a left skewed gaussian pattern for FR-2 type VPCB and WPCB respectively. For FR-4 type VPCB, it has been found that the activation energies do not follow any particular pattern, whereas FR-4 type WPCBs follows the gaussian pattern.
- The thermodynamic analysis discloses that the existence of in-situ metals in WPCB causes complex degree of reaction, confirming the catalytic effect of the in-situ metals on the pyrolysis process.
- The FTIR & NMR of pyro-oil revealed that the oil is rich in aromatics, amines and unsaturated compounds. FTIR of pyro-char revealed that it contains unreacted Acrylonitrile butadiene styrene (ABS). The pyrolysis reaction mechanism based on Šesták-Berggren model has been identified as a combination of nucleation reactions with simultaneous phase boundary reactions, while diffusion has been determined to be rate controlling, for both FR-2 and FR-4 type VPCB and WPCB.
- The optimization by Response Surface Methodology (RSM) revealed that, in case of metal + glass fibre recovery, both (A) pyrolysis time and (B) percentage of FR-4 in FR2-FR4 mixture are the two most significant input parameters. The Genetic Programming (GP) reiterated similar result. In case of pyro-oil yield, it has been predicted by RSM that (B) percentage of FR-4 in FR2-FR4 mixture is the most significant input parameter. However, GP overpredicts in this case.
- Maximum decomposition of WPCB is achieved at 973K for FR4 and 923K for FR2 WPCB in the experimental investigation of steam gasification aided pyrolysis. The gas composition analysis reveals that steam gasification aided pyrolysis of FR-2 and FR-4 WPCB contains 45.97% H₂; 40.18% CO; 13.84 % other gases and 36.59% H₂; 36.78% CO; 26.62% other gases respectively. In both cases, CO₂ was found to be in negligible volume. This is a significant improvement of the quality of the pyro-gas while allowing recovery of metal and glass fibre. The surface morphology reveals the suitability of FR-2 WPCB steam gasification aided pyrolysis char as adsorbent for wastewater treatment while the same for FR-4 WPCB could be considered as a precursor for developing tailored carbonaceous materials. As confirmed by the EDX and FTIR analysis, using steam gasification aided pyrolysis helps in bromine fixation in the steam gasification aided pyrolysis char whereas in conventional pyrolysis bromine migrates to the pyro-oil.
- This analysis on Material Recovery from E-waste (MREW) depicts the culmination of the of the experimental outputs amalgamated with the field survey which is focused on the MREW featuring pyrolysis and steam gasification aided pyrolysis as pre-treatment

technologies with a holistic landscape. Two industrial case studies in Indian and Chinese scenario respectively depicts the state-of-the-art scenario of the recycling process of MREW technology. Three frameworks for integrated MREW facilities, without (option -1) pyrolysis, with pyrolysis (option -2) and with steam gasification aided pyrolysis (option -3) have been conceptualized. The comprehensive qualitative energy and environmental assessment employing LCA principles on the three frameworks guided the design of process modelling for pyrolysis and steam gasification-assisted pyrolysis approaches.

- The ASPEN plus model of pyrolysis of mixed WPCB revealed satisfactory results as it was able to simulate compositions of metal mixture, glass fibre, char and pyro-oil. On the other hand, the model of steam gasification aided pyrolysis of mixed WPCB was able to simulate acceptable results consisting of compositions of syn-gas, metal mixture and glass fibre.
- The generic “Utilization-to-cradle” MREW supply chain network successfully describes the market dynamics of the MREW system. The results show that the hybrid AHP-PCA ranking method is superior to the standalone AHP method of ranking. However, certain cases emerged where the hybrid method over-estimated the dynamics of the system. The model was able to identify the operation windows for the supply chain managers for reinvigoration of the policies. Volume of carbon dioxide and energy consumption emerged as the most important parameters while energy consumption was the most sensitive parameter for an MREW system. The model also identifies that for social accountability practice, the decision should be purely guided by the budget constraints to maintain a sustainable business. On the other hand, the product sales which is the economic driver reflected an increasing profile with respect to the current case. The numbers and outputs are likely to change with the change in case and constraints. The study almost unerringly replicates the results which is realistic and provides a guideline for developing a cleaner production line with a sustainable profitability margin.
- Overall sustainability of MREW pre-treatment technologies has been assessed considering environmental, economic and social perspectives. The LCA analysis revealed that global warming, fossils resource scarcity, Ozone formation human health, Ozone formation terrestrial ecosystems, Fine particulate matter formation and water consumption have been found to be the highest impact categories for both pyrolysis and steam gasification aided pyrolysis. Interestingly, the post-processing step offsets the positive impacts of the pyrolysis and steam gasification aided pyrolysis processes itself. Economic analysis revealed that, total capital cost, total equipment cost and total operating cost is nearly \$50 million; \$3.9 million and \$14 million respectively for FR-2 pyrolysis plant. Whereas the

total capital cost, total equipment cost and total operating cost is nearly \$51 million; \$4.3 million and \$17 million respectively for FR-4 pyrolysis plant. The payback period is 4.86 and 1.27 years for FR-2 and FR-4 WPCB respectively. In case of gasification-based pyrolysis of mixed WPCB, total capital cost, total equipment cost and total operating cost is nearly \$60 million; \$4.5 million and \$17 million respectively. The desired rate of return is 20% per year and payback period is 8.54 years. A qualitative analysis on the societal aspects revealed that the society will be benefitted with the use of recycled products, fuels and the use of eco-friendly technologies.

Future Scope for Research

The present research study has thoroughly addressed the material recovery from FR-2 and FR-4 PCBs using green processes, namely pyrolysis and steam gasification aided pyrolysis with focus on core chemical engineering aspects such as kinetics, thermodynamics, reaction mechanism as well as supply chain performance aspects with an overall outlook of sustainability. Although, the outcome of this study lays down the groundwork to present a roadmap towards sustainable recovery of resources from printed circuit boards, further research work needs to be conducted in the following directions –

- i) Debromination of pyro-oil should be attempted for proper utilization of pyro-oil and further separation of metals from metal mixture should be investigated.
- ii) Gasification aided pyrolysis should be investigated further with different gasification agents and optimization of process parameters with focus on material and energy recovery.
- iii) Pilot-plant studies should be conducted for pyrolysis of mixed PCBs with focus on maximum recovery of material and fuel.

Sustainability of metal recovery from E-waste

Biswajit Debnath¹, Ranjana Chowdhury¹, Sadhan Kumar Ghosh (✉)²

¹ Department of Chemical Engineering, Jadavpur University, Kolkata 700032, India

² Department of Mechanical Engineering, Jadavpur University, Kolkata 700032, India

HIGHLIGHTS

- Metal recovery techniques from electronic waste reported in literature.
- Metal recovery processes followed in Industries from electronic waste.
- Sustainability analysis of metal recovery processes from electronic waste.

ARTICLE INFO

Article history:

Received 27 March 2017

Revised 24 November 2017

Accepted 26 March 2018

Available online 23 May 2018

Keywords:

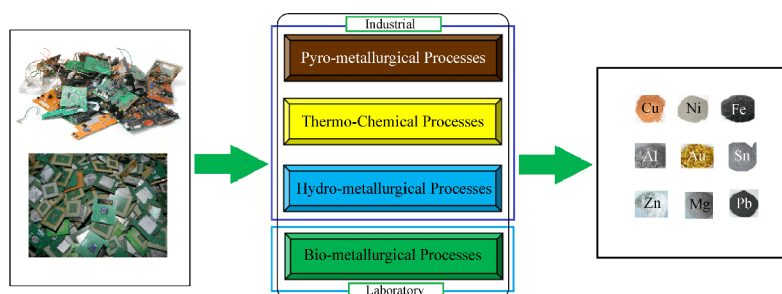
E-waste

Metal recovery

Metal Recovery from E-waste (MREW)

Sustainability

GRAPHIC ABSTRACT



ABSTRACT

The issue of E-waste disposal is concerning all the stakeholders, from policymakers to the end users which have accelerated the research and development on environmentally sound disposal of E-waste. The recovery of metals (gold, tantalum, copper, iron etc.) from E-waste has become an important focus. The mechanical recycling, thermo-chemical processes like pyrolysis, pyro-, hydro- and bio-metallurgical processes can play important roles in the Metal Recovery from E-waste (MREW) technology. For the industrial application of the MREW technology, it is important to analyze the sustainability. In this paper, two case studies have been presented on E-waste recycling industries in India and China. Based on the literature data, an attempt has been made to assess qualitatively the overall sustainability of MREW technology considering the three pillars, i.e., environmental, economic and social. Two conceptual frameworks with (Option-2) and without (Option-1) pyrolysis for integrated MREW units have been developed and the generalized energy and environmental impact analysis has been made using the principles of LCA. The impacts of two options have been compared. Option 2 has been found to be more efficient and sustainable. It has been realized that climate change, fossil fuel depletion, water depletion, eutrophication, acidification, fresh and marine water ecotoxicity are possible impact categories. The recommendations based on the generalized assessment are in good agreement with the findings of previous researchers on individual steps of MREW unit. The findings of this paper are expected to be beneficial to researchers and stakeholders for research directions and decision making on MREW.

© Higher Education Press and Springer-Verlag GmbH Germany, part of Springer Nature 2018

1 Introduction

The Electrical and Electronics Equipment (EEE) industry is one of the largest industries in the world. The electronic

industry is expected to reach \$400 billion in 2022 from \$69.6 billion in 2012 (Corporate Catalyst India 2015). The demand of EEE is ever increasing and the driving force behind this demand is often the technological advancement coupled with short innovation cycles and business strategies which shortens the lifespan of the equipments. E-waste generation is increasing exponentially every year. Huisman (2010) predicted that E-waste generation will be 19.1 kg/person/year by 2012 in 27 EU countries leading to total 10.5 million tons of E-waste by 2014. In 2014, the

✉ Corresponding author

E-mail: sadhankghosh9@gmail.com

Special Issue—Recycling Materials from WEEE (Responsible Editors: Jinhui LI & Eric David Williams)

worldwide generation of E-waste is 41.8 million metric tons and by the year 2018 it is expected to rise by 21% to 50 million tonnes (McMahon, 2016). In 2015, nearly 54 million tons of E-waste was produced globally. BRICS nations generated nearly 25% of the total E-waste generated in 2014 (Ghosh et al., 2016). Associated Chambers of Commerce of India (ASSOCHAM) reported that India generated 1.5 million tons of E-waste in the year 2015. The E-waste generation in China was estimated to be 6.033 million tonnes in 2014 (Baldé et al., 2015).

Different strategies like Material Flow Analysis (MFA), Life Cycle Assessment (LCA), Extended Producer Responsibility (EPR), Advanced Recycling Fee (ARF) etc. have been introduced for E-waste management and mostly, these have been implemented in the developed nations. However, till date recycling of E-waste is considered to be the best approach for E-waste management. While the primary resources are depleting, metals from E-waste could be an important source and Metal Recovery from E-waste (MREW) could be a potential opportunity of metal recovery from secondary resources. High content of base metal (Fe, Cu, Al, Pb and Ni) and precious metal (Ag, Au, Pt and Pd) present in E-waste results makes it a potential source of secondary resources for metal recovery. Typical metal composition of printed circuit board is presented in Table 1 and Table 2. The metal content of E-waste varies widely depending on the type of E-waste. Debnath et al. (2016) has shown in their study that the metal content in different E-waste is different based on size and operation. For example, keyboards contain 95% polymer whereas the printed circuit boards are rich in metals. Printed Circuit Boards (PCB) from a typical computer contains nearly 20% Cu and 250 mg/ton Gold, whereas the Copper percentage goes down in PCBs from mobile to 13% and Gold goes up to 350 mg/ton (Hagelüken, 2006). The metal content in printed circuit board is higher than the ores/concentrates.

MREW is a lucrative business as well as a very popular area of research. Different conventional techniques like physical processing, pyro-metallurgical processing, hydro-metallurgical and bio-metallurgical processing have been in implementation for metal recovery. Physical or mechanical recycling of E-waste is considered as a pre-treatment process. Metal rich fraction evolving from the

pre-treatment are subjected to pyro-metallurgical, hydro-metallurgical and bio-metallurgical processing for selective recovery of metals. Several studies have been reported focusing on metal recovery processes and an extensive number of them focused on comparative review, salient features, strength and weakness of the technologies. Apart from these, for the industrial application of the MREW technology, it is important to analyze the sustainability. On the other hand, there exists a distinct difference between laboratory practices and industrial practices. It is also of importance to look beyond laboratory and find out what is happening in the field. Studies focusing on these aspects have not been observed before in contemporary literature. In this study, an attempt has been made to address those issues.

2 Methodology

First, thorough literature review was undertaken exploring different databases like Science Direct, Google Scholar, Emerald Insight etc. Several keywords such as 'E-waste Recycling', 'Metal recovery from E-waste', 'Printed Circuit Board Recycling', 'Leaching of E-waste', 'Gold recovery from E-waste', 'Sustainability of E-waste recycling' etc. were used in this case. Thereafter, case study organizations were visited and their process operations were understood and reviewed thoroughly. Based on the findings, two conceptual frameworks were developed for integrated MREW. Then a generalized comparative analysis of the two scenarios was carried out from the perspectives of three pillars of sustainability.

3 Metal recovery process from E-waste

Metal recovery from E-waste is a lucrative business opportunity for the small and medium enterprises (SMEs). Many conventional thermo-chemical and bio-chemical processes have been tested both in pilot and laboratory scale for metal recovery from E-waste. Various researchers have used hydro-metallurgical (Kim et al., 2011), pyro-metallurgical (Hall and Williams, 2007) and bio-metallurgical (Ilyas and Lee, 2014) methods for this purpose.

Table 1 Typical composition of basic metals in PCB (E-waste guide info)

Name	Cu	Al	Pb	Zn	Ni	Fe	Sn
Concentration in wt%	6.9287	14.1723	6.2988	2.2046	0.8503	20.4712	1.0078

Table 2 Typical composition of rare earth and valuable metals in PCB (E-waste guide info)

Name	Sb	Au	Ag	Pd	Ga	Ge	As	Ti	Ta	Co	Se	Ni	Cd
wt%	0.0094	0.0016	0.0189	0.0003	0.0013	0.0016	0.0063	0.0157	0.0157	0.0157	0.0016	0.0002	0.0094

However, physical processes for metal recovery are quite in practice for easier operation and lower carbon footprint.

3.1 Physical recycling methods

Physical recycling methods are generally used for upgradation which helps in liberation of metals and non-metals contained in E-waste. To the best of the authors' experience in visiting several E-waste recycling facilities around the globe, physical recycling is the commonly practiced method for recycling E-waste all over the world. When it comes to the metal recovery, this is one of the efficient methods for metal recovery. Often it is considered as one of the pre-treatment step before further processing. Physical recycling includes disassembling, dismantling, chopping, shredding, crushing etc. These steps are achieved by using machineries like shredder, pre-granulator, granulator etc. After this, the separations of metal from the non-metals are achieved. Different methods such as magnetic separation, eddy current separation and density separation are used (Kang and Schoenung, 2005). It is possible to recover metal fraction containing more than 50% of copper, 24% of tin, and 8% of lead by implementing a combination of electrostatic and magnetic separation which separates the metal part from the non-metal ones (Veit et al., 2005). There are other methods reported in literature such as corona discharge method (Zhang and Forsberg, 1998; Li et al., 2007) (suitable for separation of metallic and non-metallic fractions), density based separation (Peng et al., 2004), milling (Koyanaka et al., 1997), froth floatation (Ogunniyi and Vermaak, 2009; Vidhyadhar and Das, 2012) etc.

3.2 Thermo-chemical methods

When it comes to thermo-chemical processes, pyrolysis is an important process. Pyrolysis is a thermo-chemical process which ensures thermal degradation of a targeted material in absence of air. A significant number of studies have been carried out on pyrolysis of E-waste (Sun et al., 2003; Xiong et al., 2006; Guo et al., 2010).

Vacuum pyrolysis (Qiu et al., 2009), microwave induced pyrolysis (Ruidian et al., 2007; Sun et al., 2012), catalytic pyrolysis (Hall et al., 2008) and co-pyrolysis (with biomass) (Liu et al., 2013) are different types of pyrolysis that has been reported. Though pyrolysis of E-waste is mostly limited within the laboratory, Jectec (a company from Japan) has already implemented pyrolysis in their facility. Another process which has gained attention these days is the plasma process that is being implemented for E-waste treatment and metal recovery. Plasma Technology is a high temperature and environment friendly technology. This is applied in MSW and biomedical waste disposal. Ruj and Chang (2013) reported plasma treatment of mobile phone waste and it showed that the process helps in recovery of metals. High enthalpy plasma jet (Mitrasinovic

et al., 2013), plasma reactor (Rath et al. 2012) and plasma torch (Tippayawong and Khongkrapan, 2009) has been explored for processing of E-waste. Despite very small number of available literature, it is already being used industrially in PyroGenesis Canada Inc.

3.3 Pyro-metallurgical methods

Pyro-metallurgical processes are widely employed for MREW around the world. Generally, when the metals are present in a complex matrix with other non-metals and ceramics etc, it is often difficult to recover them implementing the physical recycling processes. In that case, pyro-metallurgical method is the option. Printed circuit boards (PCB) are complex and is easier to recycle using these methods. The PCB's are first shredded or chopped into suitable pieces and then they are subjected to pyro-metallurgical processing. Smelting, refining, incineration, combustion are the common processes in this route. The state-of-art facilities available in the smelting and refining facilities are capable of extracting valuable metals from the complex matrix and are quite efficient (Antrekowitsch et al., 2006; Khaliq et al., 2014). A typical pyro-metallurgical treatment process is smelting followed by electro-chemical refining. First E-waste or metals recovered by physical recycling are fed into the furnace. The metals are collected in a molten bath and the oxides are obtained from the slag phase. Umicore, Outotec TSL, Aurubis recycling are to name a few that employs pyro-metallurgical processes for metal recovery from E-waste (Khaliq et al., 2014).

3.4 Hydro-metallurgical methods

Hydro-metallurgical methods implemented for metal recovery from E-waste are the modified version of the traditional hydro-metallurgical methods used for metal extraction from primary ores. Leaching is carried out by means of acid, alkali or other solvents to leach out metals in form of soluble salts. Impurities are removed with the gangue materials and the isolation of metals from the solution is achieved by processes such as adsorption, solvent extraction etc. Final forms of metals are achieved through electro-refining or chemical reduction processes (Shamsuddin, 1986; Khaliq et al., 2014). Four types of common leaching processes, namely—cyanide leaching (Kolodziej and Adamski, 1984), halide leaching (Quinet et al., 2005), thiourea leaching (Sheng and Etsell, 2007) and thiosulfate leaching (Chmielewski et al., 1997) are there. Copper and other precious metals such as gold, silver etc can be recovered via hydrometallurgical route and a detailed discussion can be found in the study by Wu and group (2017). Rare Earth Elements (REE) can also be recovered via this route and consolidated studies have been reported (Sun et al., 2016). Aqua regia was used as leaching agent for recovery of gold from printed circuit

board (Sheng and Etsell, 2007). Metals such as nickel (Kim et al., 2007), tin (Gibson et al., 2003), copper (Veit et al., 2006), silver (Petter et al., 2014), palladium (Quinet et al., 2005) has been reported to be recovered from E-waste. It was found that nitric acid; sulphuric acid and muriatic acid based solutions are majorly implemented for primary leaching of precious metals from E-waste. Recent focus on tin recycling from E-waste has been found among the researchers (Mecucci and Scott, 2002; Yang et al., 2017a). A green hydrometallurgical process has been developed for recovery of tin from PCBs via co-processing of waste PCBs and spent tin stripping solution which is generated during production of PCBs (Yang et al., 2017b). Umicore uses hydro-metallurgical processes for metal recovery. Industrial applications of such green processes are essential for sustainability.

3.5 Bio-metallurgical processes

Bio-metallurgical processing of E-waste is an emerging and a very promising area. There exist plenty of opportunities for research and development as well as business. Bio-metallurgical processes can be classified into two sections – a) Biosorption and b) Bioleaching. Biosorption means adsorption of metals by means of adsorbents prepared from waste biomass or abundant biomass. Metal recovery from E-waste by biosorption has been achieved by using algae (*Chlorella vulgaris*), fungi (*Aspergillusniger*), bacteria (*Penicilliumchrysogenum*), hen eggshell membrane, ovalbumin, alfalfa etc (Darnall et al., 1986; Kuyucak and Volesky, 1988; Niu and Volesky, 1999). The mechanism associated with biosorption is complex and no clear picture is available. There are certain factors that affect the process— a) Type of biological ligands accessible for metal binding, b) Type of the biosorbent (living, non-living), c) Chemical, stereo-chemical and co-ordination characteristics of the targeted metals and d) Characteristics of the metal solution such as pH and the competing ions (Tsezos et al., 2006).

According to Ilyas and Lee (2014), the mobilization of metal cations from often almost insoluble materials by biological oxidation and complexation processes is referred to as bioleaching. There are three major group of bacteria associated with in bioleaching of E-waste are – a) Autotrophic bacteria (e.g. Thiobacilli sp.), b) Heterotrophic bacteria (e.g. *Pseudomonas* sp., *Bacillus* sp.) and c) Heterotrophic fungi (e.g. *Aspergillus* sp., *Penicillium* sp.) (Schinner and Burgstaller, 1989). Typically bioleaching occurs in four steps— a) Acidolysis, b) Complexolysis, c) Redoxolysis and d) Bioaccumulation (Bosshard et al., 1996). Bioleaching has been explored by researchers for recovery of Gold, Aluminum, Copper, Nickel, Zinc and Lead from E-waste (Brandl et al., 2001; Faramarzi et al., 2004; Alan et al., 2005; Wang et al., 2009; Yang et al. 2009; Bas et al., 2013). There is no example of any industrialized process in the bio-metallurgical route.

4 Case studies

4.1 Case study organization A

Location: Karnataka, India

Capacity: Full recycling capacity of 10 ton/day but currently handling 6 ton /day

Land Area: 1.5 acres of land with 25,000 sq. ft. closed area and 60, 000 sq. ft. of open area

No. of Employees: 100 (50 men + 50 women).

Profitability trend (last five years): High.

This organization is one of the oldest E-waste recycling plants in India. The objective of this unit is to convert E-waste into beneficial raw materials (metals, plastics, glass etc.) by implementing simple, cost effective, indigenous, environmental friendly technologies suitable for Indian conditions. Its products and services includes E-waste collection, dismantling, processing, recycling; metal, plastic, glass and different other recycled products; gold recovery from printed circuit board strips etc.

This company provides the necessary logistics for collection of different types of E-waste through e-auction or direct purchase. The collected E-waste coming from the collection centers and other sources in the facility is recorded in the data entry book in terms of its weight, source and data entry records. All the E-waste is first checked for any radioactive materials before being taken in to the dismantling line/area. Different streams are segregated at the first level before actual pre-processing. The collected E-waste first undergoes manual dismantling. Trained employees with safety equipments uses basic toolkits such as hot air gun, screw driver etc. to efficiently dismantle the E-waste. Separate work tables are allocated for each person. Air suction duct is present in each table which prevents any kind of particulate emission during dismantling. The dismantled parts are further segregated and dismantled into various streams. This facilitates easier operation and efficient processing. The resulting streams are fed to respective machineries for resource recovery and recycling. The basic dismantling results into metal rich parts, printed circuit boards, plastics, wires and CRT. These streams (except CRT and wires) go through mechanical size reduction performed by Shear-shredder and hammer mills. Then density separation is carried out to separate metals and non-metals. Sister companies and other 3rd party industries are in contractual practice for metal recovery and other component recycling.

The company have developed their own process for CRT recycling. The composition and hazardous characteristics of the panel and the funnel glass are different. The recyclability of waste CRTs are substantially increased when the panel and funnel glass are separated and sold to manufacturers. These scraps then can be recycled to produce new panel and funnel glass. Electric wire heating method is used to cut CRT into two halves. This separation also facilitates removal of hazardous fluorescent color

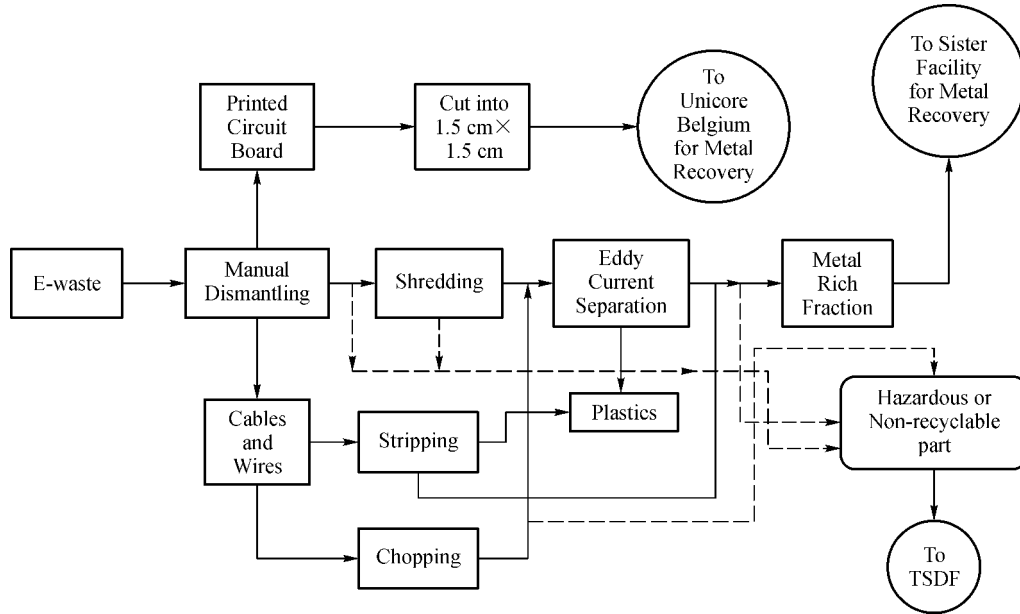


Fig. 1 Process of E-waste recycling in Indian Unit

coating from the surface of the panel glass. *Vacuum-suction method* is employed for this purpose. The glass is recycled by one of the leading TV manufacturer which uses 30% of the waste glass and rest virgin glass for manufacturing the TV glass panel. For wires, their indigenous stripping machine strips of the metal from the polymer coating. For cables with higher diameter, ranging from 2 mm to 10mm, are manually fed in the inlet holes from one end and longitudinally chopped pieces are collected from the other end, which are further manually segregated and sent to eddy current separator for separation of metals and non-metals.

The company is also associated in a social project where they have employed informal waste collectors and they buy waste printed circuit board (PCB) and other E-waste from them. These PCBs are shredded to 1.5" X-1.5" size

for smelting. It exports shredded circuit boards and components for copper smelting to Unicore Precious Melting Refining, Belgium with the approval from Ministry of Environment and Forests. All together it can be commented that this E-waste recycling plant cares about the society and environment and is working for the cleaner environment.

4.2 Case study organization B

Location: Beijing, China

Capacity: 10,000 tons/year

Land Area: 1.5 acres of land with 25,000 sq. ft. closed area and 60, 000 sq. ft. of open area

No. of Employees: 120

Profitability trend (last five years): High.

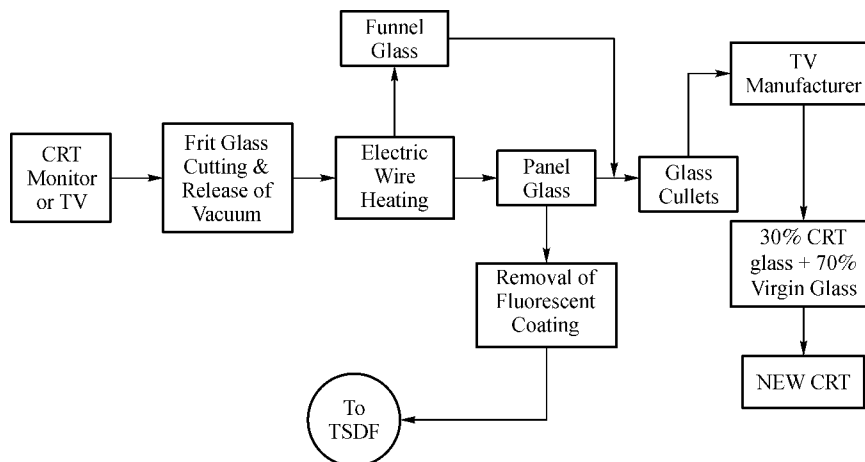


Fig. 2 Process for CRT recycling in Indian Unit

This organization is a model E-waste recycling plant for the city of Beijing, China. The unit provides waste dismantling, recycling service and disassembling E-waste as main competitive products. The company has specialized management team with professional knowledge in this sector committed to quality, honesty and value in E-waste recycling.

In the processing there are manual and semiautomatic sorting, dismantling in the E-waste recycling plant. Then the preprocessed material is sent to the processing stage. The material hence recovered are then reprocessed if required. They have separate line for refrigerators and degassing unit for safe removal of coolants. Then they are coarsely shredded and further crushed before subjecting to magnetic separation and eddy current separation for separation of metal and non-metals. Waste television sets are treated separately to take out the CRTs. The vacuum tube is cut out first. Then the glass panel and the funnel are separated out. The hazardous substances are removed before crushing the glass.

5 Sustainability of MREW technologies

Sustainability analysis of any process requires detailed intervention of the three sustainability parameters i.e. environmental, economic and social. Metal recovery from E-waste is a complex process and the heterogeneity of the material makes it even more complex. It is important to consider all three parameters for evaluation and prediction of the sustainability of metal recovery processes from E-waste. One important observation from the popular literature is that almost all the assessments of sustainability of E-waste processing are focused on determination of

environmental impacts via LCA. The economical and the social aspects have been excluded in those studies. A few studies have been identified in the social sector but the focus is on the informal sector. In this section, an effort has been made to give an overview of the sustainability of metal recovery processes from E-waste considering all three parameters of sustainability.

5.1 Generalized discussion on environmental sustainability

Environmental Sustainability of any process is generally characterized by some factors. These factors are assigned with some scores that dictate the magnitude of impact on the environment. A Life Cycle Analysis is arguably the ultimate method to assess environmental sustainability. Metal recovery from E-waste is lucrative as well as complex in nature as the metals are present within the solid polymer matrix of the printed circuit boards. To assess the environmental sustainability of the recovery processes discussed in section 3, it would require a large comparative LCA exercise to be carried out. However, a good number of standalone and comparative LCA exercises have been carried out by researchers. The standalone LCA are either on the whole treatment or technology and/or feed material specific. But the comparative LCA are just two alternatives of similar or with or without pre-treatment of a focused process.

To elucidate on the energy and environmental sustainability of MREW technologies, two conceptual scopes represented in Figs. 4 and 5, have been developed. In option 1, the metallurgical processes of pyro, hydro and bio categories are preceded by pre-treatment operations consisting only of mechanical and gravimetric types. On the other hand, the pre-treatment step is a combination of

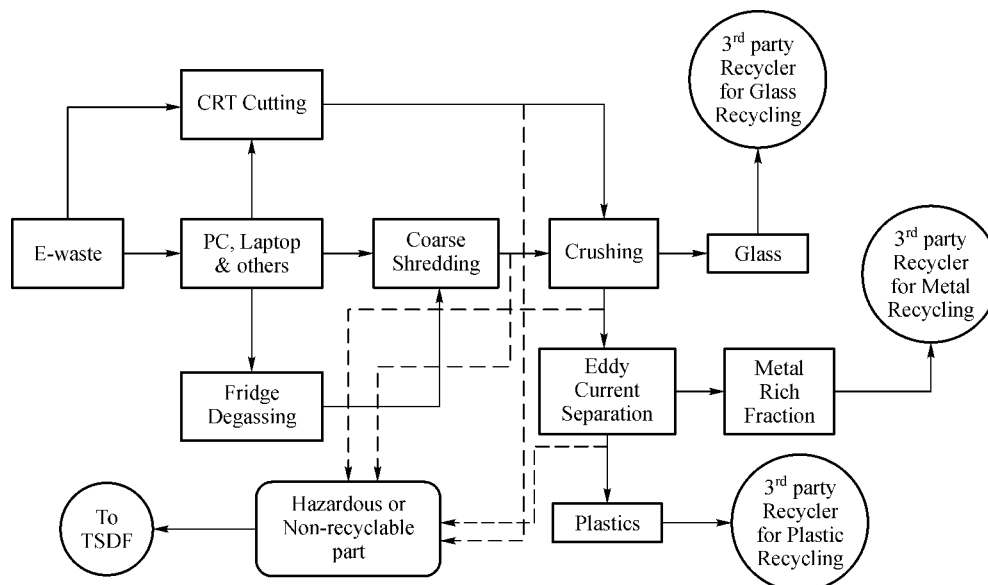


Fig. 3 Process for E-waste recycling in Chinese Unit

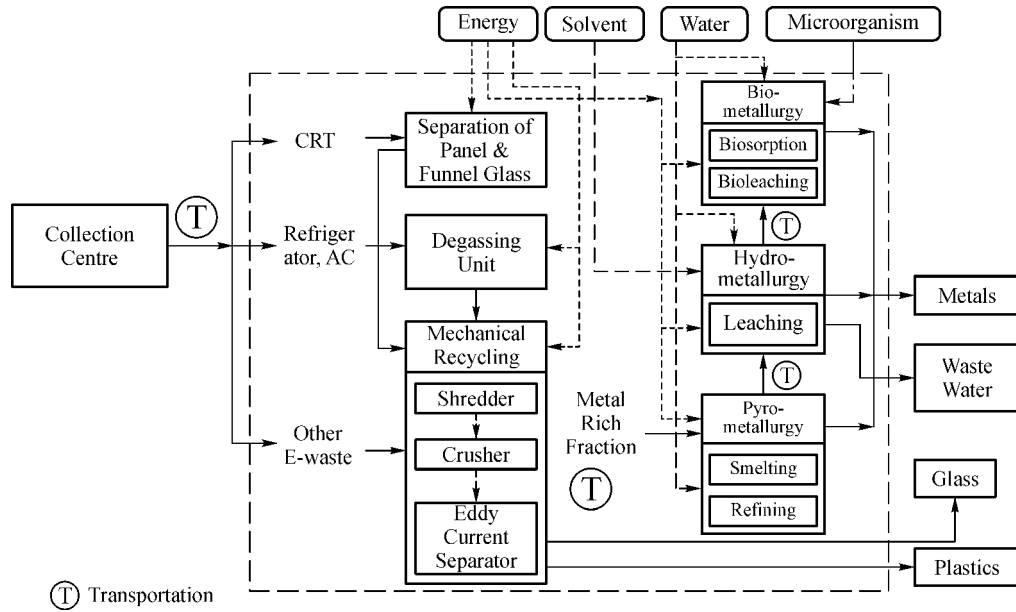


Fig. 4 Conceptual framework with conventional mechanical pre-treatment followed by metallurgical processing for MREW (Option-1)

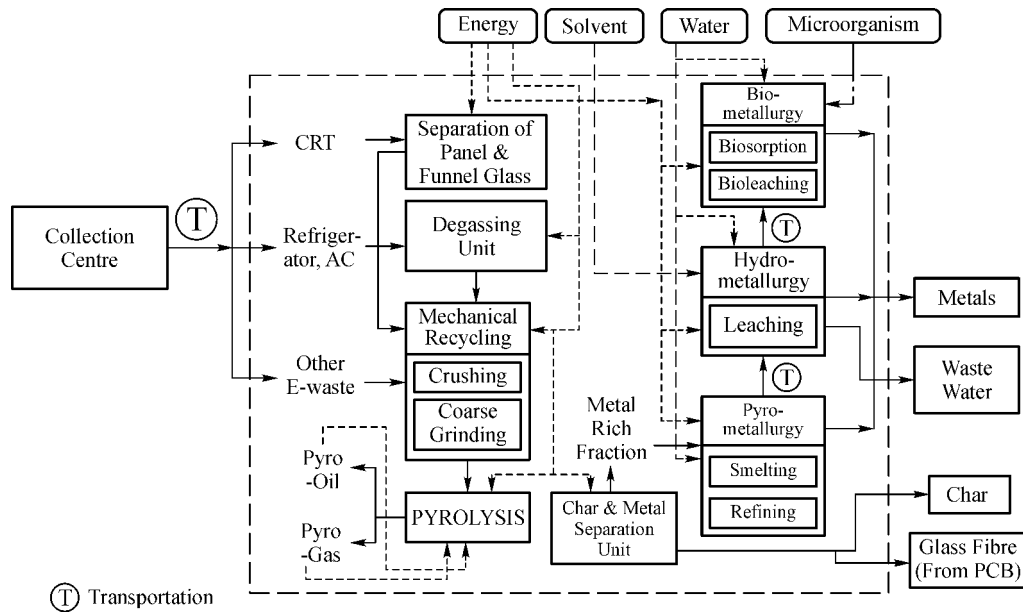


Fig. 5 Conceptual framework with light mechanical recycling and pyrolysis as pre-treatment followed by metallurgical processing for MREW (Option-2)

mechanical size reduction and a thermo-chemical process namely pyrolysis along with post separation step for isolating metal rich solids from the char residues. As per the requirement of all unit operations and chemical processes the input energy and the material resources have been clearly shown across the system boundaries. Similarly, the output streams; including metals, glass, plastic, oil, gas etc. whichever applicable have been clearly indicated. The possible emissions of carbon dioxide from

different processes and unit operations incurred due to the usage of grid energy originally generated in coal or oil or natural gas based power plants as well as transportation has been indicated. LCA could not be performed due to lack of reliable data and accurate values of energy consumption, requisite material resources and so on. However, analysis of two scenarios from the principles of LCA reveals the following points.

i) Consumption of energy and in turn the depletion of

fossil fuel is expected to be less in the pre-treatment process involving option 2 since it requires less severity of size reduction. As a consequence the carbon dioxide emission is also low in option 2.

ii) In option 2, pyrolysis process requires energy which can be supplied from the liquid gaseous products generated in the same process. The char resulting from pyrolysis can also be utilized for waste water treatment after activation.

iii) Hydro-metallurgical processing and electro-chemical refining is expected to have significant water footprint as both the processes generate waste water. Hydro-metallurgical processes use chemical solvents which contribute to COD of the waste water generated. As a result the possible contributions will be in the impact category of eutrophication, acidification, marine and freshwater ecotoxicity, human toxicity and water depletion. Recycling of the chemicals is a good option to reduce environmental impacts.

iv) Bio-metallurgical processes are expected to have similar impacts as different chemicals are required for preparation of the media for the culture and some waste water will be generated. But the magnitude of the impact is expected to be very less as it employs microorganism and toxic material generated during the process is limited.

v) The activated carbon used in waste water treatment may be manufactured from pyro-char.

vi) Usage of activated carbon prepared from waste biomass or any other waste materials instead of activated carbon prepared from virgin materials is encouraged. This will have some positive impact on the environment.

vii) Substantial amount of emission is associated with transportation of E-waste from collection centers to the recycling facility. It will be always preferred to have the

collection centers in close vicinity of the recycling center.

viii) As found from the case studies, after mechanical recycling it is sent to sister companies or third party facilities for processing and recovery of metals. This will increase the consumption of the fuel and ultimately will contribute to climate change and fossil fuel depletion.

ix) It is suggested that if the collection rate is substantially high then such processing facilities to be established in close vicinity or adjacent to the existing facility. This will reduce emissions due to transportation. However, if the rate of collection is not worthy by volume then it is better to use existing facility as new land acquisition will also have some adverse effects on the environment. Another factor, to be kept in mind that, any unit carrying out dry operations can be setup at the outskirts of any urban area as a centralized facility. If the unit to be established is for dry processing as well as metallurgical processing of E-waste, a decentralized facility will be preferred in the industrial zone. Hence, there is a trade-off between environmental aspect and social aspect.

A comprehensive presentation of LCA of individual technologies for MREW has been presented in Table 3, which reveals that the points identified by the general analysis of LCA principle is in good agreement with the reality.

5.2 Generalized discussion on economical sustainability

Economical sustainability is perhaps the most important aspect of sustainability when it comes to business. From the technological perspective, economical sustainability is there else the units would have shut down by this time. The

Table 3 Details of environmental LCA of different technologies

Technology	Type of LCA	Functional unit	Database /Method used	Geographical location	Highest impact categories
Pyrolysis (Alston and Arnold, 2011)	Comparison with landfill and incineration	E-waste containing 1 kg of plastic	Ecoinvent	United Kingdom	1. Marine aquatic toxicity 2. Freshwater aquatic toxicity 3. Carcinogens 4. Carbon Deposit 5. Climate change 6. Abiotic depletion 7. Eutrophication 8. Radiation
Pyrometallurgical processes (Ghodrat et al., 2017)	Comparison of secondary copper smelting with and without E-waste.	An input rate of 12,500 kg per hour of feed materials, (48 wt% copper scrap/metal oxides, 48 wt% waste PCB, 3.4 wt% slag and 0.6 wt% coke)	ReCiPe	Australia	1. Human Toxicity 2. Climate Change 3. Marine eutrophication 4. Freshwater eutrophication 5. Fresh water ecotoxicity 6. Water depletion
Hydrometallurgical processes (Iannicelli-Zubiani et al., 2017)	Standalone LCA	100 kg of electronic boards of mobile phones	Data obtained from pilot plant and SimaPro	EU/Italy	1. Eutrophication 2. Acidification 3. Global warming 4. Abiotic depletion 5. Human toxicity

most important thing of E-waste valorisation is metal recovery. It is nothing but chanting the '3R' mantra once again and is quite lucrative. E-waste business fostering around the world gets its maximum profit by metal reuse and recycling. Different metal recycling processes has been discussed in the section three. A summary of those processes along with their practical application in industry is presented in Table 4.

There are many economic aspects associated with the MREW units presented in Figs. 4 and 5. A generalized analysis of the two scenarios provides the following points.

(i) In option 1, mechanical recycling is rigorous and safety equipments, pollution control equipment and power consumption of the heavy machineries are few which add on extra cost of operation and maintenance, compared to option 2.

(ii) Transportation of different fractions to third party recyclers or sister companies add on extra supply chain costs but cost of setting up of new equipment and cost of land is greatly reduced.

(iii) Pyro-metallurgical processes are efficient and quite matured. These processes have evolved from their mother technologies of recovering metal from mining ores. The energy penalty of these processes is high and easily relatable to economics of the system. This is same for both option 1 and 2. However, option 2, due to pyrolysis, the load might be less.

(iv) In option 2, the resulting residue of pyrolysis contains metal, glass fiber and non-metallic char and all of these have market value. Energy input for pyrolysis is less than that of refining and smelting. The main cost associated with pyrolysis is continuous input of energy and cost of nitrogen for maintaining the inert atmosphere. Hence some cost reduction is possible at the energy input level. Additionally, the recovered materials i.e. fuels and glass fiber will generate some revenue.

(v) The hydrometallurgical processes are beneficial from

an economical point of view (Cui and Zhang, 2008). These processes does not require any energy source as the energy requirement is quite low and no extra cost associated with disposal of combustion residue in landfill or in Treatment Storage and Disposal Facilities (TSDFs) (Iannicelli-Zubiani et al., 2017).

(vi) In hydrometallurgical processes, the usage of chemicals, solvent regeneration and treatment of huge amount of waste water (i.e. leaching residue) generated is a major issue and adds on extra material and operating cost. Activated charcoal required for waste water treatment, if manufactured from waste materials or waste biomass may reduce some cost. Adsorbent regeneration and spent adsorbent disposal at TSDF may incur more cost; trade-off between these two is also possible.

(vii) Bio-metallurgical processes employ bacteria, fungi or algae to recover metal and it has a business potential. Bio-metallurgy is practised in recovering metals from ores in some places. The cost of bio-metallurgy depends on price of bacteria strain, cost of chemicals required for developing the culture medium and the culture conditions. The bio-metallurgical processes are new and more research is required to understand the kinetics, thermodynamics and further studies for scale up and process intensification to turn into a sustainable technology.

5.3 Generalized discussion on social sustainability

Social sustainability of any process is complex enough to go about. The behavior, mentality and other social indicators change with geographical region. Religion also plays a big role in this case. With respect to the technologies discussed, it is quite hard to predict the social sustainability. The social LCA is the best way to understand the social impact. Social LCA study of E-waste recycling is really scant. Umair et al. (2015) have shed some light in his study on social LCA of informal sectors

Table 4 Details of metal recovery processes from E-waste

Recovery processes	Typical industry	Input material	Expected output material	Machinery involved	Disadvantages	References
Pyrolysis	Jectec, Japan	Different PCB	Cu, Fe etc	Pyrolyzer	High energy penalty	(De Marco et al., 2008; Ghosh et al. 2014)
Plasma Process	PyroGenesis Canada Inc.	All type of PCB	Base Metals and Precious metals.	Plasma torch chamber	Very costly	(Tippayawong and Khongkrapan, 2009)
CRT Treatment	E-Parisaara India	TV, Monitor etc	Hg may be recovered	Laser Cutter	Toxic pollutants and health hazard	(Ling and Poon, 2012; Ghosh et al. 2014)
Leaching	Umicore	PCB chips or paste	Gold and other precious metals	Reactor	Toxic waste water	(Hagelüken, 2006; Kim et al., 2011)
Bioleaching	N/A	PCB chips or paste at certain %	Gold and other precious metals	Bio-reactor	Very slow process	(Alan et al., 2005)
Smelting & Electro-chemical refining	Umicore, Outotec TSL, Aurubis recycling.	All kinds of PCB	Different base metals (Cu, Fe etc) & noble metals (Ag, Au, Pt).	Smelting device	Higher emission, high energy penalty, slag generation etc	(Khaliq et al., 2014; Cui and Zhang, 2008)

associated with E-waste recycling. Considering stakeholder classification (United Nations, 2007) and the study of Umair et al. the following (Table 5) sub-categories may be taken into consideration for the formal recycling of E-waste and recovery of metals.

Table 5 Stakeholder category and sub-categories for social LCA of E-waste

Stakeholder category	Subcategories	References
Worker	Working Hours	Umair et al. 2015
	Child Labour	
	Health and Safety	
	Social Security	
	Wages	
Local community	Equal opportunities /discrimination	Umair et al. 2015
	Safety and health	
	Community engagement	
Society	Local Employment	Umair et al. 2015
	Public contribution to sustainable issues	
Governance	Contribution to economic development	Umair et al. 2015
	Corruption	
Demographics	Crime	United Nations, 2007
	Population	
Education	United Nations, 2007	Ghodrat et al., 2017
	Education Level	
	Literacy	
	Awareness	

Undoubtedly, the industrial implementation of these methods will certainly create job opportunities. The society will also be benefitted with the use of recycled products fuels and the use of green technologies in the industries. Overall, with time and advancement in the technologies, more the products will be commercialized, more it will be socially accepted and we will march toward social sustainability. However, social LCA is recommended for detailed analysis.

6 Conclusions

In this study, overall sustainability of MREW technologies has been qualitatively assessed considering environmental, economic and social perspectives. Two industrial case studies have been presented to understand the state-of-the-art scenario of the recycling process of MREW technology. Two frameworks for integrated MREW units, with (option-2) and without (option-1) pyrolysis, have been

conceptualized. A generalized qualitative energy and environmental impact analysis has been carried out using the principles of LCA. Due to scarcity of E-waste inventory data, the quantitative impact assessment through LCA could not be performed. Overall, option 2 has been predicted to be more efficient and sustainable compared to option 1 as it helps in reducing emissions and achieving circularity of materials through the reduction of milling energy along with generation of gaseous and liquid fuels, pyro-char and recyclable glass fibers from printed circuit boards etc. Generalized discussion from the perspective of economic and social aspects has been made. Climate change, fossil fuel depletion, water depletion, eutrophication, acidification, fresh and marine water ecotoxicity are possible impact categories that are evolved from the present analysis. The findings of the qualitative assessment of integrated MREW technology are in well alignment with previous standalone research outputs. The findings of the present assessment are expected to be beneficial to strategically decide on the research directions of MREW technologies.

References

- Alan N, de Klerk B J, William D D, Petrus B (2005). Recovery of precious metal from sulphide minerals by bioleaching. US Patent No. 6860919 (B1)
- Alston S M, Arnold J C (2011). Environmental impact of pyrolysis of mixed WEEE plastics Part 2: Life cycle assessment. *Environ Sci Technol*, 45(21): 9386–9392
- Antrekowitsch H, Potesser M, Spruzina W, Prior F (2006). Metallurgical recycling of electronic scrap. In: *Proceedings of the EPD Congress (899–908)*
- Baldé C P, Wang F, Kuehr R, Huisman J (2015). The global E-waste monitor–2014. United Nations University
- Bas A D, Deveci H, Yazici E Y (2013). Bioleaching of copper from low grade scrap TV circuit boards using mesophilic bacteria. *Hydrometallurgy*, 138: 65–70
- Bosshard P P, Bachofen R, Brandl H (1996). Metal leaching of fly ash from municipal waste incineration by *Aspergillusniger*. *Environ Sci Technol*, 30(10): 3066–3070
- Brandl H, Bosshard R, Wegmann M (2001). Computer-munching microbes: Metal leaching from electronic scrap by bacteria and fungi. *Hydrometallurgy*, 59(2): 319–326
- Catalyst C (India) Pvt. Ltd. (2015). A brief report on electronics industry in India. Available online at: <http://www.cci.in/pdfs/surveys-reports/Electronics-Industry-in-India.pdf> (Accessed January 4, 2016)
- Chmielewski A G, Urbański T S, Migdał W (1997). Separation technologies for metals recovery from industrial wastes. *Hydrometallurgy*, 45(3): 333–344
- Cui J, Zhang L (2008). Metallurgical recovery of metals from electronic waste: A review. *J Hazard Mater*, 158(2-3): 228–256
- Darnall D W, Greene B, Henzl M T, Hosea J M, McPherson R A, Sneddon J, Alexander M D (1986). Selective recovery of gold and

- other metal ions from an algal biomass. *Environ Sci Technol*, 20(2): 206–208
- De Marco I, Caballero B M, Chomón M J, Laresgoiti M F, Torres A, Fernández G, Arnaiz S (2008). Pyrolysis of electrical and electronic wastes. *J Anal Appl Pyrolysis*, 82(2): 179–183
- Debnath B, Roychowdhury P, Kundu R (2016). Electronic Components (EC) reuse and recycling—A new approach towards WEEE management. *Procedia Environ Sci*, 35: 656–668
- E-waste Guide Info. The composition of valuable substances in E-waste. Available online at: <http://ewasteguide.info> (Accessed September 18, 2016).
- Faramarzi M A, Stagars M, Pensini E, Krebs W, Brandl H (2004). Metal solubilization from metal-containing solid materials by cyanogenic-*Chromobacterium violaceum*. *J Biotechnol*, 113(1-3): 321–326
- Ghodrat M, Rhamdhani M A, Brooks G, Rashidi M, Samali B (2017). A thermodynamic-based life cycle assessment of precious metal recycling out of waste printed circuit board through secondary copper smelting. *Environ Dev*, 24: 36–49
- Ghosh S K, Debnath B, Baidya R, De D, Li J, Ghosh S K, Zheng L, Awasthi A K, Liubarskaia M A, Ogola J S, Tavares A N (2016). Waste electrical and electronic equipment management and Basel Convention compliance in Brazil, Russia, India, China and South Africa (BRICS) nations. *Waste Manag Res*, 34(8): 693–707
- Ghosh S K, Singh N, Debnath B, De D, Baidya R, Biswas N T, Ghosh S K, Lili L, Dey P K, Li J (2014) E-waste supply chain management: Findings from pilot studies in India, China, Taiwan (ROC) and the UK. In: Proceedings of the 9th international conference on waste management and technology, Beijing, China, 29–31 October, China: Basel Convention Regional Centre for Asia and Pacific, 1131–1140
- Gibson R W, Goodman P D, Holt L, Dalrymple I M, Fray D J (2003). U. S. Patent No. 6,641,712. Washington, DC: U.S. Patent and Trademark Office.
- Guo Q, Yue X, Wang M, Liu Y (2010). Pyrolysis of scrap printed circuit board plastic particles in a fluidized bed. *Powder Technol*, 198(3): 422–428
- Hagelüken C (2006). Recycling of electronic scrap at Umicore's integrated metals smelter and refinery. *Erzmetall*, 59(3): 152–161
- Hall W J, Miskolczi N, Onwudili J, Williams P T (2008). Thermal processing of toxic flame-retarded polymers using a waste fluidized catalytic cracker (FCC) catalyst. *Energy Fuels*, 22(3): 1691–1697
- Hall W J, Williams P T (2007). Analysis of products from the pyrolysis of plastics recovered from the commercial scale recycling of waste electrical and electronic equipment. *J Anal Appl Pyrolysis*, 79(1): 375–386
- Huisman J (2010). WEEE recast: from 4 kg to 65%: the compliance consequences. UNU Expert opinion on the EU WEEE Directive. United Nations University, Bonn, Germany
- Iannicelli-Zubiani E M, Gianni M I, Recanati F, Dotelli G, Puricelli S, Cristiani C (2017). Environmental impacts of a hydrometallurgical process for electronic waste treatment: A life cycle assessment case study. *J Clean Prod*, 140: 1204–1216
- Ilyas S, Lee J C (2014). Biometallurgical recovery of metals from waste electrical and electronic equipment: a review. *ChemBioEng Reviews*, 1(4): 148–169
- Kang H Y, Schoenung J M (2005). Electronic waste recycling: A review of US infrastructure and technology options. *Resour Conserv Recycl*, 45(4): 368–400
- Khaliq A, Rhamdhani M A, Brooks G, Masood S (2014). Metal extraction processes for electronic waste and existing industrial routes: a review and Australian perspective. *Resources*, 3(1): 152–179
- Kim E Y, Kim M S, Lee J C, Pandey B D, Pandey B D (2011). Selective recovery of gold from waste mobile phone PCBs by hydrometallurgical process. *J Hazard Mater*, 198: 206–215
- Kim E Y, Lee J C, Kim B S, Kim M S, Jeong J (2007). Leaching behavior of nickel from waste multi-layer ceramic capacitors. *Hydrometallurgy*, 86(1): 89–95
- Kołodziej B, Adamski Z (1984). A ferric chloride hydrometallurgical process for recovery of silver from electronic scrap materials. *Hydrometallurgy*, 12(1): 117–127
- Koyanaka S, Endoh S, Ohya H, Iwata H (1997). Particle shape of copper milled by swing-hammer-type impact mill. *Powder Technol*, 90(2): 135–140
- Kuyucak N, Volesky B (1988). Biosorbents for recovery of metals from industrial solutions. *Biotechnol Lett*, 10(2): 137–142
- Li J, Xu Z, Zhou Y (2007). Application of corona discharge and electrostatic force to separate metals and nonmetals from crushed particles of waste printed circuit boards. *J Electrostat*, 65(4): 233–238
- Ling T C, Poon C S (2012). Development of a method for recycling of CRT funnel glass. *Environ Technol*, 33(22-24): 2531–2537
- Liu W W, Hu C W, Yang Y, Tong D M, Zhu L F, Zhang R N, Zhao B H (2013). Study on the effect of metal types in (Me)-Al-MCM-41 on the mesoporous structure and catalytic behavior during the vapor-catalyzed co-pyrolysis of pubescens and LDPE. *Appl Catal B*, 129: 202–213
- McMahon P (2016) Electronic waste expected to rise by 21% in 2018. Available online at: <http://clareherald.com/2016/08/electronic-waste-expected-to-rise-by-21-in-2018/> (Accessed September 5, 2016)
- Mecucci A, Scott K (2002). Leaching and electrochemical recovery of copper, lead and tin from scrap printed circuit boards. *J Chem Technol Biotechnol*, 77(4): 449–457
- Mitrasinovic A, Pershin L, Mostaghimi J (2013). Electronic waste treatment by high enthalpy plasma jet. International plasma chemistry society (IPCS20) Philadelphia USA
- Niu H, Volesky B (1999). Characteristics of gold biosorption from cyanide solution. *J Chem Technol Biotechnol*, 74(8): 778–784
- Ogunniyi I O, Vermaak M K G (2009). Investigation of froth flotation for beneficiation of printed circuit board comminution fines. *Miner Eng*, 22(4): 378–385
- Peng M, Layiding W, Dong X, Jiangang G, Guanghong D (2004). A physical process for recycling and reusing waste printed circuit boards. In: Electronics and the Environment, 2004. Conference Record. 2004 IEEE International Symposium, 237–242
- Petter P M H, Veit H M, Bernardes A M (2014). Evaluation of gold and silver leaching from printed circuit board of cellphones. *Waste management*, 34(2), 475–482.
- Qiu K Q, Wu Q, Zhan Z H (2009). Vacuum pyrolysis characteristics of waste printed circuit boards epoxy resin and analysis of liquid products. *Journal of Central South University: Science and Technology*, 40(5): 1209–1215
- Quinet P, Proost J, Van Lierde A (2005). Recovery of precious metals from electronic scrap by hydrometallurgical processing routes. *Miner*

- Metall Process, 22(1): 17–22
- Rath S S, Nayak P, Mukherjee P S, Chaudhury G R, Mishra B K (2012). Treatment of electronic waste to recover metal values using thermal plasma coupled with acid leaching—A response surface modeling approach. *Waste management*, 32(3), 575–583
- Ruidian T, Tonghua W, Suxia T, Xinzhan H, Tao W (2007). Products from microwave heating of waste printed circuit boards. *Environmental Pollution & Control*, 8, 013
- Ruj B, Chang J (2013). E-waste (Cell Phone) Treatment By Thermal Plasma Technique. In: *Proceedings of the 7th International Symposium on Feedstock Recycling of Polymeric Materials (7th ISFR 2013)*, New Delhi, India
- Schinner F, Burgstaller W (1989). Extraction of zinc from industrial waste by a *Penicillium* sp. *Appl Environ Microbiol*, 55(5): 1153–1156
- Shamsuddin M (1986). Metal recovery from scrap and waste. *JOM*, 38(2): 24–31
- Sheng P P, Etsell T H (2007). Recovery of gold from computer circuit board scrap using aqua regia. *Waste Manag Res*, 25(4): 380–383
- Sun J, Wang W, Liu Z, Ma Q, Zhao C, Ma C (2012). Kinetic study of the pyrolysis of waste printed circuit boards subject to conventional and microwave heating. *Energies*, 5(9): 3295–3306
- Sun L, Lu J, Wang S, Zhang J, Zhou H (2003). Experimental research on pyrolysis characteristics of printed circuit board wastes. *Journal of Chemical Industry and Engineering—China*, 54(3): 408–412
- Sun Z, Cao H, Xiao Y, Sietsma J, Jin W, Agterhuis H, Yang Y (2016). Toward sustainability for recovery of critical metals from electronic waste: The hydrochemistry processes. *ACS Sustain Chem&Eng*, 5(1): 21–40
- Tippayawong N P, Khongkrapan P (2009). Development of a laboratory scale air plasma torch and its application to electronic waste treatment. *Int J Environ Sci Technol*, 6(3): 407–414
- Tsezos M, Remoundaki E, Hatzikioseyan A (2006). Biosorption-principles and applications for metal immobilization from wastewater streams. In: *Proceedings of the EU-Asia Workshop on Clean Production and Nanotechnologies*. Seoul, 23–33
- Umair S, Björklund A, Petersen E E (2015). Social impact assessment of informal recycling of electronic ICT waste in Pakistan using UNEP SETAC guidelines. *ResourConserv Recycling*, 95: 46–57
- United Nations Department of Economic. (2007). *Indicators of sustainable development: Guidelines and methodologies*. United Nations Publications
- Veit H M, Bernardes A M, Ferreira J Z, Tenório J A S, de Fraga Malfatti C (2006). Recovery of copper from printed circuit boards scraps by mechanical processing and electrometallurgy. *J Hazard Mater*, 137(3): 1704–1709
- Veit H M, Diehl T R, Salami A P, Rodrigues J D S, Bernardes A M, Tenório J A S (2005). Utilization of magnetic and electrostatic separation in the recycling of printed circuit boards scrap. *Waste Management*, 25(1), 67–74
- Vidyadhar A, Das A (2012). Kinetics and Efficacy of Froth Flotation for the Recovery of Metal Values from Pulverized Printed Circuit Boards In: *Proceedings of XXVI International Mineral Processing Congress (IMPC) 2012*, September 24–28, 2012, Hotel Ashok, Diplomatic Enclave, New Delhi, India, 236–243
- Wang J, Bai J, Xu J, Liang B (2009). Bioleaching of metals from printed wire boards by *Acidithiobacillus ferrooxidans* and *Acidithiobacillus thiooxidans* and their mixture. *J Hazard Mater*, 172(2-3): 1100–1105
- Wu Z, Yuan W, Li J, Wang X, Liu L, Wang J (2017). A critical review on the recycling of copper and precious metals from waste printed circuit boards using hydrometallurgy. *Front Environ Sci Eng*, 11(5): 8
- Xiong Z H, Li H B, Wu C Z, Chen Y (2006). A study on pyrolysis and kinetics of printed circuit boards wastes. *Techniques and Equipment for Environmental Pollution Control*, 10, 010
- Yang C, Li J, Tan Q, Liu L, Dong Q (2017a). Green process of metal recycling: Co-processing waste printed circuit boards and spent tin stripping solution. *ACS Sustain Chem&Eng*, 5(4): 3524–3534
- Yang C, Tan Q, Liu L, Dong Q, Li J (2017b). Recycling Tin from electronic waste: A problem that needs more attention. *ACS Sustain Chem&Eng*, 5(11): 9586–9598
- Yang T, Xu Z, Wen J, Yang L (2009). Factors influencing bioleaching copper from waste printed circuit boards by *Acidithiobacillus ferrooxidans*. *Hydrometallurgy*, 97(1): 29–32
- Zhang S, Forssberg E (1998). Optimization of electrodynamic separation for metals recovery from electronic scrap. *ResourConserv Recycling*, 22(3): 143–162

An Analysis of E-Waste Recycling Technologies from the Chemical Engineering Perspective



Biswajit Debnath, Ranjana Chowdhury and Sadhan Kumar Ghosh

Abstract Technological advancements and changes in lifestyle have led to the generation of a behemoth amount of e-waste worldwide. The demand of new Electrical and Electronic Equipment (EEE) is also increasing which is leading to rapid depletion of primary resources. Resource recovery and recycling of e-waste is the only option to keep things in balance. There are many technologies for e-waste recycling which are in practice, such as pyrolysis, gasification, leaching, biosorption. Reported literature includes stand-alone experimental works, sustainability analysis and systematic reviews of e-waste recycling technologies. Most of these recycling processes have some chemical engineering aspects which are inherent but yet overlooked in most of the cases. Studies envisaging the chemical engineering aspects of these technologies are scant. In this study, a detailed analysis of these e-waste recycling technologies from the chemical engineering perspective has been presented. Transport properties, kinetics, thermodynamics, etc., have been taken into consideration for carrying out the analysis. The findings of this paper will enable the researchers in this field for further process development.

Keywords E-waste · Technology · Recycling · Chemical engineering Kinetics

1 Introduction

The growth of electronics industry has been tremendous in the last two decades which ensured a lot of cash flow but it also contributed to the material flow stream of electronic waste. Globally, e-waste is the fastest booming waste stream in the world increasing at an annual rate of 3–5% [7, 27]. According to Basel Convention,

B. Debnath (✉) · R. Chowdhury
Department of Chemical Engineering, Jadavpur University, Kolkata, India
e-mail: biswajit.debnath.ju@gmail.com; bisuworld@gmail.com

S. K. Ghosh
Department of Mechanical Engineering, Jadavpur University, Kolkata, India

© Springer Nature Singapore Pte Ltd. 2019
S. K. Ghosh (ed.), *Waste Management and Resource Efficiency*,
https://doi.org/10.1007/978-981-10-7290-1_74

879

e-waste defined as—“*substances or objects which are disposed of or are intended to be disposed of or are required to be disposed of by the provisions of national law*” [2]. United Nations University estimated that globally 41.8 million metric tonnes of e-waste was generated in 2014 and it is forecasted to be 50 million tonnes by 2018 with a rise by 21% [1, 24]. Huisman [14] predict that by 2020, WEEE will grow by 2.5–2.7% annually making it up to 12.3 million tonnes. WEEE generation in China is estimated to be 6.033 million tonnes in 2014 which is second largest generator of WEEE while USA being the highest generator with 7.072 million tonnes in 2014 [1]. BRICS nations generated nearly 25% of the global WEEE generation in 2014 [10].

E-waste is a complex material and contains different types of materials including polymers, metals, ceramics. The lighter e-wastes such as mobile, laptop contain high amount of polymer, which are mainly flame retardants. Debnath et al. [9] reported that the amount of polymer and metals varies widely with type of e-waste based on weight, size and end application. For example, keyboards contain 95% polymer, whereas the printed circuit boards are rich in metals. There are different methods that are used for recycling e-waste. Debnath et al. [9] reported a study on different metal recovery technologies from e-waste discussed the sustainability of those processes. E-waste recycling includes physical recycling processes and chemical recycling processes. In most of the recycling units around the globe, use of physical recycling processes is dominant. However, the chemical recycling processes are required to be implemented for sustainable recycling and valorization. The only chemical recycling processes implemented in a few e-waste recycling facilities are modified versions of parent metallurgical technologies. These are mostly carried out by some third-party organization on regular or contractual basis. As reported by Khaliq et al. [19], the pyro-metallurgical and hydrometallurgical processes are followed by these industries during the metal recovery from electronic waste. However, the thermochemical processing of e-waste for the generation of fuels from the polymeric part of e-waste is still being investigated in laboratory scale. It is clear from the literature survey that most of the research studies on thermochemical conversion of e-waste are only focused on the determination of reaction kinetics of base process. For the commercial development of thermochemical processes for e-waste utilization, more thrusts should be given on reactor design along with development of process models taking both reaction kinetics and the mass and heat transfer limitations into account. This article will review the present status of the reported research studies in the area of thermochemical processing of e-waste. An attempt will be made to identify the research gaps to be mitigated for the further utilization of thermochemical processes for e-waste utilization, and finally, some recommendations will be made.

2 Methodology

Firstly, thorough literature review was carried out exploring SCI-indexed journals, Conference proceedings and Reports, etc. Different keywords such as ‘e-waste recycling’, ‘metal recovery from e-waste’, ‘printed circuit board recycling’, ‘pyrolysis of e-waste’, ‘gasification of e-waste’, ‘transport phenomena in e-waste pyrolysis’, ‘heat and mass transfer in e-waste gasification’, ‘e-waste pyrolysis kinetics’ were used for this purpose. The papers were screen and sorted. Further literature review was carried out to look for the cross references. Then, the papers were analyzed and the help of books was taken to understand the phenomena and the gaps.

3 Thermochemical Processes for E-Waste Recycling

3.1 Pyrolysis

Thermochemical processes such as pyrolysis, a common method for degradation of polymeric substances. A significant number of literature on pyrolysis of e-waste (printed circuit boards) depicts the importance and relevance of the topic [6, 11, 13, 32]. The typical product from pyrolysis of e-waste (mixed e-waste plastics) is 70.6% pyro-oil, 7.8% gases and 21.1% char and ash [13]. However, these compositions may vary depending on the type of e-waste, method of pyrolysis, presence of catalyst and additives, type of reactor, etc. Yang et al. [37] presented a review which provides insight on pyrolysis and dehalogenation of plastics obtained from e-waste. Investigation of vacuum pyrolysis of e-waste has been reported by a huge number of researchers [21, 28]. The key advantage of using vacuum pyrolysis is the low temperature and pressure. Another approach is the microwave-induced pyrolysis which is rarely adopted, though reported as a very energy-efficient process since the activation energy is much lower than other conventional pyrolysis method [29–34]. Catalytic pyrolysis is another route for treatment of e-waste (polymer fractions) [12] and has been reported by several researchers [11, 15], though maximum works focus on pure or mixture different plastics.

Different catalysts have been used—FCC catalysts [12], zeolites [30], silica-alumina [26], metal-based catalysts [15], meso-structured catalysts [22], minerals [23], low-cost materials such as red mud, limestone [35], oyster shell, calcium-based additives [15]. Co-pyrolysis, where the key is the synergistic effect of different reaction of different materials, is a good way of recycling e-waste. Co-pyrolysis of waste biomass and e-waste has been found to be beneficial [22]. This method is a green thermochemical processing alternative as it produces high-quality pyro-oil and it also prevents the generation of dioxins. Details on prevention of dioxins from pyrolysis of e-waste have been discussed and analyzed by Lai et al. [20]. Hence, pyrolysis is an environment-friendly chemical recycling method of e-waste.

3.2 Gasification

E-waste gasification is a comparatively unexplored area and a few literature reported are concentrated in either polymer gasification or polymer part of e-waste gasification. High-impact polystyrene (HIPS) resin containing poly-brominated diphenyl ethers (PBDE; mainly decabromo-diphenyl oxide), which is a brominated flame retardant, has been used as feedstock for a zero-emission recycling process which implements gasification followed by shock cooling. This method successfully prevented the formation of dioxins and furans and also recovered antimony present in the plastics in form of solids. A gaseous by-product called “thin gas” rich in hydrogen was found suitable for use as raw material in the chemical industry [36]. The effect of steam and sodium hydroxide on hydrogen production using dechlorinated PVC and activated carbon as feedstock has been reported by Kamo et al. [16]. Later, the influence of the mixed molten carbonate composition on hydrogen production by steam gasification of activated carbon derived from plastic waste materials was also reported [17]. Zhang et al. [39] performed kinetic study of epoxy resin board steam gasification in eutectic carbonate (Li_2CO_3 , Na_2CO_3 , K_2CO_3) mixture. It was revealed that the reaction follows pseudofirst-order kinetics. The order was found to be 0.91th power of the partial pressure and the activation energy was 122 kJ/mol. In case of the phenolic board, the shrinking core model and homogeneous model (kinetic controlled reactions where there are no mass transfer limitations) were used to describe the kinetics. Particles less than and equal to 0.15 mm follow the homogenous model, whereas particles greater than and equal to 1 mm follows some complex kinetics which was described using initial rapid pyrolysis, homogenous model gasification and the shrinking core model gasification [40].

4 Discussion and Analysis

The knowledge of chemical kinetics is essential to understand how the reaction proceeds. This knowledge accordingly helps in the development of the process and the design of the corresponding process equipment. Based on the available literature, it has been found that a good number of works on the kinetics of e-waste pyrolysis has been carried out. A detailed literature review has been presented in the preceding section. In most of the cases, the kinetic evaluation is limited within the primary reactions. In an ideal scenario, chemical kinetics should account for both primary and secondary decomposition reactions. Other parameters such as heating rate and possibility of autocatalysis of specific secondary reactions also play important roles. At higher pyrolysis temperature, the tar produced during the primary reactions undergoes further thermal cracking to produce more volatiles and char. These have not been considered so far in the reported literature in the kinetic evaluation processes of e-waste.

Table 1 Different reactions taking place during gasification reaction

Reaction type	Reaction
<i>(a) Carbon reactions</i>	
R _c 1 (Boudouard)	$C + CO_2 \leftrightarrow 2CO \Delta H = +172 \text{ kJ/mol}$
R _c 2 (Water-gas)	$C + H_2O \leftrightarrow CO + H_2 \Delta H = +131 \text{ kJ/mol}$
R _c 3 (Hydrogasification)	$C + 2H_2 \leftrightarrow CH_4 \Delta H = -74.8 \text{ kJ/mol}$
R _c 4	$C + 0.5O_2 \rightarrow CO \Delta H = -111 \text{ kJ/mol}$
<i>(b) Oxidation reaction</i>	
R _O 1	$C + O_2 \rightarrow CO_2 \Delta H = -394 \text{ kJ/mol}$
R _O 2	$CO + 0.5O_2 \rightarrow CO_2 \Delta H = -284 \text{ kJ/mol}$
R _O 3	$CH_4 + 2O_2 \leftrightarrow CO_2 + 2H_2O \Delta H = -803 \text{ kJ/mol}$
R _O 4	$H_2 + 0.5O_2 \rightarrow H_2O \Delta H = -242 \text{ kJ/mol}$
<i>(c) Shift reaction</i>	
R _S 1	$CO + H_2O \leftrightarrow CO_2 + H_2 \Delta H = -41.2 \text{ kJ/mol}$
<i>(d) Methanation reactions</i>	
R _M 1	$2CO + 2H_2 \rightarrow CH_4 + CO_2 \Delta H = -247 \text{ kJ/mol}$
R _M 2	$CO + 3H_2 \leftrightarrow CH_4 + H_2O \Delta H = -206 \text{ kJ/mol}$
R _M 3	$CO_2 + 4H_2 \rightarrow CH_4 + 2H_2O \Delta H = -165 \text{ kJ/mol}$
<i>(e) Steam-Reforming reactions</i>	
R _{SR} 1	$CH_4 + H_2O \leftrightarrow CO + 3H_2 \Delta H = +206 \text{ kJ/mol}$
R _{SR} 2	$CH_4 + 0.5O_2 \rightarrow CO + 2H_2 \Delta H = -36 \text{ kJ/mol}$

^aSource [3]

Kinetics for gasification reactions is well established and still a subject of intensive investigation. Gasification involves the primary reactions of pyrolysis. It is the char evolved during pyrolysis that takes active participation in the gasification reactions. There are series of reactions that take place during the char gasification, summarized in Table 1.

The determinations of kinetic parameters are imperative in case of pyrolysis of e-waste for a particular set of conditions. The deficiency of exact knowledge of the course of reactions and their degrees of completion is the main hindrance towards in-depth study of thermal behaviour of e-waste. During pyrolysis, a huge number of products, stable and unstable is evolved which makes it more complex. As a result, different set of values of reactions constant, pre-exponential factor and activation energy has been reported (Table 2). The heterogeneous nature of e-waste also plays a key role in this anomaly of different values of the aforementioned kinetic parameters.

The type of reactor used for pyrolysis or gasification plays a major role in the overall output of the process. Fixed bed reactor, fluidised bed reactor and tube reactor have been used so far for pyrolysis of e-waste and plastics derived from e-waste. Brominated high-impact polystyrene (HIPS) found in e-waste has been subjected to fast pyrolysis in fluidized bed reactor and proved to be beneficial for higher oil yield and less gas and char yield compared to the conventional pyrolysis

Table 2 Kinetic parameters of pyrolysis of e-waste reported by different authors

S. No	Type of pyrolysis	Activation energy	Frequency factor (min^{-1})	Order or reaction	References
1	Pyrolysis of e-waste from small household appliances	95.54 kJ/mol	1.06×10^8	3.38	[18]
2	Pyrolysis of PCB particle size 5, 10 and 40 mm	For 2 °C/min: 45.87–47.13 (kJ/mol)	For 2 °C/min: 1.73×10^{17} – 4.28×10^{16}	For 2 °C/min: 1.24–1.47	[5]
		For 15 °C/min: 38.16–40.44 (kJ/mol)	For 15 °C/min: 1.05×10^{14} – 9.05×10^{14}	For 15 °C/min: 1.23–1.58	
3	354 μm crashed PCB pyrolysis in fluidized bed	First-stage reaction: 90.49 kJ/mol Second-stage reaction: 137.80 kJ/mol	–	1	[11]
4	Pyrolysis of keyboard, PCB and telephone wire	Keyboard: 166.08 (kJ/mol)	Keyboard: 7.82×10^8	1	[29]
		PCB: 149.28 (kJ/mol)	PCB: 2.01×10^9		
		Telephone wire: 96.76 (kJ/mol)	Telephone wire: 2.54×10^5		
5	Microwave pyrolysis of e-waste in different carrier gas	142.99–165.04 (kJ/mol)	3.84×10^{11} – 6.87×10^9	–	[41]

[4, 15, 25]. Despite other formats, it has been an undebated choice for the researcher favouring the fluidised bed configuration. Perhaps this is the reason most of the gasification of e-waste and e-waste plastics studies has been carried out in fluidised bed reactors. From a chemical engineering point of view, it can be said that fluidised bed helps to improve polymer degradation by acting as a good agent to heat and mass transfer and thereby dispersing the melting polymer in thin layers. However, the works on gasification of printed circuit boards reported have used semi-batch reactors instead of conventional updraft or downdraft gasifiers for gasification purposes. This is probably because PCBs are complex materials and there are many other materials which does not take part or degrade during the gasification process. In case of co-pyrolysis of e-waste and biomass, good results have been obtained in a fixed bed reactor [22]. From environmental sustainability point of view, it was confirmed that the pyro-oils did not contain bromine rather most of the bromine was fixed with the char, which enables the use of pyro-oil to a good extent and chances of environmental hazard occurring from brominated

compound emission. Though this is a promising area and very less work has been done, there exists much scope for intervention. Other methods such as the use of catalysts for thermochemical conversion of e-waste have been implemented and good results have been obtained. More research in these areas is required.

5 Conclusion

E-waste is one of the fastest growing waste streams in the world and its environment-friendly disposal is now becoming harder. The challenge of developing a proper methodology for e-waste disposal is still ongoing because of the hazardous and heterogeneous nature of the waste stream. The mechanical recycling method is mostly opted globally as a recycling methodology. Other methods such as thermochemical methods have been reported for e-waste treatment. But these technologies are mostly concentrated within the laboratory. Good amount of literature is available that discusses the kinetics of e-waste pyrolysis. The choice of the reactor and the mode of pyrolysis play a big role on quality of output materials. Co-pyrolysis and fluidised bed reactor were found to be good combination for this purpose. The kinetics for gasification of e-waste is reported but not very much developed. There exists a lot of scope for reactor design and other process intensifications for gasification.

It is believed that with the contribution of stalwarts, the general modelling of pyrolysis and gasification is enriched enough. However, investigation on the mathematical modelling considering the effects of transport phenomena of e-waste pyrolysis and gasification is scant. With the growing concern of e-waste disposal, chemical treatment processes are becoming important and such investigations are required for further development and commercialization of these processes.

Acknowledgements The authors would like to acknowledge Department of Chemical Engineering, Jadavpur University, Centre for Quality Management, Jadavpur University, and International Society of Waste Management, Air and Water (ISWMAW) for their support.

References

1. Baldé, C. P., Wang, F., & Kuehr, R. et al. (2015). *The global e-waste monitor–2014*. United Nation University.
2. Basel Convention. (2014). *Basel convention on the control of transboundary movements of hazardous wastes and their disposal protocol on liability and compensation for damage resulting from transboundary movements of hazardous wastes and their disposal texts and annexes*. UNEP.
3. Basu, P. (2013). *Biomass gasification, pyrolysis and torrefaction: Practical design and theory*. Cambridge: Academic press.

4. Bhaskar, T., Murai, K., Matsui, T., Brebu, M. A., Uddin, M. A., Muto, A., et al. (2003). Studies on thermal degradation of acrylonitrile–butadiene–styrene copolymer (ABS-Br) containing brominated flame retardant. *Journal of Analytical and Applied Pyrolysis*, 70(2), 369–381.
5. Chiang, H. L., Lin, K. H., Lai, M. H., Chen, T. C., & Ma, S. Y. (2007). Pyrolysis characteristics of integrated circuit boards at various particle sizes and temperatures. *Journal of Hazardous Materials*, 149(1), 151–159.
6. Chuangzhi, X. Z. L. H. W., & Yong, C. (2006). A study on pyrolysis and kinetics of printed circuit boards wastes. *Techniques and Equipment for Environmental Pollution Control*, 10, 010.
7. Debnath, B., Baidya, R., & Ghosh, S. K. (2015). Simultaneous analysis of WEEE management system focusing on the supply chain in India, UK and Switzerland. *International Journal of Manufacturing and Industrial Engineering*, 2, 16–20.
8. Debnath, B., Roychoudhuri, R., & Ghosh, S. K. (2016). E-Waste management—A potential route to green computing. *Procedia Environmental Sciences*, 35, 669–675.
9. Debnath, B., Chowdhury, R., & Ghosh, S. K. (2016). Sustainability of metal recovery from e-waste. In *The 11th International Conference on Waste Management and Technology (ICWMT11)*. Beijing, China.
10. Ghosh, S. K., Debnath, B., Baidya, R., De, D., Li, J., Ghosh, S. K., et al. (2016). Waste electrical and electronic equipment management and Basel Convention compliance in Brazil, Russia, India, China and South Africa (BRICS) nations. *Waste Management and Research*, 34(8), 693–707.
11. Guo, Qingjie, XuehaiYue, Minghua Wang, & Liu, Yongzhuo. (2010). Pyrolysis of scrap printed circuit board plastic particles in a fluidized bed. *Powder Technology*, 198(3), 422–428.
12. Hall, W. J., Miskolczi, N., Onwudili, J., & Williams, P. T. (2008). Thermal processing of toxic flame-retarded polymers using a waste fluidized catalytic cracker (FCC) catalyst. *Energy and Fuels*, 22(3), 1691–1697.
13. Hall, W. J., & Williams, P. T. (2007). Analysis of products from the pyrolysis of plastics recovered from the commercial scale recycling of waste electrical and electronic equipment. *Journal of Analytical and Applied Pyrolysis*, 79(1), 375–386.
14. Huisman, J., (2010). WEEE recast: from 4 kg to 65%: The compliance consequences. 5 March, Bonn: United Nations University, Institute for Sustainability and Peace (UNU-ISP).
15. Jung, S. H., Kim, S. J., & Kim, J. S. (2012). Thermal degradation of acrylonitrile–butadiene–styrene (ABS) containing flame retardants using a fluidized bed reactor: The effects of Ca-based additives on halogen removal. *Fuel Processing Technology*, 96, 265–270.
16. Kamo, T., Takaoka, K., Otomo, J., & Takahashi, H. (2006). Effect of steam and sodium hydroxide for the production of hydrogen on gasification of dehydrochlorinated poly(vinyl chloride). *Fuel*, 85(7–8), 1052–1059.
17. Kamo, T., Wu, B., Egami, Y., Yasuda, H., & Nakagome, H. (2011). Influence of mixed molten carbonate composition on hydrogen formation by steam gasification. *Journal of Material Cycles and Waste Management*, 13(1), 50–55.
18. Kantarelis, E., Yang, W., Blasiak, W., Forsgren, C., & Zabaniotou, A. (2011). Thermochemical treatment of E-waste from small household appliances using highly pre-heated nitrogen-thermogravimetric investigation and pyrolysis kinetics. *Applied Energy*, 88(3), 922–929.
19. Khaliq, A., Rhamdhani, M. A., Brooks, G., & Masood, S. (2014). Metal extraction processes for electronic waste and existing industrial routes: A review and Australian perspective. *Resources*, 3(1), 152–179.
20. Lai, Y. C., Lee, W. J., Li, H. W., Wang, L. C., & Chang-Chien, G. P. (2007). Inhibition of polybrominated dibenzo-p-dioxin and dibenzofuran formation from the pyrolysis of printed circuit boards. *Environmental Science and Technology*, 41(3), 957–962.

21. Li, J., Duan, H., Yu, K., Liu, L., & Wang, S. (2010). Characteristic of low-temperature pyrolysis of printed circuit boards subjected to various atmosphere. *Resources, Conservation and Recycling*, 54(11), 810–815.
22. Liu, W. W., Hu, C. W., Yang, Y., Tong, D. M., Zhu, L. F., Zhang, R. N., et al. (2013). Study on the effect of metal types in (Me)-Al-MCM-41 on the mesoporous structure and catalytic behavior during the vapor-catalyzed co-pyrolysis of pubescens and LDPE. *Applied Catalysis, B: Environmental*, 129, 202–213.
23. Liu, M., Zhuo, J. K., Xiong, S. J., & Yao, Q. (2014). Catalytic degradation of high-density polyethylene over a clay catalyst compared with other catalysts. *Energy & Fuels*, 28(9), 6038–6045.
24. McMahon, P. (2016). *Electronic waste expected to rise by 21% in 2018*. Available from <http://clareherald.com/2016/08/electronic-waste-expected-to-rise-by-21-in-2018/>.
25. Miskolczi, N., Hall, W. J., Angyal, A., Bartha, L., & Williams, P. T. (2008). Production of oil with low organobromine content from the pyrolysis of flame retarded HIPS and ABS plastics. *Journal of Analytical and Applied Pyrolysis*, 83(1), 115–123.
26. Moqadam, S. I., Mirdrikvand, M., Roozbehani, B., Kharaghani, A., & Shishehsaz, M. R. (2015). Polystyrene pyrolysis using silica-alumina catalyst in fluidized bed reactor. *Clean Technologies and Environmental Policy*, 17(7), 1847–1860.
27. Ojeda-Benitez, S., Cruz-Sotelo, S. E., Velázquez, L., Santillán-Soto, N., Nu, M. Q., Cueto, O. R. G., & Markus, W. (2013). Electrical and electronic waste in Northwest Mexico.
28. Qiu, K. Q., Wu, Q., & Zhan, Z. H. (2009). Vacuum pyrolysis characteristics of waste printed circuit boards epoxy resin and analysis of liquid products. *Journal of Central South University: Science and Technology*, 40(5), 1209–1215.
29. Quan, C., Li, A., & Gao, N. (2013). Combustion and pyrolysis of electronic waste: Thermogravimetric analysis and kinetic model. *Procedia Environmental Sciences*, 18, 776–782.
30. Ramya, G., Sivakumar, T., Arif, M., & Ahmed, Z. (2015). Catalytic cracking using an H β catalyst for the production of green fuel: Optimization studies. *Energy Sources, Part A: Recovery, Utilization, and Environmental Effects*, 37(7), 758–765.
31. Ruidian, T., Tonghua, W., Suxia, T., Xinzhan, H., & Tao, W. (2007). Products from microwave heating of waste printed circuit boards. *Environmental Pollution and Control*, 8, 013.
32. Sun, L., Lu, J., Wang, S., Zhang, J., & Zhou, H. (2003). Experimental research on pyrolysis characteristics of printed circuit board wastes. *Journal of Chemical Industry and Engineering-CHINA*, 54(3), 408–412.
33. Sun, J., Wang, W., Liu, Z., & Ma, C. (2011). Recycling of waste printed circuit boards by microwave-induced pyrolysis and featured mechanical processing. *Industrial and Engineering Chemistry Research*, 50(20), 11763–11769.
34. Sun, J., Wang, W., Liu, Z., Ma, Q., Zhao, C., & Ma, C. (2012). Kinetic study of the pyrolysis of waste printed circuit boards subject to conventional and microwave heating. *Energies*, 5(9), 3295–3306.
35. Wu, H., Shen, Y., Harada, N., An, Q., & Yoshikawa, K. (2014). Production of pyrolysis oil with low bromine and antimony contents from plastic material containing brominated flame retardants and antimony trioxide. *Energy and Environment Research*, 4(3), 105.
36. Yamawaki, T. (2003). The gasification recycling technology of plastics WEEE containing brominated flame retardants. *Fire and Materials*, 27(6), 315–319.
37. Yang, X., Sun, L., Xiang, J., Hu, S., & Su, S. (2013). Pyrolysis and dehalogenation of plastics from waste electrical and electronic equipment (WEEE): A review. *Waste Management*, 33(2), 462–473.
38. Yang, J., Tanguy, P. A., & Roy, C. (1995). Heat transfer, mass transfer and kinetics study of the vacuum pyrolysis of a large used tire particle. *Chemical Engineering Science*, 50(12), 1909–1922.

39. Zhang, S., Yoshikawa, K., Nakagome, H., & Kamo, T. (2012). Steam gasification of epoxy circuit board in the presence of carbonates. *Journal of Material Cycles and Waste Management*, *14*(4), 294–300.
40. Zhang, S., Yoshikawa, K., Nakagome, H., & Kamo, T. (2013). Kinetics of the steam gasification of a phenolic circuit board in the presence of carbonates. *Applied Energy*, *101*, 815–821.
41. Zhang, Z., Zhao, X., Kwon, E., & Castaldi, M. J. (2010, January). Experimental research on microwave induced thermal decomposition of printed circuit board wastes. In *18th Annual North American Waste-to-Energy Conference* (pp. 15–21). American Society of Mechanical Engineers.

Urban Mining and the Metal Recovery from E-Waste (MREW) Supply Chain



Biswajit Debnath, Ranjana Chowdhury and Sadhan Kumar Ghosh

1 Introduction

E-waste has become a mini-catastrophe and its amount has reached a record level of nearly 42 million metric tonnes in 2014 [4, 10]. The demand for EEE is ever increasing and the driving force behind this demand is often the technological advancement coupled with short innovation cycles and business strategies which shortens the lifespan of the equipments [15]. In 2014, the BRICS nations were responsible for 25% of the total e-waste generated in the world [17]. It has been predicted that by 2017, 72 million tonnes of e-waste will be generated [4].

E-waste is a complex material and contains different types of basic metals, rare earth metals, polymers, glass, glass fibre, etc. (Fig. 1). With the depletion of primary resources and increasing demand for metals in the market, it is legible to recover metals from e-waste and reuse them in the manufacturing process of new ones reducing the mining activities. A comparatively new term *urban mining* has come into the picture. It extends the concept of *landfill mining* to the reclamation process of elements and compounds from the anthropogenic stockpiles [3]. The basic objective of urban mining is to recover resources from urban waste and put them back into the supply chain. It is important to extract and process the anthropogenic stocks accompanied by the economical benefits. This is the primary reason that the term urban mining has become almost synonymous with the extraction of metals from e-waste as the metal concentration (expensive and rare earth) is comparatively high [7]. Several studies have been reported in the context of urban mining. Debnath et al. [13] have proposed the frameworks for Metal Recovery from E-Waste (MREW) to address the

B. Debnath · R. Chowdhury
Department of Chemical Engineering, Jadavpur University, Kolkata, India

S. K. Ghosh (✉)
Department of Mechanical Engineering, Jadavpur University, Kolkata, India
e-mail: sadhankghosh9@gmail.com

© Springer Nature Singapore Pte Ltd. 2019
S. K. Ghosh (ed.), *Waste Valorisation and Recycling*,
https://doi.org/10.1007/978-981-13-2784-1_32

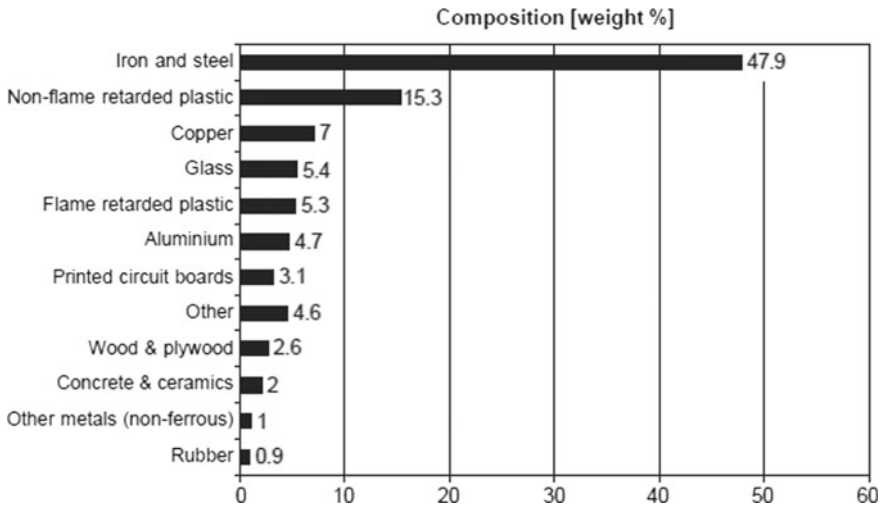


Fig. 1 Composition of e-waste [14]

issue of urban mining. Supply chain network (SCN) of e-waste is interesting and complex [9]. It is imperative to have an efficient and sustainable SCN for proper e-waste management. Aravindhnan et al. [1] have provided some insight into how supply chain strategies can help e-waste management. There are several issues and challenges in e-waste supply chains and the sustainability of the business depends on it [15219]. Country-specific supply chain mapping has been approached by different researchers. It is of great interest to identify how the supply chain of e-waste differs in developed and developing countries [9, 16]. Ghosh et al. [17] has mapped the high level supply chain for the BRICS nations and also proposed a sustainable high level SCN for them taking learning from developed nations. Barletta et al. [5] have provided the prerequisites for a high level framework for designing sustainable units in the e-waste supply chain. Reported literatures focus on country-specific supply chain mapping, optimisation models, risk assessments, etc. Hence, focus on the e-waste supply chain issues was there. However, for urban mining, it is crucial to address the issue of metal recovery and that has not been addressed in the reported literature. The research questions that arise are—how MREW can help in addressing the urban mining concept? How essential it is to have an efficient supply chain for MREW? What is the supply chain framework of the MREW? The study aims to answer these questions with the background concept of MREW. A supply chain framework for the MREW has also been developed.

Table 1 Metal percentage in PCBs

Metal	Ores (%)	PCBs (%)
Copper	0.5–3.0	12.0–29.0
Zinc	1.7–6.4	0.1–2.7
Tin	0.2–0.85	1.1–4.8
Lead	0.3–7.5	1.3–3.9
Iron	30–60	0.1–11.4
Nickel	0.7–2.0	0.3–1.6
Gold	0.0005	0.0029–0.112
Silver	0.0005	0.01–0.52

Source Bizzo et al. [6]

2 Methodology

First, a detailed literature survey was carried out. Several search engines were explored with keywords such as ‘E-waste supply chain’, ‘WEEE supply chain’, ‘Urban Mining’, etc. The literature was critically reviewed and the relevant ones were segregated. Cross-references were also considered for review. Based on the findings of Ghosh et al. [17] and Debnath et al. [13] and the authors’ experience in visiting different e-waste recycling facility around the world, a supply chain framework was developed for an MREW. The relevant literatures have been cited and additional information from the associated cross-literatures has been also properly referred.

3 Urban Mining of E-Waste

The concept of *urban mining* is associated with recovery of materials and energy from urban waste and puts them back into the economy. Such a concept must be coupled with circular economy concept to design policy frameworks for sustainable development. The anthropogenic stock available for urban mining is not limited to e-waste, but the overall concept has somehow become synonymous with resource recovery from e-waste. There is special relevance to this with respect to the goal no. 13 of the Ha Noi 3R goals which encompasses the concept of urban mining [18]. The key reason for this is due to the concentrations of metals that are more in PCBs compared to the ores (Table 1) [6].

E-waste is a heterogeneous material and contains different types of basic metals, valuable metals, rare earth elements (REE), polymers, ceramics, glass, etc. From the perspective of urban mining, all of these are resources which can be recovered via technological intervention. In general, physical recycling processes are implemented for the segregation of separate streams such as metals, glass, polymers, etc. Thermochemical, pyrometallurgical, hydrometallurgical and biometallurgical technologies

can be employed for further resource recovery from the resultant material streams from physical processing of e-waste. These technologies have been discussed in detail previous reported literatures [10, 11, 20].

4 The Relevance of MREW to Urban Mining

The business of e-waste is particularly of interest due to the presence of metals. Recovery of metals from e-waste is expected to play a major role in the resource circulation. Technologies such as pyrolysis, leaching, electro-chemical refining, pyrometallurgical extraction of metals, bio-leaching, etc. are in existence which are helpful in metal recovery from e-waste (MREW) [13]. We have discussed the concept of MREW in details in our previous work [13]. As the primary intention of urban mining is the resource recovery from 'urban ore' (or anthropogenic stockpile) and its proper circulation, the MREW has direct relevance to it. Though the metals are the particular focus, several other things can be recovered from e-waste. E-waste consists of a significant amount of polymers. These polymers may be recycled to make nice products or can be used for new product development. The printed circuit boards (PCBs) are metal-polymer-glass fibre matrix which is a source of useful materials. Pyrolysis of PCBs followed by mechanical separation can lead to recovery of metals, pyro-oil and glass fibre [12]. All of these are recyclables and have market value and pyrolysis can be considered as a pretreatment process for MREW [13]. Based on the size and average composition of e-waste, the resources that can be recovered can be estimated and accordingly the recovery path may be chosen. Another important issue is the economic sustainability, which must be ensured while realisation of urban mining via MREW facilities [8]. Some generalised insight on economic sustainability of MREW has been discussed in the previous paper [13]. Though much more innovations are required, MREW technologies are expected to play a pivotal role in urban mining of e-waste.

5 Findings and Discussions

5.1 *Supply Chain Framework for Urban Mining Considering MREW*

Despite the technological advancements and maturity over time, it is imperative to have a very efficient supply chain network to balance the supply and the demand for materials and ensure circular economy. Based on the findings of Ghosh et al. [17] and Debnath et al. [13], literature findings, brainstorming and the authors' experience in visiting several e-waste recycling facilities, a supply chain framework has

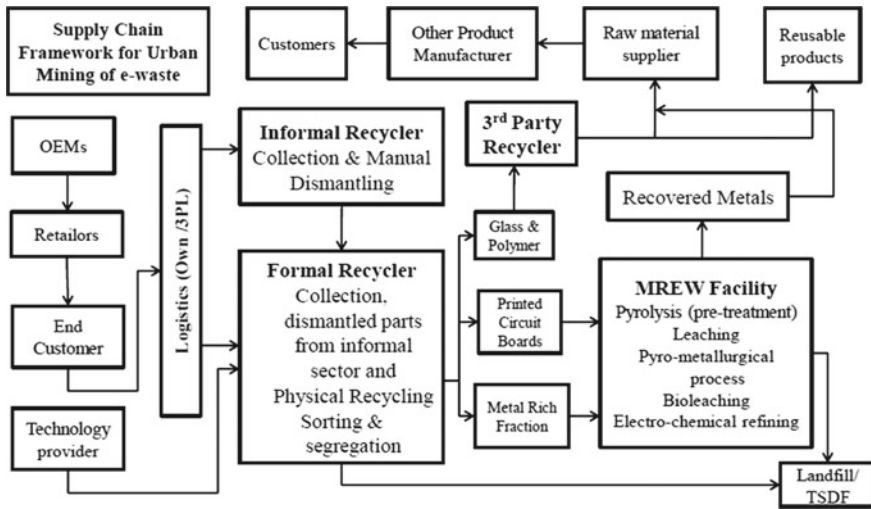


Fig. 2 Supply chain framework for urban mining of e-waste considering MREW facility

been developed (Fig. 2). The framework is intended for urban mining of e-waste considering MREW facility.

The supply chain framework can be divided into three parts—the supply side, the internal operations side and the demand side. OEMs, retailers, customers and the technology providers are in the supply side. The informal sector, formal recyclers and the MREW facility are in the internal operations side whereas; third party recyclers, raw material suppliers, reusable product manufacturer and customers of recycled products are in the demand side.

5.2 Discussions

The developed supply chain framework (Fig. 2) has considered the MREW facility for the recovery of metals from e-waste. The supply side considers the traditional stakeholder flow from OEM to end customers. The logistics for e-waste to recycling facilities has been kept as a choice of the users. To some extent, the door-to-door collection of the informal sector makes it independent of the users. After the collection and dismantling at the primary recycling facilities, the recovered fractions enter the MREW facility. In the MREW, all possible routes of metal recovery have been considered including pyrolysis as a pretreatment process. This is where the urban mining gets a boost. The existence of the dedicated MREW facility for metal recovery is the key and the strongest point here is to ensure the resource recovery. The circularity of resources is ensured by the demand side where the third party recyclers are involved in recycling the resulting fractions and the recycled product manufacturers convert

these into products which can be sold in the market. Some portion of recovered e-waste can be considered as raw materials and these are then supplied to different places by the raw material suppliers, which mean the material re-enters the value chain. This conforms to the concept of circular economy. Nonetheless, the supply chain framework will undoubtedly help in realising the concept of urban mining in a unique way and ensure sustainability.

6 Conclusions

In this paper, the concept of urban mining has been addressed with respect to e-waste as a very important anthropogenic stockpile. The concept of MREW has been taken as basis and its relevance to the urban mining of e-waste. Furthermore, a supply chain framework has been developed which considered MREW facility to address urban mining of e-waste. The urban mining is a new concept and this study focusing on enhancing urban mining of e-waste gives it a boost. The unique concept of the MREW facility will no doubt be a thing to be explored in the future for the researchers. The proposed framework will help in enhancing urban mining and ensuring sustainability. It is also believed that more studies of such kind accompanied by case studies will be beneficial for the overall community.

Acknowledgements The authors would like to acknowledge International Society of Waste Management, Air and Water (ISWMAW) for partially funding the project. Additionally, the help and cooperation from Dr. Prasanta Kumar Dey, Aston University; Centre for Quality Management Systems (CQMS) Jadavpur University, Kolkata; Consortium of Researchers for Environmental Protection, Sustainability and Climate Change (CREPSCC) are gratefully acknowledged.

References

1. Aravindhan L, Raaghavan P, Vivek Narayanji SG, Jaysri Thangam A (2012) Impact of supply chain strategies on the reduction of e-waste. *Int J Interscience Manage Rev* 2(2):26–29
2. Baidya R, Debnath B, Ghosh SK (2016) Analysis of E-waste supply chain framework in india using the analytical hierarchy process. In: *Proceedings of 6th on waste management and resource utilization IconSWM 2016, Jadavpur University, India*, pp 1181–1188
3. Baccini P, Brunner P (2012) *Metabolism of the antroposphere: analysis, evaluation, design*. The MIT Press, Cambridge. ISBN 9780262016650
4. Baldé CP, Wang F, Kuehr R, et al (2015) *The global e-waste monitor–2014*. United Nation University
5. Barletta I, Johansson B, Reimers J, Stahre J, Berlin C (2015) Prerequisites for a high-level framework to design sustainable plants in the e-waste supply chain. *Procedia CIRP* 29:633–638
6. Bizzo WA, Figueiredo RA, de Andrade VF (2014) Characterization of printed circuit boards for metal and energy recovery after milling and mechanical separation. *Materials* 7(6):4555–4566
7. Cossu R, Williams ID (2015) Urban mining: concepts, terminology, challenges. *Waste Manag* 45:1–3
8. Cossu R (2013) The urban mining concept. *Waste Manage* 33(3):497–498

9. Debnath B, Baidya R, Ghosh SK (2015) Simultaneous analysis of WEEE management system focusing on the supply chain in India, UK and Switzerland. *Int J Manuf Ind Eng* 2(1):16–20
10. Debnath B, Roychoudhuri R, Ghosh SK (2016) E-waste management—a potential route to green computing. *Procedia Environ Sci* 35:669–675
11. Debnath B, Chowdhury R, Ghosh SK (2016b) An analysis of e-waste recycling technologies from the chemical engineering perspective. In: *Proceedings of 6th waste management and resource utilization IconSWM 2016*, Jadavpur University, India, pp 1189–1195
12. Debnath B, Chowdhury R, Ghosh SK (2017) An analysis of e-waste recycling technologies from the chemical engineering perspective. In: *Proceedings of CHEMCON 2017*, Haldia Institute of Technology, India, pp 1189–1195
13. Debnath B, Chowdhury R, Ghosh SK (2018) Sustainability of metal recovery from e-waste. *Front Environ Sci Eng*, Springer (Accepted for publication.)
14. ETC/RWM (2003) European topic centre on resource and waste management (Topic Centre of the European Environment Agency) part of the European Environment Information and Observation Network (EIONET), <http://waste.eionet.eu.int/waste/6>
15. Ghosh SK, Baidya R, Debnath B, Biswas NT, De D, Lokeswari M (2014a) E-waste supply chain issues and challenges in India using QFD as analytical tool. In: *Proceedings of international conference on computing, communication and manufacturing, ICCCM 2014*, pp 287–291
16. Ghosh SK, Singh N, Debnath B, De D, Baidya R, Biswas NT, Ghosh SK, Lili L, Dey PK, Li J (2014b) E-waste supply chain management: findings from pilot studies in India, China, Taiwan (ROC) and the UK. In: *The 9th international conference on waste management and technology*, Beijing China, 29–31 October, 2014, pp 1131–1140
17. Ghosh SK, Debnath B, Baidya R, De D, Li J, Ghosh SK, Tavares AN (2016) Waste electrical and electronic equipment management and Basel Convention compliance in Brazil, Russia, India, China and South Africa (BRICS) nations. *Waste Manage Res* 34(8):693–707
18. Ha Noi Declaration (2013) Available from: <https://www.env.go.jp/en/focus/docs/files/20130318-67.pdf>. Accessed on 3 Dec 2017
19. Hazra J, Sarkar A, Sharma V (2011) E-waste supply chain management in India: opportunities and challenges. *Clean India J* 7
20. Khaliq A, Rhamdhani MA, Brooks G, Masood S (2014) Metal extraction processes for electronic waste and existing industrial routes: a review and Australian perspective. *Resources* 3(1):152–179